Vol. 94 No. 1 November 1, 1977 ISSN 0003-2670

ANALYTICA CHIMICA ACTA

International journal devoted to all branches of analytical chemistry

ELSEVIER SCIENTIFIC PUBLISHING COMPANY

ANALYTICA CHIMICA ACTA

International journal devoted to all branches of analytical chemistry
Revue internationale consacrée à tous les domaines de la chimie analytique
Internationale Zeitschrift für alle Gebiete der analytischen Chemie

PUBLICATION SCHEDULE FOR 1977 (incorporating the section on Computer Techniques and Optimization).

	J	F	M	A	M	J	J	A	S	O	N	D
Analytica Chimica Acta	88/1	88/2	89/1	89/2	90	91/1	91/2	92/1	92/2	93	94/1	94/2
Section on Computer Techniques and Optimization									95/ 1+2			95/3+4

Scope. *Analytica Chimica Acta* publishes original papers, short communications, and reviews dealing with every aspect of modern chemical analysis, both fundamental and applied. The section on *Computer Techniques and Optimization* is devoted to new developments in chemical analysis by the application of computer techniques and by interdisciplinary approaches, including statistics, systems theory and operation research.

Submission of Papers. Manuscripts (three copies) should be submitted to:
for *Analytica Chimica Acta*: Dr. A.M.G. Macdonald, Department of Chemistry, The University, P.O. Box 363, Birmingham B15 2TT, England.
for the section on *Computer Techniques and Optimization*: Dr. J.T. Clerc, Laboratorium für Organische Chemie, Swiss Federal Institute of Technology, Universitätstrasse 16, CH-8092 Zürich, Switzerland.

Information for Authors. Papers in English, French and German are published. There are no page charges. Manuscripts should conform in layout and style to the papers published in this Volume. Authors should consult Vol. 93, p. 379 for detailed information. Reprints of this information are available from the Editors or from: Elsevier Editorial Services Ltd., Mayfield House, 256 Banbury Road, Oxford OX2 7DE (Great Britain).

Reprints. Fifty reprints will be supplied free of charge. Additional reprints (minimum 100) can be ordered. An order form containing price quotations will be sent to the authors together with the proofs of their article.

Advertisements. Advertisement rates are available from the publisher.

Subscriptions. Subscriptions should be sent to: Elsevier Scientific Publishing Company, P.O. Box 211, Amsterdam, The Netherlands. The section on *Computer Techniques and Optimization* can be subscribed to separately.

Publication. *Analytica Chimica Acta* (including the section on *Computer Techniques and Optimization*) appears in 8 volumes in 1977. The subscription for 1977 (Vols. 88–95) is Dfl. 920.00 plus Dfl. 112.00 (postage) (Total approx. US $ 420.95). The subscription for the *Computer Techniques and Optimization* section only (Vol. 95) is Dfl. 115.00 plus Dfl. 14.00 (postage) (Total approx. US $ 52.75). Journals are sent automatically by air mail to the U.S.A. and Canada at no extra cost and to Japan, Australia and New Zealand for a small additional postal charge. All earlier volumes (Vols. 1–87) are available at Dfl. 115.- (plus postage).

Claims for issues not received should be made within three months of publication of the issue, otherwise they cannot be honoured free of charge.

Printed in The Netherlands

salon du laboratoire 1977

Paris, porte de Versailles

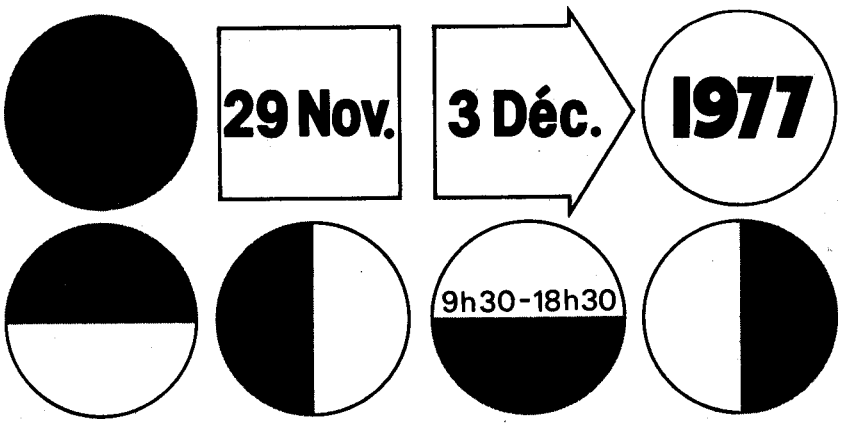

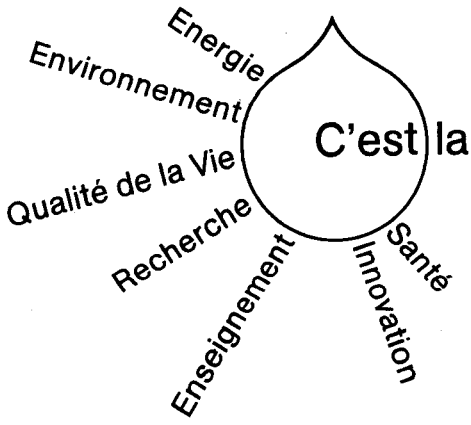

C'est la raison d'être du Laboratoire.

La 67e Exposition de Physique a lieu conjointement avec le Salon du Laboratoire. L'entrée des deux expositions est commune.

Le Congrès de Chimie Analytique - 33e Congrès du G.A.M.S. - se tiendra aux mêmes lieux et dates que ce salon.

Salon organisé par l'Association pour le Salon du Laboratoire régie par la loi de 1901
12, rue Chabanais - 75002 PARIS - France - Tél. 742.79.00

399

Verdere inlichtingen, folder en voordelig reisarrangement worden gaarne verstrekt door de STICHTING TER BEVORDERING VAN DE FRANSE VAKBEURZEN
Prins Hendrikkade 20-21 - Amsterdam-C. - Telefoon (020) 248670 en 239204

Lasers in Chemistry

Proceedings of the Conference held at the Royal Institution, London, 31 May - 2 June 1977

edited by MICHAEL A. WEST, *The Royal Institution, London.*

As lasers and associated electro-optics have been developed in the past few years, chemists have rapidly adapted and used these new light sources in many diverse ways. This conference was held in order to review and discuss the present state-of-the-art in this fast-growing field and the proceedings contain 79 papers organized into seven sections. Each section, except one, contains a review paper by an invited speaker and a set of contributed papers which, taken together, indicate the overall scope of current research and point to likely future advances in a particular area. This volume will be of value to academic, government and industrial scientists as well as to technologists in chemistry, physics and electro-optics.

In the contents listed below, the main topics of the conference are given with the total number of papers in each section noted in parentheses. Limitation of space allows titles of only a few randomly selected papers to be mentioned.

Sept. 1977 xii + 438 pages US $69.50/Dfl. 170.00 ISBN 0-444-41630-7

ELSEVIER

P.O. Box 211, Amsterdam
The Netherlands
52 Vanderbilt Ave
New York, N.Y. 10017

The Dutch guilder price is definitive. US $ prices are subject to exchange rate fluctuations.

7057

ANALYTICA CHIMICA ACTA
VOL. 94 (1977)

ANALYTICA CHIMICA ACTA

International journal devoted to all branches of analytical chemistry

ELSEVIER SCIENTIFIC PUBLISHING COMPANY

Anal. Chim. Acta, Vol. 94 (1977)

PRINTED IN THE NETHERLANDS

Analytica Chimica Acta, 94 (1977) 1—19

OPTIMIZATION OF THE MICROWAVE-INDUCED PLASMA AS AN ELEMENT-SELECTIVE DETECTOR FOR NON-METALS

J. P. J. van DALEN, P. A. de LEZENNE COULANDER and L. de GALAN

Laboratorium voor Analytische Scheikunde, Technische Hogeschool Delft, P.O. Box 5029, Delft (The Netherlands)

(Received 8th June 1977)

SUMMARY

The microwave-induced plasma in helium carrier gas at low pressure has been optimized for the detection of the elements C, H, N, O, S, P, F, Cl, Br and I. The parameters studied include the pressure, microwave power, observation height and concentration of scavenger gas. Special problems encountered with phosphorus, fluorine and silicon are discussed. Under the optimum conditions, the following analytical properties have been determined: the linear dynamic range (3—4 decades except for hydrogen), the detection limits (in agreement with other publications 0.1 ng s^{-1}) and the sensitivity (which depends on the type of compound introduced). The significance of the technique for the determination of elemental compositions is discussed.

Detectors for gas chromatography can be broadly divided into three categories: detectors that are virtually inselective, such as the catharometer and the flame-ionization detector; detectors that are highly selective but restricted in application, such as the electron-capture detector, which responds specifically to nitrogen- and halogen-containing compounds; and detectors that are both specific and widely applicable, because the type of compound to which the detector responds can be chosen at will by the operator. Examples of the last category are the flame photometric detector for S or P and the mass spectrometer set at a specific mass number.

Another example of the third type of detector is the microwave-induced plasma (MIP) operated at 2450 MHz. When the MIP is connected to the outlet of a gas chromatograph and its radiation observed with a monochromator and electro-optical readout system, element-selective detection is possible, as was first demonstrated by McCormack et al. [1]. They used argon as carrier gas, and were able to operate the MIP at atmospheric pressure. Under these conditions the eluted compounds are only partly fragmented in the plasma and the emitted spectrum consists of both atomic and complex molecular spectra. This not only raises the spectral background but also makes the sensitivity for a particular element strongly dependent on the compound involved.

The much higher electronic energy available in the low-pressure helium MIP provides a nearly complete atomization of organic compounds. Using this modification, Bache and Lisk [2] were able to detect selectively the atomic lines of halogens, phosphorus and sulfur. However, reproducible quantitative operation is impaired by the deposition of carbon on the wall of the quartz discharge tube, in which the plasma is contained.

Braun et al. [3] showed that this carbon deposit can be prevented by the addition of 0.5—5% of oxygen to the helium carrier gas. This procedure also allows the determination of carbon and nitrogen through atomic lines in the vacuum u.v. region. McLean et al. [4] reduced the oxygen concentration to 0.1—1% and used spectral lines in the visible and u.v. region for the selective detection of halogens, carbon, nitrogen, hydrogen and deuterium. When oxygen was replaced by nitrogen, oxygen could also be detected selectively. This system is commercially available as the ARL model MPD 850.

The ARL information bulletin reiterates the suggestion of some authors [4—6] that the sensitivity of the low-pressure helium MIP for a particular element is independent of the type of compound introduced, and proportional to the number of atoms of the element in the compound. If this were true, it would be possible to determine the elemental composition of unknown compounds. However, closer inspection of the published data shows that this is observed only within homologous series with exclusion of the lower members. A better perspective seems to be offered by the helium MIP at atmospheric pressure [7], for which a special cavity design has been described by Beenakker [8], but the published data are too limited to permit definite conclusions.

The potential of the MIP as a g.c. detector has been demonstrated in a number of papers that have been reviewed recently [9, 10]. Three properties are of interest here: the limit of detection, the linear dynamic range and the selectivity, defined as the ratio of the response for element-specific detection over the response to an inert compound (e.g. n-hexane for elements other than carbon and hydrogen).

The limits of detection are usually of the order of 0.1 ng of compound per second [4]. In comparison with existing selective g.c. detectors, this is not very impressive. Few data are available on the linear dynamic range. Braun et al. [3] and Beenakker [7] found a range of 4 decades in a helium MIP at reduced and atmospheric pressure, respectively, while Dagnall et al. [11] found 2—3 decades in an argon MIP at atmospheric pressure. The selectivities quoted in the literature vary from a low 100 [12] to about 10 000 [13, 14].

In addition to differences in the choice of analytical lines, an important reason for this variation appears to be the rather widely varying operating conditions used by different authors. The apparent lack of standardized pressure, power, etc., warrants a closer inspection of the MIP. Also, a closer investigation into the linearity and the sensitivity of the detector appears necessary, especially with respect to the influence of the type of compound on the detector response. This is the object of the present investigation.

Optimum conditions will be presented for the detection of ten elements (H, C, N, O, F, Cl, Br, I, S and P) and the performance of the detector under these conditions will be discussed.

EXPERIMENTAL

The equipment used will be discussed with reference to the schematic diagram shown in Fig. 1.

Equipment for plasma generation

Microwave generator (ElectroMedical Supplies, Microtron 200 operated at 2450 MHz, 0—200 W). The improved Mark III model is preferred to the earlier Mark II model, because it is more convenient to operate and less sensitive to line voltage fluctuations.

Cavity. The initially tested 1/4-wave coaxial cavity model 217 L (Electro-Medical Supplies) has the advantage of easy tuning, but several disadvantages. The reflected power remains at least 10% of the incident power and the optimum observation position appears to vary with the element concerned, the gas pressure and the microwave power. The preferred 1/4-wave Evenson-type cavity model 214L performs much better in these respects, although tuning is rather more critical. Reflected powers below 1% are now possible.

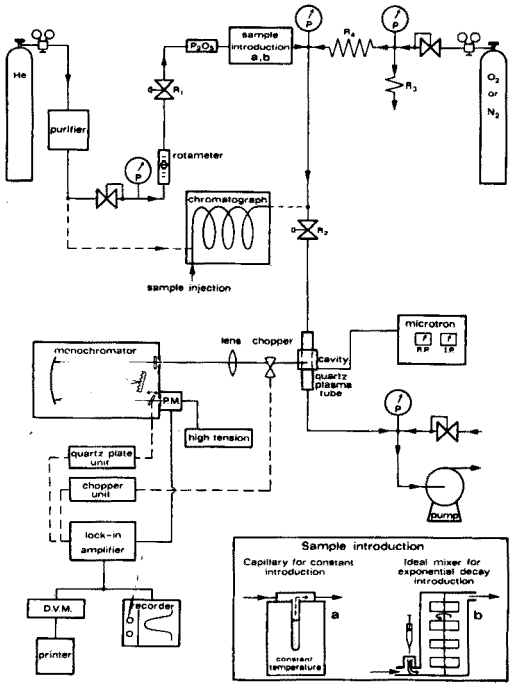

Fig. 1. Schematic diagram of the equipment; explanation in the text.

Also, by removing the end cap, the completely open cavity can be observed from any direction.

Plasma tube. The plasma is generated in an easily exchanged quartz tube of 7-mm outer diameter and 15-cm length [15]. An inner diameter of 2 mm was found to be optimal, because thinner capillaries are subject to strong erosion of the quartz, and wider capillaries are only partly and irreproducibly filled by the MIP. The plasma tube is held vertically, partly enclosed by the cavity which is adjustable in the vertical direction. This ensures that the same portion of the plasma tube is observed throughout all experiments, and avoids corrections for uneven erosion of the quartz tube.

Gases

Standard quality helium (99.995%) contains enough H, C, N, and O to permit optimization of the MIP for these elements without further sample introduction. Obviously, these impurities lead to a background signal when the MIP is used as a g.c. detector. Therefore, efforts were made to reduce the impurity level. Insertion of a "Rare gas purifier 2" (British Oxygen Company) provided only two-fold reduction. Protection of the diaphragm of the pressure regulator with aluminium polyester foil offered no further improvement. Careful cleaning of all lines with various solvents and extensive baking under a helium flow with a flame likewise gave no improvement, but insertion of a tube filled with P_2O_5 close to the plasma [4] reduced the hydrogen signal by a factor of 4. Obviously, extensive purification of the carrier gas is pointless, when the gas chromatograph contributes heavily to the impurity level of C (from the stationary phase), O (from water vapour) and H (from both).

The scavenger gases, oxygen or nitrogen, were used as received, because their helium content remains fairly low (1%, v/v). For the specific detection of oxygen, removal of oxygen from the nitrogen scavenger gas is recommended.

The scavenger gas is added when the pressure of the helium is still slightly above atmospheric pressure (0.03 atm.). The required small flow of scavenger gas is realized by means of a relatively high pressure (0.25—2.5 atm.) and a restriction (R_4 in Fig. 1). A cheap, widely variable restriction is realized with simple electric wire (7-strand silvered copper wire in a PTFE sheath of 1 mm outer diameter). An inlet pressure of 1 atm. supplied to a length of 5 m provides an oxygen flow rate of 5×10^{-9} m^3 s^{-1}. The temperature coefficient of the restriction is 0.3%/K. However, stable operation of the pressure controller requires a much higher flow rate. For this reason an additional leak of about 5×10^{-7} m^3 s^{-1} is included (R_3 in Fig. 1).

Sample introduction

In addition to a gas chromatograph, two other sample introduction systems were used. Constant introduction of a small amount of compound is achieved with a diffusion capillary (length 10 cm, i.d. 1 mm) half filled with a volatile liquid and mounted in a T-joint to the carrier gas line. The solute flow rate is

varied through the temperature of the capillary in relation to the volatility of the compound. The solute flow rate need not be known for the optimization study as long as it remains constant.

Both the sensitivity of the detector and its linear dynamic range can be determined by means of an exponential diluter [16]. The home-made equipment is made from glass and Teflon; it has a volume of 245 ml and a heated injection port for the introduction of solutes. The helium flow is regulated at constant pressure and measured with a calibrated rotameter. The pressure inside the flask is slightly above atmospheric (0.03 atm.). Solutes used were either gases (e.g. H_2S, CO_2, H_2) or low-boiling liquids of the highest purity available (see Table 1).

Vacuum system. A small mechanical vacuum pump, a vacuum pressure regulator and a barometrically compensated vacuum gauge provide and measure pressures down to 15 torr at flows of 5×10^{-6} m^3 s^{-1}.

Optics and read-out

A 1:1 image of the plasma is focused onto the entrance slit of a 0.5-m Ebert monochromator equipped with a grating with 1180 lines/mm and blazed at 750 nm. This blaze is optimal for the oxygen and nitrogen lines but less suitable for the ultraviolet carbon line used (Table 1). Even so, the detection limits for oxygen and nitrogen are 20 times poorer than for carbon.

Wavelength modulation is employed to discriminate against continuum background radiation [17, 18]. A 2-mm thick vibrating quartz plate with a peak-to-peak amplitude of 36° shifts the spectrum of 0.4 mm in the focal plane.

Theoretically this permits the use of 200-μm exit and entrance slits. In practice, slits of 100 μm stopped to a height of 2 mm were used.

A red-sensitive photomultiplier was used (Hamamatsu R 446) at a high tension between 300 and 900 V. The fundamental frequency of the vibrating quartz plate (117 Hz) is picked up with a lock-in amplifier tuned to 234 Hz and set in the f/2 mode for the reference channel. Background signal levels were measured with a d.c. current amplifier. Signals are displayed on a two-pen strip-chart recorder. One pen measures the ordinary signal, whereas the other pen measures the noise on the signal through a hi-pass filter at 100-fold higher sensitivity.

Microwave radiation. Stray radiation outside the cavity was measured with a Narda Electromagnetic Leakage detector model 8210 calibrated at 2450 MHz.

OPTIMIZATION STUDIES

Noise characteristics

Before any optimization study is contemplated, it is important to determine the noise characteristics of the system. If the dominant source of noise is source flicker noise, proportional to the net line signal, then optimization should be directed at lowering the background radiation level, because the net

signal-to-noise ratio is independent of the signal level. However, if shot noise, which is proportional to the square root of the signal, predominates, then the signal-to-noise ratio increases with the signal level and optimization should be directed at increasing the net signal.

For the MIP, noise measurements were made, with d.c. amplification, for various helium and solute element lines at different intensities. Noise was also measured for a quartz iodine lamp and a barium hollow-cathode lamp. The results presented in Fig. 2 show clearly that shot noise is the dominant source of noise in all cases. This agrees with the results of Talmi et al. [19]. The manufacturer's data for the current amplification of the photomultiplier used made it possible to convert the signals to the number of electrons emitted by the photocathode per second. Multiplication by an appropriate time span then yielded the absolute number of electrons emitted during the observation period. The square root of this number should provide the shot noise, which can be transformed into signal noise by a reverse argument. The experimental data points in Fig. 2 were measured with a 10—90% rise time of 1 s for the d.c. amplifier. The solid line was calculated (as indicated above) for a discrete time span of 1 s. The slight discrepancy between the experimental points and the theoretical line is easily attributed to a possible difference between amplifier rise time and true integration time and to the inaccuracy of the assumed current amplification of the PM tube. It is clear, however, that up to the highest intensities recorded with the MIP, shot noise from the photomultiplier is still the main source of noise.

This also means that the signal-to-noise ratio of the gross intensity (line plus background) increases with the square root of the gross intensity. This is also true for the net line intensity, if the background varies in direct proportion with the line intensity. If the background is independent of line intensity, the signal-to-noise ratio increases even faster than the square root of the gross intensity. It is only when the background increases faster than the square of the intensity, that the signal-to-noise ratio deteriorates with higher intensities. For the MIP this was never observed, and the important conclusion can be drawn that optimization of the MIP should be directed at increasing the signal levels as far as possible without impairing the stability of the signal. This will improve the sensitivity and the detection limits.

The observation zone

The MIP can be viewed in two different ways. Most authors use lateral observation through the quartz tube but a few prefer axial observation along the plasma [3, 20]; in the latter arrangement the plasma tube coincides with the optical axis and the radiation is observed through a quartz window that caps the tube a few centimeters away from the cavity. This offers the advantage that there is no deposition on, or erosion of, the observation window, but has the disadvantage that the radiation must pass through the unexcited regions next to the discharge.

When the same conditions were used here for both observation systems,

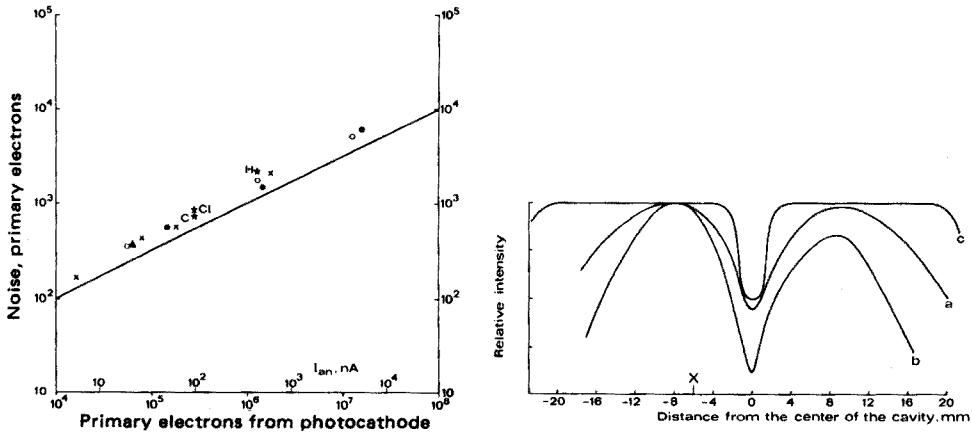

Fig. 2. The experimentally measured RMS-noise is plotted versus the emission intensity for several lines emitted by the microwave plasma. Data for H, C, Cl are starred; the symbols (•) indicate helium emission lines. For comparative purposes, additional data points refer to a quartz iodine continuum source (○) and a Ba hollow-cathode lamp (×) at various intensities. The background plasma signal is indicated by (▲). The intensities are expressed as the anode current of the photomultiplier and converted to the number of primary electrons emitted by the photocathode. The solid line designates the square root of this number and demonstrates that the observed noise is predominantly shot noise.

Fig. 3. Spectral line intensities as a function of the axial position in the microwave plasma. (a) Atom lines, e.g. C, H, N, P. F. (b) Ion lines, e.g. Cl, Br, I, S. (c) Oxygen atom line. Point × marks the position of the coupling stub.

a tenfold reduction in linear dynamic range and a twofold increase in detection limits were found for axial observations in comparison with lateral observation. For this reason further experiments with the axial arrangement were discontinued.

If the plasma tube is parallel to the entrance slit of the monochromator, then the height of observation becomes of interest. The data in Fig. 3 show that a more or less defined maximum intensity is observed between 8 and 10 mm at either side of the center of the cavity. A similar optimum position has been reported by Houpt [21]; it is independent of pressure and microwave power. Because the upstream optimum position of observation may become clouded by deposited carbon, the downstream optimum position is preferred. The direction of the flow is chosen so that the coupling stub of the 214L cavity is close to this optimum. Figure 3 also shows that observation windows between 2 and 4 mm are suitable for all elements. At very high flow rates (4×10^{-6} m^3 s^{-1}), the entire pattern may be shifted downstream by 1 mm.

Gas flow rates

The influence of the carrier gas flow rate on the detector signal is shown for carbon as a typical example in Fig. 4. A constant concentration of the

solute (in ng cm^{-3}) was realized by measuring the carbon impurity in the helium carrier gas; the signal was then largely independent of the carrier gas flow. The more usual chromatographic situation of a constant introduction rate of the solute (in ng s^{-1}) was imitated by means of the diffusion capillary filled with diethyl ether. The signal then showed the inverse relation with flow rate, which is indicative of a concentration-dependent detector. This behaviour is expected, because the emission intensity of the plasma is proportional to the volume concentration of the excited element. Nevertheless, the combination of a destructive but also concentration-dependent detector is a little unusual in gas chromatography.

In view of Fig. 4, it is obviously advantageous to keep the carrier gas flow rate as small as possible. In practice, the minimum flow rate will be dictated by the chromatographic separation. In this respect not only the peak broadening inside the g.c. column is important, but also the extra-column broadening caused by the dead volume of the plasma detector (about 0.3 cm^3).

When the MIP is operated on pure helium carrier, most organic solutes tend to produce carbon deposits on the quartz tube. This can be prevented by the addition of oxygen [3, 4] or nitrogen [4], which keep the carbon volatile through the formation of CO or CN radicals. Two problems arise here: first, the minimum level of scavenger gas required, and secondly the possible influence of the scavenger gas on the response for other elements. The latter question is of interest, because the concentrations proposed in the literature vary between 0.1 and 5% (v/v) [3, 4], whereas Brassem et al. [22] have shown that for a low-pressure MIP the excitation conditions change abruptly at foreign gas concentrations exceeding 1% (v/v).

Therefore, the spectral background and the element-specific response were studied as a function of the concentration of the scavenger gas. The analytes were introduced by the diffusion capillary technique, with liquids such as CH_2Cl_2, CH_2Br_2, C_3H_7I, CS_2, etc. The responses for nitrogen and oxygen could be analysed through the natural impurities of these elements in the helium used.

The results for oxygen are presented in Fig. 5. Up to 0.5% (v/v) of oxygen, the continuum background of the spectrum remained essentially equal to the level observed in the pure helium spectrum, and interfering oxygen lines or bands were not observed for any of the spectral lines in Table 1. The only exception is an extremely weak band close to the carbon line at 248 nm, which will not introduce a significant error in any practical analysis. Hence, only the influence on the line intensities needs to be studied. Figure 5 shows that the sensitivity for hydrogen and nitrogen is virtually unaffected by the added oxygen, whereas the sensitivity for sulfur and the halogens decreases steadily with increasing concentration of oxygen. Consequently, the concentration of oxygen should not be higher than the minimum required to prevent carbon deposit. This level naturally depends on the amount of carbon supplied to the plasma and the oxygen content of the compound. As a rule of thumb, the concentration of oxygen must be a few times the

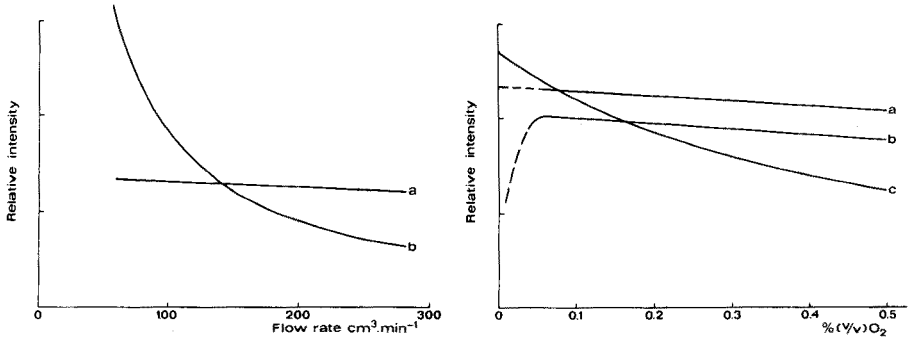

Fig. 4. Net intensity of the C 248-nm line versus carrier gas flow rate. Curve (a) is for a constant concentration (ng cm^{-3}) of carbon in helium. Curve (b) is for a constant rate of introduction (ng s^{-1}).

Fig. 5. The influence of the oxygen scavenger gas concentration on net line intensities. (a) H, N. (b) C. (c) S, halogens.

concentration of carbon in the plasma. Because the upper limit of the linear dynamic range lies at about 0.1% (v/v) C (see below) this means that an oxygen level of 0.25% (v/v) is sufficient to prevent carbon deposit for all solutes separated by the gas chromatograph.

However, this amount is inadequate when a solvent is used in the g.c. analysis, because the solvent peak may easily give rise to a temporary carbon concentration of 10% (v/v). Because a substantial increase in the oxygen concentration would lead to an unacceptable reduction of the detection sensitivity for many elements, two other possibilities are offered to avoid carbon deposits from solvent peaks.

One solution [23] is to extinguish the plasma momentarily and reignite it after the solvent peak has passed through the discharge tube. However, the consequent cooling and rewarming of the plasma tube disturbs the stability of the detector response. Indeed, cooling the tube leads to a momentary increase in the concentration and hence an initial increase of the signals following the solvent peak. After warm-up of a few minutes the signals level off to their usual value.

Consequently, it is better to keep the discharge going continuously. Carbon deposits from solvent peaks can then be prevented by introducing a bypass behind the column outlet, which can be automatically triggered by an inselective and non-destructive, low-sensitivity detector such as a catharometer.

Use of oxygen as a scavenger gas is clearly impossible if the specific detection of oxygen is desired. In that case, nitrogen must be considered; a concentration of 0.4% in helium was found to be sufficient to prevent carbon deposit from all eluted solutes except the solvent. It was also observed that the influence of nitrogen on the net line intensities is quite similar to that of oxygen. Unfortunately, however, the introduction of nitrogen gives rise to strong molecular bands throughout the spectrum. This not only

severely enhances the continuum background, but also produces serious spectral interferences for all selected element lines (Table 1) except carbon, oxygen and phosphorus. In general, therefore, the use of nitrogen as a scavenger gas can be recommended only for the specific detection of oxygen (and phosphorus, see below).

Microwave power and gas pressure

The influence of the microwave power and the gas pressure were found to be interdependent. Over the pressure range of interest (10—100 torr) most line intensities increase steadily with increasing microwave power supplied to the MIP (Fig. 6). This suggests the use of the highest power available, i.e. 200 W, but the quartz tube then becomes very hot and starts to erode. The exact power at which the erosion becomes unacceptable depends on the geometry of the plasma tube. For a particular arrangement, the erosion is readily apparent from the intensity of the silicon line monitored at 215.6 nm without added scavenger gas (Fig. 6). The addition of 0.1% (v/v) oxygen effectively suppresses the silicon signal (probably through formation of silicon oxides), but it does not prevent erosion of the quartz tube. With the presently employed tube (2-mm i.d.), strong erosion can be avoided and forced air cooling is unnecessary as long as the applied microwave power remains below 100 W.

For the 1/4-wave Evenson cavity used here, most authors recommend pressures for MIP in helium between 0.25 and 10 torr. At these reduced pressures, the plasma appears brighter and is easier to ignite and operate than at higher pressures, where the stability may present problems [3, 24]. However, a higher pressure would provide a greater density of emitting species which would be beneficial for the analyte line intensities. Recently, Houpt [21] extended the pressure range to 60 torr without adverse influence on the plasma stability. With the present equipment, the MIP could be sustained at all pressures up to and including atmospheric pressures by careful tuning. However, at pressures over 200 torr the discharge behaved erratically and the intensities became irreproducible. In going from 10 to 200 torr, the visual brightness of the discharge decreases because the higher pressure promotes radiationless de-excitation of excited helium levels, but the analyte line intensities are significantly enhanced.

The results presented in Fig. 7 show that the line intensities for carbon and oxygen increase with the gas pressure, whereas for all other elements the influence of the pressure is rather small. In practice, therefore, neither the microwave power nor the gas pressure is a critical parameter, although obviously both variables must be kept constant to achieve good reproducibility. A pressure of 90 torr and a microwave power of 75 W are recommended here.

The selective detection of fluorine, silicon and phosphorus

It is well known that fluorine released from fluorine-containing organic compounds attacks the quartz tube used in an MIP [4]. Even small quan-

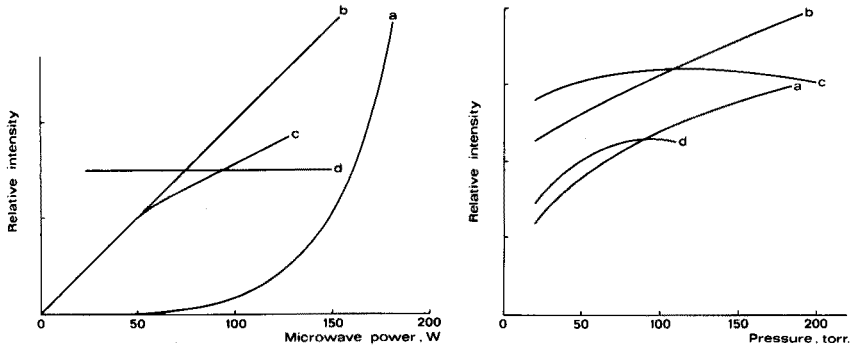

Fig. 6. The influence of microwave power on net line intensities. Curve (a) (Si 252 nm) was measured without scavenger gas and is due to erosion of the quartz tube. Curves (b), (c), and (d) were measured with 0.2% oxygen in helium: (b) Br, I, S; (c) Cl, C, H, N; (d) O.

Fig. 7. The influence of pressure on net line intensities. (a) C. (b) O. (c) H, N. (d) Cl, I, Br, S.

tities of such compounds produce a strong silicon signal from volatile SiF_4. Although a fluorine signal is also observed, reliable and reproducible results cannot be obtained in this way. For example, detuning the cavity and thus increasing the reflected power doubles the fluorine signal. Consequently, quartz tubes cannot be used for the detection of fluorine.

Much better results are obtained with an MIP sustained in a translucent alumina tube (1.5 mm i.d., 6.25 mm o.d.). Because alumina has a much higher dielectric loss factor, the microwave power must be increased to 150 W at a pressure of 60 torr. Air cooling is required to counteract the heat losses in the alumina tube. Optimum observation height and oxygen concentration are the same as discussed before for the other elements. Nitrogen cannot be used as a scavenger gas because of strong spectral interference.

Because silylated derivatives are frequently utilized in g.c. separation of involatile compounds, the specific detection of silicon is also of interest. In the usual arrangement, this is not possible for several reasons. In the absence of a scavenger gas, carbon is deposited and sensitivity is low. Addition of oxygen improves the carbon signal but suppresses the silicon signal almost completely. Replacement of oxygen by nitrogen improves both the carbon and the silicon signals appreciably, possibly through preventing the formation of silicon carbides in the discharge. Even so, such high microwave powers are required that most of the silicon signal is due to erosion of the quartz tubes. Preliminary experiments with alumina tubes demonstrated that unacceptably high microwave powers are required to overcome the heat loss to the alumina tube and still provide sufficient intensity for the silicon line. Possibly, the cavity recently developed by Beenakker [8] would give better results. Eventually, it was concluded that silicon could not be determined in the low-pressure MIP. Also, for the determination of carbon in silylated

compounds, nitrogen must be preferred to oxygen as the scavenger gas, because it provides a more complete atomization of carbon.

Another element for which nitrogen offers a slight advantage over oxygen is phosphorus. When oxygen was used as a scavenger gas for the optimization of the phosphorus signal at 253.6 nm, with dimethylmethyl phosphonate (b.p. 186°C) in the diffusion capillary, displacement of the cavity along the stationary plasma tube produced a transient peak or dip of the phosphorus signal before it attained a stable value. Also on injection of a phosphorus-containing compound into the gas chromatograph, a small but significant and reproducible time lag was observed between the carbon signal and the phosphorus signal for the same compound. Closer investigation showed that both effects are due to a temporary reaction of phosphorus oxides with the hot quartz wall of the tube [25]. McCormack et al. [1] have described the presence of white deposits on the quartz in the presence of large amounts of sulfur and phosphorus. When nitrogen is used as a scavenger gas no such effects are noted and the sensitivity of the detector response is increased twofold. Fortunately, nitrogen does not produce an interfering spectral background in the vicinity of the phosphorus line.

Microwave stray field

Absorption of microwave radiation by body tissues can be hazardous, especially for those parts where the heat cannot be carried away, such as the eye. Safety regulations in the U.S.A. and in most European countries are concerned with microwave radiance up to 10 mW cm^{-2}, whereas the U.S.S.R. maintains a much stricter upper limit of 0.01 mW cm^{-2} for continuous exposure and 1 mW cm^{-2} for short periods. Previous publications have considered the influence of cavity design and shielding [26] and of carrier gas and pressure [27] on the microwave stray field, but they do not refer to a typical laboratory environment. Stray radiation levels around the MIP set at the optimum conditions discussed earlier were therefore measured.

Clearly, the distribution of the microwave stray field in a normal laboratory will be very inhomogeneous because of reflection and absorption by surrounding pieces of equipment. Consequently the following data provide only a rough picture; all data refer to a distance of about 25 cm from the cavity. It appears that the microwave stray field increases by an order of magnitude when the carrier gas pressure is reduced from 150 to 10 torr or when the applied microwave power is raised from 50 to 175 W. For a completely open cavity, a maximum radiance of 2 mW cm^{-2} is measured at the selected optimum conditions of 90 torr and 75 W. This is clearly not acceptable for prolonged exposure, hence some sort of shielding is required.

If, as recommended by the manufacturer, the end cap is fitted onto the cavity, the stray field is reduced by an order of magnitude except in the direction of the coupling stub where the level remains at 1 mW cm^{-2}. However, with the end cap fitted, the selected optimum observation position for the MIP is obscured, so that this procedure cannot be used. Fortunately, the stray

level can be similarly reduced by a simple aluminum shielding box around the cavity. When holes are provided for optical observation and for the coupling and tuning stubs, the stray radiance is again reduced to about 0.1 mW cm^{-2} except in the direction of the protruding stubs. Obviously, completely safe shielding requires that the aluminum box encloses the coupling and tuning stubs. Provisions should be made to manipulate these stubs from outside the shielding box. The microwave stray level is then brought down to an acceptable value of 0.1 mW cm^{-2} in all directions.

ANALYTICAL PROPERTIES

Data collection

Under the optimum conditions described above, the following analytical properties were determined: the sensitivity, the linear dynamic range and the lower limit of detection. All three quantities can be determined simultaneously by using an exponential dilution flask [28, 29]. For these measurements the monochromator was adjusted to the emission line of the element considered and wavelength modulation was used to correct for the continuum background under the line.

If at time $t = 0$ a certain amount of a compound is introduced into the dilution flask, the detector signal at any time $t > 0$ is given by

$$x(t) = Sc(t) = S\frac{\rho An}{MV}\exp\left[\frac{-t\phi}{V}\right] + x_b \qquad (1)$$

where $x(t)$ is the detector signal in V, S is the sensitivity in V m^3 mol^{-1}, $c(t)$ is concentration at time t in mol m^{-3}, ρ is the density of the compound in kg m^{-3}, A is the volume of liquid compound introduced into the diluter in m^3, n is the number of atoms of the relevant element present in the compound, M is the molecular weight of the compound in kg mol^{-1}, V is the volume of the dilution flask in m^3, ϕ is the flow rate (m^3 s^{-1}) of the carrier gas at 293 K and atmospheric pressure, and x_b is the blank signal in V.

This expression is valid under the conditions of linear response, rapid mixing and negligible contribution of the connecting tubes in comparison to the volume of the dilution flask. The latter two conditions are easily fulfilled in the present equipment and the first condition can be verified from the experimental decay curve. The decaying intensity described by eqn. (1) is displayed on a strip chart recorder and also fed into a printer which prints the signal at constant time intervals so that about seven data points are printed for each decade. After correction for the blank value (Fig. 8a) the logarithm of the net intensity is plotted versus time.

From the example presented in Fig. 8b for carbon, the extraction of the relevant data can be easily perceived. The slope of the linear portion of the curve is calculated and compared with the expected slope V/ϕ. When there is no significant difference, the detector response over this intensity range is considered to be linear. Extrapolation of this linear portion to time

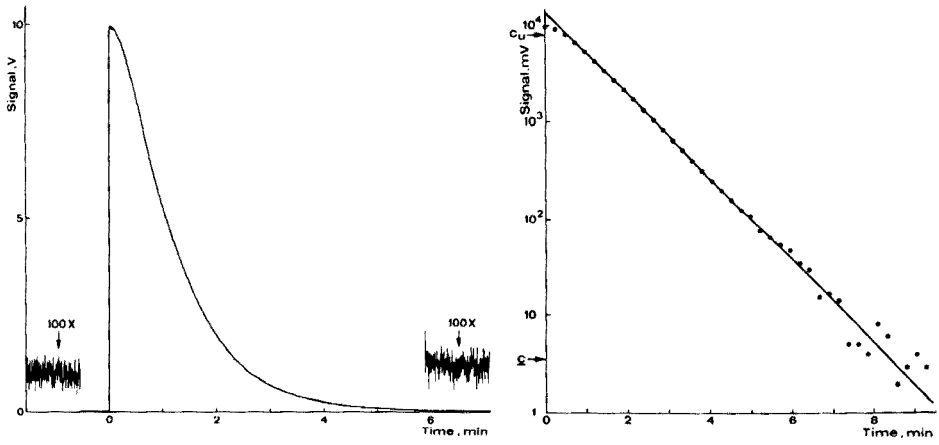

Fig. 8. The experimental measurement of sensitivity, linear dynamic range and lower limit of detection with an exponential diluter. (a) Shows an example of the signal measured for the C 248 nm line after injection of an amount of carbon slightly above the upper limit of linearity; the noise in the background before and after analytical signal was measured at 100-fold sensitivity. (b) Shows the same signal converted to a semilogarithmic scale; c_u is the upper limit of linearity, $\underline{c}$ is the lower limit of detection calculated from the background noise shown in (a); the dynamic range is log $c_u/\underline{c}$ = 3.2 decades.

$t = 0$ then yields the sensitivity S from eqn. (1). Secondly, the first few data points deviate clearly from the linear curve and the final data point for which this is observed signifies the upper limit of the linear dynamic range. Finally, the noise in the blank signal (Fig. 8a) together with the calculated sensitivity yields the lower limit of detection as $\underline{c} = 2s_x/S$, where s_x is the standard deviation of the blank signal, which is roughly equal to one fourth of the peak-to-peak noise. Obviously, the logarithm of the ratio of the upper limit of linear response and the lower limit of detection is equal to the dynamic range in decades.

The results of the measurements are collected in Table 1. The relative sensitivity is preferred to the absolute sensitivity, to emphasize the differences observed for one element between different compounds. Obviously, the absolute sensitivity varies from one element to the next, because of differences in photomultiplier response and excitation energies for the transitions considered. The upper limit of linear response and the lower limit of detection are expressed as atomic density (mol m^{-3}) in the discharge gas for 293 K and 90 torr because this is the decisive quantity for the detector. Insofar as the excitation conditions in the MIP remain unaffected, the data are independent of the carrier gas flow rate (compare Figs. 4 and 7). They can easily be converted to the chromatographically more meaningful units of ng s^{-1} at atmospheric pressure through multiplication by $M_A \phi p_0/p$, where M_A is the atomic weight of the element, ϕ is the flow rate of the carrier gas, and p_0 and p are atmospheric pressure and the pressure used in the MIP. This conversion

TABLE 1

Analytical properties of the microwave-induced plasma

Element + analysis line (nm)	Compound	Relative sensitivity	c_{upper} (mmol m^{-3})[a]	Detection limit		Dynamic range (decades)
				(μmol m^{-3})[a]	(ng s^{-1})[b]	
Br 470.47	Bromobenzene	1.00	0.32	0.26	0.69	3.1
	1-Bromopentane	1.05	0.18	0.26	0.69	2.8
	Dibromomethane	1.26	0.47	0.17	0.43	3.5
C 247.86	Benzene	1.44	6.8	0.98	0.40	3.8
	Carbon disulfide	1.22	1.2	0.92	0.37	3.1
	Ethyl acetate	1.42	4.8	0.69	0.28	3.8
	Hexane	1.52	3.5	0.75	0.30	3.7
	Nitromethane	1.00	3.7	1.13	0.46	3.5
	2-Propanone	1.24	6.4	0.92	0.37	3.8
	Tetrachloromethane	1.23	1.7	0.92	0.37	3.3
	Toluene	1.32	7.4	1.07	0.43	3.8
Cl 479.45	Chlorobenzene	1.00	0.22	0.51	0.61	2.6
	Tetrachloroethane	1.08	1.4	0.59	0.71	3.4
	Tetrachloromethane	1.24	1.2	0.52	0.62	3.4
F 685.60	Trifluorotoluene	1.00	0.28	0.17	0.11	3.2
H 486.13[c]	Benzene	1.15	4.4	2.55	0.09	3.2
	1,4-Dimethylbenzene	1.00	5.0	2.94	0.10	3.2
	Hexane	1.60	5.3	1.87	0.06	3.5
	Hydrogen	1.03	11.0	2.61	0.09	3.6
I 516.12	1-Iodopropane	1.00	0.44	0.13	0.56	3.5
	2-Iodopropane	1.11	0.33	0.11	0.46	3.5
N 746.88	Methyl cyanide	1.00	1.9	11.3	5.3	2.2
	Nitrogen	1.15	27.0	8.88	4.2	3.5
	Nitromethane	1.00	2.4	11.3	5.3	2.3
O 777.19	Carbon dioxide	1.01	3.4	8.59	4.6	2.6
	Methanol	1.00	2.5	22.2	12.0	2.0
	Nitromethane	1.31	2.8	8.48	3.0	2.7
	2-Propanone	1.71	2.1	5.03	2.7	2.6
S 545.39	Carbon disulfide	1.84	0.50	0.71	0.77	2.8
	Hydrogen sulfide	1.03	1.1	1.28	1.4	2.9
	Sulfur dioxide	1.00	1.1	1.34	1.4	2.9

[a] Calculated for 293 K and 90 torr. [b] Calculated from preceding column for helium carrier flow rate of 4 $cm^3 s^{-1}$; at normal g.c. flow rates (0.4 $cm^3 s^{-1}$) all values will be ten times lower. [c] Data for hydrogen are uncertain, owing to the non-linear response observed.

is shown in the last column of the Table for an MIP pressure of 90 torr and a flow rate of 4×10^{-6} $m^3 s^{-1}$. Under normal chromatographic conditions the flow rate is an order of magnitude less. In that case, both the upper limit of linear response and the lower limit of detection will be reduced by a factor of ten, when expressed in ng s^{-1}; their ratio remains equal to the dynamic range of the MIP which is also given in the Table.

Dynamic range and upper limit of linearity

The data in Table 1 show several interesting features of the MIP detector. For most elements the dynamic range is 3 decades or more. This may not be particularly impressive in comparison with some non-specific g.c. detectors, but it is certainly better than the range offered by other specific g.c. detectors. In fact, this is the usual dynamic range for atomic spectrometric methods of analysis. In itself this is surprising, because the usual upper limiting factor for linearity in atomic emission spectrometry — self-absorption — can hardly be operative for the non-resonance transitions measured in the MIP. Nor can saturation of the photomultiplier be the reason for the deviation from linearity, because the upper limit of linear response is not improved by reducing the radiative intensity through filters or masking.

Tentatively, the following explanation may be offered. Brassem et al. [22] have found that in a MIP at 1 torr, the excitation conditions deteriorate significantly when the foreign gas density exceeds 1% of the carrier gas density. A rough calculation shows that at the upper limit of linearity this same proportion is approached in the present MIP. For example, in the case of benzene, a density of 0.007 mol m^{-3} for carbon atoms corresponds to a partial carbon pressure of 1.0 torr, which is 0.15% of the total pressure of 90 torr. To this must be added an equal amount of hydrogen atoms (0.15%) and the oxygen atoms from the scavenger gas (0.4%), bringing the total concentration of foreign atoms to 0.7% of the helium carrier atoms.

If the departure from linearity is in fact due to changed excitation conditions as suggested above, the upper limit of linearity should depend on the composition of the compound introduced into the MIP. Indeed, for tetrachloromethane, the upper limit for carbon is lower than for benzene, hexane or 2-propanone. For other elements, the observations are similar. The high upper limit for pure nitrogen can be related to the absence of additional foreign atoms, that reduce the upper limit for nitrogen in methyl cyanide and nitromethane. The low upper limits generally found for chlorine, bromine and iodine can also be related to the comparatively large amounts of other atoms in the compounds.

Obviously, this explanation does not cover all the observed variations. The low values for the upper limit of linearity for sulfur and carbon in carbon disulfide, remain unexplained. Consequently, the explanation is only semi-quantitative at present. If true, however, the upper limit of linearity (when expressed in mol m^{-3}) should increase with the total pressure in the MIP, provided that the excitation conditions remain unaffected with increasing pressure.

Lower limit of detection

Whereas the upper limit of linear response varies significantly with the compound studied, the lower limit of detection is largely independent of the type of compound. This is to be expected, because the limit of detection is determined primarily by fluctuations in the blank value and because the sensitivity does not vary much with the type of compound.

Naturally, the limit of detection varies significantly with the element considered. In agreement with other authors, higher values were found for oxygen and nitrogen (10^{-5} mol m^{-3}) than for carbon, hydrogen, sulfur and the halogens (10^{-6} mol m^{-3}). These values correspond to the range 0.1—5 ng s^{-1} for the rather high flow rate used here. As stated above, a further reduction by a factor of ten seems possible at normal carrier gas flow rates of 4×10^{-7} m^3 s^{-1} (24 ml min^{-1}). Even then, the values are not as good as those reported for other specific g.c. detectors. The electron-capture detector (for Cl and N), the flame photometer detector (for S) and the thermionic detector (for P) all reach limits of detection of about 1 pg s^{-1}.

A further reduction of the limits of detection in the MIP could be realized in two ways. First, the limits of detection are determined by shot noise and could benefit from improved optics and a more sensitive photomultiplier tube. In a second approach, the proportion of a compound in the helium carrier gas might be increased by introducing a separator as is done in g.c.—m.s. connections. This would leave the detection limits expressed in mol m^{-3} unaffected, but by increasing its partial pressure in the MIP, the limits of detection would be improved in terms of ng s^{-1}.

It is doubtful, however, whether this is a sensible approach, because the upper limit of linearity would also be reduced (in terms of ng s^{-1}). In conclusion, it seems that the selected pressure of 90 torr represents a good compromise between useful upper limits and lower limits of detection. The strong potential of the MIP as a g.c. detector lies in its versatility for selecting particular elements combined with acceptable values for the lower limit of detection and the dynamic range.

Sensitivity variations

The sensitivity of the detector does not vary much with the type of compound analyzed. For quantitative analysis, this should offer the interesting possibility of calibrating the instrument with a reference compound different from the analyte. If an internal standard is used, equality of response per atom might be assumed. However, closer inspection of the sensitivity data in Table 1 reveals that this is true only to a first approximation. For carbon, the inherent uncertainty will be within 25%, but for other elements errors up to 200% might be observed. Many examples can be visualized where such errors would still be acceptable. However, even for carbon the variation of the sensitivity between different compounds is much too large for the elemental composition of an unknown compound to be derived from a few simple calibration standards. This conclusion disagrees with the suggestions of McLean et al. [4] and Beenakker [7] based on less data.

The response for hydrogen warrants further discussion. For all other elements, the slope of the semilogarithmic decay curve agrees within 5% with the theoretically expected value of V/ϕ (eqn. 1). For hydrogen, however, the slope of the linear portion of the semi-logarithmic curve is 30% higher than

for the corresponding carbon signal of the same compound. Consequently, when plotted on a linear scale the signal from the MIP detector is far from linear but proportional to $[H]^{1.3}$. Consequently, on a linear scale the analytical curve for hydrogen is concave. Also, at high concentrations the signal falls below the extrapolated straight line, whereas at low concentrations it runs above this line.

Several possible causes for this effect were investigated. Incomplete dissociation of hydrogen molecules does not offer an explanation, because this would produce a convex analytical curve. Nor can traces of water released from the quartz tube be responsible. Extensive degassing of the connecting lines and the discharge tube brought no improvement. Moreover, such traces of water would have a more pronounced influence at lower hydrogen concentration and again cause a convex analytical curve. Reaction of hydrogen with the scavenger gas, oxygen, is ruled out as a possible explanation, because a similar non-linear response was observed for pure hydrogen gas in helium.

Another possibility is adsorption of hydrogen molecules on the quartz wall. If this takes place at the initially high concentration levels and desorption occurs at the lower concentrations, this would account for the S-shaped decay curve. Adsorption was demonstrated as follows. A large excess of hydrogen was introduced into the MIP: when the signal had reached its maximum, the discharge was turned off and the plasma tube rapidly cooled while helium was passed for several minutes; when the MIP was reignited a clear and rapidly decaying hydrogen signal was observed. However, adsorption cannot account for the slope observed for hydrogen. Possibly, ionization of hydrogen is responsible, for this would give rise to a concave analytical curve. But it is not then clear why ionization occurs only for hydrogen and not for sulfur and carbon with similar ionization energies.

CONCLUSION

The microwave-induced plasma operated at reduced pressure in helium is a very promising device for the specific detection of non-metallic elements in gas chromatography. For the detection of H, C, N, Cl, Br, I and S, a single set of optimum operating conditions can be formulated, i.e. observation height, 8—9 mm downstream from the center of the discharge; carrier gas flow rate 30 ml min^{-1} or less; oxygen concentration in the carrier gas, 0.25% (v/v); pressure, 90 torr; microwave power 75 W.

When nitrogen is used as the scavenger gas (0.4% v/v), the specific detection of oxygen and carbon is possible and that of phosphorus improved. When the quartz tube is replaced by translucent alumina, the detection of fluorine is possible at increased power (150 W).

Except for hydrogen the detector shows a linear response for all elements over about three decades. Under normal g.c. conditions, the lower limits of detection vary from 0.01 ng s^{-1} for hydrogen to 0.05 ng s^{-1} for halogens, sulfur and carbon. Higher spectral background levels for oxygen and nitrogen raise the detection limits for these elements to 0.4 ng s^{-1}.

The authors gratefully acknowledge the mediation of Mr. P. M. Houpt from TNO-Delft in purchasing a quartz oscillator, and of Dr. C. I. M. Beenakker from Philips Research Laboratories, Eindhoven in supplying the translucent alumina tube.

REFERENCES

1 A. J. McCormack, S. C. Tong and W. D. Cooke, Anal. Chem., 37 (1965) 1470.
2 C. A. Bache and D. J. Lisk, Anal. Chem., 39 (1967) 786.
3 W. Braun, N. C. Peterson, A. M. Bass and M. J. Kurylo, J. Chromatogr., 55 (1971) 237;
4 W. R. McLean, D. L. Stanton and G. E. Penketh, Analyst, 98 (1973) 432.
5 B. J. Lowings, Analusis, 1 (1972) 510.
6 K. Durrant and R. H. Tyas, CSI XVII (Florence) Acta Vol. III (1973) 165.
7 C. I. M. Beenakker, Spectrochim. Acta, Part B, 32 (1977) 173.
8 C. I. M. Beenakker, Spectrochim. Acta, Part B, 31 (1976) 483.
9 S. Greenfield, H. McD. McGeachin and P. B. Smith, Talanta, 22 (1975) 553.
10 R. K. Skogerboe and G. N. Coleman, Anal. Chem., 48 (1976) 611A.
11 R. M. Dagnall, T. S. West and P. Whitehead, Anal. Chim. Acta, 60 (1972) 25.
12 C. A. Bache and D. J. Lisk, J. Ass. Offic. Anal. Chem., 50 (1967) 1246.
13 C. A. Bache and D. J. Lisk, Anal. Chem., 43 (1971) 950.
14 R. M. Dagnall, T. S. West and P. Whitehead, Anal. Chem., 44 (1972) 2074.
15 P. M. Houpt and H. Compaan, Analusis, 1 (1972) 27.
16 J. E. Lovelock, Anal. Chem., 33 (1962) 162.
17 W. Snelleman, T. C. Rains, K. W. Yee, H. D. Cook and O. Menis, Anal. Chem., 42 (1970) 394.
18 R. W. Spillman and H. V. Malmstadt, Anal. Chem., 48 (1976) 303.
19 Y. Talmi, R. Crosmun and N. M. Larson, Anal. Chem., 48 (1976) 326.
20 L. R. Layman and G. M. Hieftje, Anal. Chem., 47 (1975) 194.
21 P. M. Houpt, Anal. Chim. Acta, 86 (1976) 129.
22 P. Brassem, F. J. M. J. Maessen and L. de Galan, Spectrochim. Acta Part B, 31 (1977) 537.
23 C. A. Bache and D. J. Lisk, Anal. Chem., 37 (1965) 1477.
24 C. A. Bache and D. J. Lisk, Anal. Chem., 38 (1966) 1757.
25 J. Binkowski, S. Giziński, R. Kamiński and W. Reimschüssel, Mikrochim. Acta, (1976) I, 623.
26 J. L. Stanley, H. W. Bentley and M. B. Denton, Appl. Spectrosc., 27 (1973) 265.
27 J. J. De Corpo, J. T. Larkins, H. V. McDowell and J. R. Wyatt, Appl. Spectrosc., 29 (1975) 85.
28 J. Ševčik, Detectors in Gas Chromatography, J. Chromatogr., library, vol. 4, Elsevier, Amsterdam 1976.
29 D. Jentzsch and E. Otte, Detektoren in der Gas-Chromatographie Methoden der Analysen in der Chemie, Band 14, Akademische Verlagsgesellschaft, Frankfurt a/M, 1974.

Analytica Chimica Acta, 94 (1977) 21—27

ANALYSIS OF POLYCYCLIC AROMATIC HYDROCARBONS IN PARTICULATE MATTER BY GLASS CAPILLARY GAS CHROMATOGRAPHY*

ALF BJØRSETH

Central Institute for Industrial Research, Blindern, Oslo 3 (Norway)

(Received 8th June 1977)

SUMMARY

A method for analysis of polycyclic aromatic hydrocarbons in particulate matter is based on a Soxhlet extraction of the particulates with cyclohexane, liquid—liquid extraction of cyclohexane with dimethylformamide:water (9:1), back-extraction into cyclohexane by the addition of water, and a concentration step. The polycyclic aromatic hydrocarbons are separated by glass capillary gas chromatography and the chromatographic peaks are integrated electronically. The advantages of this system are discussed in terms of recovery, precision, separation efficiency, and sensitivity.

Polycyclic aromatic hydrocarbons (PAH) are widespread contaminants in the environment, produced by high-temperature reactions such as incomplete combustion and pyrolysis of fossil fuels and other organic materials [1]; major sources of PAH are traffic, domestic heating, refuse burning, and various industrial activities [2]. Because of the great number of chemical events which may take place in a combustion process, the mixture of PAH emitted from these sources may be extremely complex.

There are several problems involved in the determination of PAH. Firstly, by adequate clean-up, PAH must be separated from a complex mixture of other organic substances which are often encountered in airborne particulate matter. Furthermore, a high degree of separation efficiency is necessary. Besides the many different compounds with a wide boiling point range that may be formed during a high-temperature reaction, there also exist many possibilities for structural isomers of PAH; the biological effect may differ for isomeric molecules although the chemical and physical properties are very similar. A detailed knowledge of the sample composition is therefore required for estimating the potential hazard of PAH in the environment. Finally, a high sensitivity of detection is required both for analyzing small samples

*This work is part of a joint Norwegian project on "Polycyclic aromatic hydrocarbons in the work environment" between the Institute of Occupational Health, The Engineering Research Foundation at the Technical University of Norway, and the Central Institute for Industrial Research.

collected over a relatively short period of time and for detecting minor components in the mixture which may be of biological significance.

Because of their environmental importance, PAH have been studied extensively, and a number of analytical methods exist. These include column chromatography and spectrophotometry [3, 4], fluorescence [5], paper and thin-layer chromatography [6, 7], gas chromatography [8], high-pressure liquid chromatography [9] or combinations of these techniques [10, 11]. More recently, gas chromatography—mass spectrometry has been used [12]. These methods vary in respect of speed, resolution, reproducibility, and sensitivity, and have been used with varying degrees of success.

In principle, gas chromatography is a simpler, more direct method for determination of PAH than many other methods, provided, however, that a suitable column can be found. The technique of glass capillary gas chromatography has been brought to a level where excellent reproducibility, high sensitivity and high resolution between individual isomers of PAH may be obtained on a routine basis [13]. In this laboratory, several hundred PAH samples of different origins have now been analysed. This paper reports on the methodology of determination of PAH in particulate matter by high-resolution glass-capillary gas chromatography. Recovery and reproducibility are good; the sensitivity and separation efficiencies are demonstrated by means of standards and actual samples.

EXPERIMENTAL

Chemicals and samples

Solvents were purified by distillation in glass apparatus with a column (1 m high) filled with steel chips. Dimethylformamide (DMF) was distilled under reduced pressure and stored under nitrogen in a refrigerator.

The purity of the PAH standards, supplied commercially, was checked by g.l.c. The standards were prepared by dissolving weighed amounts in cyclohexane.

Particulates from cyclone cleaning equipment of potroom gases in an aluminium reduction plant were used as standard materials. This material contains a wide variety of PAH compounds [14].

Laboratory equipment

All glassware was thoroughly rinsed and finally cleaned by heating to 550°C.

Procedure

The clean-up procedure used is a modified version of that of Grimmer and Böhnke [15]. Samples of the particulate material (ca. 50 mg) to which were added the internal standards 3,6-dimethylphenanthrene, β,β'-binaphthalene and/or m,m'-tetraphenyl, were extracted with 50 ml of cyclohexane in a Soxhlet apparatus for 16 h. Further extraction with cyclohexane or benzene did not give any PAH. The extract was shaken with 50 ml of DMF:water

(9:1) in a separatory funnel, the layers were allowed to separate, and the DMF:water phase was transferred to another separatory funnel. The cyclohexane phase was extracted once more with 25 ml of DMF:water (9:1) and the two DMF:water phases were combined. By the addition of 75 ml of water and 50 ml of cyclohexane, the PAH were back-extracted into the cyclohexane. The extraction of PAH was repeated once with 25 ml of cyclohexane. The cyclohexane extracts were combined, washed with water, and dried with sodium sulphate.

Frequently, absorption flasks with ethanol (or other organic solvents) are placed behind the sampling filters used to collect the volatile compounds. The PAH, extracted from alcohol with cyclohexane by the addition of water [16], were subsequently subjected to the clean-up procedure described above.

The cyclohexane extract was concentrated to ca. 10 ml in a water bath with a modified Vigreux column under nitrogen at reduced pressure. The temperature was kept below 50°C and the pressure above 10 torr to ensure minimum loss and decomposition of PAH during the concentration step. Further concentration was performed in a centrifuge tube at 30°C by directing a gentle stream of highly purified nitrogen onto the liquid surface.

The analysis was carried out on a Carlo-Erba Fractovap 2101 AC gas chromatograph with glass capillary column and flame ionization detector (FID). The cyclohexane extract (ca. 2 μl) was injected by the splitless injection technique [17]. The chromatographic conditions were as follows: the columns were (a) glass capillary, 50 m × 0.34 mm i.d. coated with OV-1, and (b) glass capillary, 20 m × 0.25 mm i.d. coated with OV-101; carrier gas, hydrogen at 4 ml min^{-1}; flame ionization detector; injector and detector temperature, 275°C; initial column temperature, 100°C; programmed temperature, 3 deg min^{-1}; final temperatures, 250°C (column a) 260°C (column b). The techniques for handling, cleaning and mounting the glass capillary columns (H. & G. Jaeggi, 9043 Trogen, Switzerland) have been described in detail [18].

The chromatographic peaks were displayed on an OmniScribe (Houston Instruments) recorder; peak areas were measured by electronic integration (Autolab Minigrator, Spectra-Physics). A simple computer program compared the areas of the internal standards with the peak areas, giving the amount of each compound in the sample.

The peaks in the chromatogram were identified by comparing retention times with those of standards and by analysis on a Hitachi-Perkin-Elmer GC/MS model RMU-5 single-beam mass spectrometer with a Biemann-Watson molecule separator.

The peaks were quantified by comparing the integrated peak area with that of the nearest internal standard. When possible, the quantification was corrected for relative response factors.

RESULTS AND DISCUSSION

The analytical method described was tested with respect to recovery, precision, sensitivity and separation efficiency on standard mixtures and actual samples.

Recovery

The recovery was tested by adding a standard mixture consisting of 15 PAH compounds to 50 ml of cyclohexane followed by a complete clean-up. The recoveries of the individual compounds (average of nine parallel determinations) are listed in Table 1. The recoveries varied between 77 and 121%; the average overall recovery was 98%. By ensuring a high reflux ratio during the concentration step, high recoveries may be achieved even for volatile substances such as naphthalene and biphenyl. For the high-molecular-weight PAH coronene, the recovery is somewhat lower, presumably because of less favourable distribution coefficients between cyclohexane and DMF/water.

The goodness of the method (δ) may be measured as the deviation of the individual recoveries from the theoretical value of 100%. The formula $\delta = ({}^{n}\Sigma_{i=1}\,{}^{m}\Sigma_{j=1}\,(100 - X_{ij})^2/nm)^{1/2}$ gives the goodness of the method for 9 parallel determinations ($n = 9$) of the PAH standard ($m = 15$) as 11.6%.

Precision

The precision of the method was tested with standard mixtures and actual samples; studies with the standard samples were made in parallel with the recovery studies. The results are presented in Table 1. Relative standard deviation (s_r) is used as measure of the precision within the set of analyses. Table 2 shows that s_r is less than 14% in all cases; the average s_r for 15 compounds is 4.8%.

TABLE 1

Relative response factors, precision and recovery test of a standard PAH-mixture.

PAH	Amount added (μg)	Response factor relative to		Recovery[a] (%)	s_r[a] (%)
		3,6-DMP	β,β'-BN		
Naphthalene	13.2	0.846	0.730	96.9	3.9
2-Methylnaphthalene	14.9	0.920	0.793	87.3	3.4
Biphenyl	14.7	0.963	0.830	94.1	3.7
Fluorene	14.8	0.962	0.830	102.5	3.9
2-Methylfluorene	11.3	1.054	0.910	88.7	2.7
Phenanthrene	16.4	1.028	0.888	121.7	3.4
1-Methylphenanthrene	13.1	0.967	0.835	113.2	1.4
Fluoranthene	15.0	0.928	0.802	94.9	5.6
Pyrene	14.6	1.014	0.877	94.6	5.1
Benzo(b)fluorene	13.8	1.075	0.929	95.5	4.9
Chrysene	13.0	1.170	1.006	104.9	2.7
Benzo(e)pyrene	14.1	1.129	1.042	102.2	2.1
o-Phenylenepyrene	13.3	1.429	1.218	99.2	5.5
Anthanthrene	8.0	1.855	1.578	97.8	13.5
Coronene	6.8	1.982	1.684	77.0	10.7

[a] Average of 9 parallel determinations.

TABLE 2

Determination of PAH in airborne particulate matter

Peak number	PAH	Average value (ppm)	s_r(%)
1	Phenanthrene	160	2.8
2	Fluoranthene	1525	7.2
3	Pyrene	1106	4.0
4	Benzo(a)fluorene	250	3.3
5	Benzo(b)fluorene	105	1.9
6	Benzo(c)phenanthrene	157	5.0
7	Benz(a)anthracene	438	1.6
8	Chrysene/Triphenylene	1850	2.2
9	Benzo(b and k)fluoranthenes	2097	3.2
10	Benzo(e)pyrene	956	2.8
11	Benzo(a)pyrene	202	5.3
12	*o*-Phenylenepyrene	236	6.2
13	Benzo(ghi)perylene	248	3.9
14	Coronene	80	9.7
15	Dibenzopyrene	76	8.4

As a further test of the reproducibility of the method, a set of 5 equivalent samples of the particulates from an aluminium reduction plant was analyzed. Figure 1 shows a typical chromatogram of PAH in the particulates and Table 2 gives the results for 15 of the compounds identified; these 15 components represent both major and minor components in the sample. Table 2 shows that the precision is better than 10%, with an average of 4.5%. There are no apparent significant differences between the precision of the major and minor components.

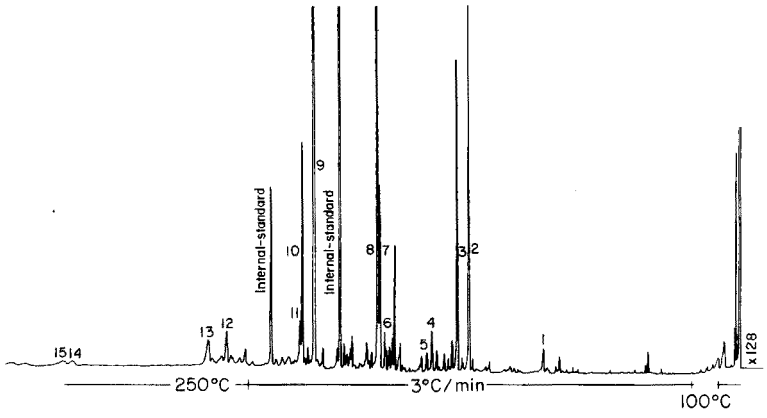

Fig. 1. Gas chromatogram of PAH in airborne particulate matter from an aluminium reduction plant; peak identity given in Table 2.

Sensitivity

In terms of the minimum detectable amount, capillary columns are superior to packed columns because of their higher resolution, i.e. they give peaks with a much higher ratio of height to width at half height. The sensitivity of this method is determined from the recovery test of the standard samples. If the detection limit is defined as 10 times the noise level [19], the sensitivity is about 1 ng of fluoranthene per 2.0 μl of the standard mixture injected.

Separation efficiency

It is important to achieve as high a separation efficiency as possible in analyses of PAH, particularly for some pairs of isomers where one isomer is carcinogenic and the other is not. Figure 2 shows a chromatogram of a standard mixture containing 45 PAH components; this shows that the glass capillary column is capable of producing a high separation efficiency over a large volatility range. Among the most important features are the separation of benzo(a)pyrene (carcinogenic, +) from benzo(e)pyrene (not carcinogenic, —) and benz(a)anthracene (+) from chrysene (—) and triphenylene (—) [2]. Complete separation of benzo(b) fluoranthene (+) from benzo(k)fluoranthene (—) is, however, not achieved with the stationary phases used in this work, but recent progress in this laboratory has shown that these isomers may be partly separated on the stationary phase SE-54.

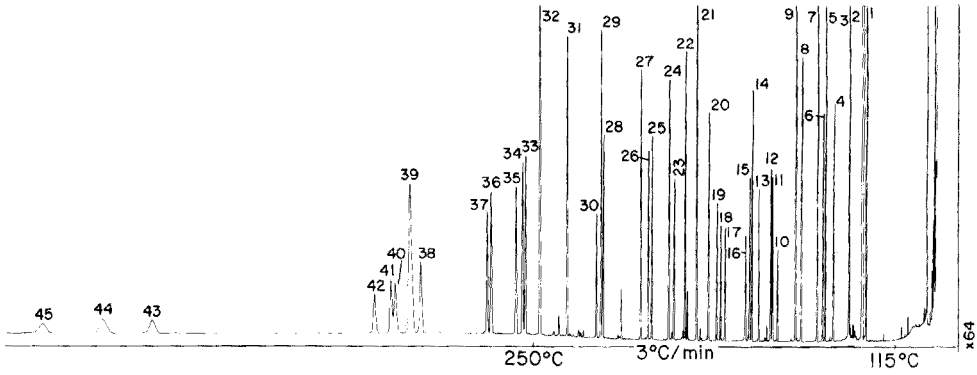

Fig. 2. Gas chromatogram of a complex PAH standard mixture. The peak identities are as follows. 1 2-Methylnaphthalene. 2 1-Methylnaphthalene. 3 Biphenyl. 4 Acenaphthylene. 5 Acenaphthene. 6 4-Methylbiphenyl. 7 Dibenzofuran. 8 Fluorene. 9 9-Methylfluorene. 10 9,10-Dihydroanthracene. 11 2-Methylfluorene. 12 1-Methylfluorene. 13 Dibenzothiophene. 14 Phenanthrene. 15 Anthracene. 16 Acridine. 17 Carbazole. 18 2-Methylanthracene. 19 1-Methylphenanthrene. 20 9-Methylanthracene. 21 3,6-Dimethylphenanthrene. 22 Fluoranthene. 23 Pyrene. 24 9,10-Dimethylanthracene. 25 Benzo(a)fluorene. 26 Benzo(b)fluorene. 27 1-Methylpyrene. 28 Benz(a)anthracene. 29 Chrysene/triphenylene. 30 Naphthacene. 31. β,β-Binaphthalene. 32 9,10-Dimethylbenz(a)anthracene. 33 Benzo(e)-pyrene. 34 Benzo(a)pyrene. 35. Perylene. 36 3-Methylcholanthrene. 37 *m,m'*-Tetraphenyl. 38 *o*-Phenylenepyrene. 39 Dibenz(a, h)anthracene. 40 Picene. 41 Benzo(ghi)perylene. 42 Anthanthrene. 43 1,2:3,4-Dibenzopyrene. 44 Coronene. 45 3,4:9,10-Dibenzopyrene.

Applications

The method described is well suited for the determination of PAH in airborne particulate matter; some applications on samples from work atmospheres and long range transported dry depositions will be described elsewhere. With a few modifications to the clean-up procedure, the method may also be used for biological material, food, water and marine organisms [20].

The author is indebted to Dr. G. Lunde for stimulating discussions and interest in this work. M. Skogland and B. Olufsen are thanked for skilful technical assistance. Financial support from the Royal Norwegian Council for Scientific and Industrial Research under contract B.1551.4879 is gratefully acknowledged.

REFERENCES

1 G. M. Bagder, Nat. Cancer Inst. Monogr., 9 (1962) 1.
2 Particulate Polycyclic Organic Matter, National Academy of Science, Washington D.C., 1972.
3 G. E. Moore, R. S. Thomas and J. L. Monkman, J. Chromatogr., 26 (1967) 456.
4 E. E. Sawicki, R. C. Corey, A. E. Dolley, J. B. Gisclard, J. L. Monkman, R. E. Neligan and L. A. Ripperton, Health Lab. Sci., 7 (1970) 31.
5 E. Sawicki, R. C. Corey, A. E. Dolley, J. B. Gisclard, J. L. Monkman, R. E. Neglian and L. A. Ripperton, Health Lab. Sci., 7 (1970) 45.
6 G. Biernoth, J. Chromatogr., 36 (1968) 325.
7 L. Zoccolillo and A. Liberti, J. Chromatogr., 120 (1976) 485.
8 D. A. Lane, H. K. Moe and M. Katz, Anal. Chem., 45 (1973) 1776.
9 H.-J. Klimisch and D. Ambrosius, J. Chromatogr., 120 (1976) 299.
10 W. Giger and M. Blumer, Anal. Chem., in press.
11 T. Doran and N. G. McTaggert, J. Chromatogr. Sci., 12 (1974) 715.
12 R. C. Lao, R. S. Thomas, H. Oja and L. Dubois, Anal. Chem., 45 (1973) 908.
13 K. Grob and G. Grob, J. Chromatogr. Sci., 7 (1969) 584.
14 A. Bjørseth and G. Lunde, Technical report 74 03 12-2, Royal Norwegian Council for Scientific and Industrial Research (1975).
15 G. Grimmer and H. Böhnke, Z. Anal. Chem., 261 (1972) 310.
16 L. Fishbein, Chromatography of Environmental Hazards, Vol. II. Elsevier, Amsterdam 1973.
17 K. Grob and G. Grob, J. Chromatogr. Sci., 7 (1969) 587.
18 K. Grob and J. J. Jaeggi, Chromatographia, 5 (1972) 382.
19 K. Grob, K. Grob Jr., and G. Grob, J. Chromatogr., 106 (1975) 299.
20 A. Bjørseth, Proceedings, 12th Nordic Symposium on Water Research, NORDFORSK, Helsinki (1976).

Analytica Chimica Acta, 94 (1977) 29—34

HIGH-PRESSURE LIQUID CHROMATOGRAPHY OF METAL DIETHYLDITHIOCARBAMATES WITH U.V. AND D.C. ARGON-PLASMA EMISSION SPECTROSCOPIC DETECTION

PETER C. UDEN and IMOGENE E. BIGLEY

Department of Chemistry, GRC Tower I, University of Massachusetts, Amherst, Massachusetts 01003 (U.S.A.)

(Received 16th May 1977)

SUMMARY

The separation of copper(II), nickel(II) and cobalt (III) diethyldithiocarbamates is reported by adsorption high-pressure liquid chromatography on 8-μm diameter spherical silica. Best resolution is found with a 5:15:80; acetonitrile:diethyl ether : Skelly B (petroleum hydrocarbon) mobile phase, any on-column degradation being avoided by pretreatment of the column with pyridine. U.v. detection limits at 254 nm are established in the 5—10 ng of metal region. An interfaced d.c. argon-plasma emission spectroscopic detection system in series with the u.v. detector, is used to confirm the metal content of eluted peaks and permit specific element detection.

High-pressure liquid chromatography (h.p.l.c.), initially employed almost exclusively for the separation of organic compounds, is now being increasingly applied to the separation of metallic compounds.

An important advantage of h.p.l.c. is the availability of a variety of separation modes including ion-exchange, partition, adsorption and exclusion. The efficiency of separations was formerly limited by the size of the substrate particles, typically 30—75 μm in diameter, but the recent development of commercially available substrates in the 5—10-μm diameter range has increased h.p.l.c. column efficiencies, making the results analogous to those in gas chromatography, particularly when spherical particles are used.

A review of the literature shows Seymour and Fritz [1] using forced-flow ion exchange to separate metal ions, and Huber et al. [2] separating acetylacetonates and trifluoroacetylacetonates of a variety of metals via a ternary liquid—liquid partition system. The separation of copper(II) and nickel(II) Schiff base chelates on microparticulate silica and reversed-phase partition phases has been reported [3, 4]. Gaetani et al. [5] subsequently also examined the separation of metal chelates of β-ketoamines on microparticulate reversed-phase substrates, achieving separation of cobalt(III), nickel(II) and copper(II) with a methanol : phosphate buffer (pH 7.8; 65:35) as the mobile phase. Copper(II) and nickel(II) were also separated on an amine-bonded column with a similar mobile phase.

Metal dialkyldithiocarbamates have recently attracted chromatographic interest and a range of different metal complexes has been successfully gas-chromatographed [6—8]. Parallel h.p.l.c. studies have been commenced with a view to analytical applications of this very versatile chelating system, and the present paper describes the separation of the cobalt(III), copper(II) and nickel(II) diethyldithiocarbamates.

EXPERIMENTAL

Preparation of metal complexes

The copper(II), nickel(II) and cobalt(III) chelates were formed by the reaction of aqueous metal ion solutions with aqueous sodium diethyldithiocarbamate solution. The precipitated complexes were extracted into chloroform and recrystallized. The purified complexes gave single peaks on h.p.l.c., and their mass spectra showed characteristic fragmentation patterns.

High-pressure liquid chromatography

A Tracor-Chromatec model 3100 liquid chromatograph was employed; a u.v. detector with single wavelength detection at 254 nm, a full-scale sensitivity of 0.01 A (absorbance units) and a 8-μl flow cell well used. The 4-mm i.d. × 25-cm stainless steel column was packed with 8-μm diameter Spherisorb SGP (Phase Sep. Inc.); a balanced density technique was used with a 1:1 bromoform : tetrachloroethylene solvent and an air-driven fluid pump (DST-122, Haskel Engineering and Supply Corp.) operating at 5800 psi.

Mass spectrometry

Mass spectra of the chelates were obtained on a Hitachi Perkin-Elmer RMU .6L single-focusing mass spectrometer operated at an ionizing voltage of 70 eV. The source temperature was kept at 265 ± 5°C, and solid samples were evaporated into the source by means of a direct insertion probe.

Ultraviolet spectrophotometry

A Perkin-Elmer 202 instrument was employed in the range 190—390 nm, with a deuterium source; 1-cm quartz cells were used. Solutions were made up in 10% methylene chloride in diethyl ether and run against similar blanks.

D.C. plasma emission spectrometry

A prototype Spectraspan III instrument (Spectrametrics, Inc., Andover, Mass.) was used as a metal-specific detector. It consists of a d.c. argon plasma and a 3/4-m modified Czerny-Turner optical system incorporating an echelle grating with an internal quartz prism cross disperser. The interface used for transfer of the hydrocarbon-based eluent from the column to the argon plasma has been described separately [9].

RESULTS AND DISCUSSION

Dithiocarbamates have been used extensively in analytical chemistry as reagents for trace analysis, colorimetry and extraction. A review by Hulanicki [10] discusses complexation reactions of a variety of dialkyldithiocarbamates. Bode and Neumann [11] published a study of extraction properties of 22 diethyldithiocarbamate chelates. Studies [10—17] have also shown the feasibility of using thin-layer chromatography on silica for the separation of various metal dithiocarbamates. With such a background of data available, including established analytical techniques, it is useful to examine the adsorption behaviour of some of these complexes in the h.p.l.c. mode for potential analytical utility.

A distinct advantage of the diethyldithiocarbamate anion over many other ligand systems is its insolubility in organic solutions. Thus a typical extraction into chloroform or carbon tetrachloride would transfer only neutral metal complexes and leave behind the excess of ligand, thus precluding its possible further reaction on the h.p.l.c. column.

The present study concerned the nickel(II), copper(II) and cobalt(III) complexes.

Mass spectra were taken of the purified metal dithiocarbamates and characteristic fragmentation patterns were observed. The major peaks are given in Table 1 along with relative intensities. These results agree with spectra found in the literature [18].

Separation of $Ni(DDTC)_2$, $Cu(DDTC)_2$ and $Co(DDTC)_3$ was best achieved with a solvent system containing acetonitrile : diethyl ether : Skelly B (light petroleum hydrocarbon) (5:15:80) on an 8-μm Spherisorb column, which had been previously washed with a solution of 0.5% pyridine in Skelly B to reduce the possibility of any on-column degradation of the complexes (Fig. 1).

TABLE 1

Principal features of mass spectral fragmentation patterns of the chelate (P indicates the parent ion, L the ligand and M the metal. R.I. = Relative Intensity. Most fragment ions below M + L are not included. Based on Ni (58), Co (59) and Cu (63).)

	Chelate					
	$Ni(DDTC)_2$		$Co(DDTC)_3$		$Cu(DDTC)_2$	
Ion	M/e	R.I.	M/e	R.I.	M/e	R.I.
P^+	355	100	503	2	360	87
$(M + 2L)^+$	—	—	355	58	—	—
$(M + L)^+$	206	4	207	13	211	20
HL^+	149	22	149	15	149	24
$(L—S)^+$	116	43	116	79	116	100
$(C_2H_5)NCS^+$	87	51	87	100	87	90
CS_2^+	76	7	76	38	76	75

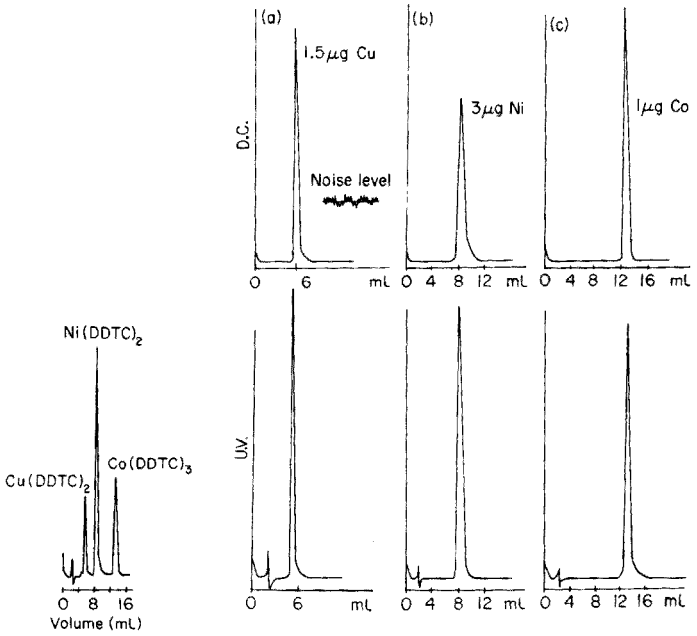

Fig. 1. High-pressure liquid chromatographic separation of $Cu(DDTC)_2$, $Ni(DDTC)_2$ and $Co(DDTC)_3$. Column (25 cm × 4 mm i.d.), 8-μm Spherisorb. Solvent, 5:15:80 CH_3CN : diethyl ether : Skelly B. Flow rate, 2.2 ml min^{-1}.

Fig. 2. High-pressure liquid chromatograms of chelates. Detection by both u.v. and d.c. plasma. (a) $Cu(DDTC)_2$, λ = 324.7 nm, (b) $Ni(DDTC)_2$, λ = 305.1 nm and $Co(DDTC)_3$, λ = 345.3 nm. Chromatographic conditions as in Fig. 2.

This system has adequate resolution for the quantification of the three metals; the resolution factors calculated are 2.8 for Cu/Ni, 3.6 for Ni/Cu and 7.6 for Cu/Co. The theoretical plates were calculated to be 1030, 1430, and 1550 for $Cu(DDTC)_2$, $Ni(DDTC)_2$ and $Co(DDTC)_3$, respectively.

To verify that the peaks observed corresponded to the metal dithiocarbamates and not to degradation products, a d.c. argon-plasma emission spectrometer system was used as a metal specific detector. The column effluent first passed through the u.v. detector and then into the d.c. argon-plasma. Monitoring specific wavelengths for the output from the plasma proved the presence of the specific metals in each case. The results are shown in Fig. 2, which also mentions the optimal wavelengths. This specific detection system is presently under further development [9].

Ultraviolet spectra in the range 190—390 nm, were obtained for each of the chelates (Fig. 3). The molar absorptivities of each of the chelates at 254 nm were calculated to be $Cu(DDTC)_2$, 13 100; $Ni(DDTC)_2$, 14 800; and $Co(DDTC)_3$, 21 800 l mol^{-1} cm^{-1}.

Quantitative studies were carried out for each of the metal chelates to determine their linearity and range of response. $Co(DDTC)_3$ and $Ni(DDTC)_2$

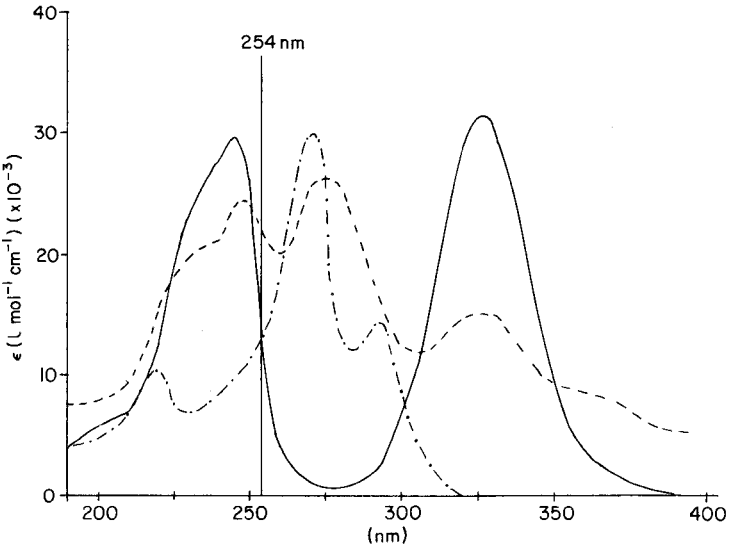

Fig. 3. Plot of molar absorptivity against wavelength for chelates: (a) (——) $Ni(DDTC)_2$; (b) (—·—·) $Cu(DDTC)_2$; (c) (·····) $Co(DDTC)_3$.

have linear ranges for 5—500 ng of metal, and $Cu(DDTC)_2$ has a linear range for 10—500 ng of copper. The detection limits were taken at a detector signal-to-noise ratio of 2:1. The detection limits could be extended by utilization of a variable wavelength detector, for $Co(DDTC)_3$ and $Cu(DDTC)_2$ have molar absorptivities between 25 000 and 30 000 l mol^{-1} cm^{-1} at 270 nm, and $Ni(DDTC)_2$ has a molar absorptivity of 31 000 l mol^{-1} cm^{-1} at 326 nm. The upper linearity limits were not specifically determined, but other metal chelates with similar molar absorptivities have shown linearity over three orders of magnitude [3].

The results of this investigation indicate the applicability of adsorption h.p.l.c. as a means of rapid separation and quantification of copper, nickel and cobalt diethyldithiocarbamates. The effect of pH on extraction efficiency and possible liquid chromatographic interferences from other metals is currently being investigated along with the separation of other metal dithiocarbamates. Quantitative applications will be reported later.

We acknowledge the support of the National Science Foundation through Grant CHE73-05207. We thank Bruce D. Quimby for assistance with the d.c. argon plasma spectrometry and Professor Ramon M. Barnes and William G. Elliott for useful discussions. Our thanks are also due to Dr. Terence J. Cardwell for his interest in this project and to Phase Sep. Inc. for a sample of Spherisorb SGP.

REFERENCES

1 M. D. Seymour and J. S. Fritz, Anal. Chem., 45 (1973) 1632.
2 J. F. K. Huber, J. C. Kraak and H. Veening, Anal. Chem., 44 (1972) 1554.
3 P. C. Uden and F. H. Walters, Anal. Chim. Acta, 79 (1975) 175.
4 P. C. Uden, D. M. Parees and F. H. Walters, Anal. Lett., 8 (1975) 795.
5 E. Gaetani, C. F. Laureri, A. Mangia and G. Parolari, Anal. Chem., 48 (1976) 1725.
6 J. Krupcik, J. Garaj, S. Holotik, D. Oktavek and M. Kosik, J. Chromatogr., 112 (1975) 189.
7 J. Masaryk, J. Krupcik, J. Garaj and M. Kosik, J. Chromatogr., 115 (1975) 256.
8 T. J. Cardwell, D. J. Desarro and P. C. Uden, Anal. Chim. Acta, 85 (1976) 415.
9 R. M. Barnes, I. E. Bigley, W. C. Elliott, B. D. Quimby and P. C. Uden, Paper presented at the Joint Chemical Institute of Canada/American Chemical Society Conference, Montreal, June 1977.
10 A. Hulanicki, Talanta, 14 (1967) 1371.
11 H. Bode and F. Neumann, Z. Anal. Chem., 172 (1960) 1.
12 A. Galik, Anal. Chim. Acta, 67 (1973) 357.
13 M. Kiboku, Jpn. Anal., 17 (1968) 722.
14 F. J. Onuska, Anal. Lett., 7 (1974) 327.
15 F. I. Onusha, Anal. Lett., 3 (1970) 41.
16 J. Rai and V. P. Kukreja, Chromatographia, 3 (1970) 499.
17 D. M. Smith and J. R. Hayes, Anal. Chem., 31 (1959) 898.
18 J. F. Villa, D. A. Chatfield, M. M. Bursey and W. E. Hatfield, Inorg. Chim. Acta, 6 (1972) 332.

Analytica Chimica Acta, 94 (1977) 35—47

DETERMINATION OF INOSITOL PHOSPHATE ESTERS IN LAKE SEDIMENTS

WALTER C. WEIMER* and DAVID E. ARMSTRONG

Water Chemistry Program, University of Wisconsin, Madison, Wisconsin 53706 (U.S.A.)

(Received 6th May 1977)

SUMMARY

A procedure for the determination of the total inositol polyphosphate content of lake sediments is presented and evaluated. This technique involves extraction with NaOH, cleanup of the extract, and isolation and identification of two groups of inositol phosphate esters by ion-exchange chromatography. Radioisotope dilution is employed to correct for losses during the extraction, cleanup and isolation steps. Recoveries of the radiotracer inositol phosphates have averaged 85% during the analysis of approximately 40 calcareous and non-calcareous sediment samples and more than 20 soil samples.

The increased awareness of the advanced eutrophic conditions present in many lakes has focused attention on the cycling of nutrients in aquatic systems. Since phosphorus is generally acknowledged to be the nutrient most frequently limiting algal productivity [1], potential sources and sinks of phosphorus have been the subjects of considerable research activity. Lake sediments are one potentially important phosphorus source that has been investigated. There are considerable data available concerning the nature of the inorganic phosphorus components in lake sediments [2]. However, although as much as 70% of the sediment phosphorus may be organic phosphorus [3—5], there is little information concerning the chemical nature of this component. Because of this quantitative significance and the possibility of organic phosphorus hydrolysis to yield inorganic phosphorus that may be released from the sediments to the overlying waters, it is very important to understand the role of organic phosphorus in the aquatic phosphorus cycle.

The organic phosphorus in lake sediments may be somewhat comparable to that in terrestrial soils because of similar origins (synthesis by green plants) and since terrestrial soils are eroded and washed into lakes and comprise a substantial portion of the sediments. Characterizations of soil organic phosphorus have indicated that the major phosphorus-containing constituents identified in all soils are the phosphate esters of hexahydroxycyclohexane, or inositol [6]. The quantitative importance of inositol phosphates in terrestrial soils suggested an investigation of their significance in lake sediments.

---

*Present address: Battelle-Northwest Laboratories, 329 Building/300 Area, Richland, Washington 99352, U.S.A.

The presence of some inositol polyphosphates in lake sediments has been reported [7—10]. However, the analytical techniques used in these studies were neither selective for inositol phosphates nor did they measure the total inositol polyphosphate contents. The purpose of the present investigation was to develop and evaluate a determination of the total inositol phosphate content of lake sediments based on procedures for determination of inositol phosphates in terrestrial soils. The analysis for inositol phosphates consists of two separate phases: (1) the extraction of inositol polyphosphates from lake sediments and cleanup of the extract, and (2) the isolation of these polyphosphates from other phosphorus species in the sediment extract, and quantitative measurement of the inositol phosphates.

EXPERIMENTAL

Sample and pretreatment

Samples of lake sediments and watershed soils were freeze-dried for storage. The samples were ground in a mortar to pass a 100-mesh sieve immediately before analysis.

Total phosphorus analysis

Samples for total phosphorus analysis were digested with HNO_3:$HClO_4$:H_2SO_4 (17:10:3, volume ratio). The phosphomolybdenum blue colorimetric method [11] was used to complete the determination. After color development, the absorbance at 883 nm was measured with a Unicam Model 600 spectrophotometer.

Radiotracer preparation

Inositol hexaphosphate labelled with radiophosphorus (^{32}P and ^{33}P) was prepared by a biological synthesis technique involving the germination of mung beans (*Phaseolus aureus*) in a medium containing inorganic radiophosphorus as the sole phosphorus source [12, 13]. After germination, the beans were blended with 6 M HCl and extracted at 110°C for 3 h. After cleanup, a portion of this extract was adjusted to pH 4, hydrolyzed for 16 h at 110°C to produce a mixture of labelled inositol phosphates, and neutralized. The labelled compounds produced were identified through separation by ion-exchange chromatography and analysis of individual aliquots for phosphorus:carbon atom ratios.

Liquid scintillation counting of radiophosphorus

All determinations of the radiophosphorus content of samples were performed by liquid scintillation counting [14] of an aliquot of the sample in a Packard Model 3320 TriCarb spectrometer. The liquid scintillation solution used was a modification of the Bruno and Christian cocktail [15]. Since the counting efficiency of the liquid scintillation solutions varied with the sample, it was necessary to correct each sample to a standard counting

efficiency by using the automatic external standard (AES) procedure [16]. Quenching curves of AES counts/min vs. efficiency were determined for standard ^{32}P and ^{33}P samples with varying amounts of nitromethane as the quenching agent. The use of radiophosphorus-labelled inositol polyphosphates as isotope dilution tracers allowed correction of the data for sample loss during extraction, cleanup, and isolation procedures.

EXTRACTION OF INOSITOL PHOSPHATES FROM AQUATIC SEDIMENTS AND EXTRACT CLEANUP

Methods for the determination of inositol phosphate esters in soils have been based on approaches to the extraction and cleanup which differ principally in the rigor of the initial sediment extraction. Three combinations of extraction and cleanup techniques have been evaluated with lake sediments [17].

Evaluation of extraction and cleanup techniques

Inositol phosphate esters can be determined in terrestrial soils in two ways. In the first approach [18], inositol phosphates and other organic phosphorus compounds or complexes are removed from the soils with little alteration of their chemical nature. Soil organic matter—inositol phosphate complexes are apparently not disrupted, and subsequent interactions between anion-exchange resins and inositol phosphates during isolation steps are therefore not predictable. This technique was found to be suitable for the observation of general classes of organic phosphorus compounds in lake sediments, but was limited in its ability to determine specific organic phosphorus compounds [9]. The second approach [19, 20] involves a rigorous extraction to disrupt any complexes formed between the inositol phosphates and humic materials.

In the present research on lake sediments, the extraction and cleanup procedures were designed to yield a final extract containing free inositol phosphate esters which would interact predictably with anion-exchange resins. Three extraction and cleanup techniques were evaluated for routine use. The major criterion was the recovery of a large amount of inositol phosphate phosphorus in the purified extract.

Method I. This is similar to a determination of inositol phosphates in terrestrial soils [20] and involves a rigorous basic extraction of the sediment samples (3 M NaOH at 100°C). This extraction, together with acid preextraction, dissolves hydrous oxide coatings on sediment particles and frees inositol phosphates from complexes with sediment organic materials. Sesquioxides are then precipitated from the extract and discarded, and the inositol phosphate esters are precipitated with barium acetate.

Method II. This is a modification of another procedure for terrestrial soils [19]. An extraction (1 M NaOH at 60°C) milder than that of Method I yields an extract that contains the sediment organic phosphorus components

in a partially altered state. Cleanup steps include precipitation and removal of humic materials followed by oxidation with hypobromite. Cosgrove [19] precipitated the extracted inositol phosphates with iron(III) chloride, but precipitation with barium acetate in an ethanol:water (1 + 1) solution at pH 8—9 was preferred here. Anderson [21] has reported incomplete recoveries during the precipitation of inositol phosphate esters with $FeCl_3$ in acidic solution, apparently because of the presence of excess iron in the solution and the formation of soluble iron—inositol phosphate complexes. Although the proper choice of reagent quantities could circumvent this precipitation problem for well-defined samples, significant concentrations of native iron in sediments could enhance the formation of these soluble complexes. Since iron concentrations in lake sediments are highly variable, different inositol phosphate recoveries would probably be obtained for each different lake sediment examined if $FeCl_3$ were used as the precipitant.

Method III. This involves extraction with 3 M NaOH at 100°C, humic acid precipitation, oxidation with hypobromite, and precipitation with barium acetate.

Table 1 summarizes the amounts of organic phosphorus and inositol phosphate phosphorus recovered for each method from samples of calcareous sediment from the 23.8-m depth of Lake Mendota, Dane County, Wisconsin. The largest quantity of sediment organic phosphorus was recovered by using Method I. Methods II and III, which differed only in the extraction technique used, recovered similar amounts of organic phosphorus from the sample; however, these recoveries were significantly less than those obtained with Method I. Estimates of the total inositol phosphate content in each extract are also listed in Table 1 (see below for the methods of isolation and identification). The lowest recovery of inositol phosphates was obtained by Method II. Since Method III yielded the greatest recovery of inositol phosphates, the lower recovery found by Method II was apparently due to the mild extraction employed. Although Method I recovered significantly more organic phosphorus than did Method III, much of this apparently was non-inositol phosphorus that the additional cleanup steps of Method III removed.

TABLE 1

Organic phosphorus recovered from a Lake Mendota sediment

Extraction and purification method[a]	Organic P recovered	Estimate of total inositol polyphosphate conten	
	μg P/g dry sediment[b]	μg P/g dry sediment[c]	% of total sediment organic P
Method I	196	49[d]	12.1
Method II	130	38	9.3
Method III	142	51	12.7

[a]Methods are described in text. [b]Average values of duplicate samples. [c]Average values of duplicate samples chromatographed in triplicate. [d]Single sample chromatographed in triplicate.

A final procedure based on the 3 M NaOH extraction at 100°C was selected because of the higher inositol phosphate recovery obtained. No significant beneficial effects from the hypobromite cleanup step were noted. However, the humic acid precipitation removed a considerable amount of material from some samples which would interfere during later isolation steps; therefore, this step was included in the purification. Finally, Method I was selected, with the addition of humic acid removal. The details of this method are given below.

Extraction and cleanup procedure

A dried sediment sample (5 g) ground to pass a 100-mesh sieve is suspended for 2 h in 0.1 M HCl (after carbonate dissolution). The acid extract and distilled water washes are discarded. This extraction removes calcium and magnesium from the samples. Large amounts of iron and inorganic phosphorus and small amounts of organic phosphorus are also extracted. Labile organic phosphorus compounds such as sugar phosphates are hydrolyzed [22], and nucleic acid fragments and very small quantities of inositol phosphates may be removed [5, 6].

A 40-ml aliquot of 3 M NaOH is added to the remaining sediment, and the sample is extracted at 110°C for 16 h. After cooling, the extract and two distilled water washes are combined, and the remaining sediment is discarded. This rigorous extraction removes all organic phosphorus and much of the remaining iron and aluminum from the samples. Possible complexes of inositol phosphates and natural organic matter or of iron, organic matter, and inositol phosphates are destroyed [23]. Organic phosphorus compounds such as ribonucleic acids and phospholipids are hydrolyzed to at least the monophosphate esters [24—26].

The extract is adjusted to pH 4 with HCl and the pH is then raised to 8—9 with NaOH. After at least 15 min, the solution is centrifuged, the supernatant liquid is removed, the precipitated sesquioxides are washed with distilled water, and the extract and washings are combined and retained. The remaining precipitate is discarded. Acidification of the extract to pH 4 destroys any hydroxide complexes that formed during the NaOH extraction, thereby facilitating sesquioxide precipitation on adjustment of the solution to pH 8—9.

The combined extract and washings are made ca. 1 M in HCl. After at least 15 min, the suspension is centrifuged, the supernatant liquid is removed, the precipitated humic acids are washed with distilled water, and the washing and extract are combined and retained. The solids are discarded. This precipitation of the humic acids prevents their inclusion and interaction with the inositol phosphates during the precipitation of the organic phosphorus constituents with barium(II).

NaOH is added to the extract until the pH is 8—9, and a volume of 95% ethanol equal to the total extract is added, followed by 15 ml of 30% (w/v) barium acetate solution. The precipitate is flocculated by heating for 10 min,

and the solution is cooled, covered, and left overnight. This precipitation of barium-inositol phosphates removes some other organic phosphorus compounds as the barium salts. Most of the remaining inorganic phosphorus is also precipitated. The barium-phosphates precipitate is collected, washed twice with 50% ethanol to remove much of the excess barium ion, and allowed to drain-dry. Distilled water and 25 ml (wet volume) of strong acid cation-exchange resin (H^+ form) are added to the precipitate and suspended for 16 h. This equilibration redissolves the barium-phosphates precipitate. Since not all the material precipitated with barium acetate dissolves, the residue is removed by filtration through a 0.45-μm membrane filter. The dissolution of the barium precipitate by contact with the resin lowers the pH of the extract to ca. 2—3. The sample is then adjusted to pH 7 to inhibit chemical hydrolysis of the inositol phosphates and to prepare the extract for ion-exchange chromatography.

Inositol phosphate recovery during extraction and cleanup

The extraction procedure completely removes the inositol polyphosphates and other organic phosphorus compounds from the lake sediments. During the subsequent cleanup, some extracted materials may be lost. The recovery of inositol phosphates through the cleanup was evaluated with a standard mixture of radiophosphorus-labelled inositol phosphates.

Typically, the inositol phosphate radiotracers were added to the lake sediment samples after the HCl pre-extraction. For one sample set, the fraction normally discarded during each step of the extraction and cleanup procedures was examined to determine the extent of loss of the radiotracers. Several sediments of varying composition were evaluated to encompass the range of recoveries that would be expected. Samples of Trout Lake (Vilas County, Wisconsin) and Lake Mendota (Dane County, Wisconsin) sediments were used. The sediments from Lake Mendota are of a calcareous nature, whereas the Trout Lake sediments are non-calcareous and also contain large concentrations of iron [27, 28]. The radiophosphorus loss during each step varied somewhat with sample type (see Table 2).

The data in Table 2 indicate the trend of the organic radiophosphorus (^{32}P) losses. The amount of tracer inositol polyphosphates recovered in the final extract varied by ca. 20% and was generally lower for the Trout Lake sediments than for the Lake Mendota sediments. The greater losses for the Trout Lake sediments appeared to occur during the sesquioxide precipitation (this precipitate was much bulkier for the Trout than for the Mendota sediments because of high iron concentrations) and during the precipitate dissolution with the ion-exchange resin. This latter loss may have involved interaction between the inositol phosphates, the resin, and the large amounts of fulvic acid materials in the Trout Lake sediment extracts. The largest loss of the added tracer organic phosphorus for both sediment types occurred during incomplete precipitation of the inositol phosphates with barium acetate and may be eliminated by careful flocculation techniques. The

TABLE 2

Estimated losses of ^{32}P-labelled inositol polyphosphate phosphorus during sediment extraction and cleanup steps[a]

Lake sediment sample number	Added ^{32}P lost during					Added ^{32}P in final extract
	Sediment extraction	Sesquioxide precipitation	Humic acid precipitation	Ba-P precipitation	Resin dissolution	
M-1	0.5	1.5	0.2	11.6	0.2	91.0
M-1	0.4	1.1	0.3	6.7	0.4	97.9
M-2	0.5	2.9	0.3	7.8	0.2	97.4
M-2	0.5	1.6	0.4	5.3	0.3	95.2
M-5	0.8	3.1	0.1	4.8	0.5	95.8
M-5	0.3	3.5	0.2	3.7	1.0	89.9
M-6	0.4	1.2	0.3	7.0	0.5	93.1
M-6	0.4	0.8	0.7	7.3	0.9	92.6
T-2-W	0.8	5.0	0.5	4.8	0.5	89.9
T-2-W	1.2	5.1	0.8	7.1	0.7	79.2
T-3-W	0.8	9.0	0.2	6.6	1.2	82.4
T-3-W	0.4	7.6	1.0	5.4	1.8	83.5
Average	0.6	3.5	0.4	6.5	0.7	90.7

[a]Expressed as percent of ^{32}P-labelled inositol polyphosphates added initially.

relatively small losses of ^{32}P activity during all of the cleanup steps show that this technique, while removing considerable quantities of interfering materials, does not remove significant quantities of the inositol phosphate esters.

To determine whether inositol phosphate esters were lost during the initial treatment with dilute HCl, tracer inositol polyphosphates were added to triplicate dried samples of Trout Lake and Lake Mendota sediments. The samples were then allowed to dry completely, and extracted for 2 h with 0.1 M HCl. Aliquots were taken from the combined acid extract—distilled water washes. Approximately 14% of the tracer inositol phosphate mixture added to the Trout Lake sample was removed by the acid extract; approximately 8% was removed from the Lake Mendota sediments. These results are similar to the findings of Dormaar [29] that a loss of 4—17% of the "total" organic phosphorus occurred during a 0.2 M HCl extraction of soil samples, and to the results of Sommers [5], which indicated that about 3% of added inositol phosphate was lost during 1 M HCl extraction of two sediment samples. Since the mechanisms retaining the native inositol phosphates in the lake sediments are probably different from the mechanisms holding the added tracer inositol phosphates, the tracer phosphates may be extracted more readily than the native inositol phosphates. Thus the amounts of radiophosphorus recovered in the 0.1 M HCl extract probably represent the maximum loss of native inositol phosphate expected during the pre-extraction.

ISOLATION AND IDENTIFICATION OF INOSITOL PHOSPHATE ESTERS

The final sediment extracts contain several phosphorus species, including inorganic phosphorus, some organic phosphorus of an unknown nature (presumably monophosphate esters), and inositol phosphates. The isolation of specific groups of inositol phosphate esters and separation of these esters from the other phosphorus species were done by ion-exchange chromatography on Bio-Rad AG1-X2 (100-200 mesh; Bio-Rad Laboratories, Richmond, California).

The optimum delineation of inositol phosphate ester content in a sample can be achieved by continuous linear-gradient elution with 0.0—1.0 M HCl [19]. The separation of a pure standard mixture of inositol phosphate esters by this method is shown in Fig. 1. The specific phosphate esters eluted in these peaks and the relative composition of this standard are listed in Table 3. This standard mixture was used throughout this investigation.

Although the continuous linear-gradient elution allows determination of each inositol phosphate ester group, the desired fractionation of phosphorus constituents in the sediment was simply a separation of the inorganic phosphorus and non-inositol organic phosphorus from the inositol di-, tri- and tetra-phosphate esters and a separation of these esters from the inositol penta- and hexa-phosphate esters. This latter division allows examination of the relative quantitative significance of each of these classes of inositol

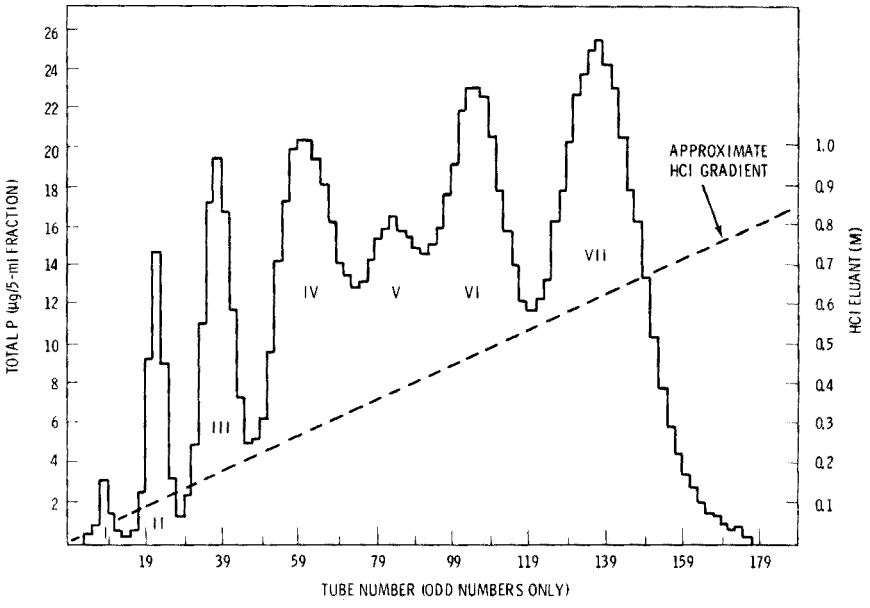

Fig. 1. Ion-exchange chromatography of standard inositol polyphosphate mixture by linear-gradient elution with HCl. Sample: standard inositol polyphosphate mixture free of inorganic phosphorus. Column: 15 cm × 1 cm AG1-X2, 100-200 mesh, Cl^- form. Eluant: HCl. Flow rate: 3.8 ml min^{-1} cm^{-2}.

TABLE 3

Characterization of standard inositol polyphosphate mixture by ion-exchange chromatography with linear-gradient elution

Peak[a]	Tube number[b]	P:C weight ratio		Inositol phosphate ester	P in peak	
		Computed	Measured			
					μg	%[b]
I	6	0.43	0.31	Monophosphate	8	0.4
II	20	0.86	0.93	Diphosphate	80	3.8
III	—	1.29	—	Triphosphate	191	9.0
IV	64	1.72	1.61	Tetraphosphate	413	19.5
V	82	2.15	2.11	Pentaphosphate	271	12.8
VI	104	2.15	2.06	Pentaphosphate	494	23.4
VII	—	2.58	—	Hexaphosphate	658	31.1

[a]Refers to Fig. 1. [b]Percent of total eluted organic phosphorus.

phosphates and comparison of the proportion of the total that each represents in lake sediments and in terrestrial soils from surrounding watersheds.

The HCl elution (Fig. 1) can be compared with the elution pattern obtained by a continuous linear gradient elution with neutral 0.0—1.5 M ammonium formate of an aliquot of the same standard mixture of esters plus inorganic phosphorus (Fig. 2). This formate eluant does not separate the hexa- and penta-phosphate esters of inositol. Thus, only five organic phosphorus peaks from the monophosphate through hexaphosphate esters appear. Since the mono-phosphate esters are eluted along with inorganic phosphorus by either HCl or $HCOONH_4$, inositol monophosphate esters cannot be determined in samples which contain inorganic phosphorus.

Attempts were made to develop a reliable standard procedure for the desired group separation of inositol phosphate esters by step-gradient elution chromatography. This procedure would separate Peak I from Peaks II, III, and IV, and those peaks from Peak V in Fig. 2. The step-gradient procedure developed utilized 75 ml of neutral 0.35 M ammonium formate to elute Fraction 1, 215 ml of neutral 0.525 M ammonium formate to elute Fraction 2, and 100 ml of neutral 1.5 M ammonium formate to elute Fraction 3. The separation of inositol phosphate standards obtained by a step-gradient elution similar to this is shown in Fig. 3. However, a smaller volume of eluant was used for Fraction 2 than is indicated in Fig. 3. When this reduced volume was employed, elution of Fraction 3 did not begin until the 1.5 M ammonium formate was added. Inositol phosphate separation in all sediment extracts was achieved by this step-gradient elution.

When sediment extracts are separated by this ion-exchange procedure, Fraction 1 contains inorganic phosphorus, some organic phosphorus of unknown character (probably monophosphate esters) that does not interact strongly with the resin, and any inositol monophosphate in the sediment

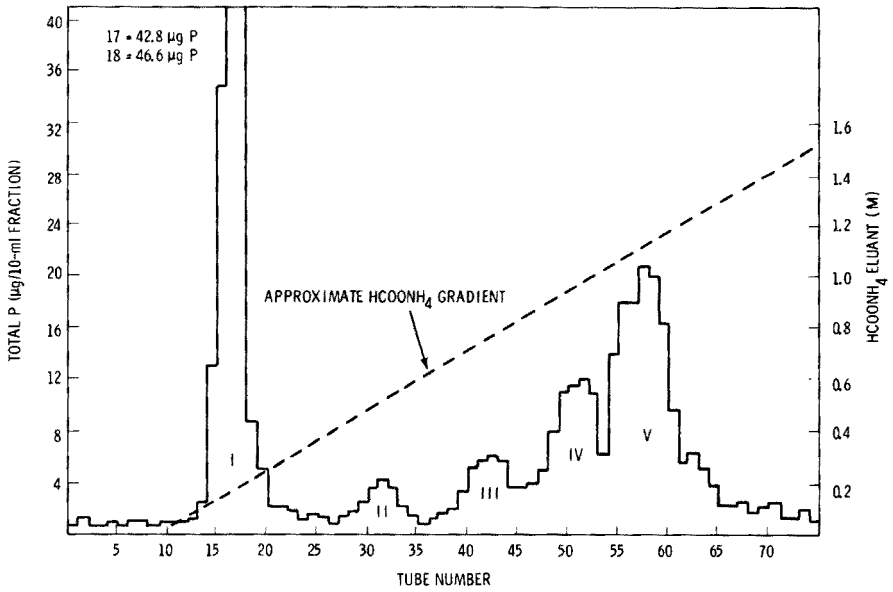

Fig. 2. Ion-exchange chromatography of standard inositol polyphosphate mixture by linear-gradient elution with $HCOONH_4$. Sample: standard inositol polyphosphate mixture plus inorganic phosphorus. Column: 15 cm × 1 cm AG1-X2, 100-200 mesh, $HCOO^-$ form. Eluant: neutral $HCOONH_4$. Flow rate: 2.7 ml min^{-1} cm^{-2}. Peak I, inorganic P + inositol monophosphate. Peaks II—IV, inositol di-, tri- and tetra-phosphates. Peak V, inositol penta- and hexa-phosphates.

extract. Inositol monophosphate is not readily separable from inorganic phosphorus and non-inositol phosphorus mono-esters. Therefore, any inositol phosphate in this fraction cannot be quantified and is not included in the inositol phosphate contents of the samples. Fraction 2 contains di-, tri- and tetra-phosphate esters of inositol, and Fraction 3 contains penta- and hexa-phosphates. The "total" inositol phosphate contents are determined by summing the total phosphorus contents in Fractions 2 and 3. No naturally-occurring organic phosphorus esters have been identified in soils other than the inositol polyphosphates that survive these extraction and purification procedures and elute in Fraction 2 or 3.

USE OF ISOTOPE DILUTION TRACERS

. Preliminary work indicated that the recovery of inositol hexaphosphate added to lake sediments varied with individual sediments and ranged from 70 to 100%. Therefore, the use of radiophosphorus-labelled inositol phosphates is an integral part of the procedure; these tracers allow corrections to be made for loss of the added and native inositol polyphosphates during the extraction, cleanup, and isolation procedures.

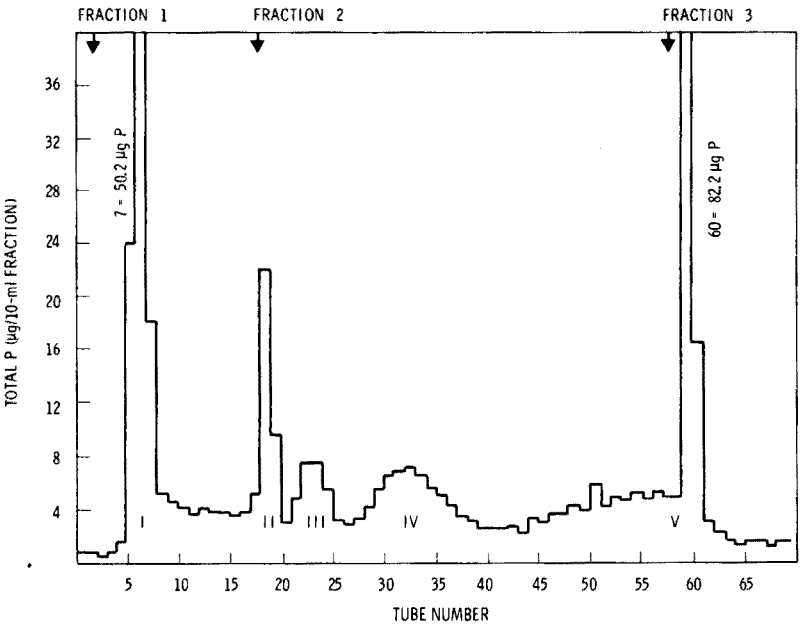

Fig. 3. Ion-exchange chromatography of standard inositol polyphosphate mixture by $HCOONH_4$ step-gradient elution. Sample: standard inositol polyphosphate mixture plus inorganic phosphorus. Column: 15 cm × 1 cm AG1-X2, 100-200 mesh, $HCOO^-$ form. Eluant: neutral $HCOONH_4$. Flow rate: 0.9—1.5 ml min^{-1} cm^{-2}. Peaks I—V, as in Fig. 2.

A well-characterized mixture of labelled inositol polyphosphates (described in Table 3) was added to the sediment samples immediately before the NaOH extraction and solubilization of all the native inositol polyphosphates. This tracer contained known quantities of inositol di- through hexa-phosphate esters. After isolation of the inositol phosphates from the sediment extract by ion-exchange chromatography, the recoveries of these labelled esters were measured by liquid scintillation counting [15]. The total phosphorus concentration in each fraction eluted was also determined and the amounts were corrected for the carrier phosphorus added with the radiotracers.

DISCUSSION AND CONCLUSION

The procedure detailed for the determination of the inositol polyphosphate content of lake sediments has been thoroughly tested during the analysis of more than 40 samples of both calcareous and non-calcareous sediments and over 20 soil samples [17]. The recoveries of radiotracer inositol phosphates after sample extraction and cleanup were 70—100% of that added; recoveries were generally greater than 85% and averaged 93.3% for 48 samples. Some loss of the radiotracer occurred during the ion-exchange chromatographic

separation of the phosphorus constituents, ranging from 0 to 25% of the tracer added to the resin column. This irreversible loss averaged 9.7% for 72 chromatographic separations. The overall recoveries through the total analysis procedure averaged ca. 85% for a great diversity of samples.

The error associated with each estimate of inositol phosphate content for these samples was calculated from replicate determinations. The standard deviation associated with the estimate of the higher ester content (penta- and hexa-phosphates) and the lower ester content (di- through tetra-phosphates) of each sample was calculated for $(n-1)$ degrees of freedom. The standard deviations were typically 10—20% of the mean estimate for the higher ester content and averaged 17%. Standard deviations of greater than 16% of the mean were obtained only for samples of low inositol phosphate content (21 $\mu g\ P\ g^{-1}$ or less). The standard deviations of estimates of the lower ester content were 16% or less of the mean value for all samples and averaged 9%.

This technique will be useful in evaluating the relative significance of the inositol phosphate esters to the pool of potentially available inorganic phosphorus in lake systems. Since inositol polyphosphates are a major constituent of both plant materials and lake sediments [17, 30], these compounds may play a major role in the aquatic phosphorus cycle. Additional research is necessary to evaluate the potential for hydrolysis of these inositol polyphosphates or their permanent immobilization in lake sediments.

This investigation was supported in part by Environmental Protection Agency Project No. 16010 EGR, and by Eastern Deciduous Forest Biome, US-IBP (National Science Foundation, and Energy Research and Development Administration, Oak Ridge National Laboratory). The cooperation and support of the University of Wisconsin Engineering Experiment Station is acknowledged.

REFERENCES

1 A. Bartsch, Environmental Protection Agency Report No. EPA-R3-72-011, 1972.
2 J. K. Syers, R. F. Harris and D. E. Armstrong, J. Environ. Qual., 2 (1973) 1.
3 C. L. Schofield, Cornell University Water Res. and Marine Science Center Technical, Report No. 13, Ithaca, New York, (1968).
4 J. J. Latterell, R. F. Holt and D. R. Timmons, J. Soil Water Conserv., 26 (1971) 21.
5 L. E. Sommers, Ph.D. Dissertation, University of Wisconsin, Madison, Wisconsin (1971).
6 G. Anderson, A. D. McLaren and G. H. Peterson (Eds.), Soil Biochemistry, M. Dekker, New York, 1967, p. 67.
7 C. L. Schofield, Cornell University, Water Res. and Marine Science Center Technical, Report No. 29, Ithaca, New York (1968).
8 J. Shapiro, W. T. Edmondson and D. E. Allison, Limnol. Oceanogr., 16 (1971) 437.
9 L. E. Sommers, R. F. Harris, J. D. H. Williams, D. E. Armstrong and J. K. Syers, Soil Sci. Soc. Am. Proc., 36 (1972) 51.
10 R. E. Wilding and R. L. Schmidt, Environmental Protection Agency Report No. EPA-53-73-024 (1973).
11 J. P. Murphy and J. P. Riley, Anal. Chim. Acta, 27 (1962) 31.
12 S. Biswas and B. B. Biswas, Biochim. Biophys. Acta, 108 (1965) 710.

13 J. K. Martin, Anal. Biochem., 36 (1970) 233.
14 W. C. Weimer, M. G. Rodel and D. E. Armstrong, Environ. Sci. Tech., 9 (1975) 966.
15 G. A. Bruno and J. E. Christian, Anal. Chem., 33 (1961) 1216.
16 C. H. Wang and D. L. Willis, Radiotracer Methodology in Biological Science, Prentice-Hall, Englewood Cliffs, New Jersey, 1965.
17 W. C. Weimer and D. E. Armstrong, Limnol. Oceanogr., submitted.
18 J. K. Martin and A. K. Wicken, N.Z. J. Agr., Res., 9 (1966) 529.
19 D. J. Cosgrove, Aust. J. Soil Res., 1 (1963) 203.
20 R. B. McKercher and G. Anderson, J. Soil. Sci., 19 (1968) 47.
21 G. Anderson, J. Sci. Food Agric., 14 (1963) 352.
22 G. Anderson, J. Sci. Food Agric., 11 (1960) 497.
23 G. Anderson and R. J. Hance, Plant Soil, 19 (1963) 296.
24 J. A. Lovern, The Chemistry of Lipids of Biochemical Significance, Methuen, London, 1955.
25 G. B. Ansell and J. N. Hawthorne, Phospholipids: Chemistry, Metabolism, and Function, Elsevier, New York, 1964.
26 T. C. Brucie and S. J. Benkovic, Bioorganic Mechanisms, Vol. II, Benjamin, New York, 1966.
27 G. C. Bortleson and G. F. Lee, Environ. Sci. Technol., 6 (1972) 799.
28 G. C. Bortleson and G. F. Lee, Limnol. Oceanogr., 19 (1974) 794.
29 J. F. Dormar, Soil Sci., 104 (1967) 17.
30 W. C. Weimer and D. E. Armstrong, Environ. Sci. Tech. submitted.

Analytica Chimica Acta, 94 (1977) 49—55

AN INTEGRATED SCHEME FOR THE RECOVERY OF THE SIX PLATINUM-GROUP METALS AND GOLD AFTER LEAD FUSION AND PERCHLORIC ACID PARTING AND A COMPARISON WITH THE LEAD CUPELLATION, TIN, AND NICKEL SULPHIDE COLLECTION SCHEMES

A. DIAMANTATOS

J.C.I. Minerals Processing Research Laboratory, Knights 1413, Transvaal (South Africa)

(Received 14th April 1977)

SUMMARY

An integrated scheme is proposed for the determination of all six platinum-group metals and gold from a single lead collector button. The button is parted with perchloric acid and acetic acid after heating at 160—180°C. Iridium and ruthenium remain unattacked as the metals together with most of the osmium; some osmium is volatilized and collected in alkali. Pt, Pd, Rh and Au pass completely into the lead perchlorate filtrate, from which they are quantitatively recovered by precipitation with 2-mercaptobenzothiazole. Ru and Os are separated by distillation, whereas Ir is recovered from the residual still liquid by solvent extraction. Comparative results on the recoveries of the precious metals in various platiniferous materials by the proposed method, and the lead cupellation, tin collection and nickel sulphide collection schemes, show that the wet-chemical analysis of the lead button yields the highest recoveries in all cases.

Recent papers have described methods for the determination of iridium [1], of ruthenium and osmium [2], and of platinum, palladium, rhodium, iridium and gold [3], respectively, after lead collection and perchloric acid parting. Although it is often more convenient to determine the two volatile metals, ruthenium and osmium, in one portion of the sample and the non-volatile metals in another portion, it is useful to have a more flexible scheme that will allow the determination of all the platinum-group metals and gold in a single sample.The integrated scheme recommended here is based on previous work [1—3].

This paper also describes a comparison of the efficiencies of the proposed wet-chemical analysis of the lead button, and the lead cupellation, tin and nickel sulphide collection techniques. Arguments about the efficiency of lead as a collector have sometimes been unnecessarily complicated by the fact that judgements have been based on the analytical results for the platinum metal content of the prill obtained after cupellation of the lead collector button. It is well known that although the six platinum metals and gold may all be quantitatively collected in the lead button [4—7], the subsequent cupellation results in an almost complete loss of osmium, appreciable losses

of ruthenium and iridium, and small losses of platinum, palladium, rhodium and gold [4, 9, 10]. Despite this, claims for the efficiency or even the superiority of the newer collectors, such as tin or nickel sulphide, have been supported [11, 12] by comparing the results obtained from wet-chemical treatment of their collector buttons with those obtained after wet-chemical attack of the prill resulting from cupellation of the lead button. Such comparisons can be unconvincing. For each technique applied, the collection stage ceases with the preparation of the collector button. Any subsequent loss of the precious metals in the particular procedure used to treat the button cannot be considered to result from inefficient collection. The proposed lead—perchloric acid parting procedure, being a non-cupellation method, permits direct evaluation of the efficiency of the lead button collector, and gives a valid comparison with the newer collectors.

EXPERIMENTAL

Apparatus and reagents

The fire-assay furnace and related equipment, the spectrophotometers and the lead flux, were the same as described recently [1]. The standard copper—nickel matte has been described [3].

Recommended procedure (See Fig. 1)

Fuse the sample with lead flux and prepare the 4-mm thick disc as described previously [3]. (Re-fuse the slag if high quantities of ruthenium, osmium or iridium are present.) Place the lead disc in a 1-l distillation flask fitted with a dropping funnel and air admission tube, and connected to two 250-ml flasks containing 100 ml of water (trap) and 100 ml of 20% NaOH solution, respectively. Introduce 300 ml of 70% perchloric acid and 30 ml of glacial acetic acid through the funnel and draw air through the apparatus at a rate of 1—3 bubbles/s. Dissolve the lead by heating at 160—180°C; some osmium volatilizes and is absorbed in the alkaline solution. After complete dissolution of lead, continue heating for 20 min at 140—150°C to ensure complete dissolution of platinum, palladium, rhodium and gold. Allow the solution to cool. Dilute the lead perchlorate solution with 200 ml of water, via the tap funnel, and mix well by increasing the bubbling rate. Disconnect the distillation apparatus and keep the alkaline receiving solution. Filter the diluted perchlorate solution through a No. 540 filter paper into a 1-l squat beaker and dilute the filtrate to 600 ml with water. Proceed with the group precipitation and determination of platinum, palladium, rhodium and gold in the lead perchlorate medium, with 2-mercaptobenzothiazole exactly as reported earlier [3]. To recover the ruthenium, osmium and iridium, wash the filter paper thoroughly with hot water, wet the filter with a 20% sodium hydroxide solution and transfer to a zirconium crucible. Char, ignite at 550°C in a muffle furnace and then fuse the residue with 3 g of powdered sodium peroxide. Leach the melt with water and combine the alkaline leach with the

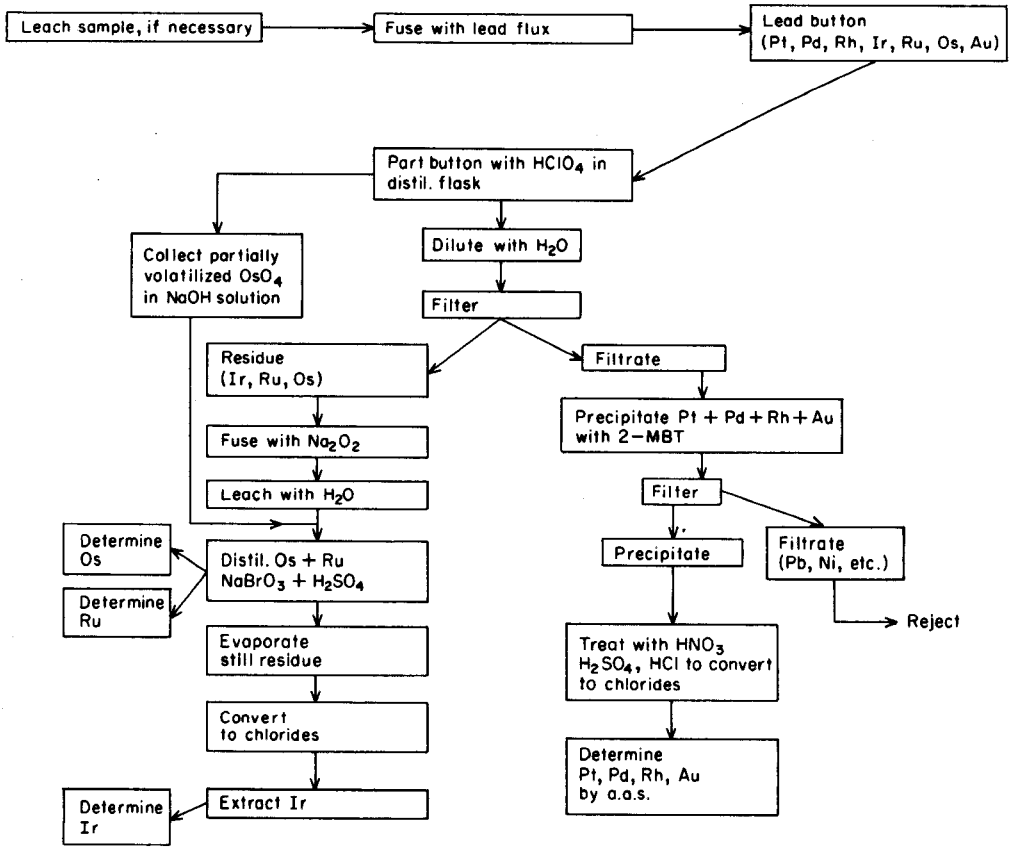

Fig. 1. Flow-sheet of the integrated analytical scheme for Pt, Pd, Rh, Ir, Ru, Os, Au.

20% sodium hydroxide solution containing the portion of osmium volatilized during the initial parting of the lead button. Proceed with the bromate—sulphuric acid distillation and determine ruthenium and osmium as described previously [2]. Transfer the solution left in the still after the distillation to a 600-ml beaker and evaporate to dryness. Boil the residue with 40—50 ml of 11 M hydrochloric acid and evaporate to dryness again. Dissolve the residue in water by boiling, and extract and determine iridium as detailed previously [1].

RESULTS AND DISCUSSION

The determination of all the platinum-group metals and gold from a single lead button

A sample (5 g) of the "standard" platiniferous copper—nickel matte [3] containing 9.82 mg of total precious metals was leached with 200 ml of 11 M hydrochloric acid and 50 g of ammonium chloride by boiling for about

2 h, to remove the bulk of the base metals. After dilution with 200 ml of water, the warm solution was filtered and the insoluble residue containing the noble metals was fused with 180 g of the lead flux. The lead—noble metals button was parted and analyzed by the recommended procedure. The individual results obtained (in ppm), were as follows: 951 Pt, 531 Pd, 91.8 Rh, 23.9 Ir, 203 Ru, 18.4 Os and 46.1 Au; the matte contained 958 Pt, 536 Pd, 93 Rh, 24.6 Ir, 205 Ru, 19 Os and 47.9 Au. These recoveries confirm the satisfactory accuracy of the proposed integrated scheme.

Comparison of the application of different methods to various platiniferous materials

A South African ore, a Canadian ore, a copper—nickel matte, a black sands sample and a sample of spent platinum-catalyst were chosen for analysis because of their different origins, compositions and ratios of precious metal content. For these analyses, all samples were weighed out in succession and fused, and the resulting buttons were treated exactly according to the recommended procedure for each method (lead—perchloric acid [2, 3], lead cupellation [9], tin [11], nickel sulphide [12]). For the tin and nickel sulphide collections, the slag was re-fused and the two buttons were combined for parting in each case. This was decided because losses to slag when only one nickel sulphide fusion is used are about 10% or more [13]. Only one fusion was used for the lead—wet chemical and lead-cupellation procedures. Care was taken to determine the noble metals concurrently and in essentially the same way, thus eliminating any errors which might have arisen from the use of different final measurement techniques. For example, when the nickel sulphide method was used, the sample was fused with the recommended flux, the slag re-fused, the buttons combined and parted exactly as recommended, and the undissolved residue filtered off. The precious metals were brought into solution and converted to their chloro complexes in hydrochloric acid solution. The noble metals were then separated by solvent extraction [14] before determination. For comparative purposes, this approach had the advantage that the final measurements were made on essentially pure solutions of each precious metal. This should minimize any unknown or unrecognized inter-elemental effects possible in the measurement of more complex solutions, the composition of which could vary with the collection method. In general, molecular absorption spectrophotometric procedures were used for the final measurements, but atomic absorption measurements were sometimes applied because of the extremely low concentration of some precious metal present. The volatile elements, ruthenium and osmium, were determined from a separate button in all cases.

Because of the lack of an international reference material, it has been assumed that the highest analytical result represents the best available value. However, the standard matte sample has been used for more than two years as a reference standard for all the precious metals, and has, during this time, been analyzed many times as a control sample by different analysts. In

addition, because of the relatively high noble metals content, the standardized figures have been obtained by methods involving acid attack of the sample without any concentration fire-assay technique. Thus these figures have been obtained by a method sufficiently different from the proposed method for it to be considered independent and reliable.

The results in Table 1 show that the lead—perchloric acid method yields recoveries for ruthenium, osmium and iridium which are at least equal to those obtained by tin and nickel sulphide collectors; but the proposed method generally gave significantly higher results for platinum and palladium than were obtained by the other methods. The nickel sulphide collection gave very low results for platinum in the Black Sands and Platinum Spent catalyst samples, possibly because these materials contain no copper, whereas the ores and the matte do. In the nickel sulphide collection, the "extractibility" of the noble metals during the fusion, appears to depend on the presence of some copper; and in fact, nickel—copper sulphide matte is a known collector [15] of the noble metals. The low results for gold by the nickel sulphide procedure are not surprising; it has already been reported [14] that this technique gives erratic and often poor yields of this metal. The primary criterion for assessing the efficiency of any collector, must centre on the collection of platinum, palladium and gold. Although efficient recovery of

TABLE 1

Comparison of noble metal recoveries by various collection procedures (all results in ppm)

Sample	Collection method	Average results (mean of 3 determinations)						
		Pt	Pd	Rh	Ir	Ru	Os	Au
South African ore	Pb cupellation	4.06	1.71	0.33[a]				0.34[a]
50 g	Sn	4.08	1.73	0.28[a]				0.31[a]
	NiS	3.96	1.71	0.28[a]				0.27[a]
	Pb—wet analysis	4.49	1.76	0.32[a]				0.34[a]
Canadian ore	Pb cupellation	2.51	14.99					0.60[a]
50 g	Sn	2.61	14.88					0.58[a]
	NiS	2.58	14.89					0.47[a]
	Pb—wet analysis	2.77	15.68					0.59[a]
Cu—Ni matte	Pb cupellation	947	524	92.3	—	—	—	46.1
5 g	Sn	931	519	91.6	21.6	191	16.8	45.4
	NiS	923	512	91.6	22.7	202	17.9	42.2
	Pb—wet analysis	957	532	92.5	23.7	202	18.0	46.1
Black sands	Pb cupellation	4.6			—		—	199
12 g	Sn	4.1			6.0		13.0	196
	NiS	3.8			6.0		13.9	188
	Pb—wet analysis	5.2			6.0		13.8	219
Spent Pt-catalyst	Pb cupellation	7065		10[a]				
3 g	Sn	6814		7[a]				
	NiS	6429		7[a]				
	Pb—wet analysis	7105		10[a]				

[a]Determined by a.a.s.

the minor elements is also important, the major elements are of greater interest for industrial purposes. The lead—wet chemical method appears more efficient than the other collection methods.

CONCLUSION

Although the proposed scheme permits the determination of all seven noble metals from a single lead button, it is preferable to determine the two volatile elements, ruthenium and osmium, from a separate button [2]. The button used for the determination of the other precious metals can then be parted more conveniently with perchloric acid in a beaker [3], without any precautions for losses of osmium. The residue after parting is used for the determination of iridium. The two buttons can be parted more or less simultaneously, which saves time and gives increased accuracy, especially in unskilled hands. The use of two samples is also recommended for the tin and nickel sulphide collector methods when high accuracy is required [11, 12].

The recommended procedure can, of course, be substantially shortened when only partial analyses are required; for example, this is possible for the spent platinum catalyst which contains only platinum and traces of rhodium. If ruthenium and osmium are absent, or of no interest, or if iridium alone is required, the recommended method provides a very simple isolation procedure [1] for this element. In addition, since iridium is completely unattacked by the controlled parting procedure used, and so can be isolated by simple filtration, it could be determined finally by spectrographic techniques.

In the recommended procedure, the (Pt, Pd, Rh, Au)—2-mercaptobenzothiazole precipitate is finally converted to a hydrochloric acid solution and then analyzed by atomic absorption spectrometry. The precipitate could also be dissolved in a solvent, e.g. methyl isobutyl ketone, for direct atomization. This approach would substantially reduce the time needed for a complete analysis and would be useful in more routine work. These examples indicate how the scheme may be altered to accommodate individual requirements.

A possible use of the proposed method should be mentioned. In fire-assay laboratories using the classical lead-cupellation procedure, correction factors are generally applied to compensate for losses during cupellation; normally, the large numbers of samples analyzed are of very similar composition. The proposed lead—wet chemical method could serve as an arbitration method to establish accurate correction factors for determinations of platinum, palladium and gold.

In conclusion, the lead—perchloric acid method yields accurate results, with no discernible bias, and with good precision [1—3]. It improves on the classical lead-cupellation procedure by obviating the cupellation step, so that ruthenium, osmium and iridium can be determined and the recoveries of platinum and palladium improved. Although it loses the advantage of the simplicity of lead removal, which is typical of the cupellation procedure, it retains the lead collector with its known efficient collection properties. It is,

to the best knowledge of the author, the first integrated scheme which depends on recovery of all the platinum-group metals and gold, directly after parting the lead button with perchloric acid. Organic precipitants other than 2-mercaptobenzothiazole for the recovery of the noble metals may be found, which would improve the schemes for the wet analysis of the collector button.

The author is indebted to Professor A. A. Verbeek (University of Natal) for helpful discussions and suggestions.

REFERENCES

1 A. Diamantatos, Anal. Chim. Acta, 90 (1977) 179.
2 A. Diamantatos, Anal. Chim. Acta, 91 (1977) 281.
3 A. Diamantatos, Anal. Chim. Acta, 92 (1977) 161.
4 F. E. Beamish, Analytical Chemistry of Noble Metals, Pergamon Press, 1966.
5 W. F. Allen and F. E. Beamish, Anal. Chem., 22 (1950) 451.
6 J. I. Watterson, R. V. D. Robert and E. van Wyk, Nat. Inst. Metall., Rep. S. Afr., Rep. No. 1048, 1970.
7 R. R. Keays and T. Donnelly, paper presented at the Conference on Platinum Metals, Melbourne, 5—6th October, 1971.
8 F. E. Beamish and J. C. van Loon, Min. Sci. Eng., 4 (1972) 3.
9 H. R. Adam, J. Chem. Metall. Min. Soc. S. Afr., 28 (1928) 106.
10 K. Beyermann, Z. Anal. Chem., 200 (1964) 161.
11 G. H. Faye and P. E. Moloughney, Talanta, 19 (1972) 269.
12 R. V. D. Robert, E. van Wyk, R. Palmer and T. W. Steele, Nat. Inst. Metall., Rep. S. Afr., Rep. No. 1371, 1971; J. S. Afr. Chem. Inst., 25 (1972) 179.
13 K. Dixon, E. A. Jones, S. Rasmussen and R. V. D. Robert, Nat. Inst. Met., Rep. S. Afr., Rep. No. 1714, 1975.
14 A. Diamantatos, Anal. Chim. Acta, 67 (1973) 317.
15 W. R. Schoeller and A. R. Powell, The Analysis of Minerals and Ores of the Rarer Elements, Charles Griffin, London, 3rd edn., 1955.

Analytica Chimica Acta, 94 (1977) 57—62

EFFECTS OF QUATERNARY AMMONIUM BASES ON VALENCE-SATURATED BUT COORDINATION-UNSATURATED CHELATES
Part IV. Extraction of some Divalent Metal 8-Hydroxyquinolinates

SHINICHIRO NORIKI and MASAKICHI NISHIMURA

Analytical Chemistry Division, Department of Chemistry, Faculty of Fisheries, Hokkaido University, Hakodate 041 (Japan)

(Received 8th March 1977)

SUMMARY

The effect of zephiramine on the chelate formation and extraction of some divalent metals with oxine is reported. In the presence of zephiramine, the non-extractable 1:2 zinc— and cadmium—oxine chelates as well as the extractable 1:2 nickel— and manganese—oxine chelates become highly coordinated ternary complexes, $M(Q)_3$ (zeph), which are easily extracted into 1,2-dichloroethane. Copper is easily extracted into 1,2-dichloroethane as $Cu(Q)_2$, which is not affected by zephiramine.

8-Hydroxyquinoline (oxine) reacts with at least 43 metals which usually form hydroxides with ammonia. Divalent and trivalent metal oxinates have the general formulae $M(Q)_2$ and $M(Q)_3$, respectively, where Q denotes 8-hydroxyquinolinate. Some of these divalent metal oxinates are neutral but coordination-unsaturated chelates which are poorly extracted into inactive solvents [1, 2].

It has been reported [3—5] that coordination-unsaturated chelates become coordination-saturated and can be extracted into inactive solvents when a quaternary ammonium base is present. For example, magnesium oxinate [4], $Mg(Q)_2 \cdot 2H_2O$, is not extracted into inactive solvents, but the highly coordinated, extractable $Mg(Q)_3 \cdot$ (zephiramine) complex is formed in the presence of tetradecyldimethylbenzylammonium chloride (zephiramine).

This paper shows that zephiramine has a similar effect on zinc, cadmium, nickel and manganese oxinates. These metals are also quantitatively extracted into 1,2-dichloroethane in the presence of zephiramine, as the ternary complex $M(Q)_3$ (zeph).

EXPERIMENTAL

Reagents

Standard metal solution (1×10^{-2} M). Solutions of cadmium, zinc, nickel, or manganese were prepared by dissolving cadmium nitrate or the other metal sulfates, and standardized with EDTA.

Oxine solution (1×10^{-2} M) in 1,2-dichloroethane, and aqueous zephiramine solution (2×10^{-2} M) were prepared. Acetate (for pH < 6.2) and borate (for pH > 6.2) buffers were used. All the chemicals used were of analytical-reagent grade.

Procedure

The solutions of ion, buffer and zephiramine were placed into a separating funnel and diluted to 20 ml with water. An equal volume of oxine solution was added and the funnel was shaken for 10 min. The organic phase was dried by filtration through paper, and the absorbance was measured against a reagent blank solution. The distribution ratio was calculated from the metal concentration in the aqueous phase determined by atomic absorption spectrometry.

RESULTS AND DISCUSSION

Zinc

Zinc oxinate, $Zn(Q)_2 \cdot 2H_2O$, is not extracted into inactive solvents, but zinc is quantitatively extracted with oxine in the presence of zephiramine. The absorption spectrum of the extracted species is shown in Fig. 1. The bright yellow zinc oxinate solution has a strong absorption and the reagent shows no absorption at 400 nm. The molar absorptivity at 400 nm is 7.0×10^3 l mol^{-1} cm^{-1}.

After the conditions for extraction had been determined, the composition of the extracted zinc species was examined. The extraction curves against pH of the aqueous solution are shown in Fig. 2. The $pH_{\frac{1}{2}}$ values (50% extraction) are 7.28 and 8.38 at 0.01 M and 0.001 M concentration of oxine (Table 1). The difference between these $pH_{\frac{1}{2}}$ values is almost unity, which shows that there is no adduct formation by neutral oxine molecules. The slopes of the extraction curves indicate that three protons are released by formation of the zinc—oxine chelate. The dependence of the logarithm of the distribution

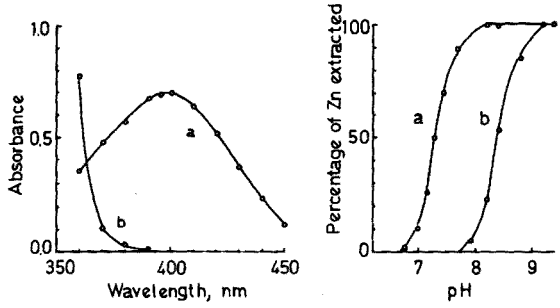

Fig. 1. Absorption spectra. (a) Zn—oxine—zephiramine complex vs. reagent blank. (b) Reagent blank vs. water. Zn = 10^{-4} M, HQ = 10^{-2} M, zeph = 10^{-3} M, pH 9.0.

Fig. 2. Effect of pH on extraction of Zn—oxine chelate. (a) HQ = 10^{-2} M, and (b) HQ = 10^{-3} M. Zn = 10^{-4} M, and zeph = 10^{-3} M.

TABLE 1

8-Hydroxyquinoline complexes in the presence of 10^{-3} M zephiramine

Complex extracted	Absorption maximum (nm)	ϵ (l mol^{-1} cm^{-1})	$pH_{\frac{1}{2}}$	
			0.01 M[a]	0.001 M[a]
$Zn(Q)_3$ (zeph)	400	7.0×10^3	7.28	8.38
$Cd(Q)_3$ (zeph)	400	6.5×10^3	6.82	7.96
$Ni(Q)_3$ (zeph)	400	7.3×10^3	4.18	5.25
$Mn(Q)_3$ (zeph)	400	7.6×10^3	7.30	—
$Mg(Q)_3$ (zeph)[b]	390	6.5×10^3	8.95	—

[a]8-Hydroxyquinoline concentration. [b]Reported previously [4].

ratio on log [HQ] is shown in Fig. 3 (curve a); the straight line for zinc with a slope of 3 indicates that a $[Zn(Q)_3]^-$ species is extracted. The continuous variations methods (Fig. 4) show that the molar ratio of $Zn:Q^-$ is 1:3 and the ratio of Zn : zeph is 1:1.

It can be concluded that the quaternary ammonium base, zephiramine, changes the ordinary zinc chelate, $Zn(Q)_2$, to a $Zn(Q)_3$ (zeph) ternary complex which is extractable into 1,2-dichloroethane.

Cadmium

Although it has been reported [2, 3] that cadmium forms an extractable chelate, $Cd(Q)_2 \cdot 2(HQ)$, the chelate is unstable and is decomposed during the extraction. Therefore, cadmium is not practically extracted with oxine.

The extracted chelate in the presence of zephiramine has an absorption maximum at 400 nm, and the molar absorptivity is 6.5×10^3 l mol^{-1} cm^{-1}. The equilibrium shift method (Fig. 3, curve c) and the continuous variations

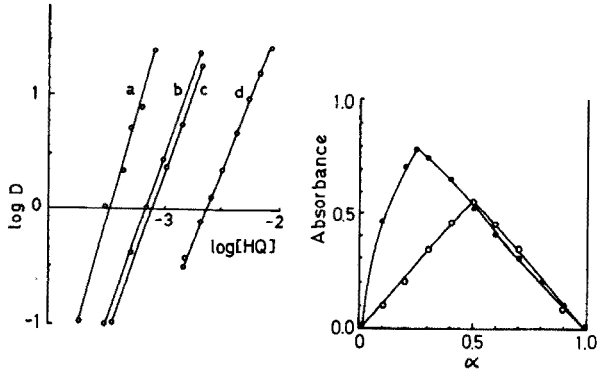

Fig. 3. Dependence of log D on log [HQ] in the presence of 10^{-3} M zephiramine. (a) Zn at pH 8.5; (b) Mn at pH 8.5; (c) Cd at pH 8.0; and (d) Ni at pH 4.95.

Fig. 4. Continuous variations method for zinc—oxine and zinc—zephiramine. ○ α = Zn/(Zn + zeph); Zn + zeph = 2×10^{-4} M, and HQ = 5×10^{-3} M; ● α = Zn/(Zn + HQ); Zn + HQ = 5×10^{-4} M, and zeph = 10^{-3} M.

method indicate that the extracted cadmium chelate has the composition metal : oxine : zeph = 1 : 3 : 1.

Nickel

Since the ordinary nickel oxinate has no coordinated water molecules, $Ni(Q)_2$ can be extracted into organic solvents in the absence of zephiramine. In the presence of zephiramine, however, another type of oxinate is formed. This complex is more easily extracted and the extraction equilibrium is attained more rapidly, compared with the ordinary oxinate [1]. As shown in Fig. 5, the absorbance increases and the wavelength of absorption maximum shifts from 370 nm to 400 nm in the presence of zephiramine. The molar absorptivities of the nickel chelates are 4.0×10^3 l mol^{-1} cm^{-1} at 370 nm in the absence of zephiramine and 7.3×10^3 l mol^{-1} cm^{-1} at 400 nm in the presence of zephiramine.

From Figs. 3 (curve d) and 6, and the $pH_{\frac{1}{2}}$ values (Table 1), it is concluded that the extracted nickel chelate has a Ni : oxine ratio of 1 : 3. In the case of nickel, the continuous variations method cannot be applied to the determination of the Ni : zeph ratio, as both the ordinary and the higher chelates are extracted simultaneously. Another approach was therefore tried. The extraction system is assumed to be as follows: in the absence of zephiramine,

$$Ni^{2+} + 2HQ \underset{K_{ex},\,1}{\rightleftharpoons} Ni(Q)_2 + 2H^+$$

and in the presence of zephiramine,

$$Ni^{2+} + 3HQ + n\ zeph^+ \underset{K_{ex},\,2}{\rightleftharpoons} Ni(Q)_3\,(zeph)_n^{n-1} + 3H^+$$

where K_{ex} denotes the extraction constant. Both chelates are quantitatively extracted into the organic phase above pH 5.5. Thus:

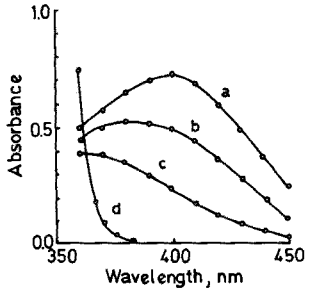

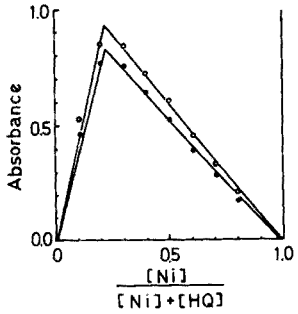

Fig. 5. Absorption spectra. (a) Ni—oxine chelate vs. reagent blank in the presence of 10^{-3} M zephiramine; (b) in the presence of 4×10^{-4} M zephiramine; (c) in the absence of zephiramine, and (d) reagent blank vs. water. Ni = 10^{-4} M, HQ = 10^{-2} M, pH 4.95.

Fig. 6. Continuous variations method for Ni—oxine chelate. Ni + HQ = 10^{-3} M, zeph = 5×10^{-3} M, and pH 5.8. ○ at 400 nm, and ● at 420 nm.

$$\frac{K_{ex,2}}{K_{ex,1}} = \frac{[Ni(Q)_3(zeph)_n]^{n-1}_{org}\,[H^+]}{[Ni(Q)_2]_{org}\,[HQ]_{org}\,[zeph^+]^n} \quad (1)$$

In the presence of 10^{-3} M zephiramine, nickel is completely extracted as a $Ni(Q)_3(zeph)_n$ species, and its molar absorptivity is 7.30×10^3 l mol^{-1} cm^{-1} at 400 nm; in the absence of zephiramine, the molar absorptivity of $Ni(Q)_2$ is 2.35×10^3 l mol^{-1} cm^{-1} at 400 nm. When the concentration of zephiramine is less than 10^{-3} M at pH 5.5, the absorbance of the organic phase at 400 nm is given by

$$\begin{aligned} Abs_{400\,nm} &= \epsilon_1[Ni(Q)_2] + \epsilon_2[Ni(Q)_3(zeph)_n] \\ &= \{2.35 \times 10^3 \times X + 7.30 \times 10^3 \times (1 - X)\} \times C_{Ni} \end{aligned}$$

or

$$Abs_{400nm} = (7.30 - 4.95X) \times 10^3 \times C_{Ni} \quad (2)$$

where ϵ_1 and ϵ_2 are the molar absorptivities of $Ni(Q)_2$ and $Ni(Q)_3(zeph)_n$, respectively, X is the proportion of $Ni(Q)_2$ in the extracted chelates, and C_{Ni} is the total concentration of nickel.

Equation (1) can be rewritten as follows:

$$\frac{K_{ex,2}}{K_{ex,1}} = \frac{[1 - X]\,[H^+]}{[X]\,[HQ]_{org}\,[zeph^+]^n} \quad (3)$$

The absorbances at 400 nm were measured at various concentrations of zephiramine. From eq. (2), the value of X was calculated at a low concentration of zephiramine, and the dependence of log ([1 − X]/[X]) on log [zeph] is shown in Fig. 7. The straight line with a slope of 1 (Fig. 7) indicates that $n = 1$; thus the extracted nickel complex has a Ni: zeph ratio of 1:1. Accordingly, the composition $Ni(Q)_3(zeph)$ is confirmed for the ternary complex formed in the presence of zephiramine.

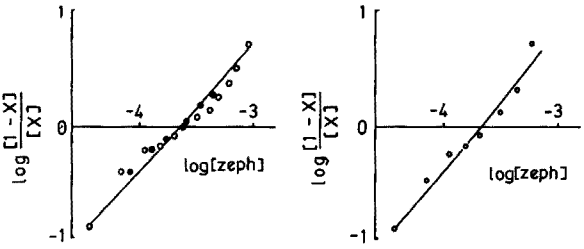

Fig. 7. Dependence of formation of the Ni—oxine—zephiramine complex on zephiramine concentration. HQ = 10^{-2} M, and pH 5.5. ○ Ni = 10^{-4} M. ● Ni = 5×10^{-5} M.

Fig. 8. Dependence of formation of Mn—oxine—zephiramine complex on zephiramine concentration. Mn = 10^{-4} M, HQ = 10^{-2} M, and pH 9.2.

Manganese

The ordinary manganese—oxine chelate is extractable, but manganese is also easily extracted as the ternary complex $Mn(Q)_3$(zeph) in the presence of zephiramine (Fig. 3, curve b, and Fig. 8). The absorbance is enhanced and the wavelength of absorption maximum shifts from 390 nm to 400 nm in the presence of zephiramine. The molar absorptivities of the extracted chelates are 4.8×10^3 at 390 nm in the absence of zephiramine and 7.6×10^3 l mol^{-1} cm^{-1} at 400 nm in its presence.

Copper

Copper is easily extracted into 1,2-dichloroethane as $Cu(Q)_2$, and zephiramine has no effect on the chelate as in the case of the Cu-*o*-(salicylideneamino)phenol chelate [3].

REFERENCES

1 J. Stary, The Solvent Extraction of Metal Chelate, Pergamon, Oxford, 1964, p. 80.
2 J. Stary, Anal. Chim. Acta, 28 (1963) 132.
3 M. Nishimura, S. Noriki and S. Muramoto, Anal. Chim. Acta, 70 (1974) 121.
4 S. Noriki and M. Nishimura, Anal. Chim. Acta, 72 (1974) 339.
5 S. Noriki, Anal. Chim. Acta, 76 (1975) 215.

Analytica Chimica Acta, 94 (1977) 63—73

THE DETERMINATION OF ZINC IN BLOOD PLASMA BY ATOMIC ABSORPTION SPECTROMETRY §

GERALD P. BUTRIMOVITZ

Department of Chemistry, University of Maryland, College Park, MD 20742 (U.S.A.)

WILLIAM C. PURDY*

Department of Chemistry, McGill University, 801 Sherbrooke Street West, Montreal, Quebec, H3A 2K6 (Canada)

(Received 26th April 1977)

SUMMARY

Atomic absorption spectrometry has been used in the analysis of plasma zinc because of its sensitivity and simplicity. Dilution techniques reduce the viscosity of plasma and facilitate direct analysis, but viscosity differences can produce deviations in aspiration rates between sample and standard, and so cause errors. A direct (1 + 4) dilution of plasma with deionized water is suggested. Working zinc standards are prepared in 5% glycerol to approximate the viscosity characteristics and aspiration rates of the diluted plasma samples. The analytical curves for diluted plasma samples and 5% glycerol working standards proved identical. Plasma zinc concentrations are accurately calculated from a daily working curve. The accuracy of the method exceeds 99% and recovery of added inorganic zinc to a pooled plasma averages 99.8%. The precision is primarily limited by baseline drift. A confidence interval of ± 2 μg/100 ml was achieved by means of six contiguous 10s-integration readings. The method is free of nebulizer clogging and matrix interferences and is not subject to significant day-to-day variations. Because the method is accurate, sensitive, reliable and specific, it should be useful in the clinical laboratory.

Plasma zinc has been assayed by various procedures including colorimetry, neutron activation, fluorimetry and atomic absorption spectrometry (a.a.s.) [1, 2]. A.a.s. has been used for most routine analysis because of its low cost of operation, sensitivity and precision [2, 3]. Even in the presence of a complex ionic matrix, analysis for zinc can be interference-free [4]. Before the advent of the Boling burner, which is suited to high solids matrices, sample preparation required precipitation of the plasma proteins by trichloroacetic acid [5]. The method was time-consuming and costly, and trace contaminants could be introduced [6]. Sprague and Slavin [7] suggested a direct method for plasma zinc requiring a (1 + 1) dilution with water. The zinc standards were also prepared in water. Although the method was free of chemical interferences, the burner head had to be modified to prevent clogging

§ Taken in part from the Ph.D. dissertation of Gerald P. Butrimovitz, University of Maryland, 1977.

from plasma proteins. Accuracy was poor, perhaps because of flow rate or viscosity differences between sample and standard. Hackley et al. [8] also used a (1 + 1) dilution with water; the zinc working standards were prepared in 3% dextran solution to match the viscosity of the diluted plasma and recoveries averaged 99%. Reinhold et al. [9] further explored the effect of various flow rates and viscosities on plasma zinc analysis. They pointed out that when dilute plasma samples were aspirated through thin capillaries, significant changes occurred in flow rate and absorbance readings, because of apparent viscosity differences between plasma sample and standard. They concluded that a minimum twofold dilution was necessary for precise and accurate measurements.

In order to obviate errors from clogging, others [10—13] suggested 10- and 20-fold dilutions, but a lowered signal sensitivity necessitated the addition of nitric acid or n-butanol as enhancing agents [10, 11]. Extreme dilution may also contribute to reduced precision from greater pipetting errors, inhomogeneity of the dilute sample and a relatively low signal-to-noise ratio [10]. Because the viscosity effect of dilute plasma cannot be totally reduced by extreme dilution, Pekarek et al. [13] suggested a method utilizing (1 + 4) dilution of plasma, which gave higher signal sensitivities without capillary clogging. Although reproducible values were obtained with aqueous standards, the accuracy of the values was not confirmed.

It has been suggested [14] that the largest source of error in flame methods arises from differing viscosities and thus flow rates between sample and standard. Glycerol has been previously used as a viscosity adjuster for clinical measurements [13]. Its versatility comes from its capacity to maintain homogeneity with buffer solutions over a wide range of concentrations. Its flow and viscosity characteristics are well defined [14, 15]. An a.a.s. methods handbook [16] suggests that the viscosity of a (1 + 4) diluted serum sample nearly matches the viscosity of zinc standards prepared in 5% glycerol.

In the method described below, the one-step dilution of plasma with a fourfold addition of deionized water is recommended. Working zinc standards are prepared in 5% glycerol solutions to approximate the viscosity and aspiration rates of the diluted plasma samples [9, 14, 16]. Because the technique is accurate, sensitive, reliable and specific, it is suitable for routine clinical laboratories [17].

EXPERIMENTAL

Reagents and materials

All reagents, diluents and containers utilized were regarded as possible sources of zinc contamination and were subjected to a continuous quality control program. Although sources of materials are given, other sources may prove satisfactory.

All volumetric glassware must meet NBS Class A specifications. Glassware and Pasteur pipets are acid-washed (No-Chromix, Godax Laboratories,

New York, N.Y. 10013), soaked in 1% Na_2EDTA solution for 24 h and rinsed 6 times with deionized water.

Disposable serological pipets 0.5 ml (Borosilicate glass; Kimble-Division, Owens-Illinois, Pittston, Pa. 18640) and polystyrene tubes (16 × 25 mm; Falcon Division, Becton, Dickinson and Co., Oxhard, California 93030) were routinely found not to contribute detectable concentrations of zinc and required no pretreatment.

Glycerin (Certified A.C.S., 99.4%, Fisher Scientific Company, Silver Spring, Maryland 20910) was used to prepare a 5% (v/v) glycerol solution in deionized water. The deionized water had a specific resistance of at least 10^6 ohms at 25°C.

Stock zinc standards. For the primary zinc standard (1000-ppm zinc), dissolve 1.000 g of zinc metal (Zinc Powder-200 mesh, Alfa Inorganics, Beverly, Mass.) in 50 ml of dilute (1 + 4) nitric acid (Ultrex Nitric Acid, J.T. Baker Chemical Co.) and further dilute to 1 l.

The secondary standard (1000-ppm zinc) was Fisher Scientific Certified Standard.

Working standards are prepared as follows. Deliver 1 ml of 1000-ppm zinc standard to a 100-ml volumetric flask and dilute with 5% glycerol to produce a 10-ppm zinc—5% glycerol solution. Invert the solution 16 times. Add 1, 2, 3 and 4-ml aliquots of this solution to 100-ml volumetric flasks and dilute with 5% glycerol to produce 10, 20, 30 and 40 μg/100 ml zinc working standards. Invert the solutions 16 times. Plot these standards on the working curve as apparent concentrations of 50, 100, 150, 200 μg/100 ml, because plasma samples are diluted to one-fifth their original concentration. The zinc concentration of the plasma samples are thus read directly from the working curve. Prepare standards daily.

Pooled plasma standards. Plasma (e.g., obtained from plasma packs) is pooled, centrifuged at 900 g for 20 min and decanted. Aliquots are stored in polyethylene vials (which were found to contribute no zinc) at −20°C and are stable for at least one year.

Collection and handling of specimens

Collect 3—5 ml of blood by venipuncture with all plastic polyethylene syringes (Peel A Way Scientific, So. El Monte, California 91733) and stainless steel needles (Monojet-250. Sherwood Medical Industries, Inc., Delano, Florida 32720) or Butterfly (21 or 23) infusion sets (Abbott Laboratories, North Chicago, Ill., 60064). Add 2 drops (0.10 ml) of a 30% (w/v) sodium citrate (reagent grade) anticoagulant solution to the syringe before blood collection. Centrifuge promptly at 900 g for 20 min with the syringe serving as the centrifuge tube. Pipette the plasma into polyethylene vials (Mini-Scintillation Vials; Fisher Scientific, Cat. No. 3-337-20) and freeze at −20°C. Care is taken not to disrupt the buffy coat or packed cells. Hemolyzed samples are discarded; platelets and red cells introduce high levels of zinc into the sample [18, 19].

Procedure

Prepare working standards as described above. Thaw plasma samples at room temperature and invert 6 times. Transfer a 0.5-ml sample with a serological pipet to a 125-mm test tube. Add 2 ml of deionized water. Cover the tube with a parafilm slip and vortex for 30 s. Repeat this for plasma samples in groups of 10. Prepare a pooled plasma sample similarly.

Establish instrumental and gas flow settings precisely as listed in Table 1. Once the aspiration rate is established for 10-ml samples of water, lock the nebulizer flow adjustment in place; to facilitate the re-establishment of the aspiration rate, a groove may be etched onto the assembly. Aspirate a 5% glycerol solution and establish the baseline in the absorbance mode to read 0.000 ± 0.001. A baseline reading is taken before and after each sample and re-established as required.

Aspirate the zinc working standards sequentially, from most dilute to most concentrated, until stable readings (±0.001) are achieved and record the following six contiguous 10-s-integration absorbance readings. Three readings produce slightly inferior precision. Take the average for each standard. Use these values to establish the daily working curve, preferably by a regression least-squares fit. Vortex a pooled plasma sample again and aspirate. Calculate the concentration by interpolation from the working curve. Results must be within 2 μg/100 ml of the established value. (Though a plasma zinc standard is not yet available, a laboratory reference standard can be established by the method of additions [20]. The precision of this method may fluctuate with the condition of the equipment.) Finally vortex plasma samples and read similarly in groups of ten. Aspirate working standards after each group.

TABLE 1

Instrumental settings for the Perkin-Elmer 403 atomic absorption spectrophotometer with Boling burner head and zinc intensitron lamp

Instrumental settings			
Wavelength	213.8 nm	Gain	Midscale
Slit width	4	Lamp focus	Grazing burner head[a]
Mode	Absorbance—10-s integration	Burner height	7.75[a]
Lamp Current	15 mA	Flame	Luminescent (fuel-rich)

Gas flow settings	Pressure (psi)	Flowmeter
Air	30	54
Acetylene	9	38

Aspiration rate (H_2O) 6.0 ± 0.1 ml min^{-1}

[a]Burner height is adjusted just to intersect the lamp beam.

RESULTS AND DISCUSSION

Standard working curve

Figure 1 illustrates a typical working curve for zinc standards prepared in 5% glycerol. Several plasma samples of known zinc concentration (Table 5) are also plotted. The analytical curve formed by these plasma samples is identical with the curve for the working standards (Table 2). Thus the plasma matrix at a fourfold dilution has no marked effect on zinc measurements within the physiological range. The linearity of these curves was established to 200 μg/100 ml.

Effects of varying glycerol concentrations

When zinc standards are prepared in 0 and 10% glycerol solutions, the resulting curves (Fig. 2) are significantly different than either the zinc—5% glycerol or plasma zinc curves ($P < 0.05$, Table 2). The multiplicative errors that would arise in estimating a pooled plasma from these standard curves are reported in Table 3. Though the errors appear slight, they are significant. The aspiration rates for these solutions are also presented, illustrating the well-known fact that the population of zinc atoms measured in the flame is regulated in part by the velocity of sample aspiration, which is controlled by the viscosity of the solution [14]; 98—99% of the viscosity of the plasma is accounted for by the protein concentration [22]. Viscosity measurements were carried out on 0%, 5%, 10%, glycerol and diluted plasma samples with a capillary Cannon—Master viscometer [23] at 25°C (Table 4). Clearly, the viscosity of a 5% glycerol solution approximates that of a diluted pooled plasma.

Harkness [22] presented a viscosity (cP)—total protein (T.P.) plot for normal plasma solutions. By extrapolating this semi-log plot to 0 g% T.P., theoretical viscosity values were calculated for dilute plasma solutions (Table 4). A fourfold dilution of the pooled plasma (T.P. = 6.2 g%) produced

TABLE 2

t-Test for two slopes[a]

Slopes tested[b]	t Value	Significance between slopes
5—0% glycerol	$t = 4.04$	$P < 0.01$
5—10% glycerol	$t = 3.54$	$P < 0.05$
0—10% glycerol	$t = 7.58$	$P < 0.01$
Plasma—5% glycerol	$t = 1.23$	N.S.
Plasma—0% glycerol	$t = 2.37$	$P < 0.05$ (1 sided)
Plasma—10% glycerol	$t = 4.39$	$P < 0.01$

[a] $t = (b - b')/S_{yx}\left(\frac{1}{SSX} + \frac{1}{SSX'}\right)^{1/2}$ [21]. Note "b" is the slope.

[b] Figs. 1 and 2.

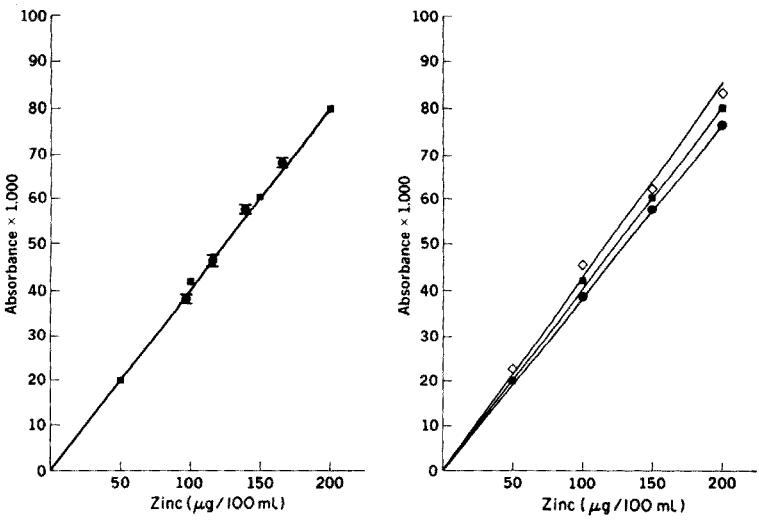

Fig. 1. Standard working curve for zinc in 5% glycerol (▪). Plasma samples of known zinc concentration (± 2 s.d.) are also plotted (•).

Fig. 2. Standard working curves for zinc. ◇ 0% glycerol. ▪ 5% glycerol. • 10% glycerol.

a solution with a protein content of 1.24 g%. Calculation of viscosity from this relationship yielded a theoretical value of 0.98 cP, identical to that found experimentally. Further validity of these measurements was established through the viscosity measurement of water. A value of 0.90 cP was found, in agreement with the literature value of 0.89 cP.

TABLE 3

Errors arising from the use of different standard curves.

	Matrix			
	0% glycerol	5% glycerol	10% glycerol	Pooled plasma
Relative concentration readings (μg/100 ml)[a]	84.1	91.7	95.3	91.9
Aspiration rate, (ml min^{-1})	6.0	5.7	5.4	5.8
Viscosity (cP): experimental[b]	0.90	1.04	1.25	0.98
theoretical[c]	0.89			0.98
Flow (ml min^{-1})	2.00	1.76	1.50	1.84

[a]Concentrations were calculated from an absorbance of 0.038 with respect to each working curve.
[b]Measurements of viscosity and flow were taken at 25.0°C with a Cannon-Master viscometer with flow times exceeding 125 s.
[c]Calculated from reported data [22].

TABLE 4

Viscosity measurements

Viscometer[a]	Matrix	ml[b]	t_{av} (s)	Flow (ml min^{-1})	Kinematic viscosity $t_{av} \times C$	d_{ave}[c] (g ml^{-1})	Absolute viscosity η_{abs}
M104	Water	3.64	108.94	2.00	0.89993	0.997	0.897
M104	5% glycerol	3.64	124.39	1.76	1.02756	1.011	1.039
M105	10% glycerol	3.54	141.20	1.50	1.21856	1.025	1.249
M104	Plasma[d]	3.64	118.52	1.84	0.97907	1.002	0.981
Calculated Viscosity[e]							
	(g% protein)						
	1.24[d]						0.98
	1.32—1.68[f]						0.98—1.02
	0.75[g]						0.93

[a]Cannon-Master Viscometer at 25°C. [b]Volume of aqueous charge in viscometer. [c] Density measured with a Hubbard Pycnometer at 25°C. [d]Value represents a fourfold dilution of a pooled plasma (6.2 g%). [e]Data approximated from published data [22]. [f]Values represent a fourfold dilution of normal plasmas (6.6—8.4 g%).[g] Value represents a ninefold dilution of a typical plasma (7.5 g%).

Normal plasma protein concentration may range from 6.6 to 8.4 g%. Through fourfold dilution, the otherwise wide viscosity range is minimized. The contribution of proteins to the viscosity of ninefold diluted plasma is still substantial (Table 4). It appears that aqueous zinc solutions are inappropriate as working standards in the measurement of diluted plasma. The similar zinc concentrations, aspiration rates, viscosities, and flow rates for the 5% glycerol standard and diluted pooled plasma sample (Table 3) confirm the need for adjusting the aspiration rate of the standard to the sample.

Standard addition curve

The method of standard additions [21] was utilized to establish the zinc concentration of a plasma pool as 91.9 μg/100 ml. The concentration of the plasma pool was calculated from the 5% glycerol working curve to be 91.7 μg/100 ml. The essential identity of these results indicates that there are no chemical interferences in the determination of zinc in fourfold diluted plasma.

Recovery study

Accuracy was further tested through recovery studies in which varying concentrations of inorganic zinc(II) was added to a pooled plasma. Recovery was calculated from the zinc—5% glycerol working curve (Table 5); the average recovery was 99.8%. Plasma zinc concentrations could therefore be calculated accurately from the zinc—5% glycerol working curve.

Newer a.a.s. instruments are equipped with direct concentration readouts. Once linearity of the working curve has been established, the instrument is calibrated with a single zinc standard. In a typical series of analyses (6 separate runs) of a pooled plasma sample by the factor method, the average zinc recovery was 99.2% (± 2.1% s.d.), when a 20 μg Zn/100 ml—5%

TABLE 5

Recovery of zinc added to pooled plasma

Zinc added (μg/100 ml)	Found (μg/100 ml)	Expected (μg/100 ml)	Recovery (%)
0	92	—	—
25	114	117	97.4
50	143	142	100.7
75	169	167	101.2
			$\bar{X}$ = 99.8 ± 2.1

glycerol working standard was set to read 100 μg/100 ml; for this series, each of the six values was the average of six successive readings on each sample. Although a daily working curve is required to insure accuracy, reasonable accuracy may be achieved through duplicate preparation and determination of a working standard.

Precision

A study based on a hierarchical design [21] was undertaken to evaluate the contribution of components creating variance (Table 6). The components evaluated were arranged in tiers as "samples" to account for sampling discrepancies, as "determinations" to account for drifts in the baseline perhaps caused by gas and sample flow fluctuations and inhomogeneity of the sample,

TABLE 6

Precision (hierarchical design)[a]

Samples	A		B		C	
Determinations	a	b	a	b	a	b
Readings	38	39	39	41	39	39
	39	39	41	40	39	38
	39	38	39	39	40	38
	40	40	40	41	40	37
	39	40	40	41	41	38
	39	39	40	40	40	39

$\bar{X}$ = 39.4, s.d. = ± 1.0, r.s.d. = 2.5%

Analysis of variance

$$F = \frac{\text{samples}}{\text{(determinations within samples)}} = 1.42 \quad (2,3\ \text{DF}) \quad \text{N.S.}$$

$$F = \frac{\text{(determinations within samples)}}{\text{Error within determination}} = 5.50 \quad (3,30\ \text{DF}) \quad P < 0.01$$

[a]Values are given as Absorbance × 1000

and as "readings" to account for instrumental noise. A plasma pool was sampled in triplicate and each sample determined in duplicate. A mean absorbance reading of 0.0394 was calculated with a standard deviation of ±0.0010.

The results of the analysis of variance indicated that (a) the sampling procedure did not contribute to the variance ($P > 0.05$), and (b) that significant variance ($P < 0.01$) was introduced from within the series of determinations. The variance from within the series of determinations might be caused by baseline drift. This further suggests a need for vortexing the sample and establishing the zero baseline prior to each sampling period (see Procedure). Duplicate determinations will obviously increase the precision of the method.

Confidence intervals [21] were calculated from these data based on one, three, and six readings and converted into concentration intervals (Table 7); accordingly, six readings are suggested to achieve high precision, although the use of three readings results in only a minor loss of precision.

Interday variation

The use of a daily working curve reduces the effects of interday instrumental and gas fluctuations [20]. An interday variation study was therefore undertaken. Thirty-four samples representing a random selection from eighty previously analyzed samples were re-analyzed (Table 8). The *t*-test for paired samples [21] showed no significant difference ($P > 0.05$) between the two sets of data. The results further illustrate that samples can be stored at −20°C, thawed, and accurately re-analyzed.

Ion interference

High salt concentrations interfere with the accurate determination of zinc in water [5], but the degree of interference varies with the salt concentration [7].

The effect of interfering ions at physiological levels can be limited by dilution techniques. Although plasma ion concentrations remain rather constant in the adult, they may increase as a result of disease [24]. To evaluate the limit of accuracy of this method in elevated states, major ions reported to interfere [7] were added to a plasma pool (Table 9). The concentrations added were equal to eight times the standard deviation of normal ion

TABLE 7

Confidence intervals

	Absorbance (× 1000)	Concentration (μg/100 ml)
For a single reading	39.4 ± 2.0	88.7 ± 4.5
For three readings	39.4 ± 1.2	88.7 ± 2.7
For six readings	39.4 ± 0.8	88.7 ± 1.8

TABLE 8

Interday variation

10/75	63	75	68	60	75	90	48	85	80	70	55	53	70	60	80	73	80
6/75	63	78	70	60	78	95	55	85	80	75	55	60	70	68	88	73	85
10/75	53	50	65	78	55	80	65	70	65	75	55	95	70	95	80	65	85
6/75	50	50	63	75	55	83	68	68	75	65	53	95	63	90	70	58	85

t-test (paired observations) (N= 34)
t = 0.63 $P > 0.05$ N.S.
Mean difference ($\bar{X}$) = 0.529
Standard error (SX) = 4.876

plasma concentrations [24]. The plasma pool was sampled in triplicate and each sample was determined in duplicate; analysis of variance indicated that there is no significant effect of these ions on plasma zinc determinations ($P > 0.05$).

Conclusion

An accurate, sensitive and specific method for the determination of zinc in human plasma by a.a.s. through a fourfold dilution with water has been studied. Similar analytical curves, aspiration rates and viscosities were achieved with pooled plasma and zinc—5% glycerol working standards. Significant errors were incurred when water or zinc—10% glycerol working standards were utilized. The concentrations of zinc in a plasma pool calculated from an additions curve and from a zinc—5% glycerol working curve were identical. Recovery of plasma zinc was 99.2% when calculated from a single standard.

The precision of the method was evaluated by a hierarchical design. The standard deviation was ±0.0010 and the confidence interval was ±0.0008 for a series of six contiguous 10-s-integration absorbance readings. The concen-

TABLE 9

Effect of ions added to pooled plasma

Ion (salt)[a]	Meq Added	Absorbance × 1000	t-paired
K^+(KCl)	4.0	37.9	
Na^+(NaCl)	30.0	37.4	
$H_2PO_4^-$(KH_2PO_4)	3.2	37.8	t = 1.45, N.S.
$H_2PO_4^-$(NaH_2PO_4)	3.2	37.6	$dF = 4$[b]
—	—	37.3	

Analysis of variance $F = 0.687$; $P > 0.05$; $dF_1 = 4$[c]; $dF_2 = 25$.[d]

[a]Reagent grade. [b]Degrees of freedom — total. [c]Degrees of freedom — samples. [d]Degrees of freedom — measurements.

tration confidence interval was ±1.8 μg/100 ml for six readings. The significance of the variables contributing to the precision of the method was evaluated by analysis of variance for a hierarchical design. Baseline drift was a major cause of the variance, whereas sampling errors were not. Effects from day-to-day variation and matrix interferences were non-significant.

We acknowledge the helpful suggestions and technical support of Dr. James C. Smith, Jr., of the Veteran's Administration Hospital, Washington, D.C., and we thank Texas Instruments, Inc., for their gift of the mini-computer used.

REFERENCES

1 F. W. Sunderman, Jr., Human Pathol., 4 (1973) 549.
2 J. A. Halsted, J. C. Smith, Jr., and M. I. Irwin, J. Nutr., 104 (1974) 305.
3 W. Mertz, Adv. Clin. Chem., 21 (1975) 468.
4 A. Zettner, Clin. Chem., 7 (1964) 1.
5 A. Prasad, D. Oberleas, J. A. Halsted, and R. S. Collins, J. Lab. Clin. Med., 66 (1965) 508.
6 R. E. Thiers, Methods Biochem. Anal., 5 (1957) 273.
7 S. Sprague and W. Slavin, At. Absorpt. Newsl., 4 (1965) 228.
8 B. M. Hackley, J. C. Smith, Jr., and J. A. Halsted, Clin. Chem., 14 (1968) 1.
9 J. G. Reinhold, E. Pascoe, and G. A. Kfoury, Anal. Biochem., 25 (1968) 557.
10 B. Momcilovic, B. Belonje, and B. G. Shah, Clin. Chem., 21 (1975) 588.
11 S. Meret and R. I. Henkin, Clin. Chem., 17 (1971) 369.
12 J. B. Dawson and B. E. Walker, Clin. Chim. Acta, 26 (1969) 465.
13 R. S. Pekarek, W. R. Beisel, P. J. Bartelloni, and K. A. Bostonian, Am. J. Clin. Pathol., 57 (1972) 506.
14 J. D. Winefordner and H. W. Latz, Anal. Chem., 33 (1961) 1727.
15 N. A. Lange, (Ed.), Handbook of Chemistry, 9th edn. Handbook Publishers, Sandusky, Ohio, 1949, pp. 10—289.
16 Clinical Methods for Atomic Absorption Spectroscopy, Perkin Elmer Corp., Norwalk, Conn., 1971, p. AA-znl, 1.
17 D. O. Rodgerson and N. W. Tietz, Clin. Chem., 21 (1975) 1057.
18 R. T. Lofberg and E. A. Levri, Anal. Lett., 7(12) (1974) 775.
19 B. Foley, S. A. Johnson, B. Hackley, J. C. Smith, Jr., and J. A. Halsted, Proc. Soc. Exp. Biol. Med., 128 (1968) 265.
20 G. D. Christian and F. Feldman, Atomic Absorption Spectroscopy, Wiley-Interscience, N. Y., 1970, p. 206.
21 A. Goldstein, Biostatistics: An Introductory Text, MacMillan, N.Y., 1965, pp. 47, 59, 81, 144.
22 J. Harkness, Biorheology, 8 (1971) 171.
23 J. F. Swindells, R. C. Hardy, and R. L. Cottington, J. Res. Nat. Bur. Std., 52(3), #2479 (1954).
24 N. Tietz, Fundamentals of Clinical Chemistry, W. B. Saunders, Philadelphia, 1970, p. 934.

Analytica Chimica Acta, 94 (1977) 75—81

UNTERSUCHUNGEN ZUR BESTIMMUNG SELTENER ERDEN DURCH ATOMABSORPTION MIT ELEKTROTHERMISCHER ATOMISIERUNG

KLAUS DITTRICH*, EVELYN JOHN und IRMGARD ROHDE
Sektion Chemie der Karl-Marx-Universität Leipzig, 701-Leipzig (D.D.R.)
(Eingegangen den 2. März 1977)

ZUSAMMENFASSUNG

Es wurden Untersuchungen zur elektrothermischen Verdampfung von SE-Spuren mit verschiedenen Atomisatoren (Graphitstab, Graphitküvette, Tantalschiff) durchgeführt. Die besten analytischen Ergebnisse wurden mit einem modifizierten Tantalschiffatomisator erreicht, weil in diesem Fall keine SE-Carbidbildung möglich ist. Der Einsatz von gemischten Argon—Wasserstoffatmosphären führt durch Reduktion der SEO-Radikale zur Verbesserung der Atomkonzentration im Plasma. Die apparativen und experimentellen Bedingungen der analytischen Bestimmungsmethoden wurden optimiert. Die Nachweisgrenzen sind: 25 pg Yb, 22 pg Eu, 62 pg Tm, 2000 pg Sm, 300 pg Ho, 300 pg Dy, 1300 pg Er.

SUMMARY

The determination of rare earths by atomic absorption spectrometry with electrothermal atomization

The electrothermal atomization of traces of rare earths has been investigated with different atomizers (carbon rod, graphite furnace, tantalum ribbon). The best analytical results are obtained with a modified tantalum thermal atomizer, because the formation of rare earth carbides is then impossible. Mixed argon—hydrogen atmospheres improve the concentration of atoms in the plasma, because hydrogen reduces the rare earth oxide radicals. The optimal analytical conditions are described. The detection limits are: 25 pg Yb, 22 pg Eu, 62 pg Tm, 2000 pg Sm, 300 pg Ho, 300 pg Dy, 1300 pg Er.

Obwohl die ersten Untersuchungen zur Atomabsorption der Seltenen Erden (SE) in King-Öfen durchgeführt wurden [1, 2], findet man in der Literatur nur eine Angabe über deren Bestimmung mit elektrothermischer Atomisierung. Hwang et al. [3] behandelt die Bestimmung von 37 Elementen mit Hilfe des Tantalschiffatomisators und erwähnt, daß damit 70 pg Eu nachgewiesen werden konnten. Darüberhinaus war uns lediglich eine Information über die Anwendung der Graphitrohrküvette auf die Bestimmung verschiedener SE bekannt [4]. Es konnten 500 ng Nd, 2500 ng Sm, 5 ng Eu, 250 ng Dy, 25 ng Tm und 0,25 ng Yb bestimmt werden. Diese Nachweisgrenzen sind jedoch für die Atomabsorption mit elektrothermischer Atomisierung unbefriedigend.

Demgegenüber sind viele Untersuchungen zur Bestimmung der SE durch Atomabsorption mit Flammenatomisierung durchgeführt worden. Fassel und

Mossotti [5, 6] berichteten über die Verwendung der C_2H_2—N_2O-Flamme für die Bestimmung der SE. Auf der Grundlage dieser Untersuchungen erschienen einige Mitteilungen zur analytischen Bestimmung der SE [7—13]. Eine Übersicht über die durch AAS mit Flammenatomisierung erreichten Nachweisgrenzen wird von Fassel et al. [14] gegeben. Sie liegen zwischen 4 $\mu g\ ml^{-1}$ für Gd und Pr und 0,02 bzw. 0,04 $\mu g\ ml^{-1}$ für Yb bzw. Eu. Damit wurde das für diese AAS-Technik normalerweise erreichbare Nachweisvermögen auch für die SE erreicht.

Diese Tatsache, die wenigen Mitteilungen über die Anwendung der elektrothermischen Atomisierung und die dabei erzielten unbefriedigenden Nachweisgrenzen führten uns zu der Meinung, daß letztere hauptsächlich auf eine nicht effektive Atombildung zurückzuführen sind. Eine niedrige Atomkonzentration kann im allgemeinen durch schlechte Verdampfbarkeit vorhandener oder sich beim Veraschungsprozeß bildender Verbindungen und durch ungenügende Dissoziation stabiler Moleküle oder Radikale verursacht werden. Unter diesen Gesichtspunkten sind folgende Eigenschaften der SE zu beachten. Nach ihren Siedepunkten lassen sich die SE in 3 Gruppen einteilen (vgl.a. [15])

1. Niedrigsiedende SE: Yb (1427°C), Eu (1439°C), Tm (1727°C), Sm (1900°C);
2. Mittelsiedende SE: Dy (2600°C), Sc(2730°C), Ho (2600°C), Tb (2800°C);
3. Hochsiedende SE: Er (2900°C), Y (2927°C), Gd (3000°C), Nd (3027°C), Pr (3127°C), Lu (3327°C), Ce (3468°C), La (3470°C).

Die SE bilden auch stabile Monoxide des Typs SEO mit Dissoziationsenergien zwischen 5,8 eV (EuO) und 7,4 eV (NdO) [16, 17] und stabile Carbide unterschiedlicher Zusammensetzung [18—20]. Diese Radikale bzw. Moleküle sind z.T. auch noch im Plasma stabil. Die Carbide sind außerdem schwer verdampfbar.

Außerdem können wie bei der Flammenatomisierung [21] Ionisationsinterferenzen infolge der niedrigen Ionisierungspotentiale der SE (E_i zwischen 5,5 und 6,5 eV [25]) auftreten, die gegebenenfalls durch Zusatz leicht ionisierbarer Elemente korrigierbar wären.

Wir führten unsere Untersuchungen mit der AAS durch elektrothermische Atomisierung unter Berücksichtigung dieser Gegebenheiten und den bei der Flammenatomisierung bereits erzielten Nachweisgrenzen durch. Da wegen der verhältnismäßig niedrigen Temperaturen der elektrothermisch erzeugten Plasmen zu erwarten war, daß die Siedepunkte der SE einen wesentlichen Einfluß auf die Bestimmungsmöglichkeiten haben werden, wählten wir für unsere Untersuchungen zuerst die niedrigsiedenden SE (Eu, Yb, Tm, Sm) und danach die mittelsiedenden SE (Dy, Ho) und hochsiedenden SE (Er, Y) aus. Da weiterhin zu erwarten war, daß die SE-Carbidbildung bei Anwendung von C-Probeträgern und die SEO-Bildung einen wesentlichen Einfluß haben werden, wurden zuerst Untersuchungen zur Verdampfung durchgeführt.

EXPERIMENTELLES

Geräte: AAS-Spektrometer Typ 811 (Zweistrahl-Zweikanal-Gerät; Jarrell-Ash, USA). Graphitstabatomisator (Eigenbau, vgl. [22]). Graphitrohrküvette Typ 1268 (Beckman, USA). Micro-Thermal-Atomizer Typ MTA-2 (Fisher, USA).

Lösungen: Reine SE-Oxide wurden in konzentrierter Salzsäure gelöst. Die Lösungen wurden eingedampft und der Rückstand in 1 M HCl aufgenommen. Die Konzentration der Stammlösungen war 1 mg SE ml^{-1}. Durch Verdünnen mit 1 M HCl wurden die entsprechenden Analysenlösungen hergestellt. Das Probevolumen betrug jeweils 0,01 ml.

Untersuchungen bei Verwendung verschiedener Atomisatoren am Beispiel des Ytterbiums

Obwohl wir bei früheren Untersuchungen zur Emissionsspektrographie von SE festgestellt hatten [23], daß gerade die niedrigsiedenden SE im elektrischen Lichtbogen starke Verdampfungsverzögerungen infolge von Carbidbildung aufweisen, wurde aus den oben erwähnten Gründen dieses Element für die Untersuchungen ausgewählt.

Zuerst kam der Graphitstabatomisator mit einem Graphitbecher (Außendurchmesser, 5 mm; Länge, 7 mm; Innerweite, 3 mm; Tiefe der Bohrung, 3 mm) zum Einsatz. Erst bei sehr hohen SE-Konzentrationen (ab 100 ng Yb/0,01 ml) konnten in Argonatmosphäre geringe Absorptionssignale beobachtet werden. Bei Verwendung einer Argon—Wasserstoff-Atmosphäre (140 l Ar h^{-1}, 28 l H_2 h^{-1}) wurde infolge der Reduktion der SEO-Radikale die Absorption verbessert (s. Abb. 1, Bild a, Kurve 1). Um auch die Carbidbildung zu reduzieren, wurde die Innenwand des Probeträgers mit PVC-Lösung imprägniert (Kurve 2). Die erzielte Empfindlichkeitssteigerung beweist, daß die Atomkonzentration auch von der Carbidbildung beeinflußt wird. Die mit dem Graphitstabatomisator erzielten Ergebnisse haben jedoch für die praktische Anwendung keine Bedeutung.

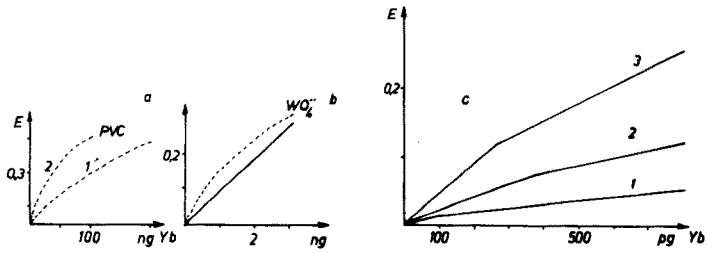

Abb. 1. Abhängigkeit der Extinktion von der Yb^{3+}-Konzentration bei AAS-Messungen mit verschiedenen Atomisatoren. (a) Graphitstabatomisator: Kurve 1, Graphitbecher ohne Imprägnierung. Kurve 2, Graphitbecher mit PVC-Imprägnierung. (b) Graphitrohrküvette, mit und ohne WO_4^{2-} Imprägnierung. (c) Micro-Thermal-Atomizer (MTA-2): Kurve 1, MTA (Variante 1), Ar-Atmosphäre. Kurve 2, MTA (Variante 1), Ar—H_2-Atmosphäre (450 l h^{-1}). Kurve 3, MTA (Variante 2), Ar—H_2-Atmosphäre (100 l h^{-1}).

Durch Einsatz der Graphitrohrküvette sollte versucht werden, evtl. entstehende Carbide bei den hier möglichen höheren Temperaturen Schneller zu verdampfen und zu zerstören. Wir wendeten Temperaturen von 3100 bis 3300°C an. Die Ergebnisse sind in der Abbildung 1 (b) dargestellt. Gegenüber dem Graphitstabatomisator ergab sich eine Empfindlichkeitssteigerung. Daraus kann man schlußfolgern, daß sich beim Graphitstabatomisator die thermische Heterogenität des Plasmas besonders negativ ausgewirkt hat. Weiterhin sollte durch Anwendung der beschriebenen Imprägnierung von Graphitrohren mit carbidbildenden Metallsalzen [24] die Carbidbildung der SE in der Graphitrohrküvette zurückgedrängt werden. Das Ergebnis, daß mit einem solchen Graphitrohr (Imprägnierung mit Na_2WO_4-Lösung) erhalten wurde, ist ebenfalls in Abb. 1 (b) dargestellt. Die erzielte Empfindlichkeitssteigerung ist gering.

Da bei den angewendeten, hohen Temperaturen die Möglichkeit besteht, daß sich die Atomkonzentration durch Ionisation vermindert, wurden den Yb^{3+}-Lösungen Alkalihalogenide zur Erhöhung des Elektronendrucks im Plasma zugesetzt. Es trat jedoch keine Verbesserung ein. Die Abb. 1 zeigt, daß Ytterbium bei Anwendung der Graphitrohrküvette mit einer Nachweisgrenze von etwa 0,5 ng Yb bestimmt werden kann.

Durch Verwendung des Tantals als Probeträgermaterial bei Einsatz des Micro-Thermal-Atomizer (MTA) sollte die Carbidbildung vollständig vermieden werden. Das Ergebnis ist in Abb. 1 (c) dargestellt. Gegenüber der Graphitrohrküvette konnte eine geringe Empfindlichkeitssteigerung erzielt werden. Der Einsatz einer Argon—Wasserstoff-Atmosphäre zur Reduktion der SEO-Radikale brachte auch beim MTA eine nennenswerte Empfindlichkeitssteigerung. Eine weitere Verbesserung ergab sich bei Verwendung eines modifizierten MTA mit verminderter Strömungsgeschwindigkeit der Schutzgase (vgl.unten). Vergleicht man die erhaltenen Ergebnisse (Abb. 1), so ist festzustellen, daß die Optimierung der Verdampfung zu einer Empfindlichkeitssteigerung um 2—3 Zehnerpotenzen führte und daß sowohl die SEO-Radikale als auch die SE-Carbidbildung die Atomkonzentration der SE im Plasma beeinflussen.

Bedingungen der AAS-Bestimmung von SE durch elektrothermische Atomisierung unter Verwendung des Micro-Thermal-Atomizers MTA-2

Atomisator 1. Variante: MTA-2; Ar (380 l h^{-1}), H_2 (56 l h^{-1}, 0,6 at).

2. Variante: MTA-2 (geschlossen); Ar (110 l h^{-1}), H_2 (14—25 l h^{-1}, 0,2—0,3 at).

Die Änderung gegenüber der kommerziellen Variante besteht darin, daß die Öffnungen der Schutzgasglocke für den Strahlengang mit Quarzfenstern verschlossen wurden. Dadurch ist die Reduzierung der Schutzgasströmungsgeschwindigkeit möglich, die zu einer höheren maximalen Atomkonzentration im Plasma und damit zu einer besseren Empfindlichkeit führt.

Probeträger Tantalschiff, 30 × 3 × 0,2 mm. Die Verringerung der Breite des Original-Tantalschiffs (6 mm) bei Erhaltung des gleichen elektrischen Widerstandes führte ebenfalls zu einer Erhöhung der maximalen

Atomkonzentration im durchstrahlten Plasma. (Trocknung: 30 s, 130°C; Veraschung: 15 s, 400°C; Atomisierung: Vgl. Tab. 1).

In der Tab. 1 sind die weiteren Bedingungen zusammengestellt. Es wurde in jedem Fall mit der Untergrundkompensation nach der Zweilinienmethode gearbeitet. Es wurde festgestellt, daß die Signalhöhe mit zunehmender Atomisierungstemperatur zuerst zunahm, danach konstant blieb (2050—2150°C), um bei noch höheren Atomisierungstemperaturen wieder abzunehmen. Da die thermische Stabilität der Tantalprobeträger bei den erforderlichen Temperaturen nicht sehr groß ist, wurde für die Atomisierung die niedrigste Temperatur bei möglichst maximaler Extinktion gewählt (vgl. Tab. 1).

ERGEBNISSE UND DISKUSSION

Die Ergebnisse der AAS-Bestimmung verschiedener SE sind in der Abb. 2 und der Tab. 2 dargestellt worden. Alle Eichkurven besitzen (Abb. 2) eine leichte Krümmung. Aus diesem Grund wurden Regressionsrechnungen nur in einem begrenzten Konzentrationsbereich durchgeführt (vgl. Tab. 2). Der tatsächlich verwendbare Konzentrationsbereich ist aus der Abb. 2 zu entnehmen. Die in der Tab. 2 angeführten reziproken Empfindlichkeiten bezogen auf die Extinktionseinheit von 0,01 sind in erster Näherung mit der statistisch berechenbaren Nachweisgrenze identisch. Die Korrelationskoeffizienten zeigen an, daß trotz des für die Regression verwendeten, geringen Konzentrationsbereiches Krümmungen vorliegen. Das führt auch zu den angegebenen absoluten Standardabweichungen für die Verfahren.

Die Ergebnisse zeigen, daß mit der entwickelten Methode Nachweisgrenzen im Picogrammbereich erzielt werden konnten. Damit wurden die Ergebnisse, die durch die AAS mit Flammenatomisierung erreicht wurden, entscheidend

TABELLE 1

Bedingungen für die atomabsorptionsspektralphotometrische Bestimmung einiger SE mit elektrothermischer Atomisierung (MTA, Variante 2)

Element	Wellenlänge der spez. u. unspez. Linie (nm)	Lichtquelle	Stromstärke (mA)	Spektrale Brandbreite (nm)	Siedepunkt des Elementes (°C)	Atomisierung	
						Zeit (s)	Temperatur (°C)
Yb	398,8	Yb-HKL	5	0,1	1427	3	1960
	397,7	Sm-HKL	10	0,2	—	—	—
	oder 397,8	Co-HKL	10	0,4	—	—	—
Eu	459,4	Eu-HKL	5	0,1	1439	3	2060
	460,1	Cr-HKL	15	0,2	—	—	—
Tm	371,8	Tm-HKL	10	0,2	1727	3	2060
	372,7	Tm-HKL	10	0,2	—	—	—
Sm	429,7	Sm-HKL	10	0,1	1900	3	2150
	431,3	Sm-HKL	10	0,2	—	—	—
Dy	421,2	Dy-HKL	10	0,1	2600	3	2250
	420,3	Dy-HKL	10	0,2	—	—	—
Ho	410,3	Ho-HKL	5	0,1	2600	3	2340
	412,8	Ho-HKL	5	0,1	—	—	—
Er	400,8	Er-HKL	7,5	0,1	2900	3	2430
	397,8	Er-HKL	7,5	0,1	—	—	—

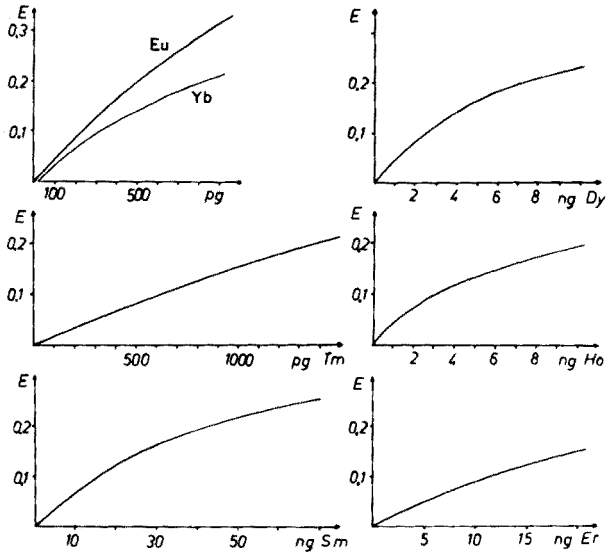

Abb. 2. Eichkurven für die Bestimmung von SE-Spuren in 1 M HCl durch AAS mit elektrothermischer Atomisierung (MTA-2, Variante 2).

verbessert. Vergleicht man die Siedepunkte der Elemente mit den erzielten Nachweisgrenzen, so stellt man mit Ausnahme des Samariums eine Korrelation fest. Das Samarium ist ein sehr linienreiches Element, für welches die Übergangswahrscheinlichkeiten in Absorption auf eine Reihe von Möglichkeiten verteilt sind.

Die vollständige Ausschaltung der SE-Carbid- und die starke Reduzierung der SEO-Bildung hat diese Nachweisgrenzen ermöglicht, womit die Voraussetzungen für die Spurenanalyse einiger SE durch AAS geschaffen wurden.

TABELLE 2

Ergebnisse der Bestimmung von SE-Spuren durch AAS mit elektrothermischer Atomisierung unter Verwendung des MTA (Variante 2)

Element	Reziproke Empfindlichkeit absolut relativ pro 0,01 *E*		Konzentrationsbereich für lineare *E*—*C*-Beziehung	Korrelationskoeffizient	Standardabweichung des Verfahrens in *E*
	(pg)	(ppb)			
Yb	25	2,5	25—300	0,98	0,012
Eu	22	2,2	22—500	0,98	0,011
Tm	62	6,2	62—700	0,99	0,006
Sm	2000	200	2000—30000	0,96	0,015
Dy	300	30	300—4000	0,99	0,009
Ho	300	30	300—3000	0,99	0,006
Er	1300	130	1300—20000	0,99	0,009

Einschränkend muß bemerkt werden, daß eine Bestimmung hochsiedender SE nur im Fall des Erbiums möglich war. Die Bestimmung des Yttriums wurde ebenfalls untersucht. Es ergab sich, daß eine Konzentration von 100 ng Y/0,01 ml bei den 3 empfindlichen Y-Linien (410,2; 414; 407 nm) keine Absorption ergab. Eine weitere Steigerung der Atomisierungstemperatur zur Verbesserung der Y-Verdampfung war aus apparativen Gründen nicht mehr möglich.

LITERATUR

1 L. F. H. Bovey und W. R. S. Garton, Proc. Phys. Soc., 67A (1954) 291.
2 R. Zalubas und M. Wilson, J. Res. Nat. Bur. Stand. Sect. A, 69 (1965) 59.
3 J. Y. Hwang, C. J. Mokeler und P. A. Ullucci, Anal. Chem., 44 (1972) 2018.
4 Fa. Perkin-Elmer, Privatmitteilung.
5 V. A. Fassel und G. V. Mossotti, Anal. Chem., 35 (1963) 252.
6 G. V. Mossotti und V. A. Fassel, Spectrochim. Acta, 20 (1964) 1117.
7 V. A. Fassel und D. W. Golightly, Anal. Chem., 39 (1967) 466.
8 D. C. Manning, At. Absorption Newslett., 5 (1966) 63, 127.
9 M. D. Amos und J. B. Willis, Spectrochim. Acta, 22 (1966) 1325.
10 J. Kinnunen und O. Lindsjo, Chemist-Analyst, 56 (1967) 25, 67.
11 Yiu-Kee Chau, Talanta, 15 (1968) 421.
12 O. H. Kriege und G. G. Welcher, Talanta, 15 (1968) 781.
13 R. L. Scott, At. Absorption Newslett., 9 (1970) 46.
14 V. A. Fassel, R. N. Kniseley und C. C. Butler, in O. B. Michelson (Ed.), Analysis and Application of Rare Earth Materials, Universitetsforlaget, Oslo, 1973, S. 71.
15 A. V. Karjakin, H. W. Laktionova und L. I. Pavlenko, Zh. Anal. Khim., 23 (1968) 1829.
16 J. Antic, Dissertation, Universität Paris, 1971.
17 V. A. Fassel und D. W. Golightly, Anal. Chem., 39 (1967) 466.
18 F. A. Cotton und G. Wilkinson, Anorganische Chemie, 2. Auflage VEB Deutscher Verlag für Grundstoffindustrie, Leipzig, 1968.
19 F. Gaume-Mahn, in LeRoy Eyring (Ed.), Progress in Science and Technology of Rare Earths, Bd. 1, Pergamon Press, Oxford, 1964, S. 275.
20 E. Saari, Ann. Acad. Sci., Fennicae, Ser., A II (1974) 7.
21 W. Ooghe und F. Verbeek, Anal. Chim. Acta, 73 (1974) 87.
22 K. Dittrich und W. Mothes, Talanta, 22 (1975) 318.
23 K. Dittrich, Ph. Luan, W. Thümmler und K. Niebergall, Z. Chem., 12 (1972) 395.
24 H. M. Ortner und E. Kantuscher, Talanta, 22 (1975) 581.
25 R. Mavrodineanu und H. Boiteux, Flame Spectroscopy, J. Wiley, New York, 1965.

Analytica Chimica Acta, 94 (1977) 83—90

BESTIMMUNG VON SPUREN SELTENER ERDEN IN ANDEREN SELTENEN ERDEN DURCH ATOMABSORPTION MIT ELEKTROTHERMISCHER ATOMISIERUNG UND DURCH EMISSIONSSPEKTROGRAPHIE MIT DEM GLEICHSTROMDAUERBOGEN

KLAUS DITTRICH* und KARIN BORZYM

Sektion Chemie der Karl-Marx-Universität Leipzig, 701-Leipzig (D.D.R.)

(Eingegangen den 28. April 1977)

ZUSAMMENFASSUNG

Die Bestimmung einiger Spuren Seltener Erden (Yb, Eu, Tm, Sm, Dy, Ho, Er) in anderen SE-Matrices durch AAS mit elektrothermischer Atomisierung (Tantalschiffatomisator) und der Spuren Tm und Dy durch AES mit Gleichstrombogenanregung wird beschrieben. Der Einfluß der Siedepunkte der Spuren und Matrices auf die Möglichkeit und die Empfindlichkeit der Bestimmungen durch AAS wird diskutiert. Die Resultate der Methoden werden verglichen. Wir erreichten die besseren absoluten und in den meisten Fällen auch die besseren relativen Nachweisgrenzen bei Anwendung der AAS.

SUMMARY

The determination of traces of rare earths in other rare earths by atomic absorption with electrothermal atomization and by d.c. arc emission spectrography

The determination of traces of some rare earth elements (Yb, Eu, Tm, Sm, Dy, Ho, Er) in matrices of other rare earths by a.a.s. with electrothermal atomization (tantalum ribbon), and of traces of Tm and Dy by a.e.s. with d.c. arc excitation is described. The influence of the boiling points of the traces and matrices on the possibility and the sensitivity of the a.a.s. determinations is discussed. The results of the methods are compared. Better absolute, and in most cases also relative, detection limits can be achieved by a.a.s.

Auf der Grundlage der von uns für einige Seltene Erden erzielten Ergebnisse der Bestimmung von Spuren Seltener Erden durch Atomabsorptionsspektrometrie mit elektrothermischer Atomisierung unter Anwendung eines Tantalschiffatomisators [1] sollten die Bestimmungsmöglichkeiten für Spuren Seltener Erden in anderen Seltenen Erden getestet werden. Die erzielten Resultate sollten für einige Beispiele mit den Ergebnissen der Mikrolösungsspektralanalyse, die unter Anwendung des Gleichstromdauerbogens nach einer modifizierten Variante des Silberstein-Verfahrens durchgeführt wurde, verglichen werden [2].

Ziel dieser Untersuchungen und des Vergleichs war die Ermittlung optimaler Bedingungen und optimaler relativer Nachweisgrenzen für die Bestimmung von Spuren Seltener Erden in Mikroproben anderer Seltener Erden.

Unter der Berücksichtigung der in unserer ersten Mitteilung [1] dargelegten Besonderheiten der Atomspektroskopie der Seltenen Erden und der im Ergebnis dieser Arbeit festgestellten negativen Korrelation zwischen dem Nachweisvermögen und den Siedepunkten der Seltenen Erden wurden die beiden genannten Verfahren hauptsächlich wegen den mit ihnen erzielbaren, unterschiedlichen Plasmatemperaturen miteinander verglichen.

EXPERIMENTELLES

Allgemeine experimentelle Bedingungen für die AAS-Untersuchungen

Spektrometer. AAS-Spektrometer Typ 811 Zweistrahl-Zweikanal-Gerät; Jarrell-Ash, U.S.A., mit Micro-Thermal-Atomizer MTA — 2 (Fisher, U.S.A.) modifiziert nach Variante 2 (vgl. [1]). Schutzgasatmosphäre: Ar (110 l h^{-1}), H_2 (14—25 l h^{-1}, 0,2—0,3 at). Probeträger: Tantalschiff, 30 × 3 × 0,2 mm. Trocknung: 30 s, 130°C. Veraschung: 15 s, 400°C. Atomisierung: s.u., Ergebnistabellen.

Lösungen. Reine SE-Oxide wurden in konzentrierter Salzsäure gelöst. Die Lösungen wurden eingedampft und der Rückstand in 1 M HCl aufgenommen. Die Konzentration der Stammlösungen war 10 mg SE ml^{-1}. Durch Verdünnung mit 1 M HCl und Mischung wurden die entsprechenden Analysenlösungen hergestellt. Das Probevolumen betrug jeweils 0,01 ml.

Folgende Seltene Erden wurden als Spuren eingesetzt: Yb (398,8 nm/397,8 nm), Eu (459,4 nm/460,1 nm), Tm (371,8 nm/372,7 nm), Sm (429,7 nm/431,3 nm), Dy (421,2 nm/420,3 nm), Ho (410,3 nm/412,8 nm), Er (400,8 nm/397,8 nm). Als Lichtquellen wurden die entsprechenden SE-Hohlkathodenlampen verwendet. Die Untergrundkompensation erfolgte nach der Zweilinienmethode (jeweils die 2. angegebene Linie) unter Verwendung der gleichen oder auch anderer Hohlkathodenlampen (vgl. [1]).

Allgemeine experimentelle Bedingungen für die AES-Untersuchungen

Spektrograph. Plangitterspektrograph PGS 2 (VEB Carl Zeiss, Jena, DDR). Gitter: 651 Strich/mm, Blaze — λ: 300 nm; Plattenmitte: 356 nm; Spaltbreite: 0,02 mm. Anregung: Universalbogenimpulsgenerator UBI — 1 (VEB Carl Zeiss, Jena, D.D.R.); Gleichstromdauerbogen: 10 A. Atmosphäre: Ar (120 l h^{-1} O_2 (80 l h^{-1}). Elektroden: vgl. Abb. 1; Abstand: 3 mm. Registrierung: Photoplatten ORWO WP — 3 extrahart, (VEB Filmfabrik ORWO, Wolfen, D.D.R.). Belichtungszeit: 21 s. Probevolumen: 0,02 ml pro Elektrode, d.h. 0,04 ml pro Analyse.

Lösungen. Wie oben, Lösungsmittel: 1 M HCl oder 1%iges $Ba(NO_3)_2$ in 1 M HCl.

Folgende Seltene Erden wurden als Spuren eingesetzt: Tm, Dy. Folgende Seltene Erden wurden als Matrices eingesetzt: Eu, Y. Damit konnten die Ergebnisse der AES für leicht- und mittel-siedende Spuren in leicht- und hochsiedender Matrix mit denen der AAS verglichen werden.

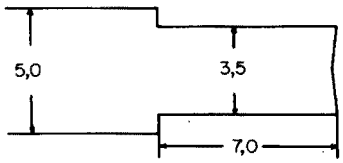

Abb. 1. Schematische Darstellung der für die Emissionsspektrographie verwendeten Elektroden.

ERGEBNISSE UND DISKUSSION

Untersuchung der Verdampfung der Seltenen Erden in Gegenwart von Matrices Seltener Erden bei elektrothermischer Atomisierung

Die Ergebnisse der Untersuchungen sind in der Abb. 2 dargestellt. Aus der Abbildung geht hervor, daß die Gegenwart von anderen Seltenen Erden als Matrices einen depressiven Einfluß auf die Meßsignale (Extinktion) der Spuren Seltener Erden ausübt. Vergleicht man die Siedepunkte der Seltenen Erden (Yb 1427°C; Eu 1439°C; Tm 1727°C; Sm 1900°C; Dy 2600°C; Sc 2730°C; Ho 2600°C; Tb 2800°C; Er 2900°C; Y 2927°C; Gd 3000°C; Nd 3027°C; Pr 3127°C; Lu 3327°C; Ce 3468°C; La 3470°C; vgl. auch [1]) mit der depressiven Wirkung der einzelnen Matrices, so stellt man fest, daß die depressive Wirkung um so höher ist, je höher der Siedepunkt der Substanz liegt. Auch der Siedepunkt der betrachteten Spur ist von Einfluß. Die niedrigsiedenden Seltenen Erden werden nicht so stark wie die mittel-und hochsiedenden durch die Gegenwart von Matrices beeinflußt.

Dieses Ergebnis legt den Schluß nahe, daß die Verdampfung und die Reduktion der Seltenen Erden in einem Schritt erfolgen: Beim Trocknungsprozeß entsteht als Rückstand basisches Chlorid, welches bei der Veraschung z.T. in Sesquioxid überführt wird. Diese Oxide sind bedeutend schwerer als die Metalle zu verdampfen. Durch die reduzierende Wirkung des H_2 werden diese Oxide während der Atomisierungsphase in die Metalle überführt und entsprechend der Reihenfolge der Siedepunkte verdampft. Es macht sich

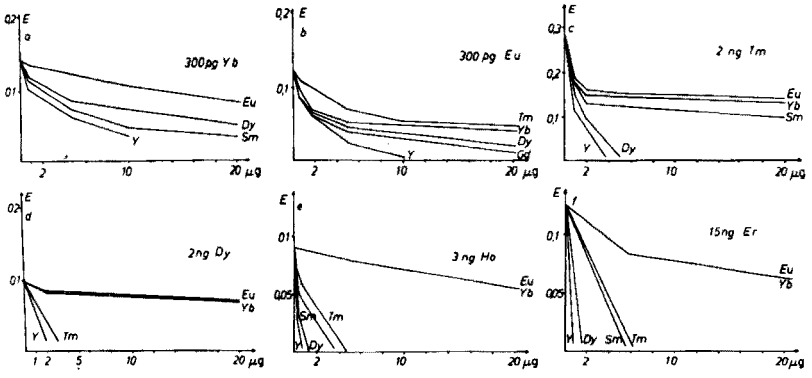

Abb. 2. Darstellung des depressiven Einflusses von Matrixsubstanzen Seltener Erden auf die Atomabsorption von Yb, Eu, Tm, Dy, Ho und Er bei elektrothermischer Atomisierung mit dem Tantalschiffatomisator.

in diesem Fall negativ bemerkbar, daß die Temperatur der Probeträger (Tantal) aus Stabilitätsgründen nicht über 2400°C gesteigert werden kann.

Der Zusatz von Alkalifluoriden (LiF, NaF, KF, NH_4F) bis zu einer Konzentration von 0,01 mg/0,01 ml übte keinen verdampfungsfördernden Einfluß aus. Eine zusätzliche depressive Wirkung wurde in Gegenwart dieser Substanzen ebenfalls nicht festgestellt. Daraus kann geschlußfolgert werden, daß der beschriebene Verdampfungsmechanismus richtig ist und daß bei den untersuchten Niedertemperaturplasmen keine Ionisationsinterferenzen auftreten.

Analytische Ergebnisse der Spurenbestimmung Seltener Erden durch AAS mit elektrothermischer Atomisierung

Die analytischen Ergebnisse der Spurenbestimmung Seltener Erden in Gegenwart anderer Seltener Erden sind in der Tabelle 1 zusammengefaßt worden. Ausgehend von der angegebenen Nachweisgrenzen umfaßt der auswertbare Konzentrationsbereich etwa eine Größenordnung. Oberhalb dieses Wertes treten in zunehmendem Maße starke Eichkurvenkrümmungen auf.

Vor allem Spurenbestimmungen der niedrigsiedenden Seltenen Erden in anderen Seltenen Erden sind bei einem Probeeinsatz von nur wenigen Mikrogramm im p.p.m.-Bereich möglich (Tab. 1). Mit Zunahme der Siedepunkte der Spuren und der Matrices wurden infolge des zunehmenden depressiven Einflusses schlechtere relative Nachweisgrenzen gefunden. So konnte z.B. Erbium (eine hochsiedende Seltene Erde) mit einer relativen Nachweisgrenze von nur 1% in der hochsiedenden Matrix Yttrium bei einem Probeeinsatz von 0,0001 mg Y bestimmt werden.

Die hier nicht genannten hochsiedenden Seltenen Erden können wegen ihrer schlechten Verdampfbarkeit und ihrer niedrigen Absorptionskoeffizienten mit dieser Methode nicht mehr bestimmt werden. In der Tabelle 2 sind einige analytische Ergebnisse angegeben, die bei der Bestimmung von Verunreinigungen in reinen Oxiden Seltener Erden erzielt wurden. Die Richtigkeit der Ergebnisse wurde jeweils mit der Additionsmethode überprüft und bestätigt.

Analytische Ergebnisse der Spurenbestimmung Seltener Erden durch Emissionsspektrographie mit dem Gleichstromdauerbogen

Es wurde für diese Untersuchungen Tm (niedrigsiedend) und Dy (mittelsiedend) ausgewählt. In Abwesenheit anderer Seltener Erden wurde zur Pufferung des Gleichstrombogens der Analysenlösung $Ba(NO_3)_2$ (1%) zugefügt. Dadurch konnten die Nachweisgrenzen beider Seltener Erden verbessert werden. Die analytischen Ergebnisse für die Bestimmung des Tm und Dy in Abwesenheit anderer Seltener Erden sind in der Tabelle 3 dargestellt.

In Gegenwart anderer Seltener Erden als Matrixsubstanzen war eine zusätzliche Pufferung des Gleichstrombogens mit $Ba(NO_3)_2$ nicht erforderlich, weil

TABELLE 1

Ergebnisse der Spurenbestimmung von Seltenen Erden in anderen Seltenen Erden durch AAS mit elektrothermischer Atomisierung

Spurenelement	Matrix (mg pro 0,01 ml)[a]		Atomisierungstemperatur (°C)	Nachweisgrenzen	
				absolut (pg)	relativ (p.p.m.)
Yb	0,02	Eu	2340	40	2
Yb	0,02	Tm	2340	50	2,5
Yb	0,01	Sm	2340	75	7,5
Yb	0,01	Dy	2430	75	7,5
Yb	0,005	Y	2430	75	15
Eu	0,01	Yb	2340	50	5
Eu	0,01	Tm	2430	50	5
Eu	0,01	Sm	2430	50	5
Eu	0,005	Dy	2430	50	10
Eu	0,002	Gd	2430	50	25
Eu	0,002	Y	2430	50	25
Tm	0,02	Eu	2340	150	7,5
Tm	0,02	Yb	2430	150	7,5
Tm	0,01	Sm	2430	150	15
Tm	0,002	Dy	2430	150	75
Tm	0,001	Y	2430	150	150
Sm	0,02	Eu	2340	3000	150
Sm	0,005	Tm	2340	3000	600
Sm	0,002	Dy	2430	3000	1500
Sm	0,001	Y	2430	3000	3000
Dy	0,02	Eu	2340	500	25
Dy	0,02	Yb	2340	500	25
Dy	0,001	Tm	2430	500	500
Dy	0,0005	Sm	2430	500	1000
Dy	0,0005	Y	2430	500	1000
Ho	0,02	Eu	2430	500	25
Ho	0,02	Yb	2430	500	25
Ho	0,001	Tm	2430	500	500
Ho	0,001	Sm	2430	500	500
Ho	0,0005	Dy	2430	500	1000
Ho	0,0001	Y	2430	500	5000
Er	0,02	Eu	2500	2000	100
Er	0,02	Yb	2500	2000	100
Er	0,002	Tm	2500	2000	1000
Er	0,002	Sm	2500	2000	1000
Er	0,0005	Dy	2500	2000	4000
Er	0,0001	Y	2500	2000	20000

[a]Es wurde jeweils die maximal mögliche Matrixmenge angegeben.

TABELLE 2

Bestimmung von Verunreinigungen Seltener Erden in anderen Seltenen Erden durch AAS mit elektrothermischer Atomisierung

Bestimmtes Spurenelement	Matrix (mg pro 0,01 ml)		Atomisierungstemperatur (°C)	Bestimmte Menge (p.p.m.) bezogen auf die SE-Matrix
Yb	0,02	Eu	2340	2
Dy	0,02	Eu	2430	15
Yb	0,0002	Tm	2340	1550
Yb	0,002	Sm	2340	47
Yb	0,002	Dy	2430	32
Eu	0,001	Yb	2340	90
Eu	0,0005	Tm	2340	70
Eu	0,0001	Sm	2340	500
Eu	0,005	Dy	2430	20
Eu	0,002	Gd	2430	50

TABELLE 3

Ergebnisse der Bestimmung von Tm- und Dy-Spuren durch Emissionsspektrographie im Gleichstromdauerbogen in Abwesenheit anderer Seltener Erden

Spur	Linien (nm)	Korr. koeff.	RSD (%)	Konzentrat.-Bereich (ng/0,04 ml)	Nachweisgrenze absolut (ng)	Nachweisgrenze relativ (p.p.m.)[a]
Tm	313,126 307,159 Ba	0,988	+24 −19	10—1500	5,6	0,14
Dy	400,048 423,957 Ba	0,989	+24 −19	50—1500	35	0,9
Dy	421,175 399,566 Ba	0,976	+29 −22	100—1500	54	1,4

[a]Bezogen auf 40 mg (0,04 ml Lösung).

die leicht ionisierbaren Seltenen Erden durch Erhöhung des Elektronendruckes im Plasma selbst die Rolle eines Puffers übernehmen.

Die Ergebnisse der Bestimmungen in Gegenwart der Matrixsubstanzen Eu (niedrigsiedend) und Y (hochsiedend) sind in der Tabelle 4 zusammengefaßt worden. Es wurde dabei versucht, mit einer möglichst großen Matrixmenge zu arbeiten, um eine möglichst niedrige relative Nachweisgrenze zu erzielen. Eine Erhöhung der Matrixmenge über 1 mg hinaus ist jedoch nicht zweckmäßig, weil in diesem Fall bei der Zündung des Bogens oftmals Substanzteile wegspritzen und somit die Reproduzierbarkeit sehr stark sinkt. Eine weitere Begrenzung für die einsetzbare Matrixmenge war der zunehmende Untergrund und das verstärkte Auftreten von Koinzidenzen.

TABELLE 4

Ergebnisse der Bestimmung von Tm- und Dy-Spuren in Eu und Y durch Emissionsspektrographie von 1 N HCl Lösungen im Gleichstromdauerbogen

Matrix (mg/0,04 ml)	Spur	Linien (nm)	Korr. koeff.	RSD (%)	Konzentrat. Bereich (p.p.m.)	Nachweisgrenze absolut (ng)	Nachweisgrenze relativ (p.p.m.)
1 Eu	Tm	313,126	0,973	+42	30—1500	27	27
		313,16		−30			
0,2 Eu	Tm	313,126	0,991	+21	100—7500	9	45
		313,16		−17			
1 Y	Tm	313,126	0,99	+26	50—1500	46	46
		312,61		−21			
0,2 Eu	Dy	421,175	0,948	+52	1000—20000	180	900
		422,069		−34			
0,2 Y	Dy	400,048	0,944	+28	500—7500	50	250
		396,761		−22			
0,2 Y	Dy	421,175	0,959	+15	7500—20000	—	—
		421,302		−13			

Die jeweils 2. Linie dient als innerer Standard und entstammt der Matrix.

Vergleich der durch Emissionsspektrographie und AAS bei der Spurenanalyse Seltener Erden erzielten Ergebnisse

Nachweisvermögen. Die absoluten Nachweisgrenzen liegen für die untersuchten Elemente bei Anwendung der AAS mit elektrothermischer Atomisierung am günstigsten. Dieses Ergebnis gilt ebenfalls für die anderen mit der AAS bestimmten, mit der Emissionsspektrographie aber nicht bestimmten Seltenen Erden.

Trotz der Tatsache, daß bei Anwendung der Emissionsspektrographie mit dem Gleichstromdauerbogen eine viel größere Menge an Matrix eingesetzt werden konnte, ergaben sich in vielen Fällen bei der AAS auch die besseren relativen Nachweisgrenzen. Lediglich im Fall hochsiedender Matrices wirkt sich die höhere Plasma- und Probeträgertemperatur bei Anwendung des Gleichstrombogens positiv aus.

Anwendbarkeit. Die Emissionsspektrographie ist prinzipiell auf alle Systeme Seltener Erden anwendbar. Sie bietet außerdem den Vorteil, daß auch direkte Untersuchungen von Feststoffen möglich sind. In diesem Fall sind auch höhere Probemengen einsetzbar, so daß gegenüber der Lösungsspektralanalyse auch bessere relative Nachweisgrenzen erzielt werden können. Allerdings kann dann nicht mehr von Mikroanalyse gesprochen werden.

Die Anwendung der AAS mit elektrothermischer Atomisierung ist begrenzt auf folgende Systeme: Niedrigsiedende Spuren in niedrig- bis hochsiedenden Matrices, mittel- und hochsiedende Spuren in niedrigsiedenden Matrices. Bestimmungen von mittelsiedenden Spuren in mittel- bis hochsiedenden Matrices sind nur mit schlechten relativen Nachweisgrenzen möglich. Mit

diesen Einschränkungen ist natürlich auch die Anwendbarkeit der Methode auf völlig unbekannte Mischungen Seltener Erden problematisch. Vernünftige Ergebnisse sind dann nur mit der Additionsmethode zu erwarten. Andererseits sind echte Spurenanalysen im Mikrobereich nur mit der AAS — z.B. zur Kontrolle von Ionenaustauschtrennungen — möglich.

Schnelligkeit. Die Bestimmungen mit der AAS sind bedeutend schneller durchführbar als mit der Emissionsspektrographie. Das ist besonders vorteilhaft, wenn die Additionsmethode eingesetzt werden muß.

Reproduzierbarkeit und Richtigkeit. Hinsichtlich dieser beiden Kriterien für Analysenverfahren bestehen nach unseren Ergebnissen zwischen den beiden angewandten Verfahren keine Unterschiede.

LITERATUR

1 K. Dittrich, E. John und I. Rohde, Anal. Chim. Acta, 94 (1977) 75.
2 A. V. Karjakin, Privatmitteilung.

Analytica Chimica Acta, 94 (1977) 91—110

ÉTUDE THERMODYNAMIQUE DE LA COMPLEXATION DES LANTHANIDES TRIVALENTS AVEC L'ACIDE HYDROXYETHYL-ETHYLENEDIAMINETRIACETIQUE ET D'AUTRES ACIDES AMINOACETIQUES

III. Détermination des Constantes de Formation des Complexes Mixtes par Titrage Potentiométrique

J. M. GATEZ, E. MERCINY et G. DUYCKAERTS

Laboratoire de Chimie analytique et Radiochimie, Université de Liège au Sart-Tilman, B-4000, Liège (Belgique)

(Reçu le 5 juin 1977)

RÉSUMÉ

Les auteurs déterminent, par titrage potentiométrique à 25°C et en milieu de force ionique égale à 1 (KCl), les constantes partielles de formation des complexes 1:2 et mixtes, protonés et non protonés, Ln—HEDTA—L, L étant respectivement la glycine, l'IMDA, le NTA et le HEDTA. Ils déterminent également les constantes de formation des espèces Ln—EDTA—HEDTA. Certaines discontinuités dans l'évolution des constantes partielles et globales de formation de ces espèces, en fonction du nombre atomique du lanthanide, sont attribuées, d'une part, à un changement dans le nombre de molécules d'eau de solvatation du complexe 1:1 LnHEDTA qui serait probablement 3 ou 2, en passant des terres cériques aux terres yttriques et, d'autre part, à une évolution de la valence coordinative de l'HEDTA dans le complexe 1:1 LnY, passant de six à cinq avec le nombre atomique du lanthanide. Une différence très nette de comportement est observée entre les complexes mixtes ou doubles dont les deux chélatants sont biazotés et ceux dont l'un est biazoté et l'autre monoazoté.

SUMMARY

A thermodynamic study of the complex formation of trivalent lanthanides with hydroxyethylethylenediaminetriacetic acid and other aminoacetic acids. Part III. The determination of the formation constants of mixed complexes by potentiometric titration.

The partial stability constants of the mixed and 1:2 complexes Ln—HEDTA—L (where Ln = La, Ce, ... and L = glycine, IMDA, NTA, HEDTA and EDTA) have been determined by potentiometric titration at 25°C and at a constant ionic strength of 1 (KCl). The changes in stability of the complexes studied (1:1, 1:2, mixed, protonated and unprotonated) vs. atomic number of the lanthanide are discussed. The changes observed in the trends of the partial and overall stability constants across the lanthanide series are attributed to the decrease in the number of water molecules in the 1:1 LnHEDTA·xH_2O from $x = 3$ for light lanthanides to $x = 2$ for heavy ones. However, in this 1:1 complex, HEDTA seems to be a hexadentate ligand in the La—Sm range of the series and a pentadentate ligand in the Gd—Lu range. Significant differences have been found between the complexes containing four nitrogen atoms, i.e. L = HEDTA, EDTA, and those with three nitrogen atoms i.e. L = glycine, IMDA, NTA.

L'interprétation de l'évolution de la stabilité des complexes de stoechiométrie 1:1 des lanthanides avec les acides polyaminopolyacétiques en fonction de la nature du complexant d'une part et du nombre atomique des lanthanides d'autre part, a fait l'objet de beaucoup de spéculations.

Choppin [1] a montré, en effet, que pour un lanthanide donné, la diminution d'énergie libre de formation du complexe augmente linéairement avec le nombre de sites coordinants du complexant. Par ailleurs, la constante de formation augmente avec le nombre atomique d'une façon plus ou moins régulière, augmentation qui a été attribuée à la contraction du rayon ionique du lanthanide et à la nature essentiellement électrostatique des liaisons entre l'ion central et le chélatant.

Il est cependant apparu rapidement que le gadolinium, correspondant au demi-remplissage de la sous-couche $4f$, présente une petite anomalie caractérisée par une stabilité systématiquement un peu plus faible, divisant ainsi la famille en deux groupes. Dans certains cas, une division en quatre groupes est proposée et appelée effet tétrade [2, 3]. Mais, c'est surtout à la suite des déterminations des ΔH et ΔS [4—12] correspondant à la formation des complexes avec l'EDTA et le HEDTA qu'il est apparu clairement que l'influence de la nature du lanthanide sur la complexation par un acide aminopolyacétique était, en réalité, beaucoup plus complexe: une discontinuité importante apparaît dans l'évolution de ces deux grandeurs thermodynamiques en fonction du nombre atomique, ces deux discontinuités se neutralisant approximativement dans la valeur de ΔG.

Ces dernières observations sont à l'origine d'un grand nombre de publications, les unes attribuant ces discontinuités en fonction de Z à un changement dans le nombre de molécules d'eau de la première sphère de solvatation du lanthanide qui passerait progressivement de neuf à huit en restant constant dans les complexes, d'autres affirmant que le nombre de molécules d'eau varie tant dans l'ion aqueux que dans l'ion complexé, d'autres enfin trouvant des arguments pour admettre qu'il est constant pour l'ion solvaté, dans toute la famille des lanthanides, mais qu'il varie dans les complexes [13—24]. Geier et Karlen [25] ont présenté des arguments en faveur de cette dernière interprétation en discutant les variations de ΔG, ΔH et ΔS des complexes mixtes Ln(EDTA)X, X étant respectivement l'ion sulfooxinate, iminodiacétate et nitrilotriacétate.

En vue de clarifier le débat, il nous a paru utile d'étendre l'étude aux complexes de l'acide hydroxyéthyléthylènediaminetriacétique (H_3Y) et c'est dans cette perspective que nous avons entrepris la détermination des constantes de formation des complexes mixtes ou doubles LnYL, L étant respectivement le glycocolle (HG), l'acide iminodiacétique (H_2X), l'acide nitrilotriacétique (H_3Z), le HEDTA (H_3Y) et l'EDTA (H_4Y'). Quelques données existent dans la littérature, mais elles concernent essentiellement les complexes non protonés [26—28]. Comme nous l'avons déjà mentionné [29, 30], nous avons déterminé également les constantes de formation des complexes mixtes et doubles protonés. Ces déterminations sont effectuées en milieu de force

ionique égale à 1 (KCl), à 25°C. Nous aborderons ultérieurement l'étude de l'évolution de ces constantes en fonction de la température.

Il nous paraît encore important de souligner qu'en extraction liquide—liquide ou en chromatographie sur échangeurs d'ions [31, 32] le complexant polyaminopolyacétique utilisé peut être en excès par rapport aux cations à séparer et, dans ces conditions, l'interprétation, et surtout la prévision des distributions en fonction du pH et de la concentration en complexant, nécessitent la connaissance non seulement de la constante de formation des complexes 1:1, mais encore celle des complexes mixtes et de leurs pK.

PRINCIPE DE LA METHODE

La méthode consiste à établir les courbes de titrage, soit par la potasse, soit par coulométrie, de l'acide aminoacétique H_nL seul, puis du même acide en présence d'une quantité stoechiométrique du complexe LnY. La première courbe de titrage permet la détermination des constantes d'acidité de l'acide chélatant [33, 34], tandis que la seconde permet d'accéder aux constantes de formation des complexes mixtes ou doubles.

Afin de simplifier, du point de vue mathématique, l'interprétation de ces courbes de titrage, les conditions sont choisies de façon à pouvoir négliger, d'une part, en milieu basique, les complexes hydroxylés LnYOH mis en évidence par Gupta et Powell [35], et, d'autre part, en milieu acide, les espèces Ln^{3+} et $LnCl_n^{(3-n)+}$ [36]. De plus, les constantes de formation du complexe 1:1 LnY sont telles que dans tous les cas examinés, à l'exception pourtant de celui de l'acide nitrilotriacétique, la formation d'espèces LnL_m (m = 1, 2 ou 3) peut être négligée. Le cas particulier du système LnYZ sera discuté plus loin.

La courbe de titrage est tout d'abord interprétée, dans son entièreté, sans tenir compte de la présence éventuelle en solution des espèces Ln^{3+}, $LnCl_n^{(3-n)+}$ ou LnYOH; on obtient ainsi des constantes approximatives mais suffisamment précises pour pouvoir évaluer le domaine de pH où ces espèces sont réellement négligeables et qui servira, dans un second traitement, pour obtenir les constantes correctes.

Une ultime vérification est réalisée grâce au programme COMICS [37] qui permet, moyennant la connaissance des constantes de formation de toutes les espèces présentes en solution, le calcul et la représentation graphique de leur répartition, en fonction du pH. On peut ainsi vérifier si, dans le domaine de pH utilisé pour le calcul des constantes de formation des complexes mixtes et doubles, les concentrations des entités Ln^{3+}, $LnCl_n^{(3-n)+}$ et LnYOH peuvent effectivement être négligées.

EXPERIMENTATION

Appareillage

Comme le montrent les Figs. 1 et 2, la différence entre les courbes de titrage de l'acide H_nL seul et de l'acide en présence du complexe LnY peut être très

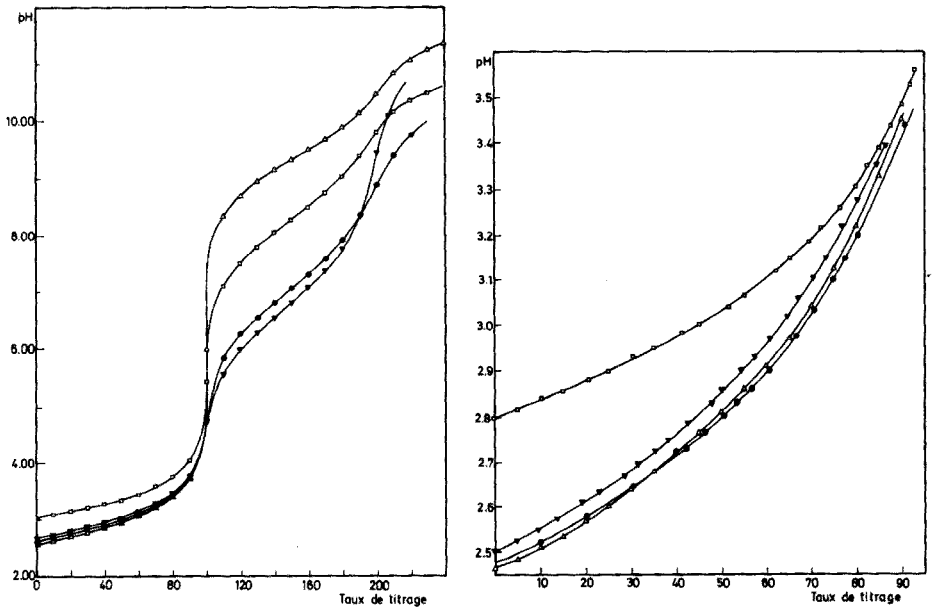

Fig. 1. Courbes de titrage de l'acide iminodiacétique seul et en présence des complexes LaY, EuY et LuY respectivement. △: IMDA. □: IMDA + LaY. ▼: IMDA + EuY. ●: IMDA + LuY.

Fig. 2. Courbes de titrage, en milieu acide, de l'acide hydroxyéthyléthylènediaminetriacétique seul et en présence des complexes LaY, EuY et LuY respectivement. △: HEDTA. □: HEDTA + LaY. ▼: HEDTA + EuY. ●: HEDTA + LuY.

faible, en milieu acide surtout, et ces courbes ne peuvent fournir des renseignements quantitatifs sur les produits de réactions entre H_nL et LnY que si elles sont établies avec une très grande précision. Ces exigences expérimentales ont nécessité la réalisation d'un titrateur automatique décrit précédemment [38] qui fournit, en tout point de la courbe de titrage, une reproductibilité, une précision et une exactitude supérieures au millième d'unité pH.

Réactifs

L'origine, la purification et l'étalonnage des acides chélatants H_nL ont été décrits en détail [33, 34]; il y est également fait mention du conditionnement des autres réactifs (KCl, Ln_2O_3), de la préparation du réactif titrant (KOH exempt de carbonate) et des caractéristiques du coulomètre.

Préparation des solutions à titrer

Toutes les solutions, à l'exception de celles des complexes de praséodyme et de terbium, sont préparées par attaque à 100°C de 0,00125 M de Ln_2O_3 par une solution contenant 0,0025 M de HEDTA, 0,0025 M de l'autre acide complexant H_nL et 0,25 M de KCl; la solution refroidie est amenée à 250,00 ml.

On obtient ainsi des solutions équimolaires en métal et en chacun des acides chélatants (0,01000 M) dont la force ionique est égale à 1. Ces conditions nous paraissent les plus favorables pour la mise en évidence des complexes mixtes; en effet, une réduction de la concentration en H_nL, tout en diminuant la concentration en complexes mixtes formés, pourrait conduire à la formation d'espèces polynucléaires; par contre, un excès du second complexant, bien que favorisant la formation des complexes mixtes, diminuerait les différences de pH entre les deux courbes de titrage et rendrait ainsi plus difficile l'obtention des informations sur les complexes mixtes; on pourrait également craindre, dans ces conditions, la formation de complexes LnL_m.

Dans le cas des oxydes non stoechiométriques Pr_6O_{11} et Tb_4O_7, on réalise une attaque à chaud par le HEDTA; après filtration de l'oxyde en excès, on refroidit la solution et le complexe 1:1 précipite. Il est filtré, séché et analysé par thermogravimétrie pour déterminer le nombre de molécules d'eau d'hydratation. Les solutions sont alors préparées par pesée de ce complexe hydraté.

Conditions des titrages

Elles sont les mêmes pour tous les systèmes étudiés et elles sont reprises au Tableau 1.

Traitement des résultats

Nous avons signalé plus haut que les conditions de travail ont été choisies pour que les proportions des espèces LnYOH, LnL_m, Ln^{3+} et $LnCl_n^{(3-n)+}$ soient négligeables et, en conséquence, les courbes de titrage des acides chélatants, en présence du complexe LnY, peuvent s'exprimer par les relations qui suivent. (Les symboles utilisés sont repris au Tableau 2.)

TABLEAU 1

Conditions des titrages pour la détermination des constantes de formation des complexes mixtes et doubles LnYL

Electrode indicatrice	H^+/H_2 sur électrode Pt/noir de Pt
Electrode de référence	Ag/AgCl ($E°$ = 0,22230 V)
Cellule de référence	KCl molal ($\gamma^{\pm}_{HCl}$ = 0,720)
Pont de jonction	KCl molal
Pression H_2	760 mm Hg
Débit H_2	100 ml min^{-1}
Température	(25,00 ± 0,01)°C
Solution à titrer	100,08 ml de solution 0,01000 M en LnY et 0,01000 M en H_nL. Force ionique égale à 1 (KCl)
Solution titrante[a]	0,0999 M en KOH. μ = 1 (KCl)
Volume d'une injection	0,1000 ml
Durée des titrages	environ 6 h par proton titré

[a]Des titrages coulométriques ont également été réalisés; les caractéristiques du coulométre utilisé ont été décrites [34].

TABLEAU 2

Symboles utilisés

$[H^+]$, $[OH^-]$	Concentrations en protons et en ions hydroxyles (mol l^{-1}). La connaissance de $\gamma^{\pm}_{HCl}$, du potentiel de jonction E_j, du produit $m_{H^+} m_{OH^-}$ et du rapport molarité/molalité dans nos conditions expérimentales, permet la transformation des mesures d'activité (pH) en molarités [33].
C_{OH}	Molarité de la solution titrante de KOH (mol l^{-1}).
C_{H_nL}	Concentration initiale de l'agent complexant H_nL (mol l^{-1}).
C_{LnY}	Concentration initiale en complexe LnY; elle est égale à la concentration initiale en métal ou en HEDTA; en effet, étant donné que les espèces Ln^{3+}, $LnCl_n^{(3-n)+}$ et LnL_m sont inexistantes, on peut considérer que le métal est entièrement complexé par le HEDTA sous forme de LnY. Rappelons en plus que nos conditions expérimentales sont choisies de telle façon que $C_{LnY} = C_{H_nL}$.
v°	Volume initial de la solution à titrer (ml).
v_i	Volume de potasse ajouté au $i^{ième}$ point de la courbe de titrage (ml).
$v_{calc.i}$	Volume de solution de potasse ajouté, calculé par l'ordinateur, au $i^{ième}$ point de la courbe de titrage (ml).
f	Facteur de dilution = $v^\circ/v^\circ + v_i$.
$C'_{H_nL} = \sum_{i=0}^{i=N} [H_iL]$	Concentration totale en complexant libre dans le volume $v^\circ + v_i$.
$\theta_i = \frac{[H_iL]}{C'_{H_nL}}$	Proportion de complexant libre sous forme H_iL.
K_j	Constante de formation partielle du complexe mixte $LnYLH_j$. $K_j = [LnYLH_j]/[LnY]\,[H_jL]$.
N	Nombre maximum de protons fixés sur le polyacide (H_nL); dans tous les cas considérés, $N = n + 1$.
M	Nombre maximum de protons fixés sur le complexe mixte; en général, $M = N = n + 1$; on aura donc $M + 1$ complexes mixtes en solution, c-à-d $M + 1$ constantes de formation à déterminer.
W	Nombre de points constituant la courbe de titrage $100 < W < 200$

Bilan en protons

$$n \cdot C_{H_nL} \cdot f = [H^+] - [OH^-] + \sum_{i=1}^{N} i\,[H_iL] + \sum_{j=1}^{M} j\,[LnYLH_j] + C_{OH} \cdot v_i/v^\circ + v_i \qquad (1)$$

Bilan en métal

$$C_{\mathrm{LnY}} \cdot f = [\mathrm{LnY}] + \sum_{j=0}^{M} [\mathrm{LnYLH}_j] \tag{2}$$

Bilan en complexant $\mathrm{H}_n\mathrm{L}$

$$C_{\mathrm{H}_n\mathrm{L}} \cdot f = \sum_{i=0}^{N} [\mathrm{H}_i\mathrm{L}] + \sum_{j=0}^{M} [\mathrm{LnYLH}_j] \tag{3}$$

Tenant compte du fait que $C_{\mathrm{LnY}} = C_{\mathrm{H}_n\mathrm{L}}$, on peut tirer des éqns. (2) et (3) la relation

$$[\mathrm{LnY}] = \sum_{i=0}^{N} [\mathrm{H}_i\mathrm{L}] = C'_{\mathrm{H}_n\mathrm{L}}$$

L'équation (2) peut alors se transformer comme suit

$$C_{\mathrm{LnY}} \cdot f = [\mathrm{LnY}] + [\mathrm{LnY}]^2 \sum_{j=0}^{M} K_j \, \theta_j \tag{4}$$

On obtient une éqn. (4) du second degré en LnY dont les coefficients, variables en chaque point de la courbe de titrage, contiennent les constantes à ajuster.

L'équation (1) peut prendre la forme

$$n \cdot C_{\mathrm{H}_n\mathrm{L}} \cdot f = [\mathrm{H}^+] - [\mathrm{OH}^-] + [\mathrm{LnY}] \sum_{i=1}^{N} i \cdot \theta_i + [\mathrm{LnY}]^2 \sum_{j=1}^{M} j \cdot \theta_j \cdot K_j + C_{\mathrm{OH}} \cdot v_i / v_i + v^\circ \tag{5}$$

En remplaçant, dans cette éqn. (5), [LnY] par sa valeur tirée de (4), on peut calculer le volume $v_{\mathrm{calc.}_i}$ de potasse ajouté au $i^{\mathrm{ième}}$ point de la courbe de titrage. Les constantes de formation des complexes mixtes K_j sont ajustées par approximations successives [33], de manière que ${}^{W}\Sigma_{i=1}(v_i - v_{\mathrm{calc.}_i})^2$ soit minimum.

Moyennant les mêmes restrictions expérimentales, un traitement analogue peut être appliqué aux complexes mixtes $\mathrm{LnY'YH}_j$; il faudra cependant tenir compte, dans ce cas, de la forme protonée du complexe 1:1 LnY'H [33].

Enfin, dans le cas des titrages coulométriques, la méthode de calcul reste en tous points semblable: la quantité d'ions hydroxyles ajoutée est déduite du nombre de coulombs injectés et le facteur de dilution est évidemment supprimé.

RESULTATS

Les valeurs des constantes de formation K_j et des pK qui en résultent sont groupées dans les tableaux 3—7.

TABLEAU 3

Constantes de formation partielles des complexes Ln—HEDTA—Glycocolle
(μ = 1 (KCl) t = (25,00 ± 0,01)°C)

Cations	$\log K_0$ $LnYG^-$	$\log K_1$ LnYGH	$\log K_2$ $LnYGH_2^+$	pK_{-1} $LnYGH_3^{2+}$	pK_0 $LnYGH_2^{2+}$	pK_1 LnYGH
H^+					pK_{H_0} = 2,48	pK_{H_1} = 9,67
La	3,11 ± 0,03	2,93 ± 0,02	3,40 ± 0,04	2,92	2,95	9,48
Pr	3,20 ± 0,05	2,86 ± 0,01	3,03 ± 0,05	2,49	2,65	9,32
Nd	3,36 ± 0,02	2,90 ± 0,01	3,03 ± 0,04	2,37	2,61	9,20
Sm	3,56 ± 0,03	3,00 ± 0,01	3,08 ± 0,03	2,17	2,56	9,10
Eu	3,58 ± 0,01	2,99 ± 0,01	3,03 ± 0,06	2,08	2,52	9,07
Gd	3,70 ± 0,01	3,00 ± 0,01	3,10 ± 0,01	2,14	2,58	8,96
Tb	3,97 ± 0,01	3,03 ± 0,01	3,11 ± 0,01	2,14	2,56	8,72
Dy	4,14 ± 0,03	3,17 ± 0,04	3,25 ± 0,03	2,14	2,56	8,69
Ho	4,24 ± 0,01	2,98 ± 0,01	3,04 ± 0,04	2,19	2,54	8,40
Er	4,32 ± 0,03	3,13 ± 0,01	3,20 ± 0,03	2,08	2,55	8,47
Tm	4,39 ± 0,03	3,01 ± 0,01	3,03 ± 0,03	2,12	2,50	8,28
Yb	4,38 ± 0,05	3,03 ± 0,02	3,06 ± 0,01	1,88	2,51	8,31
Lu	4,26 ± 0,01	2,97 ± 0,02	3,07 ± 0,01	1,69	2,58	8,37

TABLEAU 4

Constantes de formation partielles des complexes Ln—HEDTA—IMDA
(μ = 1 (KCl); t = (25,00 ± 0,01)°C)

Cation	$\log K_0$ $LnYX^{2-}$	$\log K_1$ $LnYXH^-$	$\log K_2$ $LnYXH_2$	$\log K_3$ $LnYXH_3^+$	pK_0 $LnYXH_3^+$	pK_1 $LnYXH_2$	pK_2 $LnYXH^-$
H^+					pK_{H_0} = 1,84	pK_{H_1} = 2,57	pK_{H_2} = 9,27
La	3,36 ± 0,01	0,98 ± 0,05	1,95 ± 0,03	3,61 ± 0,01	3,50	3,54	6,89
Pr	3,98 ± 0,01	1,40 ± 0,01	2,22 ± 0,02	3,04 ± 0,01	2,66	3,39	6,69
Nd	4,26 ± 0,01	1,40 ± 0,02	1,92 ± 0,02	2,83 ± 0,01	2,75	3,09	6,41
							$pK_{1,2}$ [a]
Sm	4,64 ± 0,01	—	0,95 ± 0,03	2,39 ± 0,02	3,28		4,08
Eu	4,94 ± 0,01	—	1,00 ± 0,02	2,41 ± 0,02	3,25		3,95
Gd	5,07 ±0,01	—	1,02 ± 0,04	2,39 ± 0,02	3,21		3,90
Tb	5,36 ± 0,01	—	1,08 ± 0,06	2,47 ± 0,02	3,23		3,78
Dy	5,41 ± 0,01	—	0,90 ± 0,06	2,38 ±0,07	3,32		3,67
Ho	5,49 ± 0,01	—	1,18 ± 0,02	2,41 ± 0,02	3,07		3,77
Er	5,35 ± 0,01	—	0,91 ± 0,04	2,29 ± 0,02	3,22		3,70
Tm	5,12 ± 0,01	—	0,98 ± 0,06	2,21 ± 0,02	3,07		3,85
Yb	4,79 ± 0,02	—	0,63 ± 0,08	2,04 ± 0,02	3,25		3,84
Lu	4,60 ± 0,01	—	0,70 ± 0,06	1,99 ± 0,02	3,13		3,97

[a] $pK_{1,2} = \frac{1}{2}(pK_{H_1} + pK_{H_2} - \log K_0 + \log K_2)$

TABLEAU 5

Constantes de formation partielles des complexes Ln—HEDTA—NTA

(μ = 1 (KCl); t = (25,00 ± 0,01)°C)

Cations	$\log K_0$ $LnYZ^{3-}$	$\log K_1$ $LnYZH^{2-}$	$\log K_2$ $LnYZH_2^-$	$\log K_3$ $LnYZH_3$	$\log K_4$ $LnYZH_4^+$	pK_0 $LnYZH_4^+$	pK_1 $LnYZH_3$	$pK_{2,3}$[a] $LnYZH_2^-$	
H^+						pK_{H_0} = 1,03	pK_{H_1} = 1,75	pK_{H_2} = 2,31	pK_{H_3} = 9,34
La	5,48 ± 0,01		3,00 ± 0,01	3,22 ± 0,02	5,43 ± 0,01	3,36	1,95	4,59	
Pr	5,53 ± 0,01		2,54 ± 0,01	2,73 ± 0,02	4,45 ± 0,01	2,87	1,92	4,34	
Nd	5,55 ± 0,01		2,24 ± 0,02	2,19 ± 0,05	4,10 ± 0,01	3,06	1,68	4,17	
Sm	5,85 ± 0,01		1,81 ± 0,02	1,95 ± 0,03	3,62 ± 0,01	2,82	1,87	3,81	
Eu	6,02 ± 0,01		1,63 ± 0,02	2,19 ± 0,02	3,48 ± 0,01	2,44	2,29	3,64	
Gd	6,09 ± 0,02		1,55 ± 0,03	2,11 ± 0,02	3,45 ± 0,01	2,49	2,29	3,56	
Tb	6,12 ± 0,01		1,60 ± 0,03	2,02 ± 0,03	3,47 ± 0,01	2,60	2,15	3,57	
Dy	6,16 ± 0,01		1,49 ± 0,03	1,75 ± 0,04	3,45 ± 0,01	2,85	1,99	3,50	
Ho	6,18 ± 0,01		1,63 ± 0,04	2,24 ± 0,02	3,45 ± 0,01	2,36	2,34	3,56	
Er	5,95 ± 0,01		1,64 ± 0,04	2,05 ± 0,03	3,43 ± 0,01	2,53	2,14	3,67	
Tm	5,73 ± 0,03		1,80 ± 0,05	2,25 ± 0,04	3,37 ± 0,02	2,27	2,18	3,87	
Yb	5,37 ± 0,02		1,45 ± 0,09	1,94 ± 0,06	3,18 ± 0,02	2,39	2,22	3,87	
Lu	5,25 ± 0,02		1,40 ± 0,09	2,01 ± 0,06	3,04 ± 0,04	2,18	2,34	3,91	

[a] $pK_{2,3} = \frac{1}{2}(pK_{H_2} + pK_{H_3} - \log K_0 + \log K_2)$.

TABLEAU 6

Constantes de formation partielles des complexes $Ln(HEDTA)_2$
(μ = 1 (KCl); t = (25,00 ± 0,01)°C)

Cations	$\log K_0$ LnY_2^{3-}	$\log K_1$ LnY_2H^{2-}	$\log K_2$ $LnY_2H_2^-$	$\log K_3$ LnY_2H_3	$\log K_4$ $LnY_2H_4^+$	pK_0 $LnY_2H_4^+$	pK_1 LnY_2H_3	pK_2 $LnY_2H_2^-$	pK_3 LnY_2H^{2-}
H^+						pK_{H_0} = 1,66	pK_{H_1} = 2,348	pK_{H_2} = 5,447	pK_{H_3} = 9,729
						$pK_{0,1}$[a]			
La	3,62 ± 0,01	2,02 ± 0,01	1,74 ± 0,02		3,58 ± 0,01	2,94		5,17	8,13
Pr	3,40 ± 0,01	1,65 ± 0,02	0,94 ± 0,04		2,55 ± 0,01	2,80		4,74	7,98
						$pK_{0,2}$[b]			
Nd	3,48 ± 0,01	1,70 ± 0,01			2,35 ± 0,02	3,37			7,95
Sm	3,66 ± 0,01	1,97 ± 0,01			2,07 ± 0,02	3,19			8,04
Eu	3,85 ± 0,01	2,15 ± 0,01			2,04 ± 0,02	3,12			8,04
Gd	3,91 ± 0,01	2,25 ± 0,01			1,99 ± 0,04	3,07			8,07
Tb	4,06 ± 0,01	2,42 ± 0,02			1,96 ± 0,04	3,00			8,09
Dy	4,14 ± 0,01	2,53 ± 0,01			1,95 ± 0,03	3,01			8,15
Ho	4,07 ± 0,02	2,50 ± 0,01			1,91 ± 0,03	2,96			8,15
Er	3,95 ± 0,03	2,37 ± 0,01			1,76 ± 0,04	2,95			8,15
						$pK_{0,1}$			
Tm	3,77 ± 0,01	2,11 ± 0,02	0,16 ± 0,12		1,71 ± 0,04	2,78		3,50	8,07
Yb	3,75 ± 0,01	1,90 ± 0,02	0,86 ± 0,10	0,73 ± 0,12	1,54 ± 0,06	2,47	2,04	4,31	7,91
Lu	3,56 ± 0,01	1,82 ± 0,01	1,32 ± 0,05	1,39 ± 0,04	1,59 ± 0,05	1,86	2,43	4,95	7,99

[a] $pK_{0,1} = \frac{1}{2}(pK_{H_0} + pK_{H_1} - \log K_2 + \log K_4)$.
[b] $pK_{0,2} = \frac{1}{3}(pK_{H_0} + pK_{H_1} + pK_{H_2} - \log K_1 + \log K_4)$.

TABLEAU 7

Constantes de formation partielles des complexes Ln—EDTA—HEDTA
(μ = 1 (KCl); t = (25,00 ± 0,01)°C. pK_{HEDTA} = 1,66; 2,348; 5,447; 9,279)

Cations	log K_0 $LnY'Y^{4-}$	log K_1 $LnY'YH^{4-}$	log K_2 $LnY'YH_2^{2-}$	log K_3 $LnY'YH_3^-$	pK_2 $LnY'YH_3^-$	pK_3 $LnY'YH_2^{2-}$	pK_4 $LnY'YH^{3-}$
La	Solubilité trop faible de LnY'						
Pr	Solubilité trop faible de LnY'						
Nd	3,23 ± 0,02	1,75 ± 0,04	1,82 ± 0,02	—	—	6,28	8,31
Sm	3,51 ± 0,04	2,06 ± 0,04	1,82 ± 0,04	—	—	5,97	8,34
Eu	3,53 ± 0,02	2,02 ± 0,03	1,57 ± 0,04	—	—	5,76	8,28
Gd	3,40 ± 0,02	2,06 ± 0,04	1,28 ± 0,06	—	—	5,43	8,45
Tb	3,28 ± 0,03	2,02 ± 0,03	1,29 ± 0,06	—	—	5,48	8,53
Dy	3,10 ± 0,01	1,92 ± 0,02	1,45 ± 0,06	—	—	5,74	8,61
Ho	2,82 ± 0,02	1,83 ± 0,04	1,54 ± 0,06	0,60 ± 0,02	1,51	5,92	8,80
Er	2,69 ± 0,01	1,89 ± 0,04	1,97 ± 0,04	1,22 ± 0,08	1,70	6,29	8,99
Tm	2,50 ± 0,03	1,95 ± 0,04	1,96 ± 0,03	1,74 ± 0,07	2,23	6,22	9,24
Yb	2,43 ± 0,02	1,97 ± 0,02	1,94 ± 0,02	1,58 ± 0,09	2,09	6,18	9,33
Lu	2,41 ± 0,03	1,98 ± 0,03	1,96 ± 0,02	1,63 ± 0,09	2,12	6,19	9,36

Comme pour les pK des acides aminoacétiques [33], l'écart-type d'une constante, calculé par ordinateur sur les X points d'une courbe de titrage, est en général plus faible que celui obtenu sur plusieurs expériences identiques; cela provient des erreurs expérimentales inhérentes à la préparation des solutions. L'erreur dont nous affectons nos constantes est la moyenne des différences entre chaque valeur et la valeur moyenne

$$\epsilon = 1/t \sum_{i=1}^{t} (\overline{K}_{j_i} - K_{j_i})$$

t étant le nombre de mesures expérimentales effectuées.

DISCUSSION

Les complexes non-protonés

Evolution de la constante de formation du complexe mixte ou double avec le nombre atomique du lanthanide. Il existe, dans la littérature, de nombreux exemples de complexes doubles ou mixtes non-protonés entre les lanthanides trivalents et les acides aminoacétiques; de nombreux travaux ont été consacrés à la détermination de leur constante de formation par potentiométrie, par polarographie et par spectroscopie d'absorption visible [25, 30, 39, 40—48]. C'est la raison pour laquelle nous aborderons la discussion de nos résultats par l'examen de ces espèces dont il n'est plus nécessaire de prouver l'existence.

Comme il ressort de la Fig. 1, la courbe de titrage du ligand H_nL est affectée de manière importante en milieu basique par la présence du complexe LnY. C'est bien la preuve de la formation du complexe mixte non-protoné dans ce domaine de pH; cette modification, plus ou moins importante suivant le lanthanide considéré, de la courbe de titrage du complexant H_nL facilite d'ailleurs le calcul de la constante de formation du complexe.

La Fig. 3 représente l'évolution du logarithme de la constante de formation partielle du complexe mixte non-protoné pour les systèmes Ln—EDTA—L [25] et Ln—HEDTA—L: la plupart des courbes présentent une allure en cloche dont le maximum se déplace avec la nature du ligand considéré. Plus le nombre de sites actifs augmente, plus le maximum est déplacé vers les terres rares cériques.

L'interprétation avancée par Geier et Karlen [25] pour expliquer les variations en fonction de Z des ΔG, ΔH et ΔS des réactions globales et partielles de formation des complexes mixtes LnY'L à base de EDTA d'une part et de OXS, IMDA ou NTA d'autre part, est que le nombre de molécules d'eau de la première sphère de coordination du complexe 1:1 LnY' diminue d'une unité en passant des terres cériques aux terres yttriques. Dans ces conditions, lors de la formation du complexe mixte avec OXS bidenté, on assiste à la substitution de deux molécules d'eau pour tout la série des terres rares, ce qui conduit à une augmentation continue de la constante de stabilité partielle avec Z, due à la contraction du rayon ionique.

Par contre, si le second ligand possède un nombre de sites de coordination d'au moins trois, comme dans l'IMDA ou le NTA, la formation des complexes mixtes déplace trois H_2O pour les terres cériques et deux pour les yttriques et, de ce fait, entraîne une diminution de la variation entropique (ΔS), c'est-à-dire de la stabilité.

Si maintenant on remplace l'EDTA par le HEDTA, les variations de ΔH et ΔS en fonction de Z correspondant à la formation du complexe 1:1 montrent des comportements fort analogues (Fig. 4): augmentation de ΔS et diminution concommittante de $-\Delta H$: il faut cependant remarquer que la

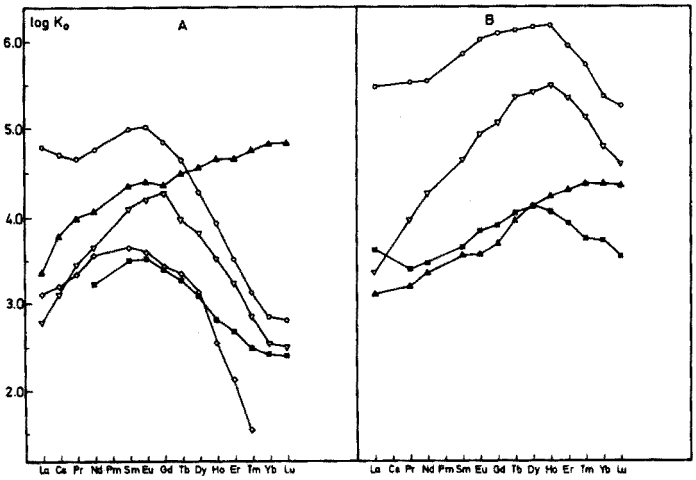

Fig. 3. Evolution, en fonction du nombre atomique des lanthanides, des constantes partielles de formation des complexes 1:2 et mixtes formés entre l'EDTA (A) ou le HEDTA (B) d'une part et divers acides aminoacétiques d'autre part. (A) ○: EDTA—NTA [25]. ▽: EDTA—IMDA [25]. ■: EDTA—HEDTA. ▲: EDTA—OXS [25]. ◇: EDTA—EDTA [40]. (B) ○: HEDTA—NTA. ▽: HEDTA—IMDA. ■: HEDTA—HEDTA. ▲: HEDTA—Glycine.

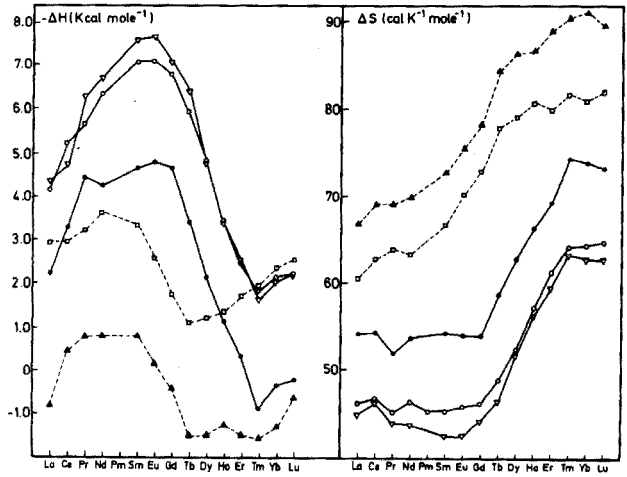

Fig. 4. Evolution, en fonction du nombre atomique des lanthanides, des ΔH et ΔS de formation des complexes 1:1 avec l'EDTA et le HEDTA. Les courbes en trait plein s'appliquent aux complexes 1:1 du HEDTA, les courbes en traits interrompus aux complexes 1:1 de l'EDTA. ○: t = 25°C, μ = 0,1 M (KCl) [12]. ▽: t = 25°C, μ = 0,5 M ($NaClO_4$) [49]. ●: t = 25°C, μ = 0,1 M (KNO_3) [50]. □: t = 20°C, μ = 0,1 M (KNO_3) [4]. ▲: t = 25°C, μ = 0,1 M KCl. [51].

discontinuité se produit plus tôt avec l'EDTA (entre Nd et Tb) qu'avec le HEDTA (entre Gd et Tm). On est tenté d'en conclure, en adoptant l'argumentation des auteurs ci-dessus, que le nombre de molécules d'eau de solvatation de LnY diminue également d'une unité en passant du Gd au Tm et que, par ailleurs, pour le même lanthanide, LnY′ contient, sans doute, une molécule d'eau de moins que LnY dans la première sphère de coordination.

Où nous conduit alors l'interprétation de Geier et Karlen [25] du point de vue de l'évolution de la stabilité des complexes LnYL en fonction du nombre atomique? Avec le glycocolle et l'IMDA, on s'attendrait à trouver une augmentation continue de K_0 avec Z, tandis que le NTA ou le HEDTA devraient produire une diminution brusque de la stabilité des terres yttriques qui serait cependant située vers des Z plus élevés que dans le cas de l'EDTA Les courbes de la Fig. 3 semblent montrer une évolution allant dans ce sens, encore que seul le glycocolle, au même titre que l'OXS pour le système EDTA, semble se comporter de cette façon, puisque, pour l'IMDA, on observe déjà une chute à partir du holmium. On est donc tenté de conclure que, dans le complexe LnY, le HEDTA, est un ligand hexadenté, au même titre que l'EDTA ou, en tous cas, qu'il déplace, par complexation, le même nombre de molécules d'eau que l'EDTA.

La Fig. 5 représente l'évolution, en fonction de Z, de la constante globale de formation des complexes mixtes et doubles avec l'EDTA d'une part et le HEDTA d'autre part: des différences assez sensibles apparaissent entre les deux systèmes; alors que les valeurs des constantes partielles de formation

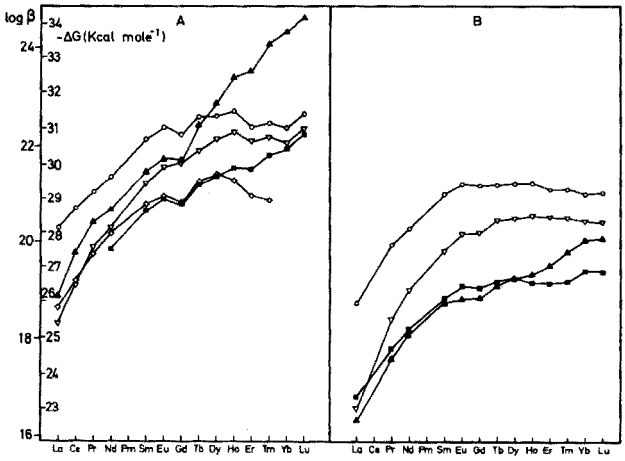

Fig. 5. Evolution, en fonction du nombre atomique des lanthanides, des constantes de formation globales des complexes 1:2 et mixtes formés entre l'EDTA (A) et le HEDTA (B) d'une part et divers acides aminoacétiques d'autre part. (A) ○: EDTA—NTA. ▽: EDTA—IMDA. ■: EDTA—HEDTA. ▲: EDTA—OXS. ◇: EDTA—EDTA. (B) ○: HEDTA—NTA. ▽: HEDTA—IMDA. ■: HEDTA—HEDTA. ▲: HEDTA—Glycine.

des complexes mixtes sont du même ordre de grandeur pour les deux systèmes considérés, (Fig. 3) les constantes globales sont 10^{-2}—10^{-3} fois plus élevées pour les complexes LnY'L si on les compare aux complexes LnYL (au niveau des terres yttriques surtout). Par ailleurs, pour le système LnY'L, on assiste à une évolution régulière de la constante en fonction de Z tant que le nombre total de coordinats ne dépasse pas 8; pour le système LnYL, même lorsque L est le glycocolle, on observe un applatissement au niveau des terres yttriques.

L'hypothèse de Geier et Karlen ne semble pas suffisante à elle seule pour interpréter tous les résultats. Certains arguments tendent à prouver que le HEDTA est hexadenté dans ses complexes simples LnY avec les terres cériques alors qu'il est pentadenté dans les complexes des terres yttriques tout en déplaçant toujours le même nombre de molécules d'eau que l'EDTA; ainsi, sur la Fig. 4, on constate une évolution similaire de ΔS pour les complexes LnY et LnY', ce qui tend à prouver que, comme l'EDTA, le HEDTA en se liant aux terres yttriques déplace, de la sphère interne de coordination du cation, une molécule d'eau de plus qu'en complexant les terres cériques. Par contre, la discontinuité dans l'évolution de ΔH est deux fois plus importante dans le cas des complexes LnY comparés aux complexes LnY'; on peut interpréter ce fait en admettant la perte par le HEDTA d'un site coordinant au niveau des terres yttriques. On peut également rappeler le travail de Merciny et al. [19] sur les complexes LnY à l'état solide qui met en évidence un comportement analogue du HEDTA en fonction du nombre atomique. Une étude par spectroscopie d'absorption visible en cours de publication semble indiquer que, dans les complexes simples LnY, le HEDTA est hexadenté au niveau des terres cériques et pentadenté pour les terres

yttriques, alors que, dans les complexes mixtes et doubles, il est toujours lié par cinq sites, quel que soit le lanthanide considéré. Une étude est actuellement en cours en vue d'étudier l'évolution des ΔH et ΔS de formation des complexes 1:2 et mixtes en fonction du nombre atomique des lanthanides: l'interprétation des premiers résultats est en accord avec l'hypothèse du changement dans le degré de coordination du HEDTA.

Sur la base de ces considérations et de l'hypothèse de Geier et Karlen, il devient possible d'interpréter nos résultats: le fait de passer de l'état hexacoordiné à l'état pentacoordiné ne diminue en rien l'encombrement stérique de la molécule de HEDTA et on peut donc admettre que le nombre de molécules d'eau déplacées pour former le complexe 1:1 est le même pour le HEDTA et l'EDTA, quel que soit le lanthanide considéré. On peut alors comprendre le fait que les deux systèmes se comportent de façon semblable du point de vue de l'évolution des constantes partielles de formation des complexes mixtes. Par contre, la constante globale de formation de ces complexes doit être affectée par ce changement dans le degré de coordination du HEDTA: les valeurs de la constante sont très inférieures à celles observées pour l'EDTA et de plus, même dans le cas des complexes avec la glycine, on observe, à partir du Sm, un plateau dans l'évolution de cette constante en fonction de Z, plateau qui n'est que le reflet de celui que l'on observe dans l'évolution de la constante de formation des complexes simples en fonction de Z: pour l'europium, cette valeur est égale à $10^{15,3}$ et elle reste constante jusqu'à l'erbium ($10^{15,4}$).

Evolution des constantes de formation des complexes en fonction du nombre de sites de fixation des ligands. Sur la Fig. 6, nous avons porté en graphique le logarithme des constantes de formation globales ($\log \beta$) de

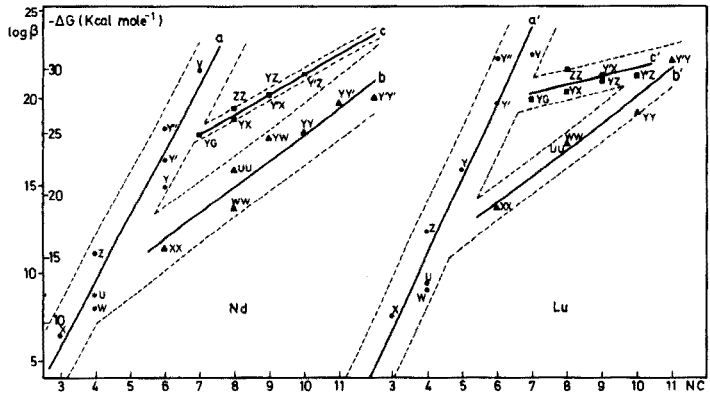

Fig. 6. Evolution des constantes globales de formation des complexes 1:1, 1:2 et mixtes formés entre deux lanthanides (Nd et Lu) et divers acides aminoacétiques en fonction du nombre de sites de coordination de ces différents chélates. Y = HEDTA. Y' = EDTA. Y'' = DCTA (acide diaminocyclohexanetétraacétique). X = IMDA. Z = NTA. G = Glycine. V = DTPA (acide diéthylènetriaminepentaacétique). W = EDDA (acide éthylènediaminediacétique). U = HIMDA (acide hydroxyéthyliminodiacétique).

complexes 1:1, 1:2, doubles et mixtes de deux lanthanides (Lu, Nd) avec divers acides aminoacétiques, en fonction du nombre total de sites de coordination disponibles avec ces chélatants (NC). Diverses constatations peuvent être faites: (1) comme l'a déjà fait remarquer Choppin [1], log β des complexes 1:1 croît grosso modo linéairement avec le nombre de sites de coordination (NC) du chélatant (zone a et a'); (2) les valeurs de log β des complexes 1:2 et mixtes ne s'intègrent pas dans cette évolution: pour un nombre de sites donné, les constantes sont systématiquement beaucoup plus petites que celles correspondant à un complexe 1:1; (3) les valeurs de log β des complexes 1:2 et mixtes peuvent néanmoins se classer dans deux zones (b et c) de pente positive mais inférieure à celle obtenue dans le cas des complexes 1:1; ces zones s'étendent jusqu'à des valeurs de NC = 11, fait plutôt surprenant puisque l'on admet généralement que le nombre de coordination maximum des lanthanides est 9; (4) les zones b et b' regroupent essentiellement des complexes 1:2 et des complexes mixtes pour lesquels les deux chélatants sont très semblables (par exemple, HEDTA—EDTA): dans la majorité des cas, les deux molécules chélatantes sont biaminées; (5) les zones c et c', par contre, groupent, à la seule exception du complexe $Ln(NTA)_2$, les complexes mixtes pour lesquels au moins l'un des chélatants est monoaminé.

Le fait que les valeurs de log β des complexes 1:2 ou mixtes soient systématiquement plus petites que celles des complexes 1:1 pour un nombre de sites de coordination donné, ne doit pas surprendre puisque l'effet entropique est plus favorable dans le second cas. La subdivision en deux groupes, à savoir type b (deux molécules chélatantes fort semblables et en général biazotées) et type c (deux molécules chélatantes différentes: en général une biazotée et une monoazotée) est plus difficile à interpréter et cette discussion sera abordée lorsque l'on disposera des valeurs de ΔH et ΔS.

Les complexes monoprotonés

Dans le cas du HEDTA, les complexes 1:2 monoprotonés LnY_2H^{2-} ont été mis en évidence par électrochromatographie et adsorption sur résine anionique [29]; leur constante de formation pour les lanthanides a été déterminée par Zur Nedden et al. [30] en milieu $NaClO_4$ à 25°C. La courbe qui représente l'évolution des log K_1 de ce complexe en fonction de Z (Fig. 7) a exactement la même allure que celle des complexes non-protonés LnY_2^{3-}; cela signifie une valeur constante du pK de LnY_2H^{2-} quel que soit le lanthanide considéré. Zur Nedden et al. interprètent cette constance du pK en admettant qu'un des groupements carboxyliques n'est pas coordiné au cation dans le complexe LnY_2^{3-} ce qui conduirait à une valeur de 9 pour le nombre de coordination des lanthanides. Si cette interprétation est correcte, on devrait observer, à fortiori, une situation analogue pour les complexes $LnY'YH^{3-}$. La Fig. 7 montre qu'il n'en est rien, pas plus d'ailleurs pour les complexes LnY'_2H^{4-} [40]. D'autre part, le nombre de coordination de 9 ne semble pas constituer une limite infranchissable (Fig. 6).

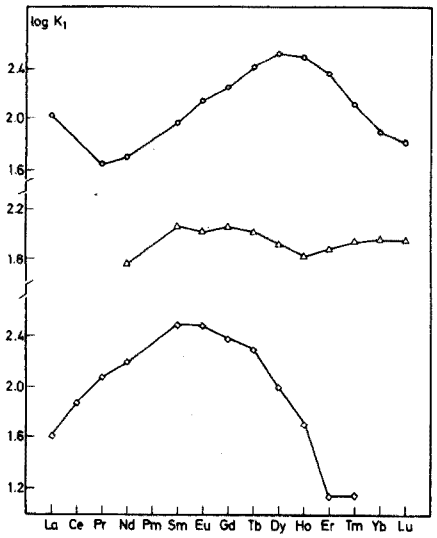

Fig. 7. Evolution, en fonction du nombre atomique, des constantes de formation des complexes 1:2 et mixtes monoprotonés que forment les lanthanides avec l'EDTA et le HEDTA. ○: LnY_2H^{2-}; △: $LnYY'H^{3-}$; ◇: LnY'_2H^{4-} [40].

En ce qui concerne les complexes mixtes que nous avons étudiés, la situation est très différente puisque le complexe monoprotoné ne semble exister que pour le système LnYG. Ainsi donc, on retrouve encore une fois pour log K_1 la subdivision en deux groupes comme dans la Fig. 6: les complexes qui peuvent fixer un proton sont essentiellement ceux du type b (deux chélatants biazotés), tandis que ceux pour lesquels la forme monoprotonée n'existe pas, sont essentiellement du type c (un chélatant biazoté l'autre monoazoté).

Il semble donc que, dans l'éventail des ligands examinés, il existe deux classes de complexes mixtes et doubles; il serait bien difficile, à ce stade, de formuler une interprétation, d'autant plus que ce classement est fait sur un nombre d'exemples assez limité et que la différence entre les deux groupes n'est pas toujours très nette. Enfin, quelle est la relation entre le nombre de coordination et le nombre de sites disponibles? La constante d'équilibre que nous mesurons est une grandeur macroscopique qui est la résultante d'un certain nombre de constantes microscopiques, chacune correspondant à une structure et un nombre de coordination donnés.

Les complexes multiprotonés

A l'exception du travail de Zur Nedden et al. [30], ces complexes multiprotonés ne sont pas signalés dans la littérature. La méthode d'investigation utilisée qui consiste à reproduire, par le calcul, les courbes de titrage en postulant la présence en solution de certaines espèces complexes ne constitue

évidemment pas une preuve irréfutable de leur existence. Comme nous l'avons vu dans les Figs. 1 et 2, on observe, en milieu acide, des décalages parfois assez importants entre la courbe de titrage de l'acide seul et celle de l'acide en présence de LnY; cela indique qu'une réaction, faisant intervenir des protons, se produit entre l'acide et le complexe en milieu acide. Il faut aussi signaler qu'il est possible de préparer des solutions 0,01 M de complexes mixtes de lanthane en milieu acide, alors que la solubilité de LaY n'est que de $5{,}5 \times 10^{-3}$ M. Enfin, il faut souligner l'excellente concordance que l'on obtient entre la courbe expérimentale et la courbe calculée en admettant l'existence des espèces multiprotonées $LnYLH_n$; ainsi, dans le cas de Sm—HEDTA—IMDA, la courbe théorique oscille de part et d'autre de la courbe expérimentale avec une amplitude inférieure à 0,006 méq (Fig. 8).

La Fig. 9 représente la variation de log K_4 en fonction de Z pour le complexe $LnY_2H_4^+$ pris comme exemple (on observe la même allure, quel que soit le système considéré). L'évolution est différente de celle obtenue pour les complexes non-protonés et monoprotonés: on observe une diminution de la stabilité en passant du lanthane au samarium, suivie d'un plateau jusqu'au holmium et d'une nouvelle diminution jusqu'au lutétium. Cette allure en escalier est très différente des courbes en cloches obtenues pour les complexes non-protonés et monoprotonés. Ce qui est remarquable, c'est que cette allure est exactement l'inverse de celle que l'on obtient pour les complexes 1:1 LnY où les constantes croissent du lanthane au samarium, gardent la même valeur jusqu'au holmium pour recommencer à croître du holmium au lutétium.

La stabilité de ces complexes est aussi tout à fait remarquable: la constante de formation des espèces $LnYLH_n^+$ est du même ordre de grandeur, voire même supérieure dans le cas des terres légères, à la constante de

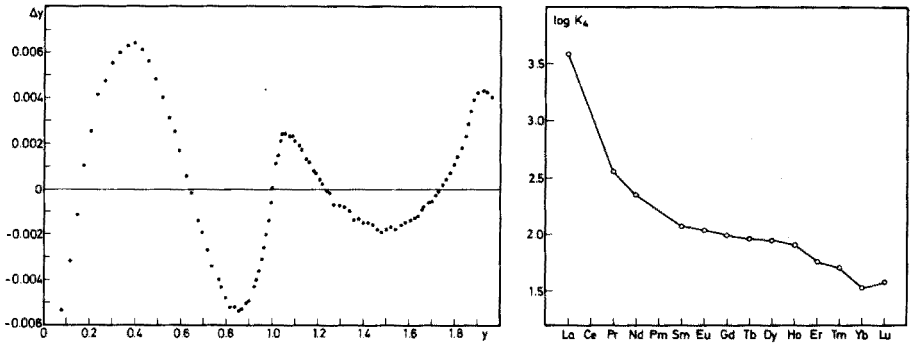

Fig. 8. Comparaison entre la courbe de titrage calculée et la courbe de titrage expérimentale dans le cas du système Sm—HEDTA—IMDA. y = nombre de milliéquivalents de OH^- ajoutés. ΔY = différence entre le nombre de milliéquivalents de OH^- ajoutés et le nombre de milliéquivalents de OH^- calculés pour une même valeur de pH.

Fig. 9. Evolution, en fonction du nombre atomique des lanthanides, des constantes partielles de formation des complexes multiprotonés $LnY_2H_4^+$.

formation des complexes non-protonés. Il est surprenant qu'en protonant un site qui était coordiné, on n'en diminue pas la stabilité. Dans l'état actuel de nos recherches, il est difficile et prématuré d'essayer d'interpréter ces résultats; il faut peut être faire intervenir un autre mécanisme réactionnel que la simple liaison cation-ligand, tel que, par exemple, une liaison par ponts hydrogène entre le complexe simple et la seconde molécule d'agent chélatant: $LnY\cdots H_nL$ Dans cette hypothèse, l'allure particulière de log K_4 en fonction de Z peut s'interpréter: l'augmentation de stabilité du complexe 1:1 LnY, lorsqu'on passe du lanthane au lutétium, implique une délocalisation de plus en plus importante des doublets électroniques des groupements carboxyliques et aminés vers l'ion central; ils sont ainsi de moins disponsibles pour une liaison par ponts hydrogène; log K_4 des complexes 1:2 et mixtes protonés doit donc diminuer en passant du lanthane au lutétium.

BIBLIOGRAPHIE

1 G. R. Choppin, Pure Appl. Chem., 27 (1971) 23.
2 D. F. Peppard, C. A. A. Bloomquist, E. P. Horwitz, S. Lewey et G. W. Mason, J. Inorg. Nucl. Chem., 32 (1970) 339.
3 S. Siekierski, J. Inorg. Nucl. Chem., 32 (1970) 519.
4 J. L. Mackey, J. E. Powell et F. H. Spedding, J. Am. Chem. Soc., 84 (1962) 2047.
5 F. H. Spedding, S. A. Crejka et C. W. de Koch, J. Phys. Chem., 70 (1966) 2423.
6 F. H. Spedding, et S. A. Crejka, J. Phys. Chem., 70 (1966) 2430.
7 F. H. Spedding, M. J. Pikal et B. O. Ayers, J. Phys. Chem., 70 (1966) 2440.
8 F. H. Spedding et K. C. Jones, J. Phys. Chem., 70 (1966) 2450.
9 L. A. K. Staveley, D. R. Markham et M. R. Jones, Nature, 211 (1966) 1172; J. Inorg. Chem., 30 (1968) 230.
10 S. L. Bertha et G. R. Choppin, Inorg. Chem., 8 (1969) 613.
11 R. J. Hinckey et J. W. Cobble, Inorg. Chem., 9 (1970) 917.
12 J. Fuger, E. Merciny et G. Duyckaerts, Bull. Soc. Chim. Belg., 77 (1968) 455.
13 W. E. Stewart et T. H. Siddal III, J. Inorg. Nucl. Chem., 30 (1968) 1513.
14 D. G. Karraker, J. Inorg. Nucl. Chem., 31 (1969) 2815.
15 C. R. Kanekar, V. R. Marothe et N. V. Thakur, Proc. Chem. Symp. 1 st, 2 (1969) 265.
16 W. E. Stewart et T. H. Siddal III, J. Inorg. Nucl. Chem., 32 (1970) 3599.
17 O. Vittori et M. Porthault, Bull. Soc. Chim. Fr., (1970) 4169.
18 P. Graham et M. Joesten, J. Inorg. Nucl. Chem., 32 (1970) 531.
19 E. Merciny, B. Gilbert et G. Duyckaerts, Bull. Soc. Chim. Belg., 80 (1971) 617.
20 F. A. Hart et F. P. Laming, J. Inorg. Nucl. Chem., 27 (1965) 1605.
21 F. A. Hart et F. P. Laming, J. Inorg. Nucl. Chem., 27 (1965) 1825.
22 S. S. Krishnamurthy et S. Soundarajan, J. Inorg. Nucl. Chem., 28 (1966) 1691.
23 T. Moeller et G. Vincentini, J. Inorg. Nucl. Chem., 27 (1965) 1477.
24 D. R. Cousins et F. A. Hart, J. Inorg. Nucl. Chem., 29 (1967) 1745.
25 G. Geier et U. Karlen, Helv. Chim. Acta, 54 (1971) 135.
26 L. G. Sillen et A. E. Martell, Stability constants of metal ion-complexes. Special Publication no. 17, The Chemical Society, London, 1964.
27 L. G. Sillen et A. E. Martell, Stability constants of metal ion-complexes. Special Publication no. 25, The Chemical Society, London, 1971.
28 A. E. Martell et R. M. Smith, Critical stability constants, vol. 1, Plenum Press, New York, 1974.
29 E. Merciny et G. Duyckaerts, J. Chromatogr., 35 (1968) 549.
30 P. Zur Nedden, E. Merciny et G. Duyckaerts, Anal. Chim. Acta, 64 (1973) 197.

31 N. Zaman, E. Merciny et G. Duyckaerts, Anal. Chim. Acta, 56 (1971) 271.
32 F. Schoebrechts, E. Merciny et G. Duyckaerts, J. Chromatogr., 79 (1973) 294.
33 J. M. Gatez, E. Merciny et G. Duyckaerts, Anal. Chim. Acta, 84 (1976) 383.
34 E. Merciny, J. M. Gatez et G. Duyckaerts, Anal. Chim. Acta, 86 (1976) 247.
35 A. K. Gupta et J. E. Powell, Inorg. Chem., 1 (1962) 955.
36 C. Pajakoff, Monatsh., 94 (1963) 482.
37 D. D. Perrin et I. G. Sayle, Talanta, 14 (1967) 833.
38 E. Merciny, J. M. Gatez, L. Swennen et G. Duyckaerts, Anal. Chim. Acta, 78 (1975) 159.
39 L. C. Thompson et J. A. Loraas, Inorg. Chem., 2 (1963) 89.
40 E. Brücher, R. Kiraly et I. Nagypal, J. Inorg. Nucl. Chem., 37 (1975) 1009.
41 S. H. Eberle et J. Bayat, Radiochim. Acta, 7 (1967) 217.
42 G. H. Carey, R. F. Boguky et A. E. Martell, Inorg. Chem., 3 (1964) 1228.
43 T. V. Ternovaya et N. A. Kostromina, Russ. J. Inorg. Chem., 16 (1971) 1580.
44 L. C. Thompson, Inorg. Chem., 1 (1962) 490.
45 G. N. Kupriyanova et L. I. Martynenko, Russ. J. Inorg. Chem., 15 (1970) 1024.
46 J. T. Bell, R. D. Baybarz et D. M. Hecton, J. Inorg. Nucl. Chem., 33 (1971) 3037.
47 N. A. Kostromina et N. N. Tananaeva, Teor. Eksp. Khim., 7 (1971) 67.
48 N. N. Tananaeva et N. A. Kostromina, Russ. J. Inorg. Chem., 17 (1972) 1243.
49 F. T. Grittmon et G. R. Choppin, Thèse de doctorat, Thallassee-Floride.
50 T. Moeller et R. Ferrus, Inorg. Chem., 1 (1962) 49.
51 R. H. Betts et O. F. Dahlinger, Can. J. Chem., 37 (1959) 91.

Analytica Chimica Acta, 94 (1977) 111—117

CALIBRATION OF BROMIDE ION-SELECTIVE ELECTRODES

R. GYENGE

Research Institute for Pharmaceutical Chemistry, Budapest (Hungary)

K. TÓTH and E. PUNGOR*

Department of General and Analytical Chemistry, Technical University, Budapest (Hungary)

E. KŐRÖS

Institute of Inorganic and Analytical Chemistry, L. Eötvös University, Budapest (Hungary)

(Received 3rd May 1977)

SUMMARY

A method based on the coulometric principle is reported for the calibration of bromide-selective electrodes. Known amounts of bromide are generated coulometrically by cathodic polarization of a silver—silver bromide electrode at a constant current. With this method, the ion-selective electrodes can be calibrated in potentiometric cells with and without transference in the concentration range 10^{-4}—10^{-7} M. In cells without transference, a PVC nitrate or perchlorate electrode is applied as reference electrode for the calibration in the presence of potassium nitrate or sodium perchlorate background electrolytes. Cells without transference are very advantageous in strongly acidic or basic solutions, where the value of the liquid-junction potential can be significant.

Many cation- and anion-selective electrodes are now used analytically. For testing purposes and for evaluation of the e.m.f. data obtained in their application, calibration is necessary. Apart from pH buffers, very few ion-buffers are available for calibration purposes. An additional problem in calibrating ion-selective electrodes is that the electrodes are generally used in unbuffered systems, and the basic principle that calibration and sample measurements should be done under similar conditions should be obeyed. Calibrations done in buffered solutions cannot be used to evaluate data measured in unbuffered solutions. (However, the handicap of this method lies in inadequate responses at very low ionic strengths and activity.) Therefore for the calibration of ion-selective electrodes, suitable standard materials and an appropriate method are essential. The calibration method can be discontinuous or continuous. The so-called injection method is an example of calibration in flowing systems [1].

The elaboration of generally utilizable activity—potential scales for the calibration of ion-selective electrodes, consistent among themselves and with the generally accepted pH convention, appears to be a general requirement [2]. In the case of pX electrodes, Bates and co-workers [3, 4] have

recommended an ion-activity scale which is based on the Stokes—Robinson hydration theory [5]. As a convention, the hydration number of the chloride ion is taken as zero, and the activity coefficients calculated on this basis are used to prepare ion-activity scales for the calibration of the electrodes.

It has become common practice to standardize ion-selective electrodes by means of diluted solutions of the completely dissociated salt appropriate to the electrode. To calibrate Cu(II), Pb(II) and Cd(II) electrodes, Růžička et al. [6—8] and Blum and Fog [9] have suggested the application of metal buffers based on metal—complex equilibria for measuring pX values over 5. Havas et al. [10] have used precipitate—solution equilibria for the calibration of halide electrodes. The disadvantage of the latter method is that heterogeneous equilibria are involved, so that the systems approach equilibrium slowly.

In some cases, it is necessary to ensure appropriate conditions for the ion to be investigated. For example, Frant and Ross [11] proposed the application of the Total Ionic Strength Adjustment Buffer (TISAB) for the calibration of fluoride-selective membrane electrodes; this buffer gives a certain pH and contains complexing agents to mask metal ions which form fluoro complexes. Orion Research Incorporation [12] recommended the so-called liter-beaker method for preparing calibration curves: small increments of standard solution are added to 1 l of distilled water, and the calibration curve is constructed by plotting electrode potential versus concentration.

For the preparation of concentration standard solutions to calibrate iodide and silver ion-selective electrodes, Bailey and Pungor [13] developed a coulometric method. A continuous calibration method was worked out by Horvai et al. [14] who used continuous dilution in a single container. This method can be considered as the reverse of the liter-beaker method.

In this paper a method for the calibration of the bromide-selective electrode in the low concentration range is described. This is of interest not only from an analytical point of view, but is very important in kinetic investigations of the Belousov—Zhabotinskii oscillatory systems [15]. Coulometric generation of bromide provides the concentration calibration technique. The method can be regarded as a version of the liter-beaker method.

EXPERIMENTAL

Instrumentation, electrodes and cells

For the preparation of the silver bromide electrode, the electrolytic generation of bromide and silver ions, and the measurement of current efficiency, a Radelkis OH-404 Universal Coulometer was used in the constant-current mode. The e.m.f. values were measured with a Radelkis Precision pH meter (Type OP-205) and a Differential Electrometer (Keithley Instrument, Model 604).

Bromide concentrations were measured with silicone rubber-based membrane electrodes produced as described by Pungor et al. [16] and with bromide-selective electrodes from Radelkis (OP-Br-711-D) and Orion Research (9435). Different types of reference electrodes were used. A saturated calomel electrode (Radelkis OP-810 or Radiometer K-401) was connected to the potentiometric cell through a 0.1 M potassium nitrate—agar salt bridge. PVC nitrate and perchlorate electrodes also were used as reference electrodes.

The silver—silver bromide electrode, required for the coulometric generation, was prepared by anodic polarization of a silver electrode in a slightly acidic potassium bromide solution [17]; electrolysis was continued for 4 h at a current density of 0.2 mA cm^{-2} to obtain an appropriate layer.

For measurement of the current efficiency, twin silver electrodes were used for end-point detection. The measuring cells and electrodes belonging to the coulometric device were used for the measurements.

Reagents and solutions

Chemicals and solvents were of analytical grade. To prepare PVC nitrate and perchlorate electrodes, an Orion 92-07-09 and a Corning 477316 nitrate liquid ion-exchanger were used [18]. To prepare the perchlorate electrode, the nitrate liquid ion-exchanger was first converted to perchlorate form by shaking with sodium perchlorate.

Methods

Bromide ions in reproducible and accurately known concentrations were generated electrolytically by cathodic polarization of the silver—silver bromide electrode at a current density of 0.15 mA cm^{-2}. Applicability of the method requires that the current efficiency be 100%. To check the current efficiency in different background electrolytes, coulometrically generated bromide at a concentration of 2×10^{-5} M was titrated with coulometrically produced silver(I). For end-point detection, the controller unit of the coulometer was used.

The rate of equilibration was low, thus the change of the ammeter current was followed visually. The end-point of the titration was detected biamperometrically by means of an electrode containing twin silver wires with a constant applied potential of 200 mV; the current through the cell was measured, reaching a minimum at the end-point. The current efficiency in different background electrolytes was 100 ± 0.05%, which provides sufficient accuracy for the calibration.

The bromide-selective electrode was calibrated in a two-compartment cell. The working cell contained the silver—silver bromide generator cathode and the bromide-selective electrode in 100.0 ml of background electrolyte; this cell was stirred magnetically. The auxiliary cell contained the platinum generator anode and the reference electrode in a 0.1 M potassium nitrate solution. The two cells were joined by a 0.1 M potassium nitrate—agar salt

bridge. The experimental arrangement is shown in Fig. 1. An aliquot of charge was passed between the generator electrode pair, and the concentration of the bromide was calculated from Faraday's law in the usual way. The potential of the indicator electrode couple was measured with the pH meter.

RESULTS

Measurements in cells with transference

Calibrations were done in different background electrolytes in the concentration range 10^{-4}—10^{-7} M, because a method based on coulometric principles is important primarily for low concentrations. The background electrolytes used were potassium nitrate, potassium perchlorate, zinc sulphate and magnesium sulphate. The calibration curves for a silicone rubber-based bromide-selective electrode in different concentrations of magnesium sulphate solution are shown in Fig. 2. Those obtained in different electrolytes (10^{-1} M) are illustrated in Fig. 3.

Measurements in cells without transference

For such measurements, PVC electrodes containing nitrate or perchlorate liquid ion-exchanger were prepared. Figures 4 and 5 show the calibration curves obtained. With the perchlorate electrode, the saturated calomel reference electrode was joined to the cell through a 0.1 M sodium chloride agar salt bridge.

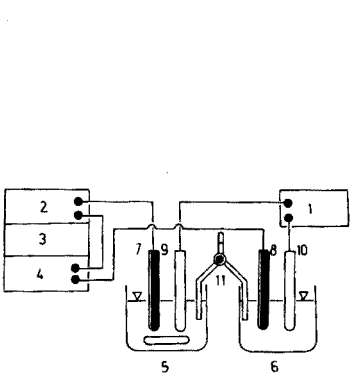

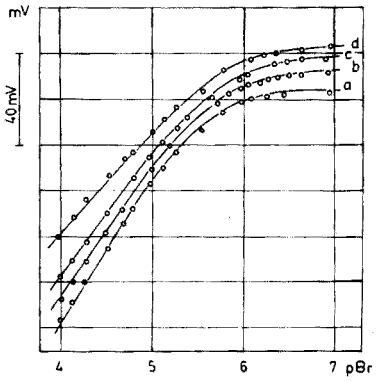

Fig. 1. Block diagram of the measuring device for the calibration of the bromide-selective electrode (1) pH meter. (2) Coulometer integrator unit. (3) Coulometer control unit. (4) Coulometer potentiostat—amperostat unit. (5) Working cell. (6) Auxiliary cell. (7) Ag/AgBr generator cathode. (8) Pt generator anode. (9) Indicator electrode: bromide-selective electrode. (10) Reference electrode. (11) 0.1 M potassium nitrate—agar salt bridge.

Fig. 2. Calibration curves for a silicone-rubber bromide-selective electrode in different $MgSO_4$ solutions. (a) 1 M, (b) 10^{-1} M, (c) 10^{-2} M, (d) 10^{-3} M.

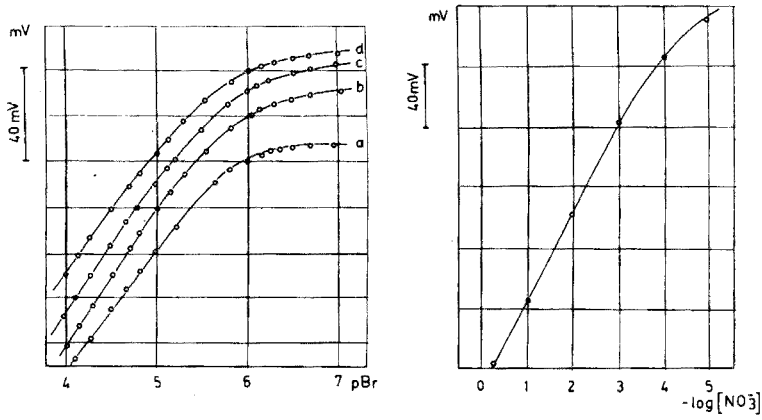

Fig. 3. Calibration curves for a silicone-rubber bromide-selective electrode in different 10^{-1} M electrolytes (vs. SCE). (a) 10^{-1} M $MgSO_4$, (b) 10^{-1} M KNO_3, (c) 10^{-1} M $KClO_4$, (d) 10^{-1} M $ZnSO_4$.

Fig. 4. Calibration curve for a PVC nitrate electrode.

The selectivity relationships of the nitrate and perchlorate electrodes for bromide ions were also examined [19]; the concentration of potassium nitrate or sodium perchlorate was kept constant (10^{-1} M, 10^{-2} M) and the concentration of bromide was varied in the range 10^{-1}—10^{-6} M. So long as the concentration of bromide was less than that of perchlorate, bromide ions did not affect the function of the perchlorate electrode.

For the measurements in cells without transference, a PVC nitrate or perchlorate electrode was used as reference electrode for calibration of the bromide-selective electrode in the presence of nitrate or perchlorate

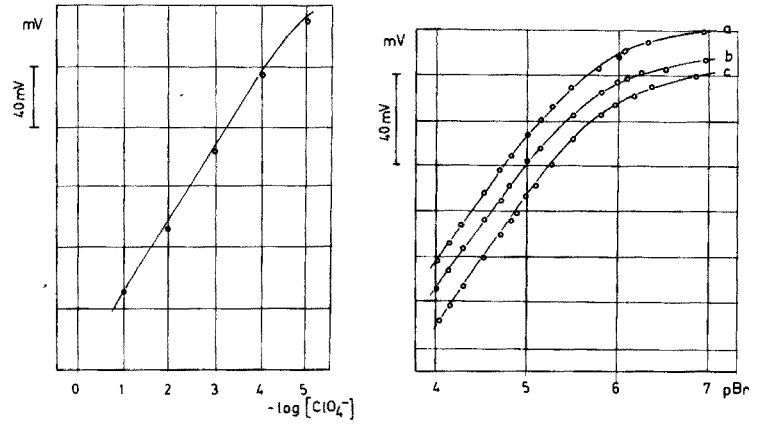

Fig. 5. Calibration curve for a PVC perchlorate electrode.

Fig. 6. Calibration curves for a Radelkis bromide-selective electrode in (a) 10^{-1} M KNO_3 with a saturated calomel electrode; and in (b) 1 M KNO_3, (c) 10^{-1} M KNO_3, both with a PVC nitrate reference electrode.

electrolyte. Bromide was generated coulometrically in 10^{-1} M or 1 M potassium nitrate background electrolytes and in a solution of pH 1 (nitric acid). The results compared to the calibration curve obtained with a saturated calomel electrode are shown in Figs. 6 and 7.

A PVC perchlorate reference electrode was examined in perchlorate background electrolytes. The curves obtained are shown in Fig. 8.

DISCUSSION

The bromide-selective electrodes were calibrated in stirred unbuffered solutions containing different background electrolytes. The responses to bromide in different 10^{-1} M electrolyte solutions did not differ significantly. Nor did the shapes of the calibration curves change when different concentrations of magnesium sulphate solutions were used as the background electrolyte. Consequently, adsorption of the electrolyte on the electrode surface plays no, or only an insignificant, role in the electrode response.

Comparison of the data obtained in cells with and without transference shows that the differences in the shapes of the calibration curves are small, presumably because in the systems investigated, the diffusion potentials are not significant enough. When the measurements are performed in strongly acidic or basic medium, the liquid-junction potential can increase considerably because equal charge transport in the boundary phase is impossible.

In these circumstances the application of the calibration method in cells without transference is recommended.

When calibration is done by serial dilution of solutions, it is difficult to obtain reproducible results in the low concentration range; even when solutions are prepared very carefully, the method is not reliable below 10^{-4} M. The advantage of the proposed method is that calibration and measurement

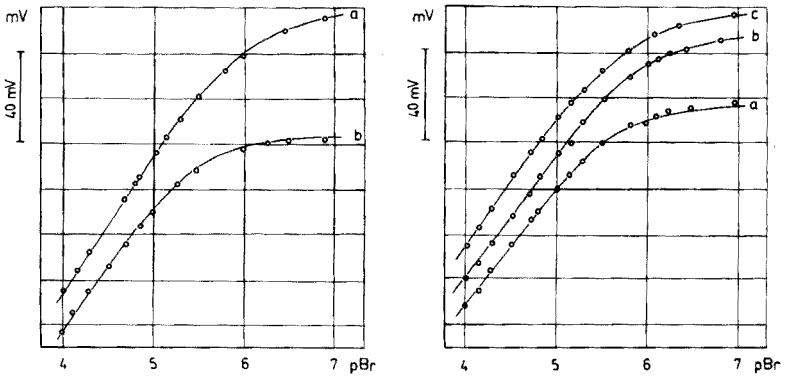

Fig. 7. Calibration curves for a Radelkis bromide-selective electrode in a solution of pH 1 (HNO_3). (a) PVC nitrate reference electrode. (b) Saturated calomel reference electrode.

Fig. 8. Calibration of a Radelkis bromide-selective electrode in (a) 1 M $NaClO_4$, (b) 10^{-1} M $NaClO_4$, both with a PVC perchlorate reference electrode; and in (c) 10^{-1} M KNO_3 with a saturated calomel electrode.

of the sample can be carried out under the same conditions. Moreover, as the ionic strength is constant in the standard solutions, the calibration curve obtained is a concentration calibration curve. A further advantage of the method is that it can readily be automated. It is rapid and does not require change of solutions and washing of the electrode between measurements.

REFERENCES

1 Zs. Fehér, G. Nagy, K. Tóth and E. Pungor, Analyst, 99 (1974) 699.
2 R. A. Durst, Ion-Selective Electrodes, NBS Spec. Publ., 1969, Chapter 6, p. 191.
3 R. G. Bates, B. R. Staples and R. A. Robinson, Anal. Chem., 42 (1970) 867.
4 R. A. Robinson and R. G. Bates, Anal. Chem., 45 (1973) 1666.
5 R. H. Stokes and R. A. Robinson, J. Am. Chem. Soc., 70 (1948) 1870.
6 E. H. Hansen, C. G. Lamm and J. Růžička, Anal. Chim. Acta, 59 (1972) 403.
7 J. Růžička and E. H. Hansen, Anal. Chim. Acta, 63 (1973) 115.
8 E. H. Hansen and J. Růžička, Anal. Chim. Acta, 72 (1974) 365.
9 R. Blum and H. M. Fog, J. Electroanal. Chem., 34 (1972) 485.
10 J. Havas, M. Kaszás and M. Varsányi, Hung. Sci. Instrum., 25 (1972) 23.
11 M. S. Frant and J. W. Ross, Anal. Chem., 40 (1968) 1169.
12 Orion Newsletter, Specific Ion-Electrode Technology.
13 P. L. Bailey and E. Pungor, Anal. Chim. Acta, 64 (1973) 423.
14 G. Horvai, K. Tóth and E. Pungor, Anal. Chim. Acta, 82 (1976) 45.
15 R. J. Field, E. Kőrös and R. M. Noyes, J. Am. Chem. Soc., 94 (1972) 8549.
16 E. Pungor, J. Havas, K. Tóth and G. Madarász, Hung. Pat. 152.106. 1963.
17 E. Bishop and R. G. Dhaneswar, Analyst, 88 (1963) 424.
18 J. E. W. Davies, G. J. Moody and J. D. R. Thomas, Analyst, 97 (1972) 87.
19 E. Pungor and K. Tóth, Anal. Chim. Acta, 47 (1969) 291.

Analytica Chimica Acta, 94 (1977) 119—127

THE APPLICATION OF DIFFERENTIAL PULSE POLAROGRAPHY TO THE DETERMINATION OF A PHARMACOLOGICALLY ACTIVE BENZHYDRYLPIPERAZINE DERIVATIVE AND ITS MAJOR ELECTROACTIVE METABOLITES IN THE PLASMA AND URINE OF ANIMALS

MALCOLM R. SMYTH[§] and W. FRANKLIN SMYTH*

Department of Chemistry, Chelsea College, University of London, Manresa Road, London SW3 6LX (England)

JOHN M. CLIFFORD

G.D. Searle and Co. Ltd., High Wycombe, Bucks. (England)

(Received 16th March 1977)

SUMMARY

Differential pulse polarography has been applied to the determination of a benzhydrylpiperazine derivative of pharmacological importance in both plasma and urine. The metabolic fate of this compound has been investigated in three animal species by the use of t.l.c. and d.p.p. procedures.

SC-13504 (I) is a benzhydrylpiperazine derivative, which has anticonvulsant activity in several animal model systems [1—4]. The mechanism of its action is not yet fully understood, although it exerts an inhibitory effect on the Mg^{2+}-dependent ATP-ase enzyme system [5].

The acid—base and polarographic behaviour of (I) (and of several structurally related benzhydrylpiperazine derivatives) has been studied [6, 7]; protonation of the N atom in position 4 greatly influences the chemical behaviour of this compound. Differential pulse polarography (d.p.p.) can be applied to the determination of (I) in the plasma and urine of experimental animals given a minimum dose of 4 mg kg^{-1}, and has been used to investigate the relationship between the anticonvulsant properties of SC-13504 and its plasma levels in photosensitive baboons (*Papio papio*) subjected to intermittent light stimulation [8]. In this study, no evidence was obtained for the existence of electroactive metabolites of SC-13504 although other work has shown that benzhydrol (II) is formed as a major metabolite in this species [9].

[§] Present address: Department of Microbiology, Colorado State University, Fort Collins, Colorado 80523 U.S.A.

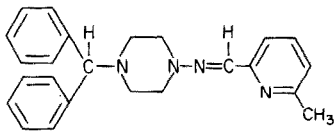

I

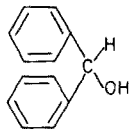

II

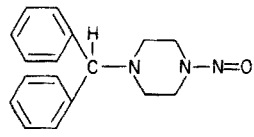

III

In studies with rhesus monkeys (*Macaca mulatta*) and beagle dogs (*Canis familiaris*), however, electroactive metabolites were detected following intravenous administration of SC-13504, one of which was believed to be SC-11808 (III) [10].

This paper discusses the application of d.p.p. to the determination of SC-13504 in the plasma and urine of baboons, rhesus monkeys and dogs and describes the methods employed for the isolation and polarographic study of the metabolic products.

EXPERIMENTAL

Apparatus

Polarographic curves in the sampled d.c. and d.p.p. modes were recorded with a PAR model 174A polarographic analyser in conjunction with a three-electrode cell system, the counter electrode being platinum and the reference a saturated calomel electrode (s.c.e.). The dropping mercury electrode used had an outflow velocity of 2.571 mg s^{-1} and a drop time of 3.46 s at the potential of the s.c.e. and a mercury pressure of 55 cm in 1 M KCl solution.

Extractions from plasma and urine were carried out in 30-cm^3 stoppered centrifuge tubes on an Eschmann blood suspension mixer.

Reagents

Samples of SC-13504 (I) and SC-11808 (III) were obtained from G. D. Searle and Co. Ltd. Stock solutions (10^{-3} M) were prepared in AnalaR methanol and stored in the dark under refrigeration.

A stock Britton–Robinson (BR) buffer solution (pH 1.8) composed of a mixture of boric acid, glacial acetic acid and orthophosphoric acid, all 0.04 M, was prepared from AnalaR grade reagents (Hopkin and Williams). From this solution, buffer solutions of varying pH were prepared by the addition of 0.2 M sodium hydroxide solution. A BR buffer of pH 3, made 10^{-3} M in EDTA (disodium salt) and containing 10% (v/v) methanol was used in the analytical investigations.

Pre-coated silica gel ($60F_{254}$) plates were obtained from E. Merck. All solvents used in extractions from plasma and urine and in t.l.c. investigations were of analytical grade.

Techniques

For the polarographic investigations, solutions were degassed with oxygen-free nitrogen for 10 min. The samples were blanketed by an atmosphere of

nitrogen and current—potential curves were recorded from —0.1 V (vs. s.c.e.). The conditions normally employed in the sampled d.c. and d.p.p. investigations were: scan rate, 1—2 mV s^{-1}; drop time, 1—2 s; modulation amplitude, 100 mV; time constant, 0.3 s.

The distribution of SC-13504 (I) and SC-11808 (III) between BR buffer pH 3 and benzene (ratio of aqueous to organic phase was maintained at 1:4) was monitored by d.p.p. The extractions were carried out at the 10^{-6} M level for 10 min of a blood suspension mixer. After centrifugation at 3000 rpm for 10 min, an aliquot (18 ml) of the organic phase was evaporated to dryness under a stream of nitrogen and taken up in 1 ml of methanol. After the addition of 9 ml of buffer pH 3 the solution was analysed by d.p.p. and the percentage extraction of (I) and (III) into the organic phase was calculated.

The administration of 4 mg kg^{-1}, 6 mg kg^{-1}, 8 mg kg^{-1} SC-13504 to the photosensitive baboons was performed by dissolving the appropriate dose level of SC-13504 in 1 ml of 0.1 M lactic acid. This was then diluted with sterile distilled water to give a pH of 2.2 and the appropriate amount (ca. 6 ml) was given intravenously (i.v.) over a period of 15 s. The rhesus monkeys and beagles received SC-13504 dissolved in 10% ethanol in polyethylene glycol (n = 400). At the appropriate time intervals, venous blood samples were taken from the saphenous, cephalic or femoral veins, collected into lithium—heparin anticoagulant tubes and centrifuged at 3000 rpm for 15 min at 0—4°C to obtain the plasma. Urine samples were collected over various time periods. All biological material was stored at —20°C until analysis.

The biological samples were thawed at room temperature and then incubated at 37°C for 15—20 min to redissolve any suspended material present after freezing. Aliquots (1 ml) of plasma (5 ml of urine) were adjusted to pH ca. 3 by dropwise addition of 0.1 M HCl, and then brought exactly to pH 3 by the addition of 4 ml of BR buffer pH 3 (5 ml for urine). These samples were then extracted with 20 ml of benzene and centrifuged as before, and 18-ml aliquots of the organic phase were taken for analysis by d.p.p. After each polarographic step, the analyte containing SC-13504 and any metabolite that may have been extracted from the body fluid were re-extracted into benzene and the organic phase thus obtained was taken to dryness under a stream of nitrogen. The residue was then taken up in 50 μl of methanol and spotted on a t.l.c. plate which was developed in ethyl acetate—1% ammonia. After elution, the plate was dried and viewed under u.v. light. Bands containing SC-13504 and possible metabolites were then scraped off the plate, taken up in 1 ml of methanol, filtered and, after addition of supporting electrolyte, analysed by d.p.p.

RESULTS AND DISCUSSION

Polarographic behaviour

The polarographic behaviour of SC-13504 at pH values less than the pK_2 value involves simultaneous saturation of the azomethine group and reductive splitting of the labile N—N bond [6].

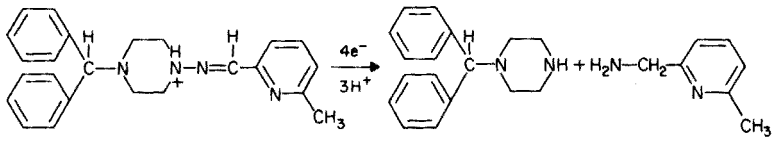

I IV V

Because of the competing hydrolytic side reaction, however, this is manifested as a $3e^-$ process and the d.p.p. peak obtained in the specified buffer pH 3 is recommended for analytical purposes.

SC-11808 (III) gives rise to well-defined waves in the pH range 2—6 corresponding to the $4e^-$ reduction of the >N—N=O moiety. Similar behaviour has been reported for *N*-nitrosopiperazine [11]. A plot of $E_{d.e.}$ vs log $i/(i_d - i)$ for the sampled d.c. wave exhibited by (III) in BR buffer pH 4 showed two linear portions, of 60 and 27.5 mV, respectively, corresponding to two rate-determining electron-consuming processes, i.e.

$$>N{-}NO \xrightarrow{2e^-,\,2H^+} >NHOH \underset{H^+}{\rightleftharpoons} >NHOH_2^+ \xrightarrow{2e^-,\,2H^+} >NH_3^+ + H_2O$$

A plot of $E_{1/2}$ vs. pH for SC-11808 between pH 2 and pH 11 yielded two linear portions of slope 80 and 37.5 mV pH^{-1} which intersected at the pK' of 6.4 (Fig. 1). At pH values above 6.4, the hydroxylamine intermediate in the electrochemical reduction of SC-11808 can no longer be protonated,

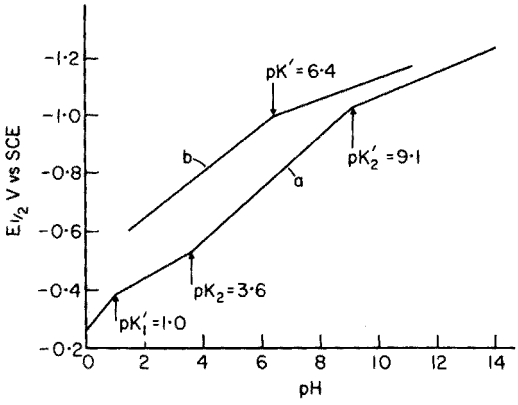

Fig. 1. Plot of $E_{1/2}$ vs. pH for diffusion-controlled wave exhibited by (a) SC-13504 and (b) SC-11808.

hence only a $2e^-$ process is involved. The waves obtained for SC-11808 above pH 10 also exhibit maxima of the first and second kind which are not useful for analytical purposes.

The greatest degree of separation in the $E_{1/2}$ values of SC-13504 and SC-11808 exists in solutions of pH 3—4 (Fig. 1) where the difference is ca. 230—240 mV. SC-11808 can therefore be determined in the presence of SC-13504 down to 0.01%. The limit of detection for SC-11808 by d.p.p. is 8 ng ml^{-1} in BR buffer pH 3, whereas 20 ng ml^{-1} SC-11808 can be detected in the presence of 100 μg ml^{-1} of SC-13504 in the same medium.

Specificity of d.p.p. assay for the determination of SC-13504 in baboon plasma and comparison with other analytical techniques

The specificity of the d.p.p. assay for the determination of SC-15304 in the plasma of two other baboons (*Papio ursinus*) was checked in the following manner. After the polarographic examination of a plasma extract (see Experimental Techniques), the substances in the analyte were re-extracted into benzene (buffer pH 3 was used in both extraction and polarographic steps) and subjected to t.l.c. After elution, the u.v.—visible zones of the t.l.c. support system (relating to R_F values of 0.0—0.2, 0.2—0.4 etc.) were scraped off, eluted with methanol and taken up in supporting electrolyte. In extractions from baboon plasma, no t.l.c. spot (as visualized under u.v. light) or d.p.p. peak was found other than that shown by SC-13504. In addition, solvent extraction studies on a potential metabolite X-6646 (VI) (which exhibits similar polarographic behaviour to SC-13504 in acid media [7] and which could be formed following liberation of benzhydrol (II) from SC-13504), showed that it could not be extracted under the conditions of the experiment.

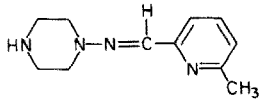

VI

A comparison was also carried out between the plasma levels obtained for SC-13504 in baboon plasma by the d.p.p. method and those employing radiochemical and gas chromatographic (g.c.) procedures. For these studies, plasma samples taken from a baboon (6.1 kg) given 6.6 mg kg^{-1} of ^{14}C-SC-13504 (^{14}C label at the benzyhydryl methine C atom) intravenously during a 20-min infusion were split, and both parts were extracted for SC-13504; roughly similar levels of ^{14}C-SC-13504 and SC-13504 were found by the radiochemical and the d.p.p. assay, respectively [8]. Another baboon (12.4 kg) was given 12.5 mg kg^{-1} of SC-13504 intravenously. The plasma samples were split and analysed by d.p.p. and a g.c. method [9]. The results (Table 1) show good agreement. In the radiochemical experiment, d.p.p. was unable to detect any SC-13504 in the plasma 6 h after administration. The levels of radioactivity found in the plasma between 6 and 24 h

TABLE 1

Comparison of levels of SC-13504 obtained in the plasma of baboons by d.p.p. and g.c.

Time after intravenous administration (h)	Plasma levels ($\mu g\ ml^{-1}$)	
	D.p.p.	G.c.
+1/12	11.06	11.20
+1	4.84	4.90
+24	0.35	0.51

could therefore arise from non-electroactive metabolite(s) of SC-13504. The major metabolite in the rat, beagle, rhesus monkey and baboon was benzhydrol (II) [9] which would retain the radioactive ^{14}C-label after cleavage of the C—N bond between the benzhydryl methine C atom and the N-1 nitrogen atom in the piperazine part of the molecule.

An even better correlation was obtained between the g.c. and d.p.p. results from the baboon dosed at 12.5 mg kg^{-1} intravenously which suggested that d.p.p. offers a specific, accurate method for the determination of SC-13504 in baboon plasma.

Polarographic studies of the metabolic fate of SC-13504 in rhesus monkeys and beagle dogs

When SC-13504 was given intravenously to rhesus monkeys (*Macaca mulatta*), only SC-13504 was found in the plasma. The existence of an electroactive metabolite was inferred, however, after extractions from urine (Fig. 2). A positive shift in the E_p value of SC-13504 from —0.48 to —0.44 V (vs. s.c.e.) has been observed in d.p.p. examinations of urine extracts [12, 13], whereas the peaks exhibited around —0.25 V and —0.7 V arise from naturally occurring electroactive constituents in urine [10]. The peak at —0.54 V was thought, however, to be due to an electroactive metabolite of SC-13504 (M_1).

When SC-13504 was administered intravenously to beagle dogs (*Canis familiaris*), a peak was obtained at —0.57 V following extraction from plasma 1 h after administration of 12.5 mg kg^{-1} of SC-13504 (Fig. 3, a). This is probably the same metabolic product (M_1) as that encountered in the urine of rhesus monkeys (allowing for the positive shift in potential which might be due to biological interference extracted from urine) and it was the predominant species in the plasma of beagle dogs 24 h after intravenous administration of SC-13504.

In an attempt to identify this metabolite (M_1), plasma from a beagle dog, obtained 1 h after administration of SC-13504 (12.5 mg kg^{-1}) was extracted with benzene and analysed by d.p.p. (Fig. 3, b). The pattern obtained was similar to that shown in Fig. 3(a). When the analyte was re-extracted with benzene and subjected to t.l.c., spots were observed both for SC-13504 (R_F = 0.57) and a product (R_F = 0.48). When the spot relating to this

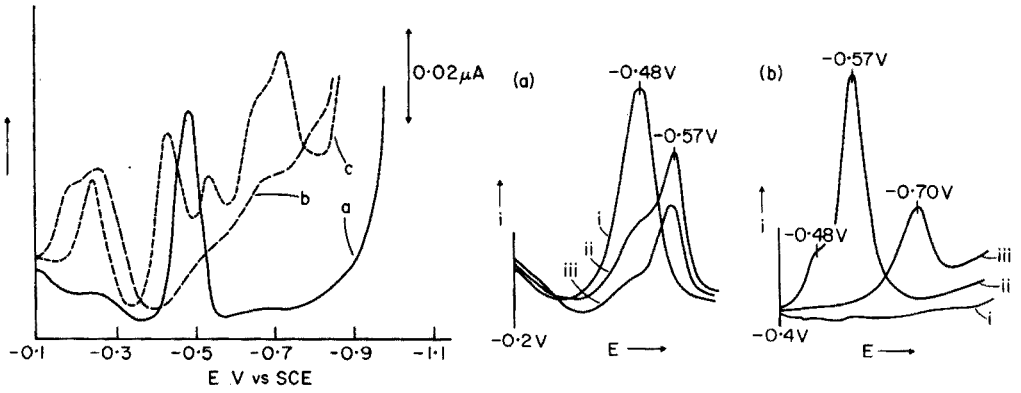

Fig. 2. Examination by d.p.p. of rhesus monkey urine extractions: (a) 1 × 10^{-6} M SC-13504 in buffer pH 3; (b) control urine extraction; (c) extract from urine obtained 1—6 h after administration of 10 mg kg^{-1} SC-13504 to a rhesus monkey. Conditions: scan rate, 1 mV s^{-1}; drop time, 2 s; modulation amplitude, 100 mV.

Fig. 3. Examination by d.p.p. of plasma extracts obtained from beagle dogs dosed with 12.5 mg kg^{-1} of SC-13504 intravenously. (a) D.p.p. of extracts obtained (i) 5 min (5 μA) (ii) 1 h (2 μA) and (iii) 24 h (1 μA) after administration of SC-13504 (current ranges employed given in parentheses). (b) D.p.p. of extracts in t.l.c. investigation of plasma samples obtained 1 h after administration of SC-13504: (i) blank t.l.c. extract; (ii) extract of sample before t.l.c.; (iii) d.p.p. of (ii) after t.l.c. separation (current range = 2 μA). Conditions: scan rate, 1 mV s^{-1}; drop time, 2 s; modulation amplitude, 100 mV.

product was eluted and subjected to d.p.p. (Fig. 3, b), its peak potential was found to be —0.7 V, similar to that observed for SC-11808. A marked decrease was also observed in the peak height which could not be explained by recovery losses from the t.l.c. support system. These results tend to suggest chemical degradation of the unknown metabolite M_1 (E_p = —0.57 V) during the above manipulations.

The urine of a beagle dog (collected 0—4 h after intravenous administration of 12.5 mg kg^{-1} of SC-13504) gave a peak corresponding to another unknown metabolite (M_2) at —0.66 V after extraction from urine. No evidence was found for the existence of SC-13504 or the other electroactive metabolite (M_1) in the urine of this species.

The production of metabolites M_1 and M_2 occurs to varying degrees in the species studied. In the baboon (*Papio ursinus*) no evidence was obtained for the existence of the unknown metabolites (M_1) or (M_2) in either the plasma or the urine. In the case of the rhesus monkey (*Macaca mulatta*), the postulated metabolite (M_1) did not appear in the plasma but did exist in the urine (Fig. 2). In the beagle dog (*Canis familiaris*) the unknown metabolite (M_1) was shown to be present in the plasma, and another unknown metabolite (M_2) species was found in the urine. A further study [14] has also been carried out on the metabolic fate of SC-13504 in rhesus monkeys when SC-13504 was given intravenously in conjunction with the 1,4-benzodiazepine,

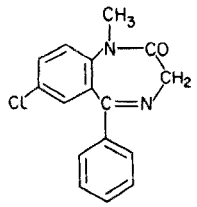

VII

diazepam VII). The results obtained for the simultaneous administration of diazepam (1 mg kg^{-1}) and SC-13504 (4 mg kg^{-1}) are shown in Fig. 4. In this case the unknown metabolite (M_1) was found to be present in the plasma of rhesus monkey 15 min after diazepam and SC-13504 had been given together thus altering the metabolic fate of SC-13504 in the rhesus monkey.

If it is assumed that the peaks due to M_1 and M_2 are due to diffusion-controlled reduction processes, the following tentative conclusions as to their structure can be drawn.

(a) *N*-oxidation at the N-4 and azomethine N atoms would give *N*-oxides that could be reducible at potentials corresponding to M_1 and M_2. If the latter *N*-oxide metabolite was unstable and degraded in vivo to SC-11808, then SC-11808 could be a metabolite.

(b) Hydroxylation, *N*-oxidation and demethylation of the picoline ring would give metabolites reducible at potentials more positive than those observed for M_1 and M_2. This has been inferred from a study of model compounds [7].

(c) *N*-oxidation at the N-1 atom would give a metabolite reducible at potentials more negative than those observed for M_1 and M_2 [15].

(d) If the C=N—N< linkage was broken to yield a picoline aldehyde or oxime, then these could possibly be reducible in the potential range observed for M_1 and M_2.

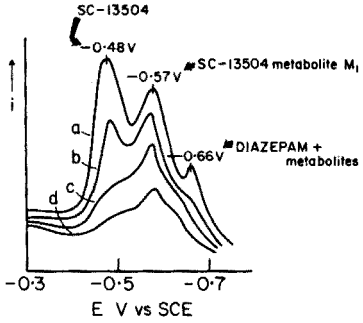

Fig. 4. Examination by d.p.p. of plasma extracts obtained (a) 15 min (b) 36 min (c) 120 min and (d) 300 min following simultaneous intravenous administration of 4 mg kg^{-1} of SC-13504 and 1 mg kg^{-1} of diazepam to a rhesus monkey. Conditions: scan rate, 1 mV s^{-1}; drop time, 2 s; current range, 0.5 μA; modulation amplitude, 100 mV. The peak at —0.48 V corresponds to reduction of SC-13504; that of —0.57 V corresponds to reduction of the SC-13504 metabolite (M_1); that at —0.66 V corresponds to diazepam and metabolites

(e) Hydroxylation of the benzhydryl moiety would be unlikely to affect the reduction potential of (I).

Studies are now in progress to elucidate the structure of the unknown metabolites M_1 and M_2.

Conclusions

The work presented is concerned with the isolation and polarographic study of the metabolites of SC-13504. Attempts to isolate and characterize the potential metabolites were hampered by their instability on the t.l.c. support system. Further work is required to isolate this compound in an intact form and to find means of removing the interferences encountered in the determination of SC-13504 and its electroactive metabolites in urine.

One of us (M. R. S.) thanks G. D. Searle and Co. Ltd. for their support throughout this work; the authors thank Dr. R. F. Palmer of G. D. Searle and Co. Ltd. for his helpful comments and criticisms.

REFERENCES

1 C. R. Craig, Arch. Int. Pharmacodyn., 165 (1967) 328.
2 L. G. Stark and H. L. Edmonds, Proc. West. Pharmacol. Soc., 16 (1973) 123.
3 R. M. Joy and H. L. Edmonds, Neuropharmacology, 13 (1974) 145.
4 H. L. Edmonds, L. G. Stark and S. Rinne, Proc. West. Pharmacol. Soc., 17 (1974) 77.
5 J. C. Gilbert and M. Wylie, Brit. J. Pharmacol., 56 (1976) 49.
6 M. R. Smyth, W. Franklin Smyth, R. F. Palmer and J. M. Clifford, Analyst, 101 (1976) 469.
7 M. R. Smyth, W. Franklin Smyth, R. F. Palmer and J. M. Clifford, Anal. Chim. Acta, 86 (1976) 185.
8 B. S. Meldrum, M. R. Smyth, W. Franklin Smyth and J. M. Clifford, Psychopharmacology, 51 (1976) 59.
9 Data on file, G. D. Searle and Co. Ltd., Chicago, Illinois, U.S.A.
10 M. R. Smyth, (1976) Ph.D. Thesis, University of London.
11 C. L. Walters, E. M. Johnson and N. Ray, Analyst, 95 (1970) 485.
12 W. Franklin Smyth and M. R. Smyth, Proc. Anal. Div. Chem. Soc., 13 (1976) 223.
13 J. A. F. de Silva, I. Bekersky, M. A. Brooks, R. E. Weinfeld, W. Glover and C. V. Puglisi, J. Pharm. Sci., 63 (1974) 1440.
14 J. M. Clifford, in Methodological Developments in Biochemistry, Vol. 5, Assay of Drugs and Other Trace Substances in Biological Fluids (E. Reid (Ed.)), N. Holland, Amsterdam, p. 203.
15 A. H. Beckett, E. E. Essein and W. Franklin Smyth, J. Pharm. Pharmacol., 26 (1974) 399.

Analytica Chimica Acta, 94 (1977) 129—133

DETERMINATION OF PERIODATE WITH PHOTOREDUCED THIONINE

F. SIERRA, C. SANCHEZ-PEDREÑO, T. PEREZ RUIZ and C. MARTINEZ LOZANO
Department of Analytical Chemistry, University of Murcia (Spain)
(Received 25th April 1977)

SUMMARY

A method for the microdetermination of periodate in the presence of iodate is presented. It is based on reduction of periodate to iodate by leucothionine generated in situ by photochemical reaction between EDTA and blue thionine. Biamperometric curves are used for evaluation, representing reduction time for the periodate versus the current generated in the oxidation of the T_{red} in excess after the end-point. A polarographic study of the process is presented. An applied potential of 100 mV is suitable for the biamperometric measurements with Pt—Pt electrodes. The method is applicable for 0.4—45 ppm periodate. Iodate does not interfere up to IO_3^- : IO_4^- ratios of 100:1.

In a series of general studies of photochemical reactions in analytical chemistry [1], a spectrophotometric determination of chromium as DCTA—Cr(III) was developed [2]. The complex was formed by reduction of Cr(VI) with leucotoluidine generated in the photochemical reaction between toluidine blue and 1,2-diaminocyclohexanetetraacetic acid (DCTA).

The present paper reports a rather similar procedure for the determination of periodate, both alone and in the presence of iodate and other anions. The reductant is leucothionine which is formed in situ by photoreduction of the blue oxidized dyestuff with EDTA in the absence of oxygen.

Many workers have studied the photochemical reduction of thionine and other thiazine, oxazine and phenazine based dyestuffs by EDTA; the mechanisms are complex and ill-defined [3—7]. The overall reaction is always irreversible, the final products being the leuco dyestuff and various oxidized species from the aminopolycarboxylate, depending on the experimental conditions.

At appropriate pH values, the leucothionine (T_{red}) formed in the photochemical reaction between T_{ox} and EDTA rapidly and stoichiometrically reduces periodate to iodate, the dyestuff being re-oxidized to its blue form. The cycle keeps repeating as long as periodate is present. The evolution of the process can be followed biamperometrically, by determining the current corresponding to oxidation of leucothionine after all the periodate has been reduced. Thus the periodate reduction time is actually measured, and this obviously depends on the periodate concentration.

The conventional methods for the determination of periodate in the presence of iodate are usually based on selective titrations, periodate being reduced to iodate in neutral medium. The micro method presented here is accurate and precise and is advantageous for periodate concentrations of 0.4—45 ppm in the presence of iodate.

EXPERIMENTAL

Apparatus

A Radiometer PO4 polarograph was coupled to the illumination device (Arrosu Electromedidas, Murcia) described previously [8]. A Radiometer rotating platinum wire electrode was used to obtain the voltammograms. Amperometric titrations were followed with two platinum electrodes of about 1-cm^2 area.

Reagents

The chemicals used were of reagent grade (Merck).

A 0.02 M solution of potassium metaperiodate was standardized with sodium arsenite in the conventional way; 10^{-3} and 10^{-4} M solutions were prepared by suitable dilution.

Acetate buffers (1 M) were used for pH 4—6 and 1 M borax buffers for pH 8—10. The pH values were always checked with a pH meter.

Distilled-deionized water was used for all solutions.

Procedure

The sample must always be prepared under diffuse light. To the reaction cell, add 5 ml of acetate buffer pH 5, 5 ml of 0.2 M EDTA (disodium salt), 2 ml of aqueous 10^{-3} M thionine solution and different volumes of standard potassium periodate solution (10^{-3} M or 10^{-4} M); the final concentration of periodate should be between 0.5 and 45 ppm. Dilute to exactly 30 ml with deionized water. Thermostat cell to 30 ± 0.5°C. Remove oxygen from the solution by bubbling pure nitrogen (99.997%) through it for 20 min. Apply an e.m.f. of 100 mV between the two platinum indicator electrodes. Then, switch on the halogen lamp of the illumination device [8] and the polarograph recorder, simultaneously, and record the i vs. t curve until the sample is decolorized.

The shapes of the curves correspond to the amperometric titration of periodate with photogenerated T_{red}, and permit evaluation of the time required for total reduction of periodate (see Fig. 2). In order to obtain reproducible results, the reagent concentrations and the light intensity must be kept constant throughout the series of measurements.

RESULTS AND DISCUSSION

When a solution containing thionine and EDTA in a medium of pH $\geqslant$ 4 and in the absence of oxygen is exposed to white light, the dyestuff is reduced,

and the blue solution becomes colourless [5]. The photoreduction process is very fast at pH 5—7 under intense light.

When periodate is added to a solution of EDTA and thionine, the photoreduced thionine is oxidized

$$T_{red} + IO_4^- \rightleftharpoons T_{ox} + IO_3^-$$

T_{ox} is photoreduced again by the EDTA, and the cycle is repeated until no periodate remains. At the end of the process the dyestuff is in its leuco form. The main factors affecting both redox processes involved are pH, temperature and light intensity.

The rate of the photochemical reaction between EDTA and thionine depends strongly on pH, reaching its maximum value at pH 6.5 [5]. The reduction of periodate by leucothionine was shown to be fast in the pH range 4—9. In order to meet both requirements and to achieve a periodate reduction time which was properly measurable under the experimental conditions, pH 5 was selected. Because of kinetic considerations, unwanted photo-oxidation of EDTA and of thionine by periodate is negligible at pH 5.

The rate of the overall redox process is affected by temperature changes. This influence is stronger above 50°C, when the periodate reduction time is substantially shorter (Table 1). A temperature of 30 ± 0.5°C was selected.

The light intensity was controlled by using in all cases a lamp of the same characteristics [8].

Electrochemical behaviour of the periodate/T_{red} reaction

To appraise the electrochemical behaviour of the systems involved and to enable the optimum conditions for biamperometric measurements to be selected, voltammetric curves were recorded (Fig. 1). The residual current of the acetate buffer is negligible (Curve 1). Curves 2 and 3 show voltammetric curves for a solution of the reactants, and for the same solution after it had been exposed to light for long enough to achieve complete reduction of periodate and produce similar concentrations of T_{ox} and T_{red}. Under the test conditions, the periodate—iodate redox system appears to be irreversible whereas the T_{ox}/T_{red} system is reversible. These current—voltage curves indicated that a potential of 100 mV is most suitable for biamperometric determinations with two platinum electrodes.

TABLE 1

Effect of temperature on the photoreduction of periodate
(Experimental conditions: 2 ml of 10^{-3} M periodate solution, 10 ml of 0.1 M EDTA, 5 ml of 1 M acetate buffer pH 5 and 2 ml of 0.001 M thionine and dilute to exactly 30 ml with deionized water.)

Temp. (°C)	25	30	35	40	50	60	70
Time (s)	283	279	273	265	232	199	175

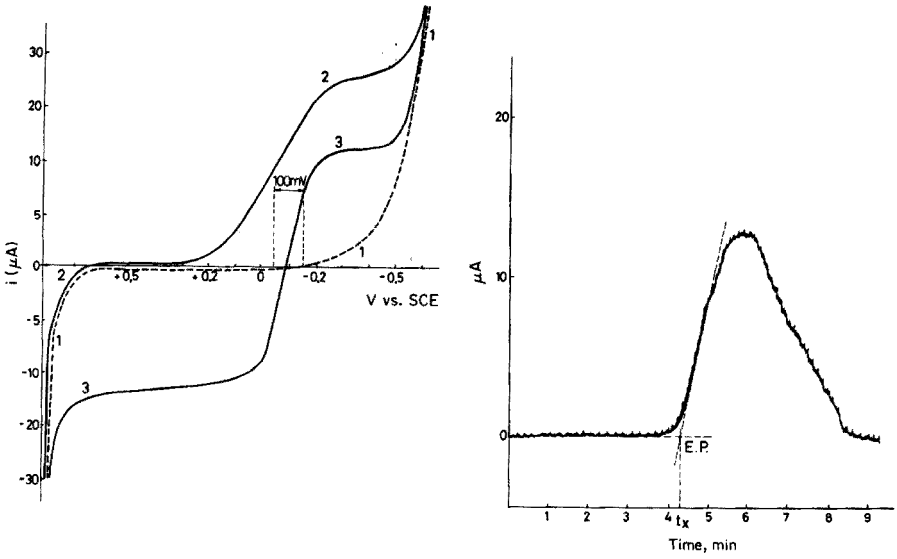

Fig. 1. Current—voltage curves at a rotating platinum microelectrode (vs.SCE). Curve 1, residual current of acetate buffer pH 5. Curve 2, voltammogram for 10^{-4} M periodate, 5×10^{-2} M EDTA and 10^{-4} M thionine in acetate buffer pH 5. Curve 3, voltammogram for the solution used for curve 2 after exposure to light.

Fig. 2. Determination of the end-point for the determination of periodate.

Figure 2 shows a biamperometric determination of periodate with photogenerated T_{red}. The total periodate reduction time can be observed accurately. The ascending portion of the curve measures the current increase after the periodate equivalence point, when the T_{red}/T_{ox} ratio increases.

Calibration graphs are prepared by plotting periodate concentration versus the time t_x required for complete reduction of periodate. Application of appropriate light intensities, which can be adjusted by changing the distance between the lamp and the reaction vessel, gives t_x values ranging from 15 to 600 s. Linear calibration graphs were obtained with 550 lux for periodate concentrations of 0.5—10 ppm (t_x = 15—550 s); under 1500 lux, linear graphs were also obtained for periodate concentrations of 6—45 ppm (t_x = 60—1000 s).

Sensitivity, reproducibility and interferences

The sensitivity of the method is ca. 0.4 ppm of periodate. This limit is imposed by the sensitivity of the instruments available (chronometers, etc.). Reproducibility in the given range of periodate concentrations (0.4 to 45 ppm) is good (Table 2).

Oxidizing anions such as MnO_4^-, $Cr_2O_7^{2-}$, VO_3^-, $Fe(CN)_6^{3-}$, etc., interfere, and also affect T_{red} at pH 5. Reducing agents such as iron(II) and tin(II) must be previously oxidized. The presence of metal ions calls for an increase in the EDTA concentration.

TABLE 2

Reproducibility at various periodate concentrations

Periodate	s_r (%) (N = 10)
2.34×10^{-6} M (0.448 ppm)	4.0
6.70×10^{-5} M (12.80 ppm)	1.2
2.34×10^{-4} M (44.80 ppm)	2.6

TABLE 3

Determinations of periodate in presence of iodate

IO_4^- taken (mg)	IO_3^- taken (mg)	IO_4^- found (mg)	Error (%)[a]
0.382	8.745	0.387	+1.3
0.382	17.49	0.389	+1.8
0.382	34.98	0.391	+2.3
0.382	43.73	0.393	+2.8
0.0764	34.98	0.0789	+3.2
0.0764	43.73	0.0793	+3.8

[a]Based on 3 samples at each level.

Table 3 shows the errors obtained in determinations of periodate in the presence of iodate.

REFERENCES

1 F. Sierra, C. Sanchez-Pedreno, T. Perez and C. Martinez, An. R. Soc. Esp. Fis. Quim., 68 (1972) 1091; 70 (1974) 595; 72 (1976) 456 and 72 (1976) 538.
2 F. Sierra, C. Sanchez-Pedreno, T. Perez and C. Martinez, An. R. Soc. Esp. Fis. Quim., 71 (1975) 382.
3 G. Oster and N. Wotherspoon, J. Am. Chem. Soc., 79 (1957) 4836; 81 (1959) 5543.
4 J. Joussot-Dubien and J. Faure, J. Chim. Phys., 60 (1963) 1214; Bull. Soc. Chim. Belg., 71 (1962) 877.
5 J. Faure and J. Joussot-Dubien, J. Chim. Phys., 63 (1966) 621.
6 K. Shimada and N. Masae, Sei. Rep. Tohoku Univ. Ser. 1, 52(3) (1969) 119.
7 M. Koizumi and Y. Usui, Mol. Photochem., 4 (1972) 57.
8 F. Sierra, C. Sanchez-Pedreno, T. Perez, C. Martinez and M. Hernandez, Anal. Chim. Acta, 78 (1975) 277 and 78 (1975) 498.

Analytica Chimica Acta, 94 (1977) 135—147

CHARACTERISTICS OF A.C. POLAROGRAMS AT HIGH SWEEP RATES

C. I. MOORING and H. L. KIES

Laboratory for Analytical Chemistry, University of Technology, Delft (The Netherlands)

(Received 9th May 1977)

SUMMARY

The single-sweep a.c. polarogram has fundamentally the same shape as the classical a.c. polarogram. It is recorded shortly before the drop detachment, which occurs every 32 s. The residual current is eliminated by subtraction of the output signals generated in a twin cell during the voltage sweep. The formula reported earlier for the peak current as a function of the amplitude and frequency, has been generalized by the introduction of 4 parameters. The equation fits most of the experimental data very well up to large amplitudes; 32 substances of great diversity have been investigated. The sweep rate does not affect the peak current for reversible systems, unless adsorption phenomena prevail. The analytically useful concentration range is 10^{-6}—10^{-3} M.

In 1938, fast voltage-sweep d.c. polarography was introduced as a variant of classical polarography. The method is commonly known as cathode-ray polarography [1]. The influence of drop growth was reduced by application of the voltage sweep during a short interval just before drop detachment [2]. The method acquired a sound theoretical base, thanks to the contributions of Ševčík [3], Randles [4] and Nicholson [5]. Commercial apparatus (Southern [6], Amel, Melabs) became available, but the method has never become widely accepted, though several of the objections to the method in its original form were removed by the introduction of the subtractive [7—9] and/or derivative [9] modes. The general method was overshadowed by the introduction of a.c. polarography [10, 11], particularly after the introduction of phase-selective detection [12, 13].

It has been suggested [14] that certain advantages of each of the above-mentioned methods could be combined by superimposing an alternating voltage of constant amplitude on the usual fast-voltage sweep. The subject has received new impetus from the contributions of Jee [15—17] and others [18, 19]. There is some overlap between these investigations, but additional information has become available, particularly with regard to comparison between theory [18, 20] and experimental results. The relationship derived earlier [20] for reversible redox systems [20] can be generalized by introduction of four empirical parameters [18]. A similar entrance signal has been proposed for studies of adsorption phenomena at the electrode [21].

It is of interest that Barker [22] mentioned the application of the fast-sweep mode, with a modified square-wave polarograph, whilst another paper on this subject was published by Saito and Okamoto [23] later.

The method presented here should not be confused with rapid a.c. polarography, introduced by Bond and O'Donnel [24—26], and examined by Ledieu and Byé [27]. The rapid a.c. method, which seems promising, is better compared with rapid d.c. polarography [28, 29].

THEORY

There are many publications on a.c. voltammetry; Breyer's monograph [10] and Smith's reviews [30, 31] provide good introductions.

A strict approach to the problems of fast-sweep a.c. polarography soon leads to insurmountable mathematical difficulties. Therefore, some simplifications are needed. First, the treatment is restricted to fast redox systems. Secondly, the electrode is considered as stationary, which is quite acceptable in view of the short duration of the voltage sweep and the long preceding period of drop growth. Further, the influence of curvature, which is in fact small for a.c. polarography [32, 33], is assumed to be a second-order effect when both redox components dissolve in the supporting electrolyte [34, 35]. Finally, all kinetic considerations are omitted.

From different studies of a.c. polarography, it can be concluded that the depth of penetration of the a.c. effect is small compared with the usual diffusion layer thickness, and that a.c. transients are negligible [30] for $(\omega t)^{\frac{1}{2}} \gg 1$. In other words, the steady state of the a.c. output signal is attained almost immediately after application of the input signal. Though it seems rather risky, it was further assumed that this situation prevails equally throughout the application of a voltage sweep. Consequently, for a given amplitude and frequency of the superimposed voltage, the a.c. output signal should be determined exclusively by the value of the direct electrode potential at each moment of the sweep; therefore, the output signal should be independent of the magnitude of the sweep rate.

A closed expression for the peak current has already been derived for this ideal case [18, 20]. For convenience, the amplitudes reported earlier can be replaced by r.m.s. values by application of the appropriate conversion factors. The formula then assumes the form

$$(i_p)_{r.m.s.} = \frac{2+\sqrt{2}}{8} nFA^* c\,(\omega D)^{\frac{1}{2}} \tanh\,(2-\sqrt{2})\,\frac{nF}{RT}\,E_{r.m.s.} \qquad (1)$$

where i_p stands for the a.c. peak current intensity, A for the drop area at the moment at which the peak potential has been reached, and E for the superimposed alternating voltage; the other symbols have their usual meanings.

The above relation was essentially confirmed by the results of various experiments concerning redox systems of known reversibility. Attempts were then made to extend the useful range of the formula by the introduction of four empirical parameters, p, q, s, and u as follows

$$(i_p)_{r.m.s.} = p\frac{2+\sqrt{2}}{8} nFA^*c\,\omega^{\frac{1-q}{2}} D^{\frac{1}{2}}\, v^s \tanh(2-\sqrt{2})\frac{nF}{RT}\, uE_{r.m.s.} \qquad (2)$$

in which v is the sweep rate (V s^{-1}). In the ideal case $p = u = 1$, and $q = s = 0$ (cf. eqn. 1).

The influence of the frequency will be discussed later; in this paper the parameter, p, and the factor $\omega^{-q/2}$ are combined to only one parameter, r, which leads to the equation

$$(i_p)_{r.m.s.} = r\frac{2+\sqrt{2}}{8} nFA^*c\,(\omega D)^{\frac{1}{2}} v^s \tanh(2-\sqrt{2})\frac{nF}{RT}\, uE_{r.m.s.} \qquad (3)$$

Many different redox systems were examined, and the sweep rate and amplitude were varied over wide ranges. As will be shown, the general equation (3) is valid for most of the experimental data.

EXPERIMENTAL

Instrumentation

For most of the experiments, the apparatus used consisted of several, partly home-made, units. Facilities for a strictly potentiostatic procedure were not provided. The advantage of the original design was its greater versatility and particularly its large choice of sweep rates. In the final stages of the study, it was found that a combination of the PAR Model 174 Polarographic Analyzer together with PAR 174/51 linear sweep module and a few additional units was a good substitute.

The principle, shown in the block diagram (Fig. 1), nearly covers both instruments; the contents of the blocks differ but their functioning is quite similar. All the elements and connections indicated by dashed lines were absent from the original device.

The drop-life timer (1) serves to activate the relay (2) which is responsible for drop dislodgement, and after a fixed time interval, to start the voltage sweep (3).

The output signal from the sweep generator passes to the summing amplifier (6) together with the output signals from the alternating voltage generator (4) and the unit (5) which supplies the starting potential. When exactly potentiostatic conditions are used, the summing amplifier also receives signals originating from the compensating device via the units (16) and (17).

The summing amplifier delivers the input signal for the polarographic cells (7 and 8). The output signals from these cells are vectorially subtracted from each other in unit (11), the output of which corresponds essentially to the faradaic component of the current through the measuring cell (7).

The usual method of phase-sensitive detection was unsuitable for sweep rates beyond 50 mV s^{-1}, as the peaks became asymmetric, and lower than they should have been. In the home-made design, a differential transformer

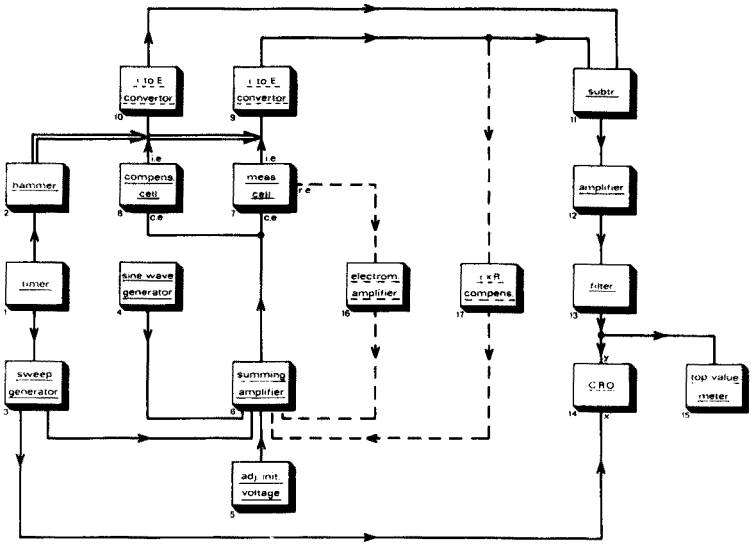

Fig. 1. Block diagram of the single-sweep a.c. polarograph. The contents of blocks 3, 5, 6, 12 and 16 form part of the PAR polarographic analyzer model 174; the contents of the blocks 1, 9, 10, 11 and 17 are accommodated within the PAR linear sweep module 174/51.

was used as subtractor [36, 37], which also removed any contributions of d.c. character. However, this transformer was unsuitable for frequencies above 100 Hz.

After amplification (12), a combination (13) of a second-order high-pass filter in series with a sixth-order low-pass filter removed the overtones from the signal, which was then supplied to the oscilloscope (14) and/or to the top-value meter (15). The oscilloscope was used partly for visual control during experiments and sometimes the traces were recorded by photography. The sweep rate used for Fig. 2 was higher than usual to permit better observation of details. The peak-value meter allows much faster operation, and is therefore recommended for routine measurements.

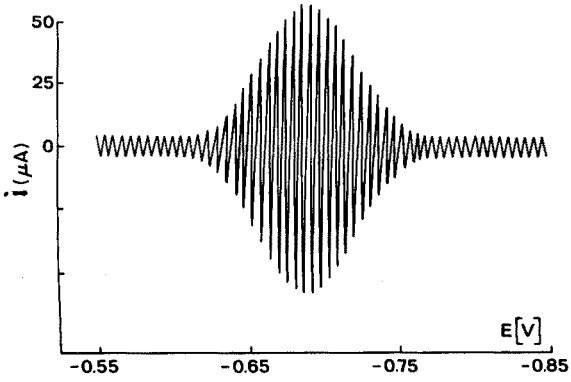

Fig. 2. Screen output for 1 mM Cd^{2+} in 0.1 M KCl. E = 22.5 $mV_{r.m.s.}$; v = 0.4 V s^{-1}.

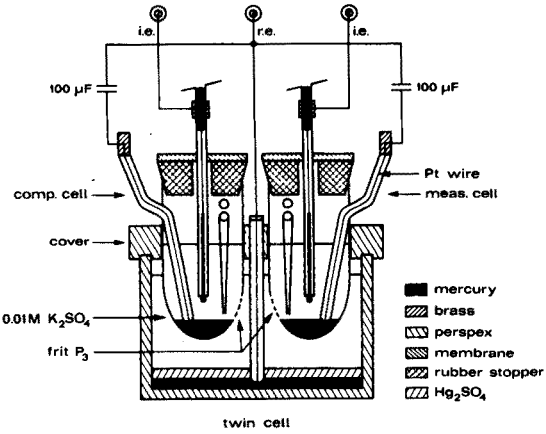

Fig. 3. Combined polarographic cells with common reference electrode.

The polarographic cell

The subtractive principle adopted requires the use of a twin-cell. The highly symmetrical twin-cell (Fig. 3) was designed according to the single cell prototype described by von Stackelberg and Hans [38]. The reference electrode is common to both cells.

In the original device, reduction of the alternating voltage drop inside the polarographic vessel was realized by short-circuiting each mercury pool via a capacitor with the reference electrode according to Breyer et al. [10, 39]. Each capillary was made by sealing a wide-bore capillary (i.d. 0.4 mm) to the lower end of a normal polarographic capillary (length ca. 90 mm, i.d. 0.04 mm). In this way, the natural drop time was variable between 20 and 120 s. Balancing of the two mercury flows was facilitated by moving one of the mercury reservoirs with a spindle. A drop time of 32 s was chosen; the sweep, having a duration of 2 s, started 28 s after the dislodgement of the preceding drop. The drop area thus increased by as little as 4% during the sweep.

Procedures

Nineteen inorganic and 13 organic test substances were selected for testing the validity of eqn. (3), which gives i_p as a function of four experimentally accessible variables, viz., $*c$, ω, v and E.

In principle, the parameter s can be derived from the slope of the logarithmic plot: $\log I_p$ vs. $\log v$ (Fig. 4). Since the hyperbolic tangent reduces for small values of the argument to the argument itself, and for large values of the argument to 1, the parameter u can be obtained from the relationship

$$u = \frac{2+\sqrt{2}}{2} \cdot \frac{RT}{nFE} \cdot \frac{(i_p)}{(i_{p,l})} \qquad (4)$$

where E refers to values of E in the lower range, and $(i_{p,l})$ stands for the

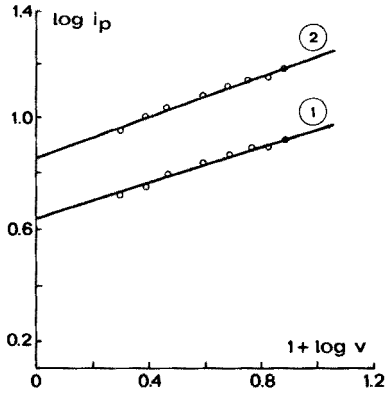

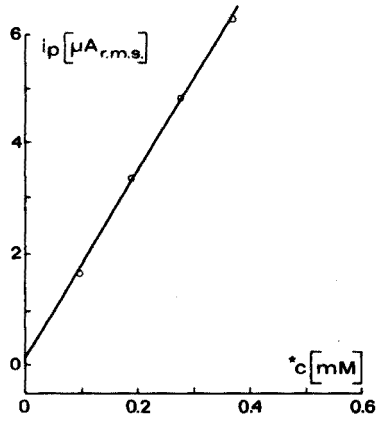

Fig. 4. Logarithmic plot for the estimation of the parameter s. 0.37 mM Ni(II) in 0.1 M KCl. i_p in μA; v in V s^{-1}. Curve 1, E = 25 $mV_{r.m.s.}$; curve 2, E = 50 $mV_{r.m.s.}$.

Fig. 5. Calibration curve for Ni(II) in 0.1 M KCl. E = 25 $mV_{r.m.s.}$; v = 0.3 V s^{-1}.

limiting peak current, which is reached at high values of E. If the parameters s and u as well as the different variables are known, the parameter r can be obtained from eqn. (3) after measurement of the peak current.

Usually, the calibration curves do not pass exactly through the origin (Fig. 5), but the intercept of the ordinate is small and vanishes when a correction is applied for the base current. The peak current as a function of the applied amplitude is shown in Fig. 6.

Unfortunately, the procedure for the determination of r, s and u does not yield very precise values, particularly if there is an inflexion point in the i_p vs. E plot (Fig. 6b). Only a rough estimation of u is then possible. However, the precision can be much improved by a curve-fitting procedure. The parameter u, together with the product $r \cdot v^s$, the values of which were

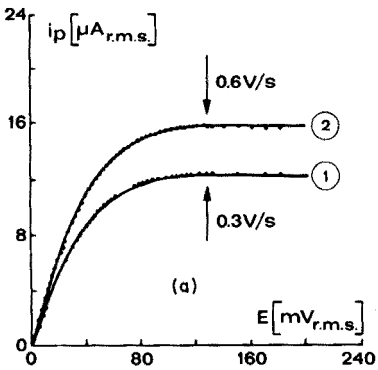

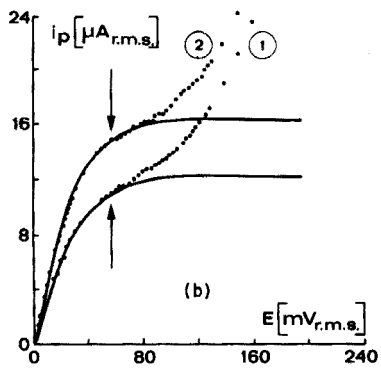

Fig. 6. Relation between peak current, i_p, and alternating voltage, E, (a) 0.37 mM Ni(II) in 0.1 M KCl. (b) 0.37 mM Ni(II) in 0.1 M KSCN. Curve 1, v = 0.3 V s^{-1}; curve 2, v = 0.6 V s^{-1}.

obtained as described above, were used as starting values of an iterative process, which is continued until the standard deviation of the ratio of the calculated to the experimental peak current does not improve further. In most cases three iterations suffice. When there is no plateau, data for points beyond a certain limit (indicated in Fig. 6 by arrows) are not used in calculating the function.

The iterative process yields fairly accurate values for the product $r \cdot v^s$ and for u. The limiting value of the peak current is also obtained.

The most reliable value for s can then be readily calculated:

$$s = \frac{\log (r \cdot v_2^s) - \log (r \cdot v_1^s)}{\log v_2 - \log v_1} = \frac{\log (i_{p,1})_{v=v_2} - \log (i_{p,1})_{v=v_1}}{\log v_2 - \log v_1} \quad (5)$$

Finally, parameter r is derived from the relationship for the limiting peak current $(i_{p,1})_{r.m.s.}$ as in eqn. (3).

$$r = 4(2 - \sqrt{2})\,(i_{p,1})_{r.m.s.}/nFA^*c(\omega D)^{\frac{1}{2}} v^s \quad (6)$$

In this eqn., A is calculated in the usual way from the time elapsed until the peak current has been reached and from the mercury flow rate. The diffusion coefficient, which depends on the medium used, can be best estimated from a classical polarogram of the same solution by application of the Ilkovič equation [40] or still better by extrapolation of the Lingane—Loveridge relationship [41].

RESULTS

When a polarogram is recorded in the normal direction, no faradaic process whatsoever takes place at the outset of the sweep. The potential sweep can also be applied in the opposite direction, but this was not tested extensively as it does not seem of analytical interest.

Normal sweep direction

The possible influence of drop growth during the sweep was shown to lie within the limits of experimental uncertainty. This was demonstrated by recording a number of polarograms, each with a different starting potential, so that the area of the drop at the moment of appearance of the peak varied in each case. (Table 1).

With a few exceptions, the peak potentials found for an applied alternating voltage of 25 $mV_{r.m.s.}$, coincided with the d.c. half-wave potentials within a margin of ca. 10 mV for reversible systems; larger deviations were found for some irreversible systems. The peak potentials were shifted slightly, usually in the positive direction, for most of the investigated systems, when the amplitude was increased; but the peaks remained symmetrical up to the highest value of the applied a.c. voltage for all reversible systems and for most of the other systems. Tailing was found for Sn^{2+}, whilst with Ba^{2+} a shoulder developed on the cathodic flank of the peak.

The large amount of data obtained are summarized in Table 2.

TABLE 1

Peak current for 10^{-3} M Cd^{2+} in 0.1 M KCl[a] ($E_{r.m.s.}$ = 22.5 mV)

E_{init} (V)	v (V s^{-1})	t_p/t_s	E_p (V)	i_p ($\mu A_{r.m.s.}$)
−0.540	0.1	0.57	0.70	81.1
−0.100	0.4	0.50	0.70	80.5
−0.600	0.2	0.18	0.70	78.3
−0.400	0.2	0.51	0.71	80.5
−0.200	0.2	0.87	0.72	80.5

[a] t_p = time delay between the application of the sweep and the moment of maximum current. t_s = duration of the sweep (3 s). E_{init} = initial potential. E_p = peak potential.

TABLE 2

Experimental results

Depolarizer	r	s	u	$\Delta u/u$ (%)	n	E_p (V)	$E_{\frac{1}{2}}$(V)	$E_p - E_{\frac{1}{2}}$ (V)	Medium[a]	σ (%)[b]
Pb^{2+}	0.977	0.00	0.916	0	2	−0.41	−0.40	−0.01	2	2.0
Cd^{2+}	0.937	0.00	0.903	0	2	−0.61	−0.60	−0.01	1	1.3
Tl^{+}	0.984	0.00	0.846	0	1	−0.47	−0.46	−0.01	1	1.8
Fe(III)	0.797	0.00	1.029	0	1	−0.22	−0.22	0.00	7	1.5
K^{+}	0.954	0.00	0.682	0	1	−2.14	−2.14	0.00	3	2.2
Na^{+}	0.933	0.00	0.626	0	1	−2.10	−2.12	0.02	3	2.6
Ba^{2+}	0.499	0.21	1.017	0	2	−1.92	−1.92	0.00	3	1.1
Zn^{2+}	0.794	0.00	0.520	0	2	−1.02	−1.01	−0.01	1	3.3
Mn^{2+}	0.402	0.33	0.992	0	2	−1.51	−1.51	0.00	1	2.1
Sr^{2+}	0.576	0.22	0.672	10	2	−2.14	−2.11	−0.03	3	1.5
Ni(II)	0.291	0.40	0.600	1	2	−0.64	−0.63	−0.01	4	2.1
Sb^{3+}	1.125	−0.02	0.154	−5	3	−0.17	−0.16	−0.01	2	10.6
H^{+}	0.231	0.34	0.677	−6	1	−1.67	−1.58	−0.09	3	1.4
Ni^{2+}	0.231	0.37	0.497	−1	2	−1.08	−1.10	0.02	1	2.3
Sn^{2+}	0.097	0.00	0.990	0	2	−0.45	−0.47	0.02	2	0.8
Co^{2+}	0.249	0.40	0.360	−6	2	−1.31	−1.20	−0.11	1	1.3
IO_3^{-}	0.269	0.40	0.203	1	6	−1.25	−1.21	−0.04	5	1.4
CrO_4^{2-}	0.051	0.47	0.154	−5	3	−1.13	−0.97	−0.16	5	2.3
Quinone	0.991	−0.09	0.605	0	2	0.18	0.16	0.02	8	2.5
Acetophenone	0.340	0.35	0.912	2	2	−1.03	−1.10	0.07	2	1.8
Fumaric acid	0.301	0.37	0.789	6	2	−0.66	−0.61	−0.05	2	2.0
Maleic acid	0.294	0.35	0.790	−10	2	−0.61	−0.56	−0.05	2	1.5
m-Nitrophenol	0.689	0.65	0.309	3	4	−0.56	−0.53	−0.03	9	2.2
Nitrobenzene	0.658	0.55	0.316	−4	4	−0.59	−0.60	0.01	9	2.0
o-Nitrophenol	0.539	0.67	0.228	2	6	−0.54	−0.54	0.00	9	3.0
p-Nitrophenol	0.433	0.60	0.240	0	4	−0.69	−0.71	0.02	9	1.2
Bromoacetic acid	0.255	0.42	0.208	−4	2	−1.61	−1.50	−0.11	9	1.7
Pyruvic acid	0.158	0.49	0.284	−10	2	−0.69	−0.60	−0.09	2	1.7
Iodoacetic acid	—	0.07	—	—	2	−0.58	−0.58	0.00	9	—
Hg–EDTA	—	0.34	0.451	−19	2	0.06	0.11	−0.05	8	1.8
EDTA	1.795	−0.15	0.526	−7	2	0.06	0.17	−0.11	8	1.6
Hydroquinone	1.179	0.00	0.698	2	2	0.20	0.19	0.01	8	1.7
Iodide	1.026	−0.18	0.584	−1	1	−0.34	−0.21	−0.13	6	1.5

[a] 1, 0.1 M KCl. 2, 0.1 M HCl. 3, 0.1 M $(C_2H_5)_4NCl$. 4, 0.1 M KSCN. 5, 0.1 M NaOH. 6, 0.1 M KNO_3. 7, 0.1 M $NaH(COO)_2$; 0.1 M $Na_2(COO)_2$; pH = 4.21. 8, 0.1 M HCH_3COO; 0.1 M Na CH_3COO; pH = 4.73. 9, 0.1 M KCl; 0.0627 M Na_2HPO_4; 0.0033 M KH_2PO_4; pH = 7.90.

[b] Standard deviation of the curve-fitting procedure.

Fast one-step redox systems. The experiments seldom gave the ideal values for the parameters, r, s, and u. Nevertheless, the deviations for Cd^{2+}, Pb^{2+} and Tl^{+} are quite acceptable in view of the approximations introduced. Independence from the sweep rate, i.e. $s = 0$, was obtained for quite a large number of reductions. It can be demonstrated that the estimated values for u are too low because the ohmic voltage drop was neglected, though even after due correction the ideal value was rarely reached.

Other redox reactions. The examples chosen cover a variety of reaction schemes. In several cases, a plateau was not reached, but instead an inflection point was observed, followed by a rising curve. Such curves were found for nickel(II) in a thiocyanate medium (a preceding chemical reaction may be expected [42—44]), for *o*- and *p*-nitrophenol [45—49], and for quinone [50, 51] during the reduction of which stable intermediates develop temporarily. Similar curves were also shown by Na^{+}, K^{+}, Sr^{2+} and acetophenone; here the interference may have been due to decomposition of the supporting electrolyte. The similar behaviour of barium(II) is difficult to explain. Manganese(II) followed the same pattern; for some reason, the product αn_a is according to the literature [52] about twice the usual value for other comparable divalent cations in neutral aqueous media.

For the rest, curve fitting gave satisfactory results. The standard deviations between calculated and experimental values were less than 3%, except for antimony(III), for which the standard deviation was 10.6%. The proposed relationship (3) clearly does not apply for antimony(III).

Quite often, another irregularity with respect to the parameter u was observed. It appeared that this parameter is sometimes slightly dependent on the sweep rate, v, contrary to the initial assumption. Table 2 shows the relative deviation ($\Delta u/u$) of u as a consequence of doubling the sweep rate (which was usually 0.3 V s^{-1}).

A curved calibration plot was observed for HgY^{-2}; in this case the shape of the electrocapillary curve provided strong indication that the complex anion was adsorbed at the mercury interface [18]. Strong adsorption was also proved for iodocetate; the behaviour of iodocetate was also unusual in that the peak current was proportional to the imposed alternating voltage over the whole range investigated. This phenomenon indicates the smallness of the parameter, u. Moreover, a non-linear calibration plot was obtained.

In addition to these cathodic processes, a few anodic processes were also investigated, namely hydroquinone, EDTA and iodide.

Some attention was also given to substances which produce tensammetric peaks, sometimes in addition to faradaic peaks. The substances investigated were acetophenone, *p*-nitrophenol and quinone. The tensammetric peaks likewise obeyed a hyperbolic-tangent relationship, but the calibration graphs were not rectilinear. The calibration curve could be represented by

$$i_p = \alpha^* c/(1 + \beta^* c) \qquad (7)$$

which is typical when there are adsorption effects [10]; plotting $1/i_p$ vs. $1/^*c$ gave a straight line (Fig. 7).

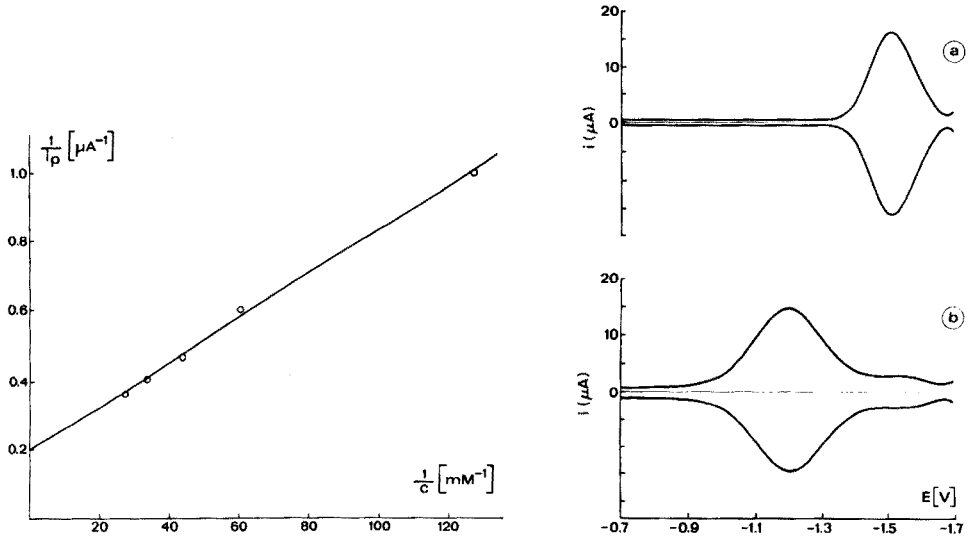

Fig. 7. Calibration curve for the tensammetric peak of *p*-nitrophenol in 0.1 M KCl, buffered at pH 7.90 with phosphate.

Fig. 8. The polarogram of 0.77 mM ZnO_2^{2-} in 1 M KOH. E = 25 $mV_{r.m.s.}$; v = 0.5 V s^{-1}. Sweep direction (a) normal; (b) reverse. Frequency 80 c s^{-1}.

Reverse sweep

The starting potential was given a value corresponding to some point on the plateau of the d.c. polarogram. However, the electrical connection with the combined d.c. and a.c. sources was not always achieved over the whole blanking period, but occasionally during a variable interval, t_e, preceding the start of the d.c. voltage sweep; the duration of this interval lay between 0.1 and 28 s.

As a first approximation it might be expected that the resulting inverse polarogram would hardly be different from the normal one, for reversible redox systems. Closer examination showed that the influence of the sphericity of the diffusion pattern became more manifest, the longer the pre-electrolysis period. This effect was intensified if there was amalgam formation during the pre-electrolysis period, t_e (see Appendix).

For irreversible redox systems the situation was quite different. A small peak was observed at the same potential as found in the normal a.c. sweep polarogram. This peak was due to diffusion of the original species, but in the small concentration present in the diffusion layer because of its depletion during pre-electrolysis. This small peak was followed by a larger one, which corresponded to electrochemical reconversion of the reaction product formed during pre-electrolysis (Fig. 8). The shift of the second peak potential compared with the position of the peak in the normal polarogram is readily explained by reference to a classical polarogram for an irreversible redox system with both components present simultaneously.

The situation outlined above is influenced by the electrode potential during pre-electrolysis, the moment at which this potential is applied, and by the magnitude of the d.c. voltage span. The heights of both peaks depend strongly on these variables.

Analytical features

The analytical value of the method proposed appears to its fullest advantage in dealing with multicomponent samples. To this end, a solution containing Pb^{2+}, Cd^{2+}, Zn^{2+}, Co^{2+} and Mn^{2+} was prepared, with concentrations of 10^{-3}, 10^{-5}, 10^{-3}, 10^{-4} and 2×10^{-5} M, respectively, in a supporting electrolyte of 0.1 M KCl. To obtain an overall view the polarogram was first recorded over a broad voltage range. Only the peaks of the main components appeared. Thereupon, four smaller voltage spans were selected and the sensitivity was adjusted suitably for the concentrations concerned. The peak heights thus obtained were easily measured, despite the neighbouring peaks of the major components. In practice, much time can be saved by reading the peak voltage meter, possibly in combination with print-out. Routine analyses can be achieved within a few minutes, provided that the solutions have been previously degassed.

The dynamic range of the method covers about 3 decades, whilst the lower limit for quantitative determination is about 10^{-6} M or somewhat lower.

APPENDIX

Before the application of a normal sweep, the drop grows for a considerable time without electrolysis taking place. Then a voltage sweep of relatively short duration occurs; this can be described by a planar diffusion model, as was done by Osteryoung et al. [53, 54] in discussing certain relationships in pulse polarography. It must be admitted, however, that this approximation is more justified in the latter case because of the much shorter times involved.

The initial condition for a reverse sweep is far more complicated, especially when electrolysis occurs during the whole period of drop growth. The effect of the pre-electrolysis process must therefore be calculated on the basis of spherical diffusion. For the sweep proper, the planar diffusion model can be used again.

Unfortunately, exact derivations for a.c. polarography at an expanding sphere are not available, but qualitative information can be obtained from Delmastro and Smith's exposition of the stationary sphere model [34]. According to these authors, the a.c. component of the output signal for a reversible redox system can be derived from the relationship for the planar model for a reversible redox system by multiplication by a time-dependent factor, $F(t)$ given by

$$F(t) = 1 + \frac{1 \mp d^{1/2}}{\exp\Phi \pm d^{1/2}} [1 - \exp(a^2 t) \operatorname{erfc}(at^{1/2})] \qquad (A1)$$

in which $d = D_R/D_O$, $\Phi = (E_{d.c.} - E_{1/2})nF/RT$, $a = (\exp \Phi \pm d^{1/2})\, D_O^{1/2}/r_0(1 + \exp\Phi)$ and r_0 is the drop radius [34]. Essentially, the factor $F(t)$ is a measure of the enhancement of the sum of the surface concentrations. The lower signs refer to amalgam formation, whilst the upper signs refer to a redox system, both components of which dissolve in the aqueous phase. In the latter case, the influence of sphericity is very small, and even vanishes for $d = 1$. (Table 3). However, as stated above, the original model was devised for a stationary electrode, whereas actually the drop is growing. Therefore, the factor $F(t)$ has merely a qualitative meaning for the present investigation.

During a normal sweep, the peak current is attained very quickly after electrolysis starts. Hence the parameter, t, is small (less than 0.3 s), which implies an almost negligible value for the correction factor. In contrast, for a reverse sweep there is a considerable delay between appearance of the peak and the start of electrolysis (about 29 s). Consequently, $F(t)$ acquires a considerable value, which results in the observed enhancement of the peak current. Only when the pre-electrolysis time is kept very short by temporary disconnection of the direct voltage source, does the reverse peak nearly equal that obtained during the normal sweep.

TABLE 3

Correction factor F for sphericity[a]

	$10^5 D_O$ (cm^2 s^{-1})	
	0.90	2.12
t_e	F	F
0.1	1.03	1.05
0.3	1.06	1.10
1.0	1.12	1.18
3.0	1.21	1.33
10.0	1.41	1.68
28.0	1.79	2.43

[a] t_e = pre-electrolysis time. $r_0 = 6.1 \times 10^{-2}$ cm.

The authors are most grateful to Dr. J. H. Sluyters and Dr. M. Sluyters-Rehbach for their interest and contributions to discussions.

REFERENCES

1 L. A. Matheson and N. Nichols, Trans. Electrochem. Soc., 73 (1938) 193.
2 G. S. Smith, Nature, 163 (1949) 290.
3 A. Ševčík, Collect. Czech. Chem. Commun., 13 (1948) 349.
4 J. E. B. Randles, Trans. Faraday Soc., 44 (1948) 327.

Piezoelectric crystals and instrumentation

The crystals were general-purpose devices with a normal resonant frequency of 9 mHz; they were of the smaller size, HC 25/U holders with the canister removed. Crystals for measuring NH_3 possessed gold electrodes, and were purchased from International Crystal Manufacturing Co. (Oklahoma); the H_2S crystals had silver electrodes and were obtained from Jan Crystals (Florida).

The instrumentation consisted of a low-frequency 1T transistor oscillator (International Crystal Mfg. Co.) powered by a Heathkit Model 28 power supply; the voltage used was a constant 9 V. The frequency output from the oscillator was measured by a Systron-Donner Model 8050 frequency meter which was modified by a digital-to-analog converter [7] so that the frequency could be recorded by a Bristol Model 570 Dynamaster recorder. Thus, data were obtained from both the frequency meter and the recorder.

The experimental procedures are described in the results section. The test solutions were obtained from C.P. ammonia or H_2S gases, or by using concentrated aqueous ammonia, either injected directly or diluted with distilled water.

RESULTS AND DISCUSSION

The crystal as an ammonia detector

Dissolved ammonia can be detected by a coated piezoelectric crystal that is separated from the aqueous solution by a gas-permeable membrane. This reaction is shown by a decrease in the frequency of the crystal caused by the adsorption of ammonia, over that caused by the adsorption of water alone. The frequency of the crystal was first measured with the crystal chamber dry and in air. After the crystal was placed into the sample cell with the membrane in contact with distilled water, and the frequency recorded, the frequency had dropped 550 Hz. After the distilled water was replaced with aqueous 1.5 M ammonia, the frequency dropped by 1150 Hz, giving a difference of 600 Hz due to ammonia. A concentration of aqueous ammonia of 0.15 M, produced a frequency difference of 135 Hz. In all cases the frequency drop was measured after a steady frequency reading was reached; this took considerable time.

To reduce the time necessary to perform the measurements, a new procedure was devised. The crystal was placed in position in the sample cell in contact with 150 ml of distilled water and the system was allowed to come to a steady frequency. Ammonia gas was then injected into the water through the capillary side arm and the frequency was again recorded after a steady frequency had been reached. In Fig. 1, the difference in frequency, ΔF, between that of distilled water and that after injection of ammonia, is plotted vs. the concentration of the solution resulting from the injection of ammonia. The concentration reported is total ammonia, i.e., corrections for equilibrium constants and solubilities were not considered. The plot in Fig. 1 shows that

Analytica Chimica Acta, 94 (1977) 149—154

MICRODETERMINATION OF AROMATIC NITRO COMPOUNDS WITH IRON(II) IN ALKALINE SORBITOL MEDIA

B. VELIKOV, J. DOLEŽAL and J. ZÝKA

Department of Analytical Chemistry, Charles University, Prague (Czechoslovakia)

(Received 16th May 1977)

SUMMARY

In titrations with iron(II) sulphate in alkaline solutions of sorbitol, the iron(III) formed is bound in a strong complex and the formal redox potential of the Fe(III)/Fe(II) system is decreased to —1.10 V (SCE; 0.5 M sorbitol, 2 M KOH). This permits reducing titrations with a stable reagent, of systems which would otherwise require unstable strong reductants (e.g. Cr(II), Sn(II), V(II), etc.). Determinations of organic mono-, di- and tri-nitro compounds are described; these can be carried out directly on the microscale, with potentiometric, bipotentiometric or biamperometric end-point detection. Nitrate does not interfere; the method can also be employed for indirect determinations of various aromatic compounds after their conversion to nitro derivatives.

The possibility of decreasing the redox potential of the Fe(III)/Fe(II) system for titrimetric purposes was studied previously; the Fe(III) formed was bound in strong complexes in alkaline solutions [1]. Recently, it was found that the best results can be obtained in alkaline sorbitol solutions, as has been verified by polarographic studies [2, 3]; the formal redox potential in 0.5 M sorbitol and 2 M KOH attains a value of —1.10 V (SCE), i.e. it equals the strongest reductants. The present work deals with titrations of organic nitro compounds, which previously could only be determined directly with unstable reductants or had to be determined indirectly, after the addition of an excess of reductant. Standard solutions of iron(II) sulphate are very stable and sorbitol is readily available; these direct titrations of nitro compounds should therefore find wide analytical application. The method, tested on mono-, di- and tri-nitro derivatives, can also be used for indirect determinations of organic compounds that can be converted to nitro derivatives. The nitro derivative formed can be titrated directly in the nitration mixture. The end-point can be detected potentiometrically, bipotentiometrically or biamperometrically. The titrations must be performed in a nitrogen atmosphere. The method also gave good results for oxo, nitroso and diazo compounds; these determinations will be described in future communications. The use of dulcitol and mannitol was also investigated, but these compounds were not as efficient as sorbitol.

EXPERIMENTAL

Reagents and apparatus

To prepare iron(II) sulphate solution (0.05 M), dissolve 6.950 g of $FeSO_4 \cdot 7H_2O$ (p.a.) in 500 ml of 0.05 M H_2SO_4. De-aerate the acid solution thoroughly before addition of the iron(II) sulphate by passage of nitrogen for 30 min. Check the titre of the solution weekly by titration of potassium dichromate in an acid medium. From this stock solution prepare 0.01 to 0.005 M Fe(II) solutions.

Prepare stock solutions of 0.05 M *o*-, *m*-, and *p*-nitrophenol, 2,4-dinitrophenol and 2,4,6-trinitrophenol (p.a.) by dissolving the appropriate amounts in distilled water made alkaline by adding 5 ml of 5 M KOH. Prepare sorbitol solutions as required.

The potentiometric, bipotentiometric and biamperometric titrations were carried out with a Seibold digital pH-meter (Austria) and operational amplifier modular sets made at the Department of Analytical Chemistry, Charles University, and the Institute of Physical Chemistry and Electrochemistry. A three-position switch permitted potentiometric, bipotentiometric and biamperometric measurements to be carried out in rapid succession; the currents measured during the biamperometric titrations are therefore given in terms of the voltages displayed on the pH meter. (In the Figures, abbreviations P, BP and BA denote potentiometric, bipotentiometric and biamperometric end-point detection, respectively.)

RESULTS

Determination of o*-nitrophenol*

The reduction of *o*-nitrophenol by iron(II) salts in alkaline sorbitol solutions is rapid and produces the amine according to

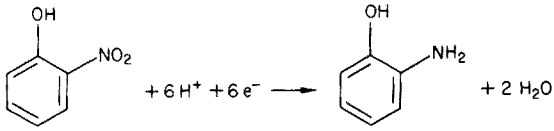

During the titration the orange solution turned yellow, became colourless around the equivalence point, and turned green on the addition of an excess of iron(II). The dependence of the titration course on the sorbitol and KOH concentrations (Table 1) indicated that the optimum solution composition is 0.25—0.5 M sorbitol and 2—3 M KOH. The potentials stabilized too slowly at lower concentrations of the two components. With the optimum concentrations, the potentials stabilized within 30 s at laboratory temperature and the slope at the potentiometric end-point, $\Delta mV/\Delta ml$, was 20 000—22 000 mV for 0.05 M Fe(II) (Fig. 1).

The optimum applied current in the bipotentiometric titration was 7—8 μA and the optimum applied voltage in the biamperometric titration

TABLE 1

The effect of the sorbitol and potassium hydroxide concentrations on the potentiometric titration of *o*-nitrophenol with 0.05 M Fe(II)
(25 ml of the solution contained 6.95 mg of *o*-nitrophenol.)

Sorbitol (M)	KOH (M)	Found (mg)	Error (%)	ΔmV/Δml
0.05	0.1	6.84	−1.58	6500
	1.0	6.88	−1.00	7000
0.1	0.1	6.87	−1.15	8500
	1.0	6.89	−0.86	11 500
	4.0	6.88	−1.00	15 000
0.25	0.1	6.99	+0.57	9000
	1.0	6.85	−1.44	14 000
	4.0	6.90	−0.72	17 500
0.5	0.1	7.03	+1.15	12 000
	0.5	7.01	+0.86	14 500
	1.0	6.98	+0.43	17 000
	2.0	6.92	−0.43	20 000
	3.0	6.91	−0.57	22 000
	4.0	6.98	+0.43	23 000
0.8	0.1	7.00	+0.72	13 000
	1.0	6.99	+0.57	16 500
	4.0	6.88	−1.00	21 000

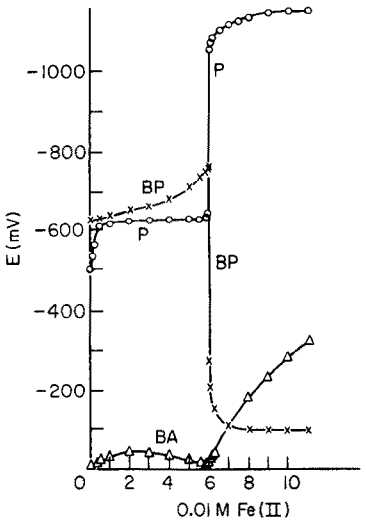

Fig. 1. Potentiometric, bipotentiometric and biamperometric titration of *o*-nitrophenol with 0.01 M Fe(II) in a solution of 0.4 M sorbitol and 3 M KOH.

was 500—600 mV. The results are virtually the same with all three detection techniques.

Amounts of 0.1—20 mg of *o*-nitrophenol were titrated precisely in 25 ml of solution. For 10 determinations, the % error ranged from +1.44% to −1.58% (average error −0.39%). The determination on the microscale (0.1—1 mg in 25 ml) is very precise ($\Delta mV/\Delta ml$ = 30 000 mV for 0.01 M Fe(II)).

Determination of m- *and* p-*nitrophenol*

The reduction of *m*- and *p*-nitrophenol in a solution of 0.25—0.5 M sorbitol and 2—3 M KOH proceeded smoothly. The yellow solution turned orange during the titration and became colourless around the equivalence point. The potentials stabilized rapidly; in the vicinity of the equivalence point, the stabilization required 1—1.5 min. The slopes of the potentiometric curves at the end-point were similar, being about 13 000—14 000 mV for 0.05 M Fe(II) (Figs. 2 and 3). The potentials during the titration of *p*-nitrophenol decreased before the equivalence point, and then the potential break occurred.

The bipotentiometric titration curve (optimum current, 9 μA) shows that an irreversible system is titrated by a more reversible one, which is typical of most organic systems (Figs. 2 and 3). The biamperometric end-point can also be precisely located with the optimum applied voltage, 900—1000 mV.

Similarly to the determination of *o*-nitrophenol, *m*- and *p*-nitrophenol can be titrated on the microscale; 0.1—25 mg of the substances were titrated in 25 ml of solution with an error not exceeding ±1.6%.

Determination of mononitrophenols in the nitration mixture

Nitrate does not interfere in direct determinations with iron(II) ions in alkaline sorbitol media. This is apparently caused by the small difference

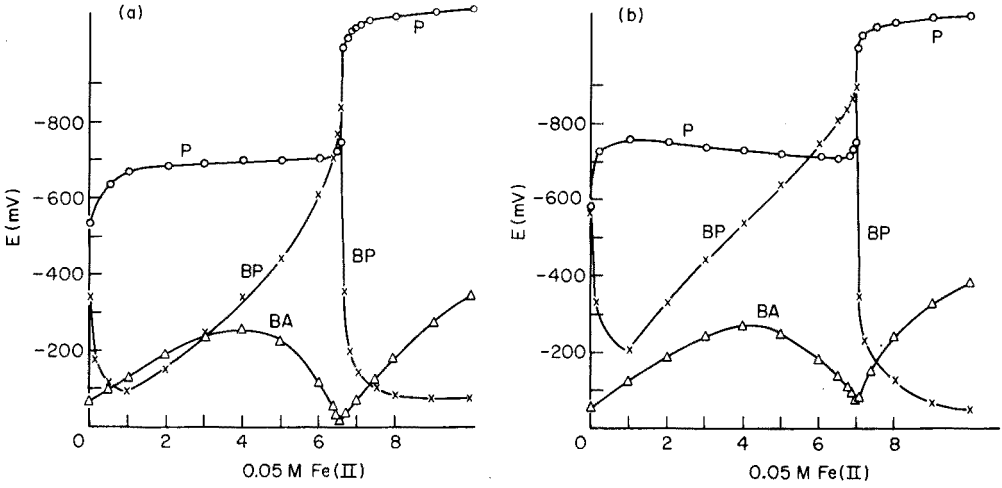

Fig. 2. Potentiometric, bipotentiometric and biamperometric titrations with 0.05 M Fe(II) in a solution of 0.4 M sorbitol and 3.5 M KOH. (a) *m*-Nitrophenol. (b) *p*-Nitrophenol.

Analytica Chimica Acta, 93 (1977) 153—159

COULOMETRIC TITRATION OF PENICILLINS AND PENICILLAMINE WITH MERCURY(II)

ULF FORSMAN

Institute of Chemistry, University of Uppsala, P.O.B. 531, S-751 21 Uppsala (Sweden)

(Received 14th April 1977)

SUMMARY

An absolute coulometric method based on the titration of hydrolysed penicillins with coulometrically generated mercury(II) is presented. An amalgamated gold plate is used as anode and the titration is performed in a pH 4.6 acetate buffer solution. The method gives values which deviate by less than 1% from values obtained by other absolute methods. The relative standard deviation for determination of penicillin G is 0.4%. The determinations of penicillamine and mixtures of penicillamine and penicilloate are also reported.

In earlier studies, titration techniques for penicillins [1] and 6-aminopenicillanic acid [2] with mercury(II) solutions were reported. These methods were based on volumetric titration of penicillins hydrolysed to the corresponding penicilloates with mercury(II) nitrate solution. Compensation for penicilloates initially present in the penicillins was made by titration of an unhydrolysed sample. For penicillamine, which is a break-down product of penicillins, volumetric titrations with mercury(II) solutions have also been published. Billabert et al. [3] used mercury(II) acetate for a titration at pH 6; two equivalence points were found, the first corresponding to formation of a sulphide and the second to formation of a chelate. Körbl and Vanicek [4] titrated penicillamine with mercury(II) perchlorate in a medium containing pyridine.

Coulometric generation of mercury(II) from the metal would serve as an alternative to these volumetric methods, and would have the advantage that no standardization is required. The use of coulometrically generated mercury (II) has been reported for several different substances. Vandenbalck et al. [5] determined aminopolycarboxylic acids with a mercury pool as anode; a back-titration procedure for metal ions was also presented. The titration of halides with electrolytically generated mercury(I and II) was reported by Przybylowicz and Rogers [6]. Three different anodes were investigated: a mercury pool, and mercury-coated silver and gold. The amalgamated gold anode was preferred and used in subsequent studies where sulphide [7] and cysteine [8] were titrated; errors of ±0.2% were reported for sulphide and <1% for cysteine. Mairesse-Ducarmois et al. [9] used coulometric mercury(II) titrations for thiols and reduced disulphides.

point the stabilization took about 2 min. During the titration the yellow solution turned deep orange and became colourless at the equivalence point. Bipotentiometry (optimum current, 7 μA) and biamperometry (optimum voltage, 450—500 mV) had no advantage over equilibrium potentiometry (Fig. 3), for which the slope of the titration curve at the equivalence point amounted to 12 000 mV for 0.05 M Fe(II) (0.5 M sorbitol and 3 M KOH).

In a volume of 25 ml, 0.4—19 mg of 2,4-dinitrophenol was determined with good precision (±1.3%). Amounts larger than 10 mg can also be determined indirectly by back-titrating an excess of iron(II) salt with standard 0.05 N Cr(VI) solution.

Determination of 2,4,6-trinitrophenol

2,4,6-Trinitrophenol was selected as representative of aromatic trinitro compounds; its reduction in alkaline hexitol solutions yields the triaminophenol, according to

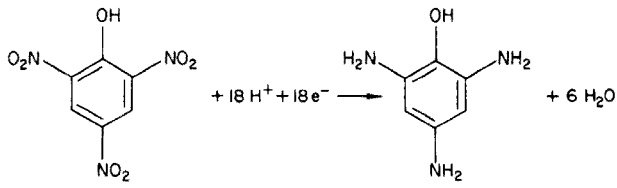

Direct titration with iron(II) sulphate was possible, but the reaction was too slow at laboratory temperature. As an exchange of 18 electrons is involved, microdeterminations were carried out at 60—70°C. The potentials stabilized rapidly during potentiometric titration in a solution of 0.5 M sorbitol and 2—3 M KOH, but around the equivalence point a delay of 3—4 min was necessary before the potential value was read. The potential break at the equivalence point was large (Fig. 3); its slope was 12 500 mV for 0.05 M Fe(II). The orange solution gradually turned colourless. The same results were obtained with the bipotentiometric (optimum current, 8 μA) and biamperometric (optimum voltage, 600—700 mV) end-point indication. By direct titration, 0.07—2.3 mg of the substance was determined in 25 ml of solution with a maximum relative error of +1.45% (mean relative error +0.71%, 7 determinations).

2,4,6-Trinitrophenol can also be determined indirectly with the same results. The reagents were added in an inert atmosphere in the following order: 12.5 ml of 1 M sorbitol, 1 ml of 0.02 M picric acid, 50—100% excess of the 0.05 M $FeSO_4$ standard solution, and 15 ml of 5 M KOH. The excess of Fe(II) was back-titrated with 0.05 N $K_2Cr_2O_7$.

REFERENCES

1 A. Berka, J. Vulterin and J. Zýka, Newer Redox Titrants, Pergamon Press, Oxford, 1965.
2 B. Velikov and J. Doležal, J. Electroanal. Chem., 71 (1976) 91.
3 J. Zýka and J. Doležal, Microchem. J., 10 (1966) 554.

Analytica Chimica Acta, 94 (1977) 155—159

MASS SPECTROMETRIC DETERMINATION OF CADMIUM IN I.A.E.A. FISH SOLUBLES

TSAIHWA J. CHOW* and CARRIE B. SNYDER

Scripps Institution of Oceanography, La Jolla, California 92093 (U.S.A.)

(Received 4th April 1977)

SUMMARY

The cadmium content of the I.A.E.A. Fish Solubles [A-6 (1975)] was determined by the isotope dilution method. After dry-ashing and dissolution of the specimen, the cadmium was equilibrated with a known amount of ^{108}Cd spike, isolated by ion exchange, purified by dithizone extraction, and converted to the sulfide form in 1% H_3PO_4 solution. The CdS precipitate was loaded onto a baked single rhenium filament for mass spectrometric analysis. The $^{108}Cd/^{110}Cd$ ratio was measured to compute the cadmium content of 0.278 ± 0.032 ppm (dry weight basis) in the Fish Solubles.

The Analytical Quality Control Service of the International Atomic Energy Agency (I.A.E.A.) in Vienna has prepared a suite of reference materials and intercomparison samples for use in the determination of stable trace elements in environmental or biomedical research. These materials provide an opportunity for laboratories dealing with trace metal studies to check their analytical performances and the elaboration of new procedures.

One of these reference materials is Fish Solubles [A-6 (1975)]; its cadmium content was included in the intercomparison study of trace elements. The results reported by 12 laboratories ranged from 0.087 to 17 ppm. By rejecting four extreme values, Görski [1] derived a mean cadmium concentration of 0.485 ± 0.181 ppm.

This study re-examines the cadmium content of the Fish Solubles by the isotope dilution method.

EXPERIMENTAL

Cadmium spike

Cadmium oxide, enriched in ^{108}Cd (Oak Ridge National Laboratory), was dissolved in 0.2 M HCl to give a spike solution containing 114.6 μg Cd ml^{-1}. Results for the isotopic composition of the spike and common cadmium are given in Table 1.

Specimen treatment

A can of the Fish Solubles reference material (I.A.E.A.) contained 100 g of dried fish serum prepared from commercial sources. The macro-homogeneity

TABLE 1

Isotopic composition of common and spike cadmium (in atom %)

Isotope	106	108	110	111	112	113	114	116
Common cadmium								
Oak Ridge	1.215	0.875	12.39	12.75	24.07	12.26	28.86	7.58
This paper	1.239	0.886	12.47	12.77	24.11	12.21	28.80	7.522
Spike cadmium								
Oak Ridge	0.45	82.35	5.30	2.99	3.66	1.58	3.00	0.67
This paper	0.352	82.95	5.336	2.965	3.428	1.476	2.827	0.664

of the specimen was achieved by thorough mixing, and no active or inactive materials were added.

Aliquots (2—15 g) of this material were dried at 110°C to constant weight and dry-ashed at various temperatures and times, as shown in Table 2. The average moisture content was 8.8%. Aliquots ashed at 400—600°C yielded

TABLE 2

Cadmium content of I.A.E.A. Fish Solubles

Sample wt. (g)	Moisture (%)	Dry ashing			Cadmium content ppm (dry basis)
		Temp (°C)	Time (h)	Ash (%)	
4.003	8.3	600	20	21.6	0.299
4.010	8.3	600	8	21.9	0.308
4.000	8.3	600	8	21.9[a]	0.284
2.006	9.6	600	4	21.9	0.354
1.999	10.0	600	4	21.8	0.309
2.004	9.7	600	4	21.9	0.278
4.008	8.2	550	8	21.9	0.297
4.001	8.3	550	8	22.0	0.307
2.002	8.3	550	8	22.0	0.283
2.005	8.3	550	8	22.0	0.270
2.001	8.3	550	8	22.0[a]	0.255
2.014	9.4	500	8	21.7	0.284
2.002	9.7	500	8	21.7	0.275
2.012	8.6	500	4	21.9[a]	0.256
2.012	9.5	450	21	21.9	0.312
2.004	8.6	450	21	21.9	0.304
8.016	9.4	450	20	21.9	0.269
15.120	8.3	450	20	22.1	0.248
2.001	8.5	400	24	22.3	0.259
2.011	9.7	400	28	22.2	0.230
2.009	8.4	350	49	26.7	0.223
2.006	8.6	350	49	27.8[a]	0.222
2.000	8.5	Wet digestion—HNO_3			0.258
2.002	8.7	Wet digestion—HNO_3			0.222

[a]Spiked in 1 M HNO_3, others in 8 M HCl.

a grey, greyish white, or white residue; those ashed at 350°C produced black charred particles, despite prolonged ashing time. Two aliquots were wet-ashed with concentrated HNO_3.

Chemical procedure

The ash of each aliquot was immersed in 10 ml of 8 M HCl or 1 M HNO_3 as indicated in Table 2. To the solution either 100 μl or 200 μl of the cadmium spike (11.46 μg/100 μl) were added and the mixture was equilibrated by evaporating to dryness. Some 10 ml of 1 M HCl were added to the residue, heated to dissolve the cadmium compound, and then centrifuged. The supernatant liquid was poured through a Dowex AG1-X8 anion-exchange column washed previously with 50 ml of 1 M HNO_3, rinsed with 50 ml of doubly distilled water, and conditioned with 10 ml of 1 M HCl. The resin column now containing the sample was washed with 25 ml of 0.02 M HCl to extract zinc that would interfere with dithizone purification, with 50 ml of 1 M HCl, and with 10 ml of doubly distilled water. The cadmium ion sorbed on the resin was eluted with 50 ml of 1 M HNO_3, although most of the cadmium was eluted in the first 25-ml portion.

The eluted cadmium(II) in 1 M HNO_3 was evaporated to dryness, dissolved in 10 ml of acidified doubly distilled water (pH 2—3), and transferred to a 30-ml separatory funnel. After adjusting to pH 9 with ammonium hydroxide, the solution was shaken vigorously with 10 ml of 0.002% dithizone in chloroform for 2 min. Sufficient additional dithizone powder was introduced to complex all cadmium. This chloroform layer showing the reddish-brown color of cadmium dithizonate was then drained into another separatory funnel, decomposed and extracted with 10 ml of acidified (pH 2–3) doubly distilled water. The acidic solution which contained cadmium was retained in the separatory funnel while the chloroform—dithizone layer was discarded. The cadmium was again extracted with 5 ml of dithizone—chloroform solution after adjusting to pH 9. Sufficient dithizone powder to complex all cadmium was added; the red chloroform layer was drained into a 5-ml beaker and evaporated to dryness.

Concentrated HNO_3 and $HClO_4$ (0.5 ml of each) were added to the beaker and evaporated to dryness to destroy the organic matter. The resulting cadmium chloride was dissolved in 0.5 ml of 1% H_3PO_4 solution, transferred to a 1-ml centrifuge tube, precipitated with filtered H_2S until the CdS coagulated, and then centrifuged.

Mass spectrometry

A single rhenium filament (1 × 30 mil) was heated in a vacuum at 2 A, corresponding to a temperature of 1000°C, for 30 min until any cadmium which might have been initially present on the filament was removed. The CdS precipitate in H_3PO_4 solution was loaded onto this filament. The acid was evaporated by heating the filament with a current of 1.5 A before mounting the sample in the mass spectrometer.

The $^{108}Cd/^{110}Cd$ ratio was measured with a single focusing, 60° sector, 30-cm radius, solid-source mass spectrometer equipped with an electron multiplier. After the pressure in the source chamber had been reduced to less than 10^{-6} mm Hg, the filament current was slowly raised to 0.8 A and held for about 30 min. At this stage, impurity peaks of masses 105, 106,107 and 109 were observed, mass 105 being the predominant peak. The current was then increased to 0.9 A, at which time the impurity peaks decreased and the intensity of the cadmium ion beam gradually increased. At the usual operating filament current (1.0—1.2 A) only the cadmium ion beam remained.

The charged cadmium ions passed through a 50% transmittance grid at the collector and impinged on the conversion dynode of an electron multiplier which had a gain of 10^5. The signal was further amplified by passing the collected ion current through a 10^8 ohm resistor connected to the input of a vibrating reed electrometer. An isotopic spectrum of common cadmium is illustrated in Fig. 1, showing a total signal strength of 7500 mV. For an ordinary analysis, about 20 pairs of $^{108}Cd/^{110}Cd$ ratios were taken.

The atomic weight correction was incorporated in the calculation as well as the square root of mass ratio correction to compensate for the velocity discrimination in the electron multiplier. The amount of cadmium in the sample was calculated from

$$M = m\ (N \times {}^{110}Cd_s - {}^{108}Cd_s)/({}^{108}Cd_w - N \times {}^{110}Cd_w)$$

where M = cadmium in the sample (μg); m = amount of ^{108}Cd spike added (μg); N = observed $^{108}Cd/^{110}Cd$ ratio with atomic weight and square root of mass ratio corrections; $^{108}Cd_s$, $^{110}Cd_s$ = atom % of ^{108}Cd and ^{110}Cd in the cadmium spike, respectively; $^{108}Cd_w$, $^{110}Cd_w$ = atom % of ^{108}Cd and ^{110}Cd in the common cadmium, respectively.

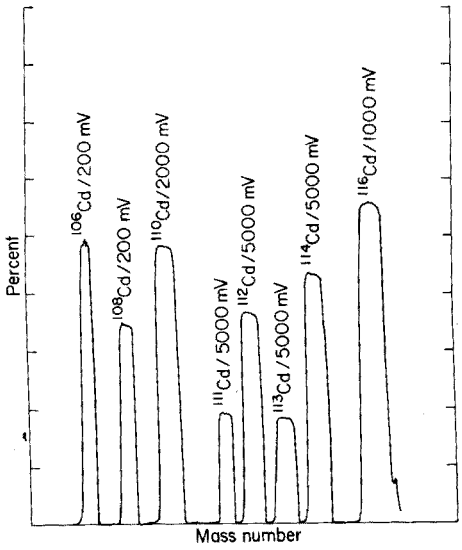

Fig. 1. Isotope spectrum of common cadmium.

Rosman and De Laeter [2] reported a silica-gel technique for sub-micro gram quantities of cadmium; however, it often had the disadvantage of the presence of small hydrocarbon peaks. The procedure described here achieves the same ion current intensity as the silica-gel technique without the hydrocarbon interference.

RESULTS

Standardization

A common cadmium standard solution of 61.47 μg Cd ml^{-1} was prepared by dissolving 0.10025 g of $CdCl_2$ in 1 l of 0.2 M HCl. Equal volumes, 100 μl each, of the cadmium spike (11.46 μg) and common cadmium solution (6.147 μg) were equilibrated in 10 ml of doubly distilled water, evaporated to dryness, and converted to CdS. The atomic $^{108}Cd/^{110}Cd$ ratio was determined at 7.086. With the atomic weight correction of 0.9818 and square root of mass ratio correction of 0.9909, the corrected ratio was 6.894, which was used to calculate the common cadmium standard solution concentration (62.19 μg ml^{-1}). The difference between the weighed and the determined cadmium concentration was 1.2%.

Procedural blank. The cadmium blank was determined by processing 12 g of 8 M HCl or 10 g of 1 M HNO_3 through the chemical and mass spectrometric procedures. The cadmium blank was 0.073 μg for HCl and 0.108 μg for HNO_3, respectively. These procedural blanks were incorporated in the Fish Solubles results.

Fish Solubles

The results for cadmium in the I.A.E.A. Fish Solubles are given in Table 1. The average cadmium concentration was 0.278 ± 0.032 ppm on a dry weight basis, ranging from 0.222 to 0.354 ppm. This range may be, in part, caused by the lack of micro-homogeneity of the specimen; heterogeneity of biological materials was reported for the lead content of tuna muscle [3]. The aliquot showing the lowest cadmium content was that ashed at 350°C. This result may be caused by the incomplete mixing of the partially ashed specimen with the spike solution; as previously mentioned, this residue contained black, charred particles. The two HNO_3-digested aliquots gave an average cadmium content of 0.240 ppm.

This work was supported by a grant from the National Science Foundation.

REFERENCES

1 L. Górski, Final Report on the Intercomposition of Trace Multielement Analysis in Fish Solubles (A-6), International Atomic Energy Agency, Report No. RL/28, Vienna, March 1975.
2 K. J. R. Rosman and J. R. De Laeter, Geochim. Cosmochim. Acta, 38 (1974) 1665.
3 T. J. Chow, C. C. Patterson and D. Settle, Nature, 251 (1974) 159.

Analytica Chimica Acta, 94 (1977) 161—168

PROTON TRANSFER IN THE LOWEST EXCITED SINGLET STATE OF 4-METHOXYACRIDINE: EXTRACTION OF KINETIC PARAMETERS FROM AN INCOMPLETE FLUORIMETRIC TITRATION CURVE

STEPHEN G. SCHULMAN* and LEONARD S. ROSENBERG

College of Pharmacy, University of Florida, Gainesville, Florida 32610 (U.S.A.)

(Received 15th March 1977)

SUMMARY

The fluorimetric pH titration curve of 4-methoxyacridine cannot be completed because of quenching of the neutral molecule above pH 14. Normalization of the points in the curve with respect to some point, corresponding to $\phi/\phi_0 < 1$, can be employed to determine the correction factor for conversion to normalization with respect to the unattainable fluorescence intensity of the neutral molecule, in the absence of excited-state proton-exchange or quenching. The excited-state dissociation constant (pK_a^*) for protonated 4-methoxyacridine, calculated from the rate constants for excited-state proton exchange determined by this approach, is in excellent agreement with the value of pK_a^* calculated from a Förster cycle.

It is well known that the variations of the relative fluorescence efficiencies of excited aromatic acids and bases, with pH, are related to the kinetics of proton-exchange in the lowest excited singlet state [1]. For example, for the reaction

$$B^* + H_2O \underset{\overleftarrow{k}}{\overrightarrow{k}} BH^{+*} + OH^- \qquad (1)$$

the relative fluorescence efficiency of B* is given by

$$\phi/\phi_0 = (1 + \overleftarrow{k}\tau_0' [OH^-])/(1 + \overrightarrow{k}\ \tau_0 + \overleftarrow{k}\ \tau_0' [OH^-]) \qquad (2)$$

and that of BH^{+*} by

$$\phi'/\phi_0' = \overrightarrow{k}\ \tau_0/(1 + \overrightarrow{k}\ \tau_0 + \overleftarrow{k}\ \tau_0' [OH^-]) \qquad (3)$$

where $\overrightarrow{k}$ and $\overleftarrow{k}$ are the rate constants for hydrolysis of B* and proton abstraction from BH^{+*} and τ_0 and τ_0' are the respective lifetimes of B* and BH^{+*}, in the absence of proton exchange [2]. If τ_0 and τ_0' can be measured, $\overrightarrow{k}$ and $\overleftarrow{k}$ can be determined from a plot of $1/[OH^-]$ vs. $\{\phi/\phi_0\}/\{(1 - \phi/\phi_0)[OH^-]\}$ which has a slope of $\overrightarrow{k}\ \tau_0$ and a vertical axis intercept of $-\overleftarrow{k}\ \tau_0'$. In most cases, however, the term $\overleftarrow{k}\ \tau_0'\ [OH^-]$, in eqns. (2) and (3) becomes vanishingly small at pH 4—10 because of the low concentration of OH^- in this

pH region. This reduces eqns. (2) and (3) to

$$(\phi/\phi_0)_{const} = 1/(1 + \vec{k}\ \tau_0) \quad (4)$$

and

$$(\phi'/\phi_0')_{const} = \vec{k}\ \tau_0/(1 + \vec{k}\ \tau_0) \quad (5)$$

In this case, $\vec{k}\ \tau_0$ can be quickly calculated, e.g.

$$\vec{k}\ \tau_0 = (1 - (\phi/\phi_0)_{const})/(\phi/\phi_0)_{const} \quad (6)$$

and $\overleftarrow{k}\ \tau_0'$ can be graphically or analytically evaluated from the portion of the fluorimetric titration where ϕ/ϕ_0 varies with pH:

$$\overleftarrow{k}\ \tau_0' = \{\phi/\phi_0(1 + \vec{k}\ \tau_0) - 1\}/\{(1 - \phi/\phi_0)[OH^-]\} \quad (7)$$

The extraction of $\vec{k}$ and $\overleftarrow{k}$ from eqns. (2) and (3), as a practical matter, depends on the fact that these equations are derived from steady-state kinetics, on the assumption that the deprotonation of $BH^{+}*$ is the only second-order process competing with deactivation of the excited molecules. However, if an extraneous second-order process, say quenching by OH^-, occurs at higher pH, it might be impossible to complete the fluorimetric titration curve and therefore, to calculate ϕ/ϕ_0 (since the region where $\phi/\phi_0 = 1$ cannot be experimentally attained) or to determine τ_0 accurately, since the fluorescence yield of B* could not be measured in the absence of a pH dependence. In this case, the determinations of $\vec{k}$ and $\overleftarrow{k}$ are somewhat more complicated than indicated by eqns. [6] and [7].

In the present work, the fluorimetric pH titration of 4-methoxyacridine, a titration which cannot be completed in alkaline solutions because of quenching (presumably by OH^-) of the fluorescence of the neutral molecule, is analyzed in order to obtain the proton-transfer rate constants $\vec{k}$ and $\overleftarrow{k}$.

EXPERIMENTAL

Chemicals and apparatus

4-Hydroxyacridine (neo-oxine; Fluka) was etherified, at ambient temperature, by dissolution, along with an equivalent amount of sodium methoxide, in dimethylsulfoxide, followed by the addition of a 20 mole-% excess of methyl iodide. The etherification is virtually quantitative in less than 1 min, as the red color of the 4-acridinolate anion is completely discharged within this time. Removal of the solvent by flash evaporation, gave a yellow residue which was recrystallized twice from absolute ethanol. The recrystallized material had a melting point and a spectrophotometrically determined pK_a in excellent agreement with the literature values for 4-methoxyacridine [3].

The instruments used have been described [4].

Procedures

Solutions of which spectra were taken, were prepared by diluting aqueous sulfuric acid or sodium hydroxide in a 10-ml volumetric flask and then delivering 100 μl of 1.00×10^{-3} M 4-methoxyacridine, in absolute ethanol, with a micropipet, to the 10-ml flask. Each solution was prepared immediately before use, to minimize decomposition errors and errors caused by change in pH of the poorly buffered solutions in the mid-pH region.

Dilute sulfuric acid and sodium hydroxide solutions were employed in preference to fairly concentrated buffer solutions, because buffer ions are known to react with excited aromatic acids and bases during the lifetime of the lowest excited singlet state [5]. This reaction often affects the mechanism and therefore, the kinetics of excited-state proton transfer. It was deemed desirable to avoid this added complication.

All solutions were purged for 5 min with dry nitrogen, before the measurement of fluorescence lifetimes, to minimize the effect of oxygen quenching which may affect the longer lifetimes.

Fluorescence, in each case, was excited at an isosbestic point in the absorption spectrum of each compound. This makes the fluorimetric titration correspond to variation of relative fluorescence efficiency with pH.

The lifetimes of the lowest excited singlet states of 4-methoxyacridine and its protonated form were measured at pH 14.0 and pH 1.0, respectively.

RESULTS AND DISCUSSION

The fluorimetric titration curve of the neutral species derived from 4-methoxyacridine is shown in Fig. 1. The absorption and fluorescence maxima and lifetimes of the lowest excited singlet state of the neutral molecule and cation are presented in Table 1. Above pH 7.3 ($pH > pK_a + 2$) the neutral molecule is essentially the only species excited. Hence the fluorescence intensity (F) at the emission maximum of the neutral molecule, is given by

$$F = 2.3\,\phi\, I_0\, \epsilon\, C_B\, l \tag{8}$$

where ϕ is the fluorescence efficiency of the neutral molecule, I_0 is the intensity of exciting radiation, ϵ is the molar absorptivity of the neutral molecule at the wavelength of excitation, C_B is the formal concentration of 4-methoxyacridine and l is the optical depth of the irradiated sample. Since I_0, ϵ, C_B and l are constant under the conditions of excitation, variations in F during the course of the fluorimetric titration must arise from variations in ϕ with pH (or $[OH^-]$). Hence, in the region where F is constant with increasing pH (i.e. where no reaction with OH^- occurs in the excited state), we may write

$$F_{const} = 2.3\,\phi_{const}\, I_0\, \epsilon\, C_B\, l \tag{9}$$

In the region near pH 13, where F increases with increasing pH, ϕ depends upon $[OH^-]$ according to eqn. (2). Theoretically, at a pH great enough that $\overleftarrow{k}\,\tau_0'\,[OH^-] \gg \vec{k}\,\tau_0$, ϕ and therefore F, should reach a maximum (ϕ_0 and

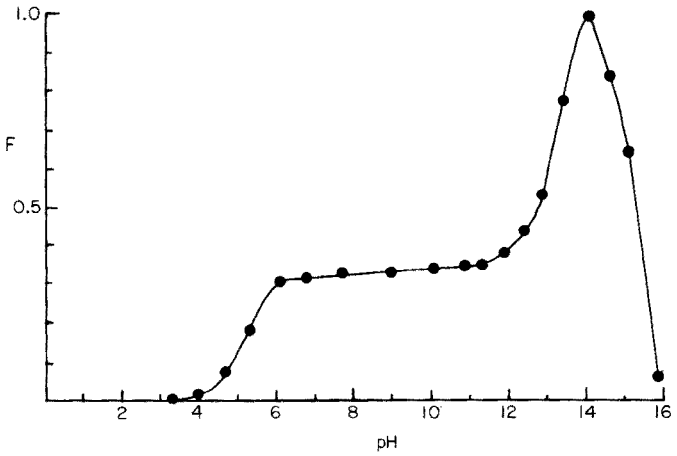

Fig. 1. Variation of the relative fluorescence intensity (F) of the neutral molecule derived from 4-methoxyacridine (1×10^{-5} M) with pH. Excitation at 364 nm, fluorescence monitored at 470 nm.

F_0) and should remain essentially constant and maximal with further increase in pH [5]:

$$F_0 = 2.3\,\phi_0\,I_0\,\epsilon\,C_B\,l \tag{10}$$

in this case

$$F/F_0 = \phi/\phi_0 \tag{11}$$

and

$$F_{const}/F_0 = \phi_{const}/\phi_0 \tag{12}$$

Moreover, the lifetime of the lowest excited singlet state of the neutral molecule, τ, is not independent of the excited-state proton-exchange, but is proportional to ϕ and has the value τ_0 only when $\phi = \phi_0$ [1].

TABLE 1

Spectral properties of 4-methoxyacridine

	Cation	Neutral molecule		Cation	Neutral molecule
$\lambda_{^1La(nm)}$	425	380	$\lambda_{f(nm)}$	552	470
$\bar{\nu}_{^1La(cm^{-1})}$	23 500	26 300	$\bar{\nu}_f(cm^{-1})$	18 100	21 300
$\epsilon_{^1La}$	3 470	5 670	τ_0(ns)	0.35[c]	20.5[a](25.0)[b]

[a]Measured by pulsed-source fluorimetry at pH 14.0.
[b]Corrected for pH dependence of fluorescence at pH 14.0.
[c]Calculated from τ_0 = 25.0 ns for neutral molecule, integrated absorption spectra of cation and neutral molecule and relative quantum efficiencies of cation and neutral molecule.

Figure 1 shows that above pH 14, the fluorescence intensity (F) of the neutral molecule which increases up to pH 14, falls with increasing pH, as a result of some, as yet undetermined, quenching process. Consequently, it cannot be assumed that the maximal fluorescence intensity at pH 14 is F_0. Nor can it be assumed that the lifetime of the lowest excited singlet state of the neutral molecule, measured at pH 14.0, is τ_0. The fluorescence of the protonated species at pH 1.0 is 91 times weaker than the fluorescence of the neutral molecule at pH 14.0. The lifetime of the excited cation (τ_0') was too short to measure with the present apparatus. Clearly, under these circumstances the titration data (Fig. 1) cannot be applied to eqns. (6) and (7), to obtain the rate constants for excited-state proton transfer in 4-methoxyacridine.

If it is assumed that at pH 14.0 the fluorescence intensity (F_n) of the neutral molecule is a function only of F_0, τ_0, τ_0' and the rates of proton-exchange in the excited state (i.e., quenching does not occur at pH 14.0), then F_n can be related to F_0 by

$$F_n = m F_0 \tag{13}$$

where m is simply a proportionality factor. If eqns. (2) and (11) are combined

$$F/F_0 = (1 + \overleftarrow{k}\,\tau_0'[OH^-])/(1 + \vec{k}\,\tau_0 + \overleftarrow{k}\,\tau_0'[OH^-]) \tag{14}$$

Substitution of F_n/m for F_0 in eqn. (14), and subsequent rearrangement, yields

$$m = F_n\,(1 + \overleftarrow{k}\,\tau_0'[OH^-])/F\,(1 + \vec{k}\,\tau_0 + \overleftarrow{k}\,\tau_0'\,[OH^-]) \tag{15}$$

Combination of eqns. (4) and (12) gives

$$F_{const}/F_0 = 1/(1 + \vec{k}\,\tau_0) \tag{16}$$

which yields, on substitution of F_n/m for F_0, and subsequent rearrangement

$$m = F_n/F_{const}\,(1 + \vec{k}\,\tau_0) \tag{17}$$

Since $[OH^-] = 1$ when $F = F_n$, it may be noted that

$$m = F_n/F_0 = (1 + \overleftarrow{k}\,\tau_0')/(1 + \vec{k}\,\tau_0 + \overleftarrow{k}\,\tau_0') \tag{18}$$

Combination of eqns. (15) and (17) gives

$$(1 + \overleftarrow{k}\,\tau_0'[OH^-])/F(1 + \vec{k}\,\tau_0 + \overleftarrow{k}\,\tau_0'[OH^-]) = 1/F_{const}(1 + \vec{k}\,\tau_0) \tag{19}$$

which is independent of F_0, F_n and m. Rearrangement of eqn. (19) leads to

$$(F - F_{const})/[OH^-] = F_{const}\,\overleftarrow{k}\,\tau_0' - F\,\overleftarrow{k}\,\tau_0'/(1 + \vec{k}\,\tau_0) \tag{20}$$

Consequently, a plot of $(F - F_{const})/[OH^-]$ vs. F should give a straight line whose slope is $-\overleftarrow{k}\,\tau_0'/(1 + \vec{k}\,\tau_0)$ and a vertical axis intercept of $F_{const}\,\overleftarrow{k}\,\tau_0'$. A plot of this type, for 4-methoxyacridine, is shown in Fig. 2. It should be noted that since eqn. (20) is independent of F_n, the determination of $\vec{k}\,\tau_0$ and $\overleftarrow{k}\,\tau_0'$ is valid even if F_n is partially determined by the quenching process, or is in error for other experimental reasons. However, the value of m, which

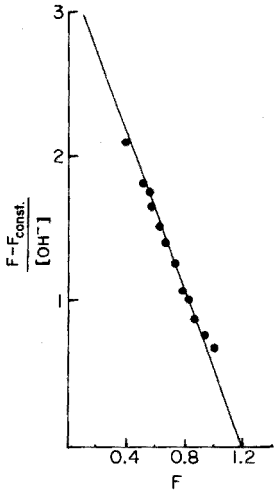

Fig. 2. Plot of $(F - F_{const})/[OH^-]$ vs. F for 4-methoxyacridine, constructed from the data represented in Fig. 1.

is a conversion factor to obtain F_0 from F_n and is necessary to calculate τ_0, will be valid only if the quenching process has not yet begun to occur at the point where F_n is taken (pH 14.0). Alternatively, F_n may be taken and the lifetime of the neutral molecule measured, at some lower pH.

Since $F_n = m\,F_0$, $\phi_n = m\,\phi_0$ and since the lifetime of the excited state is proportional to the fluorescence efficiency, $\tau_n = m\,\tau_0$, where τ_n is the lifetime of the lowest excited singlet state of 4-methoxyacridine, measured at pH 14.0. Equation (17) may be used to determine m, once $\vec{k}\,\tau_0$ is known. For 4-methoxyacridine $\vec{k}\,\tau_0 = 2.7$, $F_{const} = 0.33$ and $F_n = 1.0$ (the latter two in arbitrary units). This gives a value of 0.82 for m. At pH 14.0, τ_n was found to be 20.5 ns. Consequently, the value of 25.0 ns is assigned to τ_0. This value was checked by calculating m and determining τ_n at pH 13.0. Essentially identical results were obtained. The value of $\vec{k}$ calculated from $\vec{k}\,\tau_0$ and τ_0 is $1.1 \times 10^8 s^{-1}$.

Because τ_0' was too short to measure at pH 1.0, an estimate was made so that $\vec{k}$ could be approximated. The absolute quantum yield of fluorescence of the neutral molecule derived from 4-methoxyacridine is given by $\phi_0 = k_f\,\tau_0$, where k_f is the rate constant for fluorescence of the neutral molecule (the reciprocal of the natural lifetime of the lowest excited singlet state). The absolute quantum yield of fluorescence of the cation, in the absence of proton exchange, is given by $\phi_0' = k_f'\,\tau_0'$, where k_f' is the rate constant for fluorescence of the cation. Division of these equations and subsequent rearrangement yields

$$\tau_0' = \phi_0'\,k_f\,\tau_0/\phi_0\,k_f' \qquad (21)$$

If F_0' is the fluorescence intensity of the cation at the maximum of its fluorescence band (535 nm) and $F_0 = F_n/m$ is the fluorescence intensity that the

neutral molecule would have at its emission maximum (470 nm) if quenching did not occur at high pH, then $\phi_0'/\phi_0 = F_0'/F_0 = mF_0'/F_n$. But if F_n is taken at pH 14.0 as 1.00 and m as 0.82 and if $F_0'/F_n = 1/91$ then $\phi_0'/\phi_0 = 0.82/91 = 9.0 \times 10^{-3}$. It has been shown [6] that for a symmetrical absorption band, to a fair approximation, the rate constant for fluorescence, k_f, is given by $k_f = \bar{\nu}^2_B \epsilon_B \Delta\bar{\nu}_{B½}/3.5 \times 10^8$, where $\bar{\nu}_B$ and ϵ_B correspond to the maximum and $\Delta\nu_{B½}$ is the half-band-width of the lowest energy absorption band of the fluorescing species. Then,

$$k_f/k_f' = (\bar{\nu}_B^2 \epsilon_B \Delta\bar{\nu}_{B½})/(\bar{\nu}^2_{BH^+}\epsilon_{BH^+} \Delta\bar{\nu}_{BH^+½}) \quad (22)$$

Table 1 shows the values of $\bar{\nu}_B$, $\bar{\nu}_{BH^+}$, ϵ_B and ϵ_{BH^+} for the ^1L_a band of 4-methoxyacridine and its conjugate acid. Because of overlap of the ^1L_b bands with the short wavelength side of the ^1L_a bands in the absorption spectra of 4-methoxyacridine and its conjugate acid (Fig. 3), $\Delta\bar{\nu}_{B½}$ and $\Delta\bar{\nu}_{BH^+½}$ could not be estimated. However, if it is assumed that the ^1L_a bands are symmetrical, then the differences in $\bar{\nu}$ between the maximum and the half-maximum heights on the long wavelength sides of the respective ^1L_a bands should be equal to ½ $\Delta\bar{\nu}_{B½}$ and ½ $\Delta\bar{\nu}_{BH^+½}$ and the factor of ½ should cancel out in their ratio, in eqn. (22). Thus, $\Delta\bar{\nu}_{B½}/\Delta\bar{\nu}_{BH^+½} = 0.16 \times 10^4 cm^{-1}/0.21 \times 10^4 cm^{-1} = 0.76$. From this value and the data of Table 1, $k_f/k_f' = 1.55$. Finally, substitution of $k_f/k_f' = 1.55$, $\phi_0'/\phi_0 = 9.0 \times 10^{-3}$ and $\tau_0 = 2.5 \times 10^{-8}$ s into eqn. (23) gives $\tau_0' = 3.5 \times 10^{-10}$ s. Since $\overleftarrow{k}\ \tau_0' = 9.5\ M^{-1}$, then $\overleftarrow{k} = 2.7 \times 10^{10}\ M^{-1}\ s^{-1}$, which is characteristic of a diffusion-limited second-order process [7].

The ratio of $\overrightarrow{k}$ to $\overleftarrow{k}$ is the equilibrium constant of the excited-state hydrolysis (K_B^*) depicted in eqn. (1). For 4-methoxyacridine, $K_b^* = 4.0 \times 10^{-3}$. As the ion-product of water is 1.00×10^{-14}, then $K_a^* = 2.5 \times 10^{-12}$ or $pK_a^* = 11.60$.

It is well known that pK_a^* can also be calculated from the shifts of the absorption and fluorescence spectral maxima, accompanying protonation or dissociation and the pK_a of the corresponding ground-state equilibria [8]. For 4-methoxyacridine, $pK_a = 5.3$. In this approach, $pK_a - pK_a^* = 0.625\ (\bar{\nu}_C - \bar{\nu}_N)/T$, where T is the absolute temperature (298 K) and $\bar{\nu}_a$ and $\bar{\nu}_b$ are,

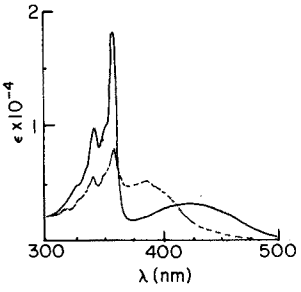

Fig. 3. Near ultraviolet and visible absorption spectra of 1×10^{-5} M 4-methoxyacridine (------) and its conjugate acid (——).

in this case, the wavenumbers of the arithmetic averages of the maxima of the ^1L_a absorption and fluorescence bands of the cation and neutral molecule respectively. From the data in Table 1, $\bar{\nu}_C = 20\ 800\ cm^{-1}$, $\bar{\nu}_N = 23\ 800\ cm^{-1}$ and $pK_a^* = 11.6$, in excellent agreement with the value of pK_a^* calculated from the rate constants for proton transfer. Hence, unless the errors involved in estimating $\vec{k}$ and $\overleftarrow{k}$ are great but cancel each other fortuitously in the calculation of pK_a^*, the procedure used to estimate $\vec{k}\tau_0$ and $\overleftarrow{k}\ \tau_0'$, in this case, is a reasonable means of obtaining kinetic information from incomplete fluorimetric pH titration curves.

REFERENCES

1 A. Weller, Prog. React. Kinet., 1 (1961) 187.
2 A. Weller, Z. Elektrochem., 61 (1957) 956.
3 A. Albert, J. Chem. Soc., (1965) 4653.
4 S. G. Schulman and R. J. Sturgeon, Anal. Chim. Acta, 00 (1977) 000.
5 S. G. Schulman and A. C. Capomacchia, J. Phys. Chem., 79 (1975) 1337.
6 T. Förster, Fluorezeng Organischer Verbindungen, Gottingen: Vandenhoech and Ruprech, 1951.
7 M. V. Smoluchowski, Z. Phys. Chem., 92 (1917) 129.
8 T. Förster, Z. Phys. Chem. N.F., 54 (1950) 42.

Analytica Chimica Acta, 94 (1977) 169—174

EXTRACTION—SPECTROPHOTOMETRIC DETERMINATION OF TRACES OF ANTIMONY AS THE FERROIN—HEXACHLORO-ANTIMONATE(V) COMPLEX

G. GOPALA RAO and S. G. VISWANATH

Department of Chemistry, Andhra University, Waltair (India)

(Received 10th May 1977)

SUMMARY

The sparingly soluble scarlet precipitate formed by the interaction of ferroin and antimony(V) in strong hydrochloric acid medium is soluble in nitrobenzene. The composition of the complex is $[Fe(phen)_3]\,[SbCl_6]_2$. The percentage extraction into nitrobenzene, determined by tracer techniques, reaches a maximum (98%) at 8—9 M hydrochloric acid. The advantages of this procedure over those employing dyes as reagents are discussed. Antimony(V) can be determined in the range 2.5—24 $\mu g\,ml^{-1}$. Interferences are described.

The determination of small amounts of antimony is often required in geochemical prospecting, in the analysis of alloys, such as phosphor bronze, cartridge brass, etc., and of biological materials. The spectrophotometric methods available are usually based on complex formation between hexachloroantimonate(V) and a large dye cation, the complex being extracted into an organic solvent for the absorbance measurement. The xanthone dye, rhodamine B [1], has been frequently used [2]. Methyl violet [3] and other triphenylmethane dyes [2] have also been studied. Unfortunately, the commercial dyes employed are often impure or of uncertain composition; for example, Brilliant green may contain at least three components [4].

The tris(1,10-phenanthroline)—iron(II) complex (ferroin) forms a scarlet precipitate with antimony(V) in hydrochloric acid medium [5]. This paper reports the development of a reliable and precise spectrophotometric determination of antimony in the range 2.5—24 $\mu g\,ml^{-1}$. The ferroin—hexachloroantimonate(V) complex is sparingly soluble in water, but readily soluble in nitrobenzene. Ferroin is easily obtained in a pure state; another important advantage of ferroin is that only a small excess of the reagent is needed to ensure complete extraction of antimony(V), whereas the dye reagents often require very large excesses.

EXPERIMENTAL

Apparatus and reagents

A Hilger Uvispek Spectrophotometer was used with matched 1-cm cells.

Ferroin sulphate solution (0.01 M) was prepared; this solution was diluted to 10^{-3} M as required.

Antimony(V) solution (0.01 M), was prepared by dissolving potassium hexapyroantimonate in 250 ml of 10 M hydrochloric acid. It was standardized by reduction with sodium sulphite [6] after the addition of sulphuric acid to prevent volatilization of antimony(V), and finally titrating antimony(III) as described previously [5]. The stock antimony(V) solution was diluted with 10 M hydrochloric acid as required.

All chemicals used were of analytical grade, where possible.

Recommended procedure

Accurately measure an aliquot (1 ml) containing 25—240 μg of antimony(V) into a 50-ml separating funnel, and add 7 ml of 10 M hydrochloric acid, 1 ml of water and 1.00 ml of 10^{-3} M ferroin solution. Immediately add 3 ml of nitrobenzene, shake for 10—20 s and remove the organic layer into another 50-ml separating funnel containing 10 ml of distilled water. Repeat the extraction with 3 ml of nitrobenzene, transfer this extract to the second funnel and shake for 20 s. Remove most of the upper aqueous phase by gentle suction. Wash the organic extract similarly with another two 10-ml portions of water. Dry the nitrobenzene extract with 1 g of anhydrous sodium sulphate, transfer it to a 10-ml volumetric flask, washing the sodium sulphate with two 1-ml portions of nitrobenzene, and dilute to 10 ml with nitrobenzene. Measure the absorbance of the extract against a nitrobenzene blank at 510 nm.

RESULTS AND DISCUSSION

Figure 1 presents the absorption curve spectrum, showing the variation of molar absorptivity (ϵ) with wavelength. The absorption spectrum of ferroin in water is also presented. The wavelengths of the absorption maxima of ferroin and the ferroin—antimony(V) complex are about the same, 510 nm. The molar absorptivity of ferroin in water is 11 000 l mol^{-1} cm^{-1} at 510 nm, while that of the ferroin—antimony(V) complex in nitrobenzene is 10 700 l mol^{-1} cm^{-1}. The differences in the spectra appear to indicate complex formation.

Optimum conditions for extraction and measurement

Two extractions with 3 ml of nitrobenzene suffice to remove all the antimony, with shaking times of about 15—20 s. The colour of the unwashed nitrobenzene extract fades rapidly, becoming almost colourless in about 35 min. The stability of the absorbance improves with the number of washes of the extract; after three washes with water, the absorbance remains stable for 90 min.

The effect of the concentration of hydrochloric acid was studied over the range 4—10 M. The molar absorptivities of the extracts at 510 nm were

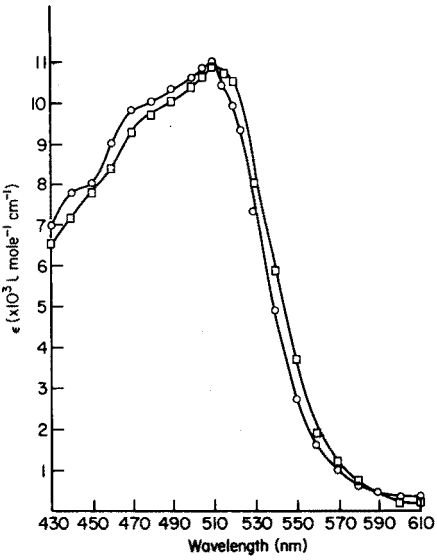

Fig. 1. Absorption spectra of the ferroin—antimony(V) complex in nitrobenzene (□) and of ferroin in water (○). The recommended procedure was used with 1.00 ml of 10^{-3} M Sb(V) solution.

7700, 9200, 10 600 and 10 700 l mol^{-1} cm^{-1} for 4, 6, 8 and 10 M HCl, respectively. Since the values for 8 and 10 M HCl were almost constant, all subsequent extractions were done from 9 HCl media.

To ascertain how large an excess of ferroin was necessary, a mole ratio plot was prepared (Fig. 2). The absorbance of the nitrobenzene extracts increased with increasing concentration of ferroin in the aqueous phase and reached a limiting value when the concentration of ferroin was 50% that of antimony(V), i.e., the stoichiometric amount required for a 2 :1 complex between antimony and ferroin. When the concentration of ferroin in the aqueous phase exceeds this ratio, ferroin remains in the aqueous phase; only the complex is extracted with nitrobenzene. Approximately double the stoichiometric amount of ferroin was used in further tests.

Composition of the complex

Job's method of continuous variations as modified by Vosburgh and Cooper [7] was used. Different volumes of equimolar solutions of ferroin and antimony(V) were mixed (total volume, 10 ml) and extracted with nitrobenzene as in the recommended procedure. Figure 3 shows that a 1:2 complex is formed between ferroin and antimony; the curves indicate that only one complex is formed and that it is quite stable.

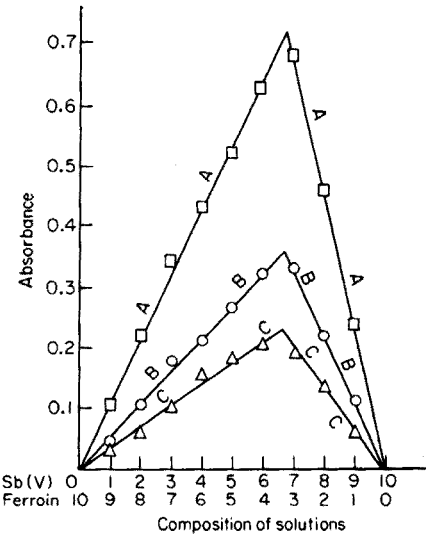

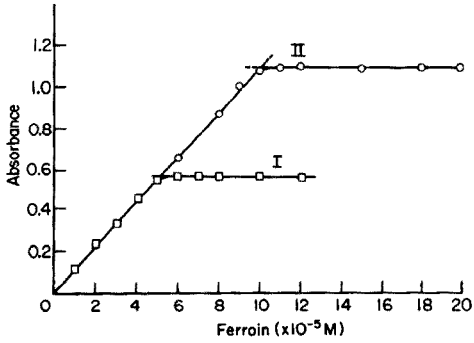

Fig. 2. Mole ratio plot. Curve I, (Sb) = 10^{-4} M. Curve II, (Sb) = 2×10^{-4} M.

Fig. 3. Continuous variations study at 510 nm. Curve A, [ferroin] = [Sb(V)] = 2×10^{-4} M. Curve B, [ferroin] = [Sb(V)] = 10^{-4} M. Curve C, [ferroin] = [Sb(V)] = 5×10^{-5} M.

Calibration curve

For the calibration curve, 0.10—2.00 ml aliquots of 10^{-3} M antimony(V) solution were treated as in the recommended procedure. Beer's law was obeyed at least over the range 2×10^{-5}—2×10^{-4} M, which corresponds to the range 2.5—24 μg Sb ml^{-1}. Numerous tests showed that the maximum relative error was 2% for the range 12—24 μg Sb ml^{-1} and 4% for amounts below 12 μg Sb ml^{-1}.

Interferences

The effects of diverse ions were investigated by adding each ion to the aqueous solution before extraction. In the determination of 12μg of antimony(V), copper(II) did not interfere up to 300 μg, or lead(II) up to 4000 μg. Arsenic(V) did not interfere up to 3 μg, but more arsenic decreased the absorbance. Tin(IV) (6 μg) could be tolerated, but even 0.2 μg of iron(III) interfered seriously. Acetate (8 μg as sodium acetate) and thiocyanate (2 μg as potassium thiocyanate) did not interfere. In all these cases, larger amounts of these ions decreased the absorbance.

Choice of the organic solvent and extraction efficiency

Various water-immiscible organic solvents were tested. Benzene, toluene, xylene and chloroform did not extract the complex, and diethyl ether extracted it only slightly. n-Amyl alcohol, isoamyl alcohol, n-butanol and iso-butanol are miscible with strong hydrochloric acid solutions. Only nitrobenzene proved to be a satisfactory extractant.

Since only the complex is extracted by nitrobenzene, the extraction efficiency was calculated by comparing the observed absorbances of the nitrobenzene extracts with the theoretical value. The percentage extraction was found to be 87% for a single extraction and 98% for a double extraction; triple extraction did not improve matters. This was checked by isotopic dilution with ^{125}Sb.

The radioactive reagent was prepared by mixing 50 ml of 10^{-3} M Sb(V) in 10 M hydrochloric acid with 0.15 ml of carrier-free ^{125}Sb tracer ($t_{1/4}$, 2.0 y; Bhabha Atomic Research Centre, Trombay, Bombay). This solution (1 ml; 3.4 mCi) was mixed in a separating funnel with varying quantities of 11 M hydrochloric acid, to give a final acidity of 4, 6, 8 or 10 M on dilution to 10 ml. Then 1 ml of 10^{-3} M ferroin was added, the solution was extracted with two 3-ml portions of nitrobenzene, and the extracts were washed with water as described above. The extracts were mixed, treated with anhydrous sodium sulphate, and diluted to 10 ml. The aqueous phase (ca. 10 ml) was also preserved. The activities of the nitrobenzene and aqueous phases were determined by γ-counting with a 1.5 × 1.5-in. NaI (Tl) crystal and a scintillation counter (Harshaw Ltd.). Each sample was counted for 1 min and the average of two counts taken. Corrections were made for background activity, but not for decay because of the long half-life of the radio-isotope. The percentage extractions from 4, 6, 8 and 10 M HCl media were 65.8, 89.2, 98.0 and 98.1%, respectively. The results obtained by the spectrophotometric and tracer procedures are in good agreement. The increase in extraction with increased acidity is undoubtedly due to an increase in the concentration of $SbCl_6^-$ ions; these are extracted with ferroin whereas hydrolysed species such as $Sb(OH)Cl_5^-$, which exist in less acidic solutions, are not.

Conclusions

It is well known that the ferroin cation forms ion-association complexes with various anions such as perchlorate, iodide, azide, thiocyanate, etc., which can be determined by extraction—photometric procedures. Ferroin also forms sparingly soluble complexes with complex metal anions, such as tetrachlorogold(III) [8], tetrabromogold(III) [9], tetracyanonickelate(II) [10], tetraiodomercuriate(II) [11], and trisoxalatotin(IV) [12], which can be extracted and determined spectrophotometrically. The ion-association complex of ferroin with hexachloroantimonate(V) does not seem to have been reported previously. Under suitable conditions, the extracted complex has the composition, $[Fe(phen)_3]\,[SbCl_6]_2$. Kuznetsov [3] was the first to suggest that an ion-association complex is formed between $SbCl_6^-$ and the methyl violet cation, and similar complexes are formed with numerous cationic dyes.

Many commercial dyes are not only inhomogeneous but impure. Ferroin is greatly superior in this respect, because it is readily obtainable pure. Another difficulty experienced with dyes such as rhodamine B [13] is that their solutions in hydrochloric acid may contain several cations (RH^+, RH_2^{2+}, and RH_2Cl^+) each of which can form insoluble benzene-extractable products.

Although the chief product in 6 M hydrochloric acid is the violet salt $RHSbCl_6$, small amounts of the orange $RH_2(SbCl_6)_2$ and $RH_2ClSbCl_6$ salts are also formed. Further problems may also arise from the extraction of the colourless lactone form of the dye, which slowly becomes coloured on standing, and from the instability of dye solutions. The proposed ferroin method does not suffer from these drawbacks, and the sensitivity, indicated by the molar absorptivity of 10 700 l mol^{-1} cm^{-1}, is adequate for many purposes.

The authors are very grateful to Prof. V. Lakshminarayana, D.Sc., F.Inst.P (Lond), Head of the Department of Nuclear Physics, for providing facilities for the isotope tracer work, and to M. M. Sreenivasa Rao, M.Sc., Research Fellow, for assistance with the nuclear instrumentation.

REFERENCES

1 W. G. Fredrick, Ind. Eng. Chem., Anal. Ed., 13 (1941) 922.
2 See, e.g., Z. Marczenko, Spectrophotometric Determination of Elements, Horwood-Wiley, Chichester, 1976.
3 V. I. Kuznetsov, Zh. Anal. Khim., 2 (1947) 179.
4 R. W. Burke and O. Menis, Anal. Chem., 38 (1966) 1719.
5 G. Gopala Rao and S. G. Viswanath, Anal. Chim. Acta, in press.
6 I. M. Kolthoff and R. Belcher, Volumetric Analysis, Vol. III Interscience, New York, 1957, p. 127 and p. 74.
7 W. C. Vosburgh and G. R. Cooper, J. Am. Chem. Soc., 63 (1967) 1176.
8 Y. Yamamoto, M. Tsubouchi and I. Okimura, Bunseki Kagaku, 16 (1967) 1176.
9 E. G. Nasouri, S. A. Shahine and R. J. Magee, Anal. Chim. Acta, 36 (1966) 346.
10 Y. Yamamoto, T. Kumamaru, Y. Hayashi, S. Mirua and S. Kimura, Nippon Kagakuzasshi, 92 (1971) 64.
11 K. Kotsuji, Bull. Chem. Soc. Jpn., 38 (1965) 402.
12 K. Hiiro, T. Tanaka, T. Shirai and Y. Yamamoto, Osaka Kogyo Gijitsu Shikensho Kihō, 20 (1969) 223; Bunseki Kagaku, 18 (1969) 563.
13 R. W. Ramette and E. B. Sandell, Anal. Chim. Acta, 13 (1955) 455.

Analytica Chimica Acta, 94 (1977) 175—180

SPECTROPHOTOMETRIC DETERMINATION OF BORON IN COBALT AND NICKEL COATINGS BY MEANS OF CARMINIC ACID

GEORGE NORWITZ* and HERMAN GORDON**

Frankford Arsenal, Philadelphia, PA 19137 (U.S.A.)

(Received 4th April 1977)

SUMMARY

A method is proposed for the determination of boron in cobalt and nickel coatings deposited from borane-type baths. The deposit is dissolved in hydrochloric acid in the presence of platinum chloride as catalyst, potassium chloride and mannitol are added, and the solution is evaporated to dryness. Boron is then distilled as methyl borate into sodium hydroxide solution, the distillate is evaporated to dryness, and the boron is determined spectrophotometrically with carminic acid. The mannitol prevents volatilization of boron during the evaporation. Evaporating the hydrochloric acid solution to dryness eliminates excess of acid and water, both of which cause incomplete recovery of boron in the distillation. The potassium, cobalt, and nickel chlorides left after the evaporation dissolve in the hot methanol during the distillation and do not interfere.

The problem of determining boron in cobalt and nickel coatings is important because of the growing use of cobalt and nickel coatings deposited from borane-type baths. Some borane-type baths [1—3] tend to give a coating containing several percent boron and the boron content of the coating can be calculated with reasonable accuracy by difference; other borane-type baths [3—9] tend to give a coating with a lower boron content and the calculation of the boron by difference is subject to large errors.

In this paper, a spectrophotometric method is proposed for the determination of boron in cobalt and nickel coatings. The sample is dissolved in hydrochloric acid in the presence of platinum chloride as a catalyst [10], potassium chloride and mannitol are added, and the solution is evaporated to dryness. Methanol is added, the boron is distilled as methyl borate into sodium hydroxide solution, the distillate is evaporated to dryness, and the boron is determined with carminic acid. Feldman [11], in a comprehensive study of the volatility of boron from solutions, has shown that mannitol prevents loss of boron when hydrochloric acid solutions containing boron are evaporated to dryness. Many investigators have used carminic acid for the spectrophotometric determination of boron in various materials [12—19].

*Present address, 2123 Hoffnagle Street, Philadelphia, PA 19152.
**Present address, 8022 Langdon Street, Philadelphia, PA 19152.

EXPERIMENTAL

Apparatus and reagents

The distillation apparatus consists of a 1500-ml beaker placed on a wire gauze over a flame. The reaction vessel (300-ml Erlenmeyer flask; Corning 7280 glass) is placed diagonally in the beaker and connected via a right-angled borosilicate glass tube with 24/40 ground-glass joints (Fisher Scientific, Cat. No. 15-322-2) to a Liebig condenser (borosilicate glass with 24/40 ground-glass joints and a 40-cm long jacket). The end of the condenser is connected via a borosilicate glass adapter and Tygon tubing to a hard plastic tube (20-cm long from a plastic wash bottle). This tube reaches diagonally to the corner of the collection vessel, which is a 250-ml beaker (Corning 7280 glass).

All chemicals used were of reagent grade.

Standard boron solutions. To prepare the stock standard (1 ml = 0.2 mg B), dissolve 0.5721 g of boric acid (reagent grade) in water and dilute to 500 ml in a volumetric flask. Prepare the working solution (1 ml = 0.02 mg B) weekly by suitable dilution.

Carminic acid solution (0.1%). Dissolve 0.500 g of carminic acid (Eastman Kodak) in 500 ml of 96% sulfuric acid.

The boron solutions should be stored in polyethylene bottles. The sodium hydroxide, carminic acid, potassium chloride, and mannitol solutions should be prepared and stored in polyethylene bottles.

Preparation of calibration curve

Transfer 1.0, 2.0, 3.0, and 4.0 ml of standard boron solution (1 ml = 0.02 mg B) to 300-ml Erlenmeyer flasks (Corning 7280 glass). Carry along a reagent blank. Add 10 ml of water, 10 ml of concentrated hydrochloric acid, 5 ml of potassium chloride solution (10%), and 10 ml of mannitol solution (10%). Move the flasks to the edge of the hot plate away from direct heat and heat until only one or two drops of liquid remain or until the salts are just dry (do not bake since this will cause the salts to be difficultly soluble). Allow to cool to room temperature. Insert stoppers (borosilicate glass), add 100 ml of methanol, and allow to stand for 1 h while swirling frequently. At the end of this time, scrape the salts from the bottom of the flasks with a steel spoon spatula, break up the salts with the spatula, and insert the stoppers.

Add 20 ml of water and 3 ml of sodium hydroxide solution (5%) (measured with a 10-ml polypropylene graduated cylinder) to a 250-ml beaker (Corning 7280 glass). Place the beaker under the exit tube of the distillation apparatus so that the tube reaches to the corner of the beaker. Attach the Erlenmeyer flask containing the methanol to the connecting tube and place the 1500-ml beaker under the flask so that the bottom of the flask is about 5 cm from the bottom of the beaker. Add tap water until the volume of water in the 1500-ml beaker is about 5 cm from the top. Place a burner under the 1500-ml beaker and heat the water to boiling; then turn down the flame so

that the water boils moderately and continue heating until dry salts remain (total heating time ca. 15 min). Lower the 250-ml beaker and wash down the exit tube with a little water. Place the beaker on a steam bath or an electric hot plate (at low heat) and evaporate just to dryness. Remove from the hot plate and allow to cool (do not cover). Add ca. 35 ml of sulfuric acid (96%) and swirl to dissolve the salts. Add 10 ml of carminic acid solution (0.1%) from a buret and swirl. Dilute with sulfuric acid to 50 ml in a polypropylene graduated cylinder (tall form) and then pour the solution back in the beaker. Cover with a watch glass. Allow to stand for 90 min and measure the absorbance at 610 nm against the reagent blank. Plot absorbance against mg of boron (per 50 ml).

Procedure

Weigh the specimen (preferably 2—2.5 cm^2 in area) and calculate the weight of the coating by deducting the original weight of the base metal. Transfer the specimen (squeezing it if necessary) to a 300-ml Erlenmeyer flask (Corning 7280 glass). Add 10 ml of hydrochloric acid and 1 drop of platinum chloride solution (5%; Fisher Scientific, Cat. No. So-P-118). Heat under reflux (air condenser; Corning 7280 glass) until the coating has dissolved. If the base metal is copper, the heating need be conducted only until the bright copper surface appears (although complete dissolution of the copper will do no harm). Add 2 ml of hydrogen peroxide (30%) and heat under reflux for 20 min to destroy peroxide. Wash down the interior of the condenser with a little water and detach the flask. Cool, dilute to 500-ml in a volumetric flask, and transfer the solution to a polyethylene bottle. Pipet a 5-ml aliquot (or an aliquot preferably containing 0.03—0.07 mg of boron) into a 300-ml Erlenmeyer flask (Corning 7280 glass). Add 5 ml of potassium chloride solution (10%) and 10 ml of mannitol solution (10%), evaporate to dryness, distil, and develop the color as described for the preparation of calibration curve. Determine the mg of boron by referring to the calibration curve and calculate the percent boron in the coating in the usual way.

DISCUSSION AND RESULTS

The advantage of evaporating the hydrochloric acid solution of the sample to dryness is that such a treatment eliminates excess of acid and water. Luke [20] has shown (with sulfuric acid solution) that the presence of excess acid and water causes incomplete recovery of boron in the distillation.

The potassium chloride serves the purpose of complexing the boron (as potassium borate) and making the cobalt and nickel chlorides more readily soluble after the evaporation to dryness. Potassium chloride is not readily soluble in methanol at room temperature but it dissolves when the methanol is heated close to its boiling point. Sodium chloride is far less soluble in methanol than potassium chloride and cannot be substituted for potassium chloride.

Sulfuric acid cannot be used in place of hydrochloric acid because it is not possible to evaporate off the sulfuric acid without loss of boron and because the mannitol would be destroyed by the hot sulfuric acid. Also, cobalt and nickel coatings do not readily dissolve in sulfuric acid, and cobalt and nickel sulfates are insoluble in methanol. Phosphoric acid cannot be used in place of hydrochloric acid because phosphoric acid cannot be volatilized and because cobalt and nickel coatings do not readily dissolve in phosphoric acid. Also, cobalt and nickel phosphates are insoluble in methanol. Nitric acid cannot be used in place of hydrochloric acid because the mannitol would be destroyed by the hot nitric acid and because residual nitrate (that would be distilled) would interfere with the development of the boron—carminic acid color.

The Erlenmeyer flask and condenser used in the dissolution of the sample must be made of Corning 7280 glass; the high temperature and acidity cause high results if borosilicate glassware is used. The beaker used for the evaporation of the alkaline solution after the distillation must also be made of Corning 7280 glass. Because of the low acidity and relatively low temperature encountered during the distillation (the boiling point of methanol is about 65°C), no significant amount of boron is picked up from the connecting tube, condenser, or adapter, all of which are made of borosilicate glass.

It is recommended that the color be developed in beakers made of Corning 7280 glass. However, previous investigators have demonstrated that borosilicate glassware (volumetric flasks) can be used for this purpose, after rinsing with sulfuric acid [18, 21].

An air condenser was used in dissolving the coatings. It was not necessary to attach a jacket (borosilicate glass) to this condenser although such a jacket is available (Corning Catalogue No. 2240, 400 mm). An alternative method of dissolving the coating, found to be as satisfactory as an air condenser, was to cover the Erlenmeyer flask with a 250-ml beaker (Corning 7280 glass) and then heat the beaker gently at the edge of the hot plate. Cobalt, nickel, and platinum salts are catalysts for the destruction of hydrogen peroxide, so vigorous boiling is not necessary.

The platinum chloride is essential for the dissolution of nickel coatings and less essential (but still recommended) for the dissolution of cobalt coatings.

The maximum amount of cobalt or nickel that can be handled in the distillation is about 0.5 g. The presence of larger amounts can cause bumping.

No residue was ever obtained on dissolution of the cobalt and nickel coatings in hydrochloric acid. This indicated that all the boron in the coatings was acid-soluble (as would be expected).

The concentration of carminic acid used for the development of the color (0.2 mg ml^{-1}) is approximately that used by several investigators [15—17]. The absorbance measurements are made at 610 nm [15, 17].

The recoveries obtained on adding the working standard boron solution to reagent-grade cobalt and nickel metal (0.5 g) and carrying the samples through the procedure with the metal sample as a blank are shown in Table 1. The

TABLE 1

Recovery of boron added to pure cobalt and nickel

Sample	B added (mg)	B found (mg)	Sample	B added (mg)	B found (mg)
0.5 g Co	0.020	0.021	0.5 g Ni	0.020	0.018
0.5 g Co	0.040	0.043	0.5 g Ni	0.040	0.040
0.5 g Co	0.060	0.068	0.5 g Ni	0.060	0.057
0.5 g Co	0.080	0.081	0.5 g Ni	0.080	0.077

TABLE 2

Results for boron in actual deposits of cobalt and nickel

Type of coating	Weight of entire specimen (g)	Weight of deposit (g)	B found (%)[a]
Co	1.4861	0.7043	0.54; 0.52
Co	2.7230	0.9318	0.59; 0.59
Co	2.8392	1.3526	0.18; 0.17
Ni	1.6937	0.8027	0.56; 0.57

[a]The results represent duplicate aliquots.

boron (acid-soluble) contents found in the reagent-grade cobalt and nickel samples (by means of the regular reagent blank) were 0.0002% and 0.0019%, respectively. The results obtained for boron are shown in Table 2.

The method is probably applicable to other materials but this was not investigated.

This work was conducted under an Army Materials Technology Program (AMS Code 53970M6350).

REFERENCES

1 K. Lang, Electroplating and Metal Finishing, 19 (1966) 86.
2 H. Narcus, Plating, 54 (1967) 380.
3 G. O. Mallory, Plating, 58 (1971) 319.
4 E. Groshart, Metal Finishing, 70, No. 4 (1972) 35.
5 T. Berzins (to E. I. du Pont de Nemours and Co.), U.S. Patent 3, 338, 726, Aug. 29, 1967.
6 F. Pearlstein and R. F. Weightman, Frankford Arsenal Report FA-TA-74031, Nov. 1974.
7 F. Pearlstein and R. F. Weightman, Frankford Arsenal Report FA-TA-74032, Nov. 1974.
8 F. Pearlstein and R. F. Weightman, U.S. Patent 3,578,468, May 11, 1971.
9 F. Pearlstein and R. F. Weightman, U.S. Patent 3,917,464, Nov. 4, 1975.
10 C. L. Luke, Anal. Chem., 30 (1958) 1405.
11 C. Feldman, Anal. Chem., 33 (1961) 1916.
12 D. F. Boltz, Colorimetric Determination of Nonmetals, Interscience, New York, 1958, p. 339.
13 J. T. Hatcher and L. V. Wilcox, Anal. Chem., 22 (1950) 567

14 W. C. Smith, A. J. Goudie, and J. N. Sivertson, Anal. Chem., 27 (1955) 295.
15 H. Kawaguchi, Jpn. Anal., 4 (1955) 307.
16 R. C. Calkins and V. A. Stenger, Anal. Chem., 28 (1956) 399.
17 D. L. Callicoat and J. D. Wolszon, Anal. Chem., 31 (1959) 1434.
18 H. K. L. Gupta and D. F. Boltz, Mikrochim. Acta, 3 (1974) 415.
19 Am. Public Health Assoc., Standard Methods for the Examination of Water and Waste Water, 13th edn, Washington, DC, 1971, p. 72.
20 C. L. Luke, Anal. Chem., 27 (1959) 1150.
21 ASTM, 1975 Annual Book of ASTM Standards, Part 12, Chemical Analysis of Metals; Sampling and Analysis of Metal Bearing Ores, Designation E 34—72, Philadelphia, PA.

Analytica Chimica Acta, 94 (1977) 181—186

Short Communication

THE USE OF A SLOTTED QUARTZ TUBE FOR THE DETERMINATION OF ARSENIC, ANTIMONY, SELENIUM AND MERCURY

R. J. WATLING

Applied Spectroscopy Division, National Physical Research Laboratory, Council for Scientific and Industrial Research, P.O. Box 395, Pretoria (South Africa)

(Received 16th March 1977)

The introduction of air—hydrogen flames and argon— or nitrogen—hydrogen flames (entrained air as the oxidant gas) into atomic absorption spectrometry significantly lowered analytical limits for such elements as selenium and arsenic [1, 2]. With these flames, however, there may be interference problems and the inconvenience of gas bottles additional to those used normally in routine laboratories. The hydride-generation techniques [3, 4], in which volatile metal hydrides are introduced direct into the flame, also suffer disadvantages such as chemical interferences and prolonged analysis time.

The application of a slotted quartz tube (s.q.t.) to the determination of ten elements has recently been described [5]; a significant increase in analytical sensitivity and precision was achieved for elements such as lead, zinc, cadmium, cobalt, silver and manganese by using an s.q.t. in conjunction with flame atomization and atomic absorption analysis. The results indicated [5] that the more volatile elements, such as zinc, cadmium and lead, were better suited to analysis with the s.q.t., than those with higher boiling points.

This communication describes the application of the s.q.t. to the determination of arsenic, antimony, selenium and mercury. The s.q.t. is used in conjunction with air—acetylene, air—hydrogen and argon (entrained air)—hydrogen flames, and the results are compared with those obtained by direct nebulization.

Experimental

Composite standards of arsenic, selenium, antimony and mercury were prepared in 10% nitric acid in the range 0.1—100 $\mu g\ ml^{-1}$. The resonance lines of the elements were used, viz. arsenic 193.7 nm, antimony 217.6 nm, selenium 196.0 nm and mercury 253.7 nm. The element concerned was determined with each of three flames; air—acetylene (F1), air—hydrogen (F2) and argon (entrained air)—hydrogen (F3), both with and without the s.q.t. (T1—T3). Flame conditions were optimized in every case. A Varian-Techtron AA6 atomic absorption spectrometer and BC6 hydrogen background corrector were used, and results were recorded on an Hitachi flatbed recorder.

Results and discussion

Sensitivity. The characteristic concentrations [6] (concentration giving 0.004 absorbance) obtained by direct nebulization of the four elements under the conditions of these experiments are compared with those determined with the s.q.t. (Table 1). The calibration curves obtained by spraying direct into each flame (F1—F3) and into the s.q.t. (T1—T3) are plotted in Fig. 1.

At low arsenic concentrations, both the air—hydrogen flame (F2) and the argon (entrained air)—hydrogen flame (F3) give better sensitivity than the air—acetylene flame (F1). When the s.q.t. is used, the air—acetylene (T1) and air—hydrogen (T2) flames both result in greatly increased absorbance signals in comparison with those obtained for all three flames in the absence of the s.q.t. A decrease in the absorbance signal is observed for arsenic when the s.q.t. is used in conjunction with an argon (entrained air)—hydrogen flame. This is probably because the low temperature of the flame maintains fewer neutral atoms inside the tube.

The air—hydrogen flame (F2) gives optimum readings for the determination of antimony by direct nebulization. The greatest increase in absorbance signal values is observed when the s.q.t. is used in conjunction with an air—acetylene flame (T1). A similar result is obtained for selenium where, for the direct flame method, the highest sensitivity is observed when the solution is nebulized into either the air—hydrogen (F2) or argon (entrained air)—hydrogen (F3) flame. The greatest increase in absorbance signal value is obtained however when the s.q.t. is used in conjunction with an air—acetylene flame (T1).

The argon (entrained air)—hydrogen flame (F3) appears to be slightly better than the air—acetylene and the air—hydrogen flames for the determination of mercury by direct nebulization. A threefold increase in absorbance signal is observed for each of the flames when the s.q.t. is used; the optimum flame is the argon (entrained air)—hydrogen flame (F3).

Precision. Improved analytical precision was achieved with the s.q.t. The results obtained with the air—acetylene and air—hydrogen flames are shown in Figs. 2 and 3. Results for argon (entrained air)—hydrogen are given only for mercury because this flame was the least sensitive for the other elements.

TABLE 1

Characteristic concentrations ($\mu g\ ml^{-1}$) obtained with (1) the flame direct and (2) the slotted quartz tube

Element	(1) Flame			(2) S.q.t.		
	F1	F2	F3	T1	T2	T3
As	2.0	0.8	0.8	0.2	0.2	2.0
Sb	0.5	0.5	0.5	0.1	0.2	0.3
Se	0.5	0.4	0.5	0.1	0.1	0.5
Hg	4.0	5.0	3.0	1.0	1.0	0.8

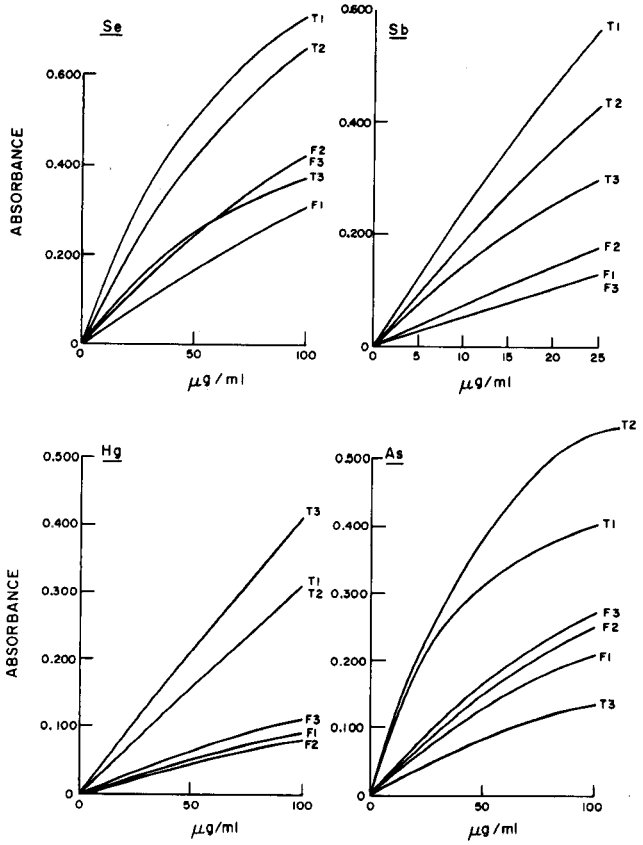

Fig. 1. Absorbance-signal enhancement with the s.q.t.

Precision data at concentrations near the characteristic concentrations of the four elements are summarized in Table 2. In all cases there is an improvement in precision at low concentrations when the s.q.t. is used, the relative standard deviations (s_r) being of the same order in the two flames. For mercury, equivalent results were obtained for the air—hydrogen and argon (entrained air)—hydrogen flames. All values were obtained from the linear portions of the calibration graphs. Up to a five-fold decrease in s_r was observed when the s.q.t. was used.

Interference studies. Two series of standards containing 10 and 25 μg ml^{-1} of the elements investigated, together with selected anions and cations in the concentration range 0—1000 μg ml^{-1}, were used to study interference effects. Solutions of sodium and potassium chlorides, and sodium, potassium, calcium, magnesium and strontium nitrates were investigated for their effects on absorbance values for each element with each of the three flames.

Severe interferences occur in the argon (entrained air)—hydrogen flame, both with and without the s.q.t. for arsenic, selenium and antimony. For

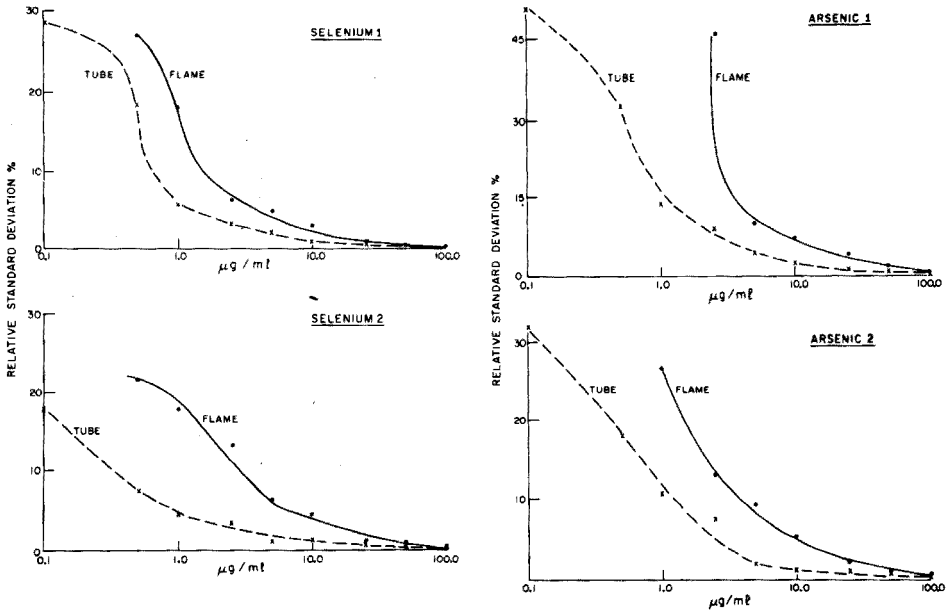

Fig. 2. Relative standard deviation—concentration graphs for selenium and arsenic.

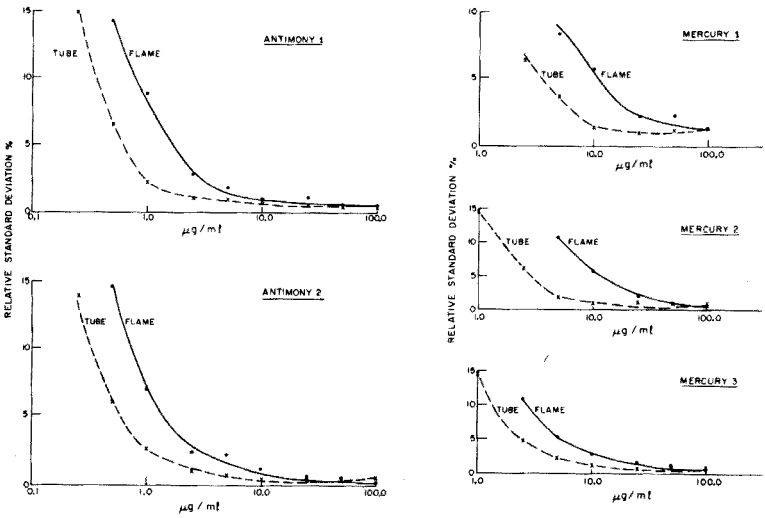

Fig. 3. Relative standard deviation—concentration graphs for antimony and mercury.

example, in the flame, 500 μg ml^{-1} calcium depressed the arsenic absorbance signal by 85%. In the case of antimony, with the s.q.t., 500 μg ml^{-1} calcium suppressed the absorbance signal by 95% while 1000 μg ml^{-1} magnesium enhanced the signal by 100%. It is concluded that these interferences, which

TABLE 2

Comparisons of precisions near the analytical limits for the flame and slotted quartz tube

Element	Concentration ($\mu g\ ml^{-1}$)	Relative standard deviation[a] (%)			
		F1	T1	F2	T2
As	2.5	46.3	9.1	12.9	7.4
	1.0		13.8	26.7	10.1
	0.5		32.7		17.9
Sb	0.5	14.5	6.6	14.6	5.8
	0.1		20.8		14.0
Se	1.0	18.2	5.7	18.0	4.5
	0.5	27.0	18.5		7.4
	0.1		28.4		17.9
Hg	5.0	8.2	3.6	10.8	1.9
	2.5		6.2		6.0
	1.0		17.0		14.7

[a] Average of 20 determinations.

have been described in detail [5], make this flame unsuitable for the determination of arsenic, selenium and antimony in samples where these interfering elements are present. In the case of mercury, no significant interferences occurred in the flame, but a general 10% enhancement was observed when the s.q.t. was used. The only interference observed in the air—hydrogen flame was a 20% suppression of the antimony absorbance signal by 1000 $\mu g\ ml^{-1}$ calcium. Interferences were not observed for arsenic determination with the s.q.t. and only a 10% enhancement of the absorbance signal occurred for mercury in the presence of 1000 $\mu g\ ml^{-1}$ sodium as the chloride and for antimony in the presence of 100 $\mu g\ ml^{-1}$ sodium both as the chloride and the nitrate. A 10% suppression of the absorbance signal was observed with the s.q.t. when selenium was determined in the presence of 1000 $\mu g\ ml^{-1}$ sodium, potassium or strontium.

Interferences were not observed for the determination of mercury, arsenic, selenium or antimony in the air—acetylene flame, nor for mercury and antimony in the same flame with the s.q.t. A 10% enhancement was observed when arsenic was determined with the s.q.t. in the presence of 1000 $\mu g\ ml^{-1}$ sodium or potassium, either as the chloride or the nitrate. This enhancement was compensated by means of a continuum background corrector. Sodium and potassium chlorides, and sodium and strontium nitrates at the 1000 $\mu g\ ml^{-1}$ cation level caused a 10% suppression of the selenium absorbance signal when the s.q.t. was used.

REFERENCES

1 A. Ando, M. Suzuki, K. Fuwa and B. L. Vallee, Anal. Chem., 41 (1969) 1974.
2 H. L. Kahn and J. E. Schallis, At. Absorpt. Newsl., 7 (1968) 5.
3 K. C. Thompson and D. R. Thomerson, Analyst (London), 99 (1974) 595.
4 E. N. Pollock and S. J. West, At. Absorpt. Newsl., 12 (1973) 12.
5 R. J. Watling, CSIR FIS 108, Special Report, 1977.
6 B. M. Gatehouse and J. B. Willis, Spectrochim. Acta, 17 (1961) 710.

Analytica Chimica Acta, 94 (1977) 187—191

Short Communication

THE SIMULTANEOUS MULTI-ELEMENT ANALYSIS OF HAIR: A NON-PARAMETRIC METHOD FOR EVALUATING THE ABILITY OF THE DATA TO DISTINGUISH BETWEEN INDIVIDUALS

J. F. ALDER*, A. J. SAMUEL and T. S. WEST§

Chemistry Department, Imperial College of Science and Technology, South Kensington, London SW7 2AY (Great Britain)

(Received 3rd May 1977)

For over 15 years, extensive studies have been made of the possibility of human identification by means of trace element analysis of scalp hair [1, 2]. The analytical technique exploited most widely for hair analysis has been neutron activation analysis, which has the advantage that, for moderate irradiation flux and time, the hair samples can be retained intact [3], and short (1 mm) sections of hair can be used [4], although to date no conclusive method of individual characterization by means of such data has been found. Several workers have compared the γ-ray spectra obtained from irradiated hair samples [5]; such comparisons have been presented as evidence in courts of law. A study of trace elements in human hair [6] was followed by the development of a statistical method for identifying individuals by means of such data, but these methods are not now used since they may give false identification [7, 8].

The method developed [9, 10] for the treatment of the data obtained from neutron activation analysis of hair was rejected for the data obtained in the present study for two reasons. The method requires the information obtained for each section of the hair to be averaged to give a mean value for the whole hair; the value of the analytical technique, i.e. its ability to measure trace metal concentrations in 1-cm lengths of hair, would therefore be lost. Secondly, Parker's method [9] assumes that the frequency distribution of trace metal concentrations in hair is known; there is, however, considerable conflict in the literature as to the frequency distribution of many elements. A non-parametric method of evaluating the information, in terms of its ability to distinguish between individuals, was thus sought. Observations of the trace metal profiles of head hair had indicated in many instances an apparent correlation between elements specific to an individual. Thus several element pairs were considered, and the data for several individuals were

§Present Address: The Macaulay Institute for Soil Research, Craigiebuckler, Aberdeen AB9 2QJ (Great Britain).

plotted in a two-dimensional graph. Areas of correlations specific to the individual were found. A test was then applied to discover whether it was possible to identify samples from a batch of unknowns vs. a batch of controls.

Experimental

Ten control hairs (from 1 head) and 10 individual hairs were taken from the heads of males, aged 22—58, with similar colour of hair. The hairs were washed for 2 h in diethyl ether (Soxhlet extractor) as in previous studies [11]. The hairs were then cut into ca. 1-cm sections from the distal end, and analysed by means of the multi-element atomic absorption spectrometric method previously described [12]. The hair samples were weighed on an Oertling Q01 quartz fibre micro-balance; the results were calculated by interpolation from calibration curves for aqueous solution.

Results and discussion

The four elements (Cu, Fe, Mn and Co) considered in this study seemed to offer the best possibility of discrimination; distribution within the individual was small compared with the distribution within the whole population studied.

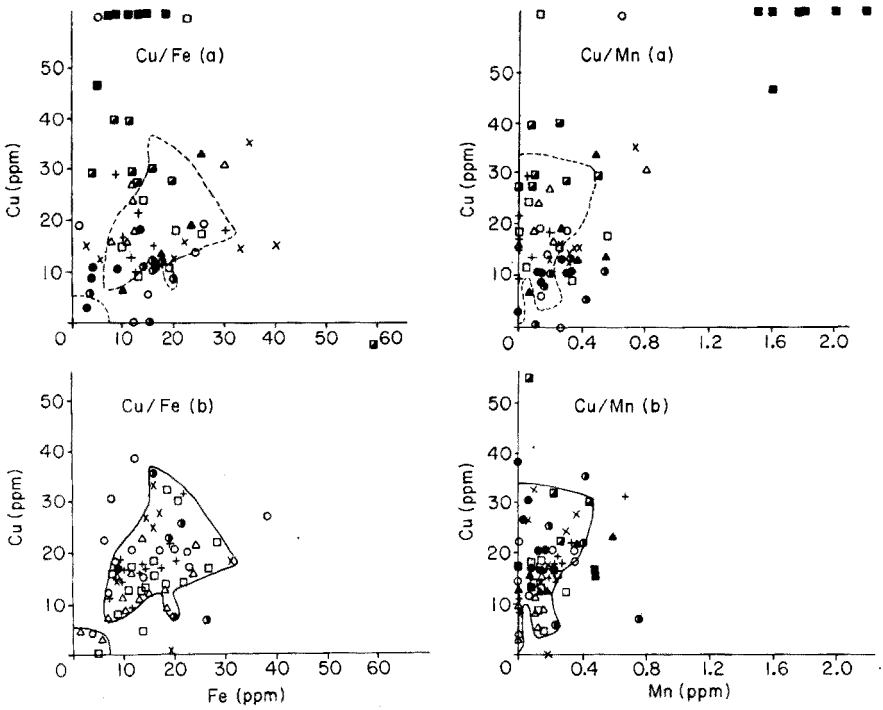

Fig. 1. Correlation between element pairs. Correlations are given between copper and iron, copper and manganese, manganese and iron, manganese and cobalt, iron and cobalt, and copper and cobalt. In each set (a) represents the unknowns, and (b) represents the controls. Symbols used are: ○ S1, U1; □ S2, U2; △ S3, U3; • S4, U4; ■ S5, U5; ▲ S6, U6; + S7, U7; × S8, U8; ◪ S9, U9; ◑ S10, U10. The figure is continued on the following page.

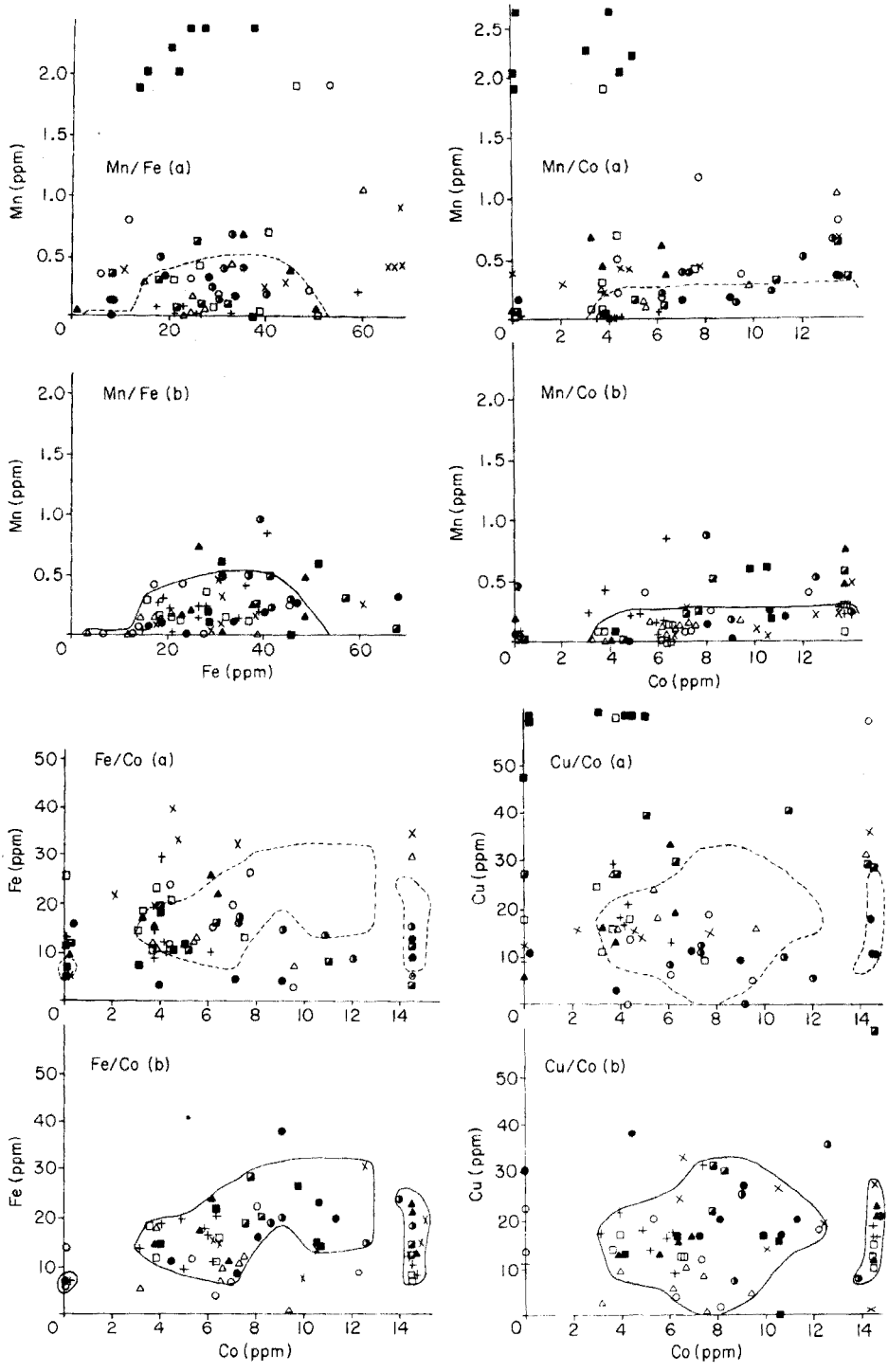
Mn/Fe (a)
Mn/Co (a)
Mn/Fe (b)
Mn/Co (b)
Fe/Co (a)
Cu/Co (a)
Fe/Co (b)
Cu/Co (b)
Mn (ppm)
Fe (ppm)
Cu (ppm)
Co (ppm)

Plots made of the six element pairs formed from these four elements are shown in Fig. 1. The unknowns and controls are plotted separately for clarity. A boundary, drawn around the controls so that the majority of the points were enclosed, was chosen so that it afforded maximum discrimination against the unknowns. The area was superimposed on the unknowns, and the numbers lying inside and outside the area were counted separately. The numbers of controls lying inside the chosen area are shown in Table 1; the number of unknowns lying within the areas is shown in Table 2. In all cases, more than 70% of the control samples are covered by the areas chosen. From the data in Table 2, sample 7 has the largest number of points within the control areas and would seem to be similar to the controls. Sample 3 has 72% of its points within the area: this is within the range for the controls and might also be considered similar. To assess the discrimination of this method the mean and relative standard deviation of the fraction of controls within the areas was found to be 82.9 ± 9.5%. This assumes that the distribution of controls, inside and outside the boundary, is normal. This cannot be rigorously defended from the data presented here but serves to give an indication of the discrimination that has been obtained. Thus the next nearest sample (No. 4) is 2.8 standard deviations away and has only a probability of 2 in 1000 of being similar to the controls: samples 3 and 7 are, in fact, from the same head as the controls. This test suffers from operator bias in the constructions of the area around the control points but it should be relatively easy to overcome this problem with a pattern recognition method such as that developed by Duewer and Kowalski [13].

Conclusions

The method of interpretation of the data obtained from the multi-element analysis of hair proposed appears to have potential in the field of discrimination between individuals. There are, unfortunately, only limited reliable data available to evaluate the method; before it can be exploited generally a study by unbiassed computer methods will be necessary.

TABLE 1

Fraction of controls falling in the enclosed areas in Fig. 1.

Sample	C1	C2	C3	C4	C5	C6	C7	C8	C9	C10
Total (%)	79	98	93	81	73	86	92	83	71	73

TABLE 2

Fraction of unknowns falling in enclosed areas in Fig. 1.

Sample	U1	U2	U3	U4	U5	U6	U7	U8	U9	U10
Total (%)	50	48	72	56	12	37	83	29	45	48

The authors are indebted to the Home Office for financial support and for lending the equipment used in this work.

REFERENCES

1 R. E. Jervis, A. K. Perkons, W. D. Mackintosh and M. F. Kerr, Proc. Int. Conf. Modern Trends Activ. Anal., 1961, p. 107.
2 L. C. Bate and F. F. Dyer, Nucleonics, 23 (1965) 74.
3 R. F. Coleman, J. Brit. Nucl. Energ. Soc., 6 (1967) 134.
4 I. Obrusnik, J. Gislaoson, D. K. McMillan, J. D'Auria and B. D. Pate, J. Radioanal. Chem., 15 (1972) 115.
5 D. E. Bryan, V. P. Guinn and D. M. Settle, General Atomic, Report No. 6152, (Chemistry), U.S.A. Energy Comm. (1965).
6 R. F. Coleman, F. H. Cripps, A. Stimson and H. D. Scott, Atomic Weapons Research Establishment Report No. 0-86/66 (1966).
7 R. Cornelis, Medicine, Science and the Law, 12 (1972) 188.
8 H. L. Schlesinger, H. R. Lukens and D. M. Settle, Proc. Int. Conf. Modern Trends Activ. Anal., Gaithersburg, 1968, p. 265.
9 J. B. Parker, J. Forensic. Sci. Soc., 6 (1966) 33.
10 J. B. Parker and A. Holford, Appl. Stats., 17 (1968) 237.
11 J. F. Alder, A. J. Samuel and T. S. West, Anal. Chim. Acta, 87 (1976) 313.
12 J. F. Alder, D. Alger, A. J. Samuel and T. S. West, Anal. Chim. Acta, 87 (1976) 301.
13 D. L. Duewer and B. R. Kowalski, Anal. Chem., 47 (1975) 526.

Analytica Chimica Acta, 94 (1977) 193—194

Short Communication

THE DETERMINATION OF URANIUM IN GEOLOGICAL SAMPLES BY AN INDIRECT ATOMIC ABSORPTION SPECTROMETRIC PROCEDURE

J. F. ALDER and B. C. DAS

Department of Chemistry, Imperial College of Science and Technology, South Kensington, London SW7 2AY (Great Britain)

(Received 3rd May 1977)

The analysis of geological samples for uranium by a.a.s. is difficult; the refractory nature of the uranium oxides results in low atomization efficiency and poor sensitivity.

The emission spectrum from the hollow-cathode lamp is complex and the line-to-background ratio at the analytical wavelengths is poor. This leads to poor sensitivity and high limits of detection. Martin [1] proposed the use of a.a.s. for the determination of uranium-based nickel—uranium catalysts, but since that time the determination of uranium has received much less attention than other elements.

Uranium can be determined indirectly by the reduction of Cu(II) to Cu(I) by U(IV), extraction of Cu(I) as its neocuproine complex, and determination of the copper by a.a.s. in an air—acetylene flame [2]. The method is accurate, sensitive and precise, and only a few species cause serious interference; the method has now been applied successfully to the analysis of standard geological materials for uranium. The samples supplied were quartz-based minerals, resistant to hydrochloric—nitric acid mixtures. Hydrofluoric acid (40%, w/v) was therefore used; as fluoride interferes in the subsequent determination [2], the bulk of it is removed by repeated evaporation to dryness with hydrochloric acid and the remaining fluoride is complexed with boric acid [3]. The uranium is extracted from the matrix with ethyl acetate in the presence of aluminium nitrate as a salting-out agent. The uranium is back-extracted into water [4] and any organic material or nitric acid is removed by evaporation of the solution to dryness with a few drops of sulphuric acid. The final solution, made up in 3 M hydrochloric acid, is used in the procedure described earlier [2].

Procedure

Weigh 0.5—1 g of sample (<80 mesh) into a clean platinum crucible. Add 10 ml of 40% HF and evaporate to dryness at about 180°C. Add 15 ml of 40% HF and 10 ml of 70% HNO_3 and evaporate to dryness. Digest the residue with 10 ml of 35% HCl for 5 min and evaporate to dryness to volatilize the HF and SiF_4. Repeat twice more with aliquots (5 ml) of HCl. Finally, dissolve the residue in 5 ml of 35% HCl and dilute to 100 ml with water.

TABLE 1

Results of analyses

Sample	Uranium (%)	Calculated amount of U in sample aliquot taken (μg)	U (μg) obtained by a.a.s.						Mean U found (μg)	s_r (%)
IGS A_1	0.25	50	49.70	50.50	48.90	49.65	49.65	49.65	49.67	±1.02
IGS A_2	0.50	50	48.70	49.70	50.50	49.66	49.70	50.50	49.79	±1.34
IGS B_1	0.026	20	19.66	19.70	20.20	19.70	20.20	19.70	19.86	±1.33
IGS 37-175	0.149	50	48.70	49.65	49.70	49.65	48.66	49.40	49.29	±1.06

[a]A known weight of ore was dissolved and the concentration of U in solution calculated from the given U content of the ore.

By pipette, add a volume of solution containing about 50 μg of uranium into a separating funnel, add 5 ml of 1 M boric acid and sufficient nitric acid to make the final solution about 5% in nitric acid. Add 6—8 ml of hot 30% (w/v) aluminium nitrate solution, mix well, and allow to cool to room temperature. Extract the uranium with 20 ml of ethyl acetate and back-extract into water [4]. In order to remove organic matter and nitrate, add a few drops of 98% H_2SO_4 and evaporate to dryness. Dissolve the residue and make up to 25 ml with 0.4 M HCl. This solution is put onto the reductor column and passed through twice at 7—10 ml min^{-1} [2]. The solution is then aerated to oxidize U(III) to U(IV); add 5 ml of acetate buffer (pH 8.5) and 5 ml of 30% (w/v) sodium citrate solution and adjust to pH 8.5 with ammonia. Add a five-fold excess of Cu(II) solution with 10 ml of 0.1% (w/v) neocuproine. After standing for 5 min, extract with two portions (10 ml and 5 ml) of chloroform. Wash the chloroform layer twice with 10 ml of buffer (pH 8.5). Back-extract the copper into 5 ml of 3 M HCl and determine in an air—acetylene flame by the usual method.

Results

Four quartz based mineral samples were analyzed. The samples, provided by the Institute of Geological Sciences, had been analyzed previously by colorimetry, polarography, x.r.f., neutron activation, and fluorimetric methods. The results shown in Table 1 compare favourably with those obtained by the above techniques. The precision is acceptable and it therefore brings the determination of uranium in geological samples within the capability of conventional a.a.s. equipment.

The authors are indebted to Dr. Brian Lister of the Institute of Geological Sciences (Geochemical Division, 64 Gray's Inn Road, London) for providing the analyzed samples, and to the Commonwealth Association, London, for the award of a scholarship to B. C. Das.

REFERENCES

1 M. S. Martin, Analyst, 96 (1971) 843.
2 J. F. Alder and B. C. Das, Analyst, in press.
3 D. A. Johnson and T. M. Florence, Anal. Chim. Acta, 53 (1971) 73.
4 R. J. Guest and J. B. Zimmerman, Anal. Chem., 27 (1955) 931.

Analytica Chimica Acta, 94 (1977) 195—197

Short Communication

THE CARBON-ROD ATOMIZER FOR THE DETERMINATION OF CADMIUM AND LEAD IN PLANT MATERIALS AND SOIL EXTRACTS
Part II. Improved Rod Geometry for Atomic Fluorescence Spectrometry

A. M. URE* and M. P. HERNANDEZ-ARTIGA§

Department of Spectrochemistry, The Macaulay Institute for Soil Research, Craigiebuckler, Aberdeen AB9 2QJ (Scotland)

(Received 11th May 1977)

The apparatus described [1] for the determination of cadmium by atomic absorption with a carbon-rod atomizer was developed as the first stage of a multi-element spectrometer. Since the multi-element capability depends on the additional use of atomic fluorescence techniques, a carbon-rod was chosen instead of a furnace atomizer. The present communication describes a carbon-rod atomizer whose rod geometry differs from that used for atomic absorption analysis and offers improved precision for atomic fluorescence spectrometry without loss of precision or sensitivity in atomic absorption.

The carbon rod (A) used for the determination of cadmium by atomic absorption [1] and that (B) used for atomic fluorescence spectrometry are shown diagrammatically in Fig. 1. Both are made from spectrographic carbon rod (Morganite Grade SG-905-J). They differ in the method used to reduce their cross-sectional area near the sample well for the purpose of localizing the heating of the rod to this region. In rod (A) this is achieved by turning down the rod diameter on both sides of the sample well and in rod (B) by drilling a hole on each side of the sample well. Figure 2 shows the flow-pattern of argon gas and vapour from the two rods obtained by spotting them with grease and then heating the rods by passing current in the normal manner. In Fig. 2(a), the column of smoke from rod (A) is elongated along the axis of the rod whereas the smoke from rod (B) rises in a well-defined cylindrical column directly above the sample well. The latter rod offers a more compact and stable atom cloud which lends itself more easily to irradiation with a narrow beam of light from an excitation source and to the collection and collimation of the emitted fluorescence.

For cadmium, neither the atomic absorption detection limit nor the non-dispersive atomic fluorescence detection limit is significantly changed by replacing rod (A) by rod (B). The precision of analysis for lead or cadmium by

§ On leave from: Departamento de Quimica Analitica, Facultad de Ciencias, Universidad de Murcia, Murcia, Spain.

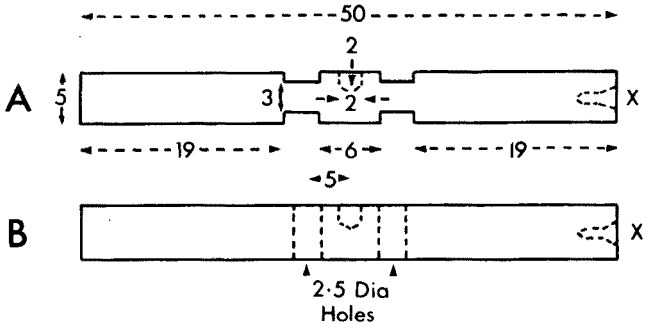

Fig. 1. Diagram showing the form and dimensions (in mm) of carbon-rod (A) and carbon-rod (B). X, centre-drilled hole for machining in lathe.

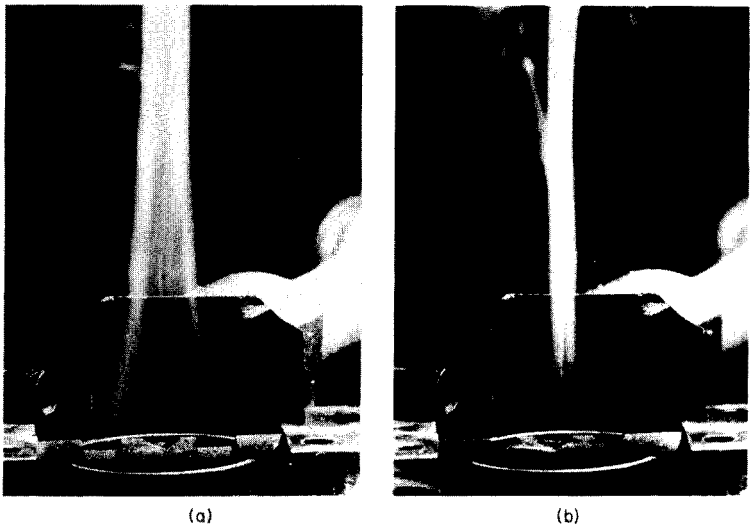

Fig. 2. (a) Smoke flow pattern for rod (A) (Fig. 1). (b) Smoke flow pattern for rod (B) (Fig. 1).

atomic absorption is essentially the same with the two types of rod. However, in the determination of cadmium by atomic fluorescence, (B) provides a marked improvement in precision compared with (A). These comparisons are shown in Table 1, and are all made with extracts of aqueous cadmium and lead solution into dithizone in chloroform.

Variation of the position and atomic concentration of the vapour column can occur along the axis of rod (A) which probably results in an increased variability in the atomic fluoresence signal as the atomic cloud moves in or out of the small, side-illuminated, fluorescence cell. This positional variation, however, has little effect on the atomic absorption signal since the variation occurs along the axis in which the atomic absorption measurement is made.

TABLE 1

The effect of rod type on the precision of analysis by atomic absorption (AA) for lead and cadmium and by non-dispersive atomic fluorescence (AF) for cadmium with dithizone-in-chloroform extracts of aqueous solutions as samples

Element	Concentration in extract (ppm)	Method of analysis	Rod type	s_r(%)
Pb	0.1	AA	A	8.2
Pb	0.1	AA	B	8.3
Cd	0.1	AA	A	3.6
Cd	0.1	AA	B	3.2
Cd	0.1	AF	A	5.6
Cd	0.1	AF	B	2.4

Simultaneous determination of cadmium by atomic fluorescence and lead by atomic absorption spectrometry, with a type (B) carbon rod atomizer will be described in Part III.

We gratefully acknowledge the award of a grant from the Spanish Ministry of Education and Science to one of us (M.P.H.A.) during the course of this work.

REFERENCE

1 A. M. Ure and M. C. Mitchell, Anal. Chim. Acta, 87 (1976) 283. (Part I).

Analytica Chimica Acta, 94 (1977) 199—200

Short Communication

DETERMINATION OF THE CHROMATE CONTENT OF CHROMATE CONVERSION FILMS ON ZINC

LINDSAY F. G. WILLIAMS

Department of Defence, Materials Research Laboratories, P.O. Box 50, 3032, Melbourne (Australia)

(Received 13th April 1977)

The chromate content of iridescent and opaque chromate conversion films on zinc or cadmium is a criterion for evaluating the corrosion performance of these films [1—3]. The chromate is adsorbed on the chromium(III) hydroxide which precipitates on the surface of the metal when immersed in an acidic dichromate solution containing added anions. On drying, an adherent film is formed; the yellow iridescent films are 0.1—0.6 μm thick and the opaque types are slightly thicker.

The normal method of removal of the chromate involves desorption in a hot sodium hydroxide solution, rinsing and final dissolution in sulphuric acid [2]. The combined solutions are then analysed spectrophotometrically for chromate with diphenylcarbazide to produce a red complex. The major disadvantages with this method are that the diphenylcarbazide solution must be prepared freshly, and that the red complex tends to be unstable. Usually, the absorbance is recorded after 10 min; to ensure the required accuracy, standards must be made up with each set of analyses. A further problem is the interference from zinc [4].

Differential pulse polarography (d.p.p.) has been used for chromate determinations [5] in concentrations below 1 ppm and should be a rapid, accurate method for determining the chromate content of chromate conversion films. The method described below simply entails a sodium hydroxide extraction of the chromate followed by d.p.p. of the resultant solution. Synthetic solutions were used to check the linear dependence of the peak current on the concentration of the chromate in the presence of cations which are likely to be present in the extracted solution.

Experimental

All reagents were AR grade and the water was doubly distilled through all-glass apparatus. High-purity nitrogen was used to deoxygenate the solutions for polarography.

A Princeton Applied Research (PAR) Model 174A Polarographic Analyser and a Moseley X-Y Recorder Model 7030A were used with a standard PAR

cell, dropping mercury electrode, drop timer assembly, Pye saturated calomel electrode (s.c.e.) and a platinum auxiliary electrode. The s.c.e. was connected to the solution via a salt bridge filled with sodium sulphate solution. Polarograms were run on 25 ml of solution after purging for 7—8 min with nitrogen. The control settings on the PAR 174A were as follows: initial potential, —0.5 V; scan rate, 2 mV s^{-1}; pulse amplitude, 25 mV; and pulse rate and drop time, 1 s.

For analyses of the chromate conversion films, 50 ml of a 6% (w/w) sodium hydroxide solution was heated to 80°C and the panel (32.3 cm^2) to be analysed was immersed in this solution for 120 s. This time was sufficient for the chromate to be desorbed from air-dried chromate conversion films. After this, the solution and washings were diluted to 100 ml and analysed by d.p.p. The standard addition method was used with 50-μl additions of a 10^{-2} M $K_2Cr_2O_7$ solution.

Results and discussion

Plots of d.p.p. peak height versus concentration of chromate in 0.75 M NaOH solutions doped with zinc sulphate and chromium(III) chloride (8×10^{-5} M each) were linear over the range 0—5 ppm Cr(VI). This linear dependence indicates that the method can be applied readily to a hydroxide solution after extraction of chromate from the film on a zinc substrate. For films on cadmium, the interference from cadmium should be negligible because of its low solubility in the hydroxide solution.

Differential pulse polarograms obtained in the analysis of chromate conversion films produced by a 4-s immersion of a zinc-plated steel panel in a Cronak [6] chromating solution at 20°C, showed well defined peaks at —0.73 V vs. s.c.e. Blank determinations gave steady baselines. The value of 5.6 μg cm^{-2} calculated from the peak currents compares with values of the chromate content of 5.6, 5.6, 5.8, 5.6 and 5.4 μg cm^{-2} obtained by a modified diphenylcarbazide method. A series of experiments showed that less than 2% of the chromate remained in the air-dried films after the 120-s immersion in the sodium hydroxide solution at 80°C. Therefore, a second extraction with sulphuric acid [2] was unnecessary.

A minimum acceptable value for the chromate content of iridescent chromate conversion films has been set at 4 μg cm^{-2} [2]. At this concentration the chromate can be readily determined by d.p.p. as evidenced by the peak current (65 nA) obtained for a film containing 5.6 μg cm^{-2} chromate.

REFERENCES

1 L. F. G. Williams, Plating, 59 (1972) 931.
2 U.S. Federal Specification QQ-Z-325b (1969).
3 Australian Standard 1791 (1976).
4 Tables of Spectrophotometric Absorption Data of Compounds Used for the Colorimetric Determination of Elements, Supplement to Pure and Applied Chemistry, IUPAC Publications, Butterworths (1963), p. 130.
5 Princeton Applied Research Application Note 122 (1974).
6 E. A. Anderson, Tech. Proc. Am. Electroplat. Soc., 31 (1943) 6.

Analytica Chimica Acta, 94 (1977) 201—203

Short Communication

DETERMINATION OF NITRILOTRIACETIC ACID IN WATER BY DERIVATIVE PULSE POLAROGRAPHY AT A HANGING MERCURY DROP ELECTRODE

B. J. A. HARING and W. v. DELFT

National Institute for Water Supply, Voorburg (The Netherlands)

(Received 20th April 1977)

The determination of nitrilotriacetic acid (NTA) at low concentrations became of interest after its application in detergents as a substitute for tripolyphosphates; because of the ability of NTA to complex many metal ions, studies of its environmental impact, e.g. the release of metal ions from sediments, and of the biodegradability of NTA, have been initiated. The present work includes an investigation of the use of derivative pulse polarography techniques for the determination of NTA. These methods are based on complex formation of NTA with suitable metal ions and on the shift of the halfwave potential of the polarographic reduction wave of these metal ions to more negative values on chelation with NTA. Spectrophotometric methods for NTA, e.g. the zinc—zincon method [1], have frequently been used but these methods suffer from interferences by other chelating agents.

As voltammetric methods are subject to interferences by metal ions that compete for complex formation with NTA, NTA is usually determined as its bismuth(III) complex at pH 2.0 where this complex is very stable. Afghan et al. [2] found that at pH 2.0 bismuth was capable of displacing NTA from most heavy metals normally found in natural waters; only Fe(III) forms an NTA complex at pH 2.0, resulting in a pre-wave close to that of the bismuth—NTA complex. The addition of vitamin C reduces Fe(III) to Fe(II) and eliminates this pre-wave. The voltammetric methods described in the literature usually involve dropping mercury electrodes in a.c. polarography or twin-cell oscillographic d.c. polarography [2—5]. In this study, a hanging mercury drop electrode was used. These electrodes make it easy to automate the method completely when a sample changer is used (P.A.R. model 316). The procedure does not involve any preconcentration or sample clean-up.

Experimental

Reagents. Stock solutions of NTA were prepared by dissolving the accurately weighed solid in water with just enough sodium hydroxide. Solutions of bismuth(III) nitrate were prepared by dissolving the solid in concentrated nitric acid, with dilution to the required concentration.

Apparatus. The P.A.R. Electrochemistry System (Princeton Applied Research, New Jersey, U.S.A.) used consisted of: a model 174 polarograph; a model 315 automated electroanalysis controller; a model 314 automated hanging mercury drop electrode (h.m.d.e.) or, when the method is completely automated, a model 316 automated cell sequencer equipped with a model 302 universal mercury electrode. All polarograms were recorded at a scan rate of 5 mV s^{-1} and 50-mV pulse amplitude. The pH values of the samples were checked with a Philips digital pH meter (PW 9414/01). The glass capillary of the h.m.d.e. was siliconized once weekly to avoid retraction of the mercury thread when the drop was dislodged.

Procedure. The water sample (25 ml) was acidified with vitamin C (ca. 1 g) and nitric acid to pH 2.0, and deaerated with nitrogen. A differential pulse polarogram of this solution (blank) was recorded by scanning the potential of the h.m.d.e. from 0 to −600 mV versus saturated calomel electrode (s.c.e.). Next bismuth(III) solution was added till a concentration of 24 ppm Bi was reached and a second polarogram was recorded. The peak of the NTA bismuth(III) chelate appears at −300 mV vs. s.c.e. The concentration of NTA was determined by the method of standard additions, i.e. the amount of NTA originally present was found by extrapolation of the signals found for spiked samples. Typical voltammograms of the Bi—NTA and Bi—EDTA chelates are shown in Fig. 1. The peak heights of the Bi—NTA and Bi—EDTA peak were found after baseline subtraction.

The detection limit for the NTA determination without clean-up of the water samples was as low as 50 $\mu g\ l^{-1}$. The calibration curve for the NTA determination was linear up to 5 mg l^{-1}. Reproducibility was within 10%.

Results and discussion

Effect of pH. To study the effect of pH on the peak height of the bismuth—NTA complex, the slopes of the calibration curves at different pH values were

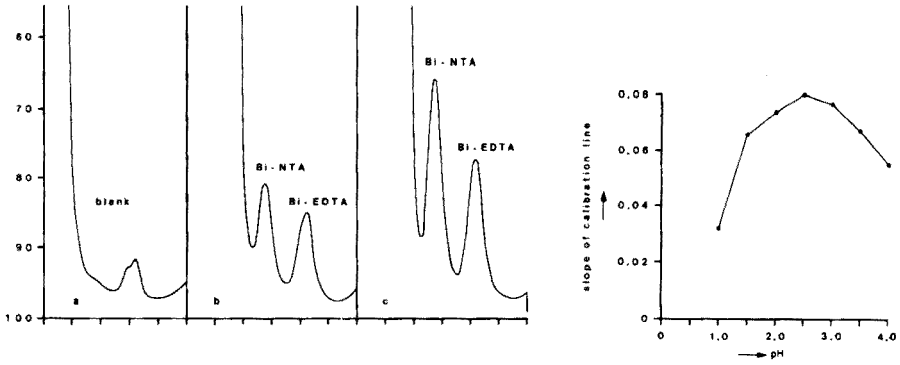

Fig. 1. Typical voltammograms of (a) blank; (b) 100 $\mu g\ l^{-1}$ NTA, EDTA; (c) 200 $\mu g\ l^{-1}$ NTA, EDTA. Instrument settings: initial potential, +70 mV; final potential, −600 mV; scan rate, 5 mV s^{-1}; pulse interval, 0.5 s.

Fig. 2. Effect of pH on slope of calibration line.

plotted versus pH (Fig. 2). Maximum response was found between pH 2 and 3. A value of pH 2 was chosen because most other metal—NTA chelates are not stable at this pH.

Interference of other metal ions. Various metal ions that form complexes with NTA were tested to see whether bismuth was capable of displacing them at pH 2.0 from their chelates with NTA. Table 1 shows the recovery of the Bi—NTA chelate from samples with different heavy metal concentrations at a concentration of NTA of 1.0 mg l^{-1}. These experiments indicated that cadmium, lead, copper and zinc do not interfere at pH 2. Measurement of the peak height of the Bi—NTA complex was difficult if the sample had a high lead concentration (>0.4 mg l^{-1}) because the two peaks were separated by less than 100 mV. Calcium, magnesium, nickel, aluminium and manganese do not interfere in acidic solution [2, 5].

Interference of chelating agents. Naturally occurring metal complexing compounds (e.g. humic acids) also form complexes with bismuth and may interfere in the NTA determination. EDTA was found not to interfere and could be determined simultaneously by measuring the peak height of the Bi—EDTA complex (Fig. 1).

TABLE 1

Displacement of NTA by bismuth from its cadmium, lead, copper and zinc complexes at pH 2

	Amount added[a] (mg l^{-1})	Recovery of Bi—NTA complex (%)		Amount added[a] (mg l^{-1})	Recovery of Bi—NTA complex (%)
Cadmium	0.4	94	Copper	0.4	92
	0.8	98		0.8	96
	2.0	101		2.0	97
	4.0	102		4.0	97
	10.0	102		10.0	103
	20.0	98		20.0	102
Lead	0.4	100	Zinc	0.4	95
	0.8	109		0.8	96
	2.0	109		2.0	100
	4.0	117		4.0	99
	10.0	114		10.0	101
	20.0	114		20.0	97

[a]All samples contained 1.0 mg NTA l^{-1}.

REFERENCES

1 J. E. Thompson and J. R. Duthie, J. Water Pollut. Control Fed., 4 (1968) 306.
2 B. K. Afghan, P. D. Goulden and J. F. Ryan, Anal. Chem., 44 (1972) 354.
3 J. P. Haberman, Anal. Chem., 43 (1971) 63.
4 F. Dietz, Z. Wasser Abwasser Forsch., 3 (1974) 74.
5 G. den Boef, R. Oostervink and F. Freese, Z. Anal. Chem., 264 (1973) 147.

Analytica Chimica Acta, 94 (1977) 205—207

Short Communication

SYNTHESIS AND APPLICATION OF PERIMIDINYLAMMONIUM BROMIDE

P. K. DASGUPTA, G. L. LUNDQUIST, K. D. REISZNER and P. W. WEST*
Louisiana State University, Baton Rouge, La. 70803 (U.S.A.)
(Received 4th April 1977)

2-Aminoperimidine hydrochloride was originally introduced by Stephen [1] as a turbidimetric reagent for sulfate offering excellent sensitivity. Since the method was plagued with interferences from various anions that also form insoluble precipitates with this reagent, field applications were limited. However, since the study and measurement of aerosol sulfuric acid and airborne sulfates became important, there has been a tremendous interest in this reagent. It was discovered that the reagent can be used with great success as an immobilizing agent in microdiffusive separation of sulfuric acid [2], that the resulting sulfate salt can be thermally pyrolyzed to yield SO_2 [3] which is easily measurable by the established West—Gaeke method [4], and that the reaction of aerosol sulfuric acid with a filter impregnated with this reagent is topochemical and free of interference from other particulate sulfates and metal oxides [5—8]. The latter [8] is currently under evaluation as the ASTM Standard Method. A colorimetric method involving the nitration of 2-aminoperimidine sulfate is also almost complete [9]. A very selective pyrolytic method that employs this reagent for determination of sulfate in water at trace levels is now completely developed [10].

Stephen synthesized the hydrochloride following Sach's original method [11]. This method is quite cumbersome, and McClure [12] developed a much simplersynthesis to produce the hydrobromide salt (perimidylammonium bromide, 2-perimidylammonium bromide, PDA—Br). The account given here, contains significant modifications of McClure's method. Changes in reaction medium and purification steps have been found to give a purer product in higher yield.

Experimental

Reagents. Cyanogen bromide was reagent grade. Benzene, acetone, diethyl ether and 1,8-diaminonaphthalene were technical grade. 1,8-Diaminonaphthalene is almost white when pure, but the pure compound is highly susceptible to oxidation and acquires a purplish color rapidly. Since purification before use is necessary in any case, using a better grade of the reagent as the starting material has no advantage.

Preparation. 1,8-Diaminonaphthalene (DAN) may be purified by recrystallization from 1:1 ethanol—water [12]; a much preferred method is two distillations under a 1.5-mm Hg vacuum at 170—175°C. The purified DAN product is pale yellow to white, and should be used immediately.

The indicated amounts are for the preparation of approximately 100 g of PDA—Br dihydrate. Purified DAN (72 g) is dissolved in 500 ml of benzene and cyanogen bromide (52 g) is dissolved in 500 ml of benzene. The latter solution is placed in an ice bath and the DAN solution is added slowly with constant stirring. The temperature is monitored, and the mixture is removed from the bath and replaced alternately, so that the temperature does not exceed 50°C. Below 20°C the reaction proceeds slowly, so overcooling should be avoided. A pale tan product begins to separate immediately and finally the mixture becomes quite viscous. After 30 min, the mixture is set outside the bath, warmed to ca. 40°C if necessary, and set aside for another 30 min to ensure complete reaction.

Purification. The product is filtered under vacuum in a large Buchner funnel and washed slowly with 50 ml of benzene, and then small volumes of acetone until the filtrate is colorless. Water (1 l) is boiled for 10 min to ensure removal of dissolved oxygen. The PDA—Br product is added to the water and stirred vigorously to help quick dissolution. The hot solution is filtered under vacuum through a bed of activated coconut charcoal. The hot filtrate is quickly transferred to a large Erlenmeyer flask, stoppered, and allowed to come slowly to room temperature; beautiful needlelike crystals then separate from the solution. The mixture is refrigerated at ca. 10°C to improve the yield and filtered. The product is recrystallized again in the above manner and the resultant product should be almost perfectly white. Any last tinges of color are removed by washing with a small volume of 1:1 ethanol—acetone.

The solid form of the reagent when freshly recrystallized from water is PDA—Br.$2H_2O$, which can be dried at 80°C for 4 h to the anhydrous compound; this absorbs moisture unless kept in a desiccator. (McClure found the form to be the dimer monohydrate.) [Analysis: calculated for $C_{11}H_{14}N_3O_2Br$: 44.0% C, 4.7% H, 14.0% N; found 44.1% C, 4.7% H, 14.0% N.] The white crystalline product has a m.p. of 265°C.

Discussion.

Nucleophilic additions to cyanogen bromide are commonly performed in polar solvents. But the use of benzene instead of dimethoxyethane [12] has advantages. First, the reaction temperature can be more carefully controlled and therefore the reaction is less violent. Secondly, the PDA—Br product is less soluble in benzene. Thirdly, benzene is more readily available and less expensive then dimethoxyethane. Further, like other ethers, the presence of peroxides in commercial dimethoxyethane aids in rapid oxidation of both diaminonaphthalene and PDA—Br, leading to undesirable intensely colored products, which often necessitate many more recrystallization steps.

The reaction is exothermic and careful monitoring is necessary to prevent the reaction from reaching explosive proportions. The heat of reaction is

TABLE 1

Influence of (a) the curing method and (b) the water content of the resin mix on the properties of a 1:1:2.5 oxine : resorcinol : formaldehyde ion exchange resin

1st Series	Original water content of resin mix (%)	Water regain ($g\ g^{-1}$)	Equilibration rate ($t_{\frac{1}{2}}$)	Metal capacities[a] ($mmol\ g^{-1}$)		
				Cu(II)	Fe(III)	Al(III)
			pH	5.0	2.8	4.0
Batch 1						
Dry cure	67	0.67	6 h	0.70	0.04	0.32
Sealed cure		1.8	25 min	3.24	1.96	1.17
Batch 2						
Dry cure	70	0.70	5.5 h	1.40	0.06	0.33
Sealed cure		5.2	8.5 min	3.15	2.05	1.11
Batch 3						
Dry cure	75	1.0	1.5 h	1.41	0.08	0.52
Sealed cure		7.8	4 min	3.10	2.05	1.39

[a]Theoretical metal capacity from nitrogen contents of the resins is 3.2 to 3.3 $mmol\ g^{-1}$ assuming 1:1 complex formation.

water content, in good agreement with Jakubovic [13]. Although equilibration rates, in terms of time to 50% resin saturation, are given here, such measurements are dependent upon resin particle size and distribution. The particle size range used (22—60-mesh fraction) is so wide that it can be argued that variation in equilibration rates, particularly in Table 2 where such variations are small, may be determined by differences in resin particle size rather than in the parameter being varied. As Parrish [8] has demonstrated and others have discussed [14, 15], the water regain values can give

TABLE 2

The effects of changing the hydrophilicity and the degree of cross-linking of an oxine-containing ion-exchange resin

2nd Series	Resorcinol	*m*-Cresol	*p*-Cresol	Oxine	Cross linking (%)	Water regain ($g\ g^{-1}$)	Equilibration rate ($t_{\frac{1}{2}}$) (min)	Copp capac
Batch 1	4		0	4	50	4.8	4.7	3.5
Batch 2	3		1	4	37.5	2.9	6.0	3.4
Batch 3	2		2	4	25	2.4	6.5	3.2
Batch 4	2	2	0	4	50	1.6		2.8
Batch 5	2	1	1	4	37.5	2.2		3.1
Batch 6	2	0	2	4	25	2.5		2.8

[a]Theoretical copper capacity, from nitrogen contents, is 3.3—3.4 $mmol\ g^{-1}$.

Analytica Chimica Acta, 94 (1977) 209—211

Short Communication

FLUORESCENT MALONDIALDEHYDE POLYMERS FROM HYDROLYSED 1,1,3,3-TETRAMETHOXYPROPANE

J. M. C. GUTTERIDGE, A. D. HEYS and J. LUNEC

Department of Clinical Biochemistry, Whittington Hospital, London, N19 (England)

(Received 1st June 1977)

The measurement of malondialdehyde (MDA) is used both as a marker for prostaglandin biosynthesis and as an indication of enzymatic and non-enzymatic catalysed lipid peroxidation [1—3]. The most widely used test depends on heating lipid oxidation products with acidified thiobarbituric acid (TBA) and measuring the resulting chromogen at 532 nm [4, 5]. These TBA-reactive compounds are usually quantitatively expressed as MDA. As an alternative to colorimetric measurement a more sensitive spectrofluorimetric technique has been introduced by Tappel and his collaborators [6, 7]. The characteristic fluorescence depends on the reaction of MDA with free amino groups to form conjugated Schiff bases. MDA standards for both spectrophotometric and spectrofluorimetric work are usually prepared by hydrolysis of 1,1,3,3-tetramethoxypropane or the corresponding ethoxy derivative. During this hydrolysis, MDA can polymerize to form several compounds with physical and chemical properties different from those of the monomer [8]. The fluorescent characteristics of several of these polymers separated by gel-filtration have been measured in both polar and non-polar phases, and the results are discussed with reference to MDA—amino Schiff bases.

Experimental

Chemicals and materials. 1,1,3,3-Tetramethoxypropane (TMP; Eastman Chemicals, Kodak Ltd., Liverpool) and Sephadex G-10 (Pharmacia Ltd) were used. Chemicals were of "AnalaR" grade (where available) and solvents of spectroscopic grade (BDH Ltd).

Hydrolysis of TMP. TMP (2 ml) was added to 1 ml of 1 M HCl and heated at 60°C for 1 h. The resulting solution (orange-brown) was allowed to stand for 10 h at 4°C.

Gel-filtration chromatography. Separation was carried out as previously described [8] with Sephadex G-10 in a 60 × 0.9-cm column. Hydrolysed TMP (0.5 ml) was applied to the column and eluted with deionized water (pH 6.8). Fifty fractions (4 ml) were collected for analysis.

Spectrofluorimetric measurements. A Perkin-Elmer MPF-3 spectrofluorimeter was used with the following instrument settings: Sensitivity, × 10;

scan speed, X 3; excitation slit, 10 nm; emission slit, 10 nm; filter, 430 nm. Samples for aqueous phase measurements were diluted (1 + 19) with water before reading. The solvent phase samples were prepared by diluting 1 ml of the column fraction with 3 ml of water and adding 4 ml of chloroform: methanol (2:1, v/v). These were mixed vigorously for 2 min and centrifuged, the upper layer was removed, and 0.3 ml of methanol was added to clarify the lower layer before reading. Appropriate water and solvent blanks were included. Fluorescence intensity was measured with reference to a standard cell (Perkin-Elmer) with excitation maximum 400 nm and concentration 5×10^{-5} M. The instrument was standardized with reference to quinine sulphate (1 μg ml^{-1} in 0.05 M H_2SO_4).

Results

Hydrolysis of TMP at high concentration resulted in the formation of an orange-brown solution. When separated by gel filtration, at least five distinct zones of characteristic colour developed on the column. The visible and u.v. absorption spectra have been described in detail previously [8]. Fraction collector samples 1, 10, 15, 20, 30 and 40 were selected as representing the midpoint of each main coloured column zone; the results are presented in Table 1.

Aqueous phase. The first fraction had an excitation maximum at 375 nm with two emission peaks at 490 and 550 nm; all other fractions had single emission and excitation peaks. Fraction 15 had the highest fluorescence intensity and the lowest excitation wavelength.

Chloroform phase. The emission and excitation spectra were similar to those obtained in the aqueous phase. Fractions 20 and 30 developed two emission peaks, similar to those seen in fraction 1, and fractions 15 and 40 displayed a shoulder to the main peaks at 480 and 460 nm. The tendency for MDA to polymerize further in chloroform has been observed previously in gas–liquid chromatographic analysis [8].

MDA–bis(bisulphite) [9] produces a single peak by g.l.c. and a single spot on thin-layer separation; it was therefore included as a monomer control. In aqueous solution, and as a chloroform extract, this showed no fluorescent

TABLE 1

Spectroscopic data for chromatographic fractions

Column fraction	Aqueous phase			Chloroform phase		
	λ_{max} (ex.)	λ_{max} (em.)	%FI	λ_{max} (ex.)	λ_{max} (em.)	%FI
1	375	490, 550	7	375	485, 555	11
10	395	480	16	395	485	7
15	365	490	75	375	480[a]	21
20	375	490	30	375	490, 550	13
30	370	490	13	375	490, 550	5
40	370	490	4	370	460[a]	6

[a]Shoulder to main peak.

properties. TMP, diluted (1 + 49) with water and then treated similarly had no significant fluorescence.

Discussion

Malondialdehyde, a characteristic product of polyunsaturated fatty acid peroxidation, reacts with free amino groups to form conjugated Schiff bases [6]. Conjugation involving both aldehyde groups of MDA results in a fluorescent product. Depending on the amino donor, these products can be either polar or non-polar in nature. Identification of these fluorescent products has proved to be a more sensitive measure and marker of tissue and organelle lipid peroxidation than the colorimetric TBA reaction [10].

Preparation of MDA standards usually involves the hydrolysis of TMP or the corresponding ethoxy derivative to form free MDA [11]. This step must be carefully controlled in order to minimize polymer formation. Carbonyls formed during polyunsaturated fatty acid peroxidation as well as polymerized MDA can yield fluorescent complexes which are not MDA—amino Schiff bases [12]. The visible and u.v. absorption spectra of certain MDA polymers formed during TMP hydrolysis have been characterized by various chromatographic techniques [8]. This work has been extended to include spectrofluorimetric measurements on the major zones identified and separated by gel filtration. The results show that different polymers of MDA have fluorescent properties similar to those described for polar (ex. 350—400 nm/em. 450—470 nm), non-polar (ex. 360—400 nm/em. 430—475 nm), MDA—amino Schiff bases and age-pigments (ex. 340—395 nm/em. 420—490 nm) [13]. During peroxidation studies, polymerization of MDA or other carbonyls could contribute as artefacts to the measured MDA—amino fluorescence (although it would still be a valid measure of overall peroxidation). Suitable fluorescence controls should be included whenever hydrolysed TMP is added to a system to study the bio-reactivity of MDA.

The authors thank the Whittington Hospital Management Committee for facilities and the MRC for financial assistance.

REFERENCES

1 R. J. Flower, H. S. Cheung and D. W. Cushman, Prostaglandins, 4 (1973) 325.
2 E. D. Wills, Boichem. J., 113 (1969) 315.
3 T. F. Slater, Free Radical Mechanisms in Tissue Injury, Pion, London, (1972) p. 38.
4 S. Patton, M. Keeney and G. W. Kurtz, J. Am. Oil. Chem. Soc., 28 (1951) 391.
5 T. C. Yu and R. O. Sinnhuber, Food Technol., 11 (1957) 104.
6 K. S. Chio and A. L. Tappel, Biochemistry, 8 (1969) 2821.
7 W. R. Bidlack and A. L. Tappel, Lipids, 8 (1973) 203.
8 J. M. C. Gutteridge, Anal. Biochem., 69 (1975) 518.
9 L. D. Saslaw and V. S. Waravdekar, J. Org. Chem., 22 (1957) 843.
10 C. J. Dillard and A. L. Tappel, Lipids, 6 (1971) 715.
11 T. W. Kwon and B. M. Watts, J. Food Sci., 29 (1964) 294.
12 V. G. Malshet, A. L. Tappel and N. M. Burns, Lipids, 9 (1974) 328.
13 A. L. Tappel, in B. F. Trump and A. V. Arstila (Eds.), Pathobiology of Cell Membranes, Vol. 1, Academic Press, New York, 1975, p. 145.

Analytica Chimica Acta, 94 (1977) 213—216

Short Communication

THE DETERMINATION OF TOTAL SULPHUR IN COAL BY A SEMI-MICRO TUBE-COMBUSTION METHOD

W. LÄDRACH and J. D. VAN DER LAARSE*

Koninklijke/Shell-Laboratorium (Shell Research B.V.), Amsterdam (The Netherlands)

(Received 22nd March 1977)

In many countries the sulphur content of fuels and/or the amount of sulphur dioxide emitted into the atmosphere are restricted, and the sulphur content of coal (which varies between a few hundred ppm and 5%) is an important aspect of quality control. Many procedures for the determination of sulphur in coal are available as national or international standards. They are generally based on combustion at high temperature (1350°C; ISO/R 351), or sintering of the coal with magnesium oxide—sodium carbonate mixtures (Eschka mineralization: ISO/R 334, ASTM 3177, DIN 51724) to convert all sulphur compounds to sulphate, which is then determined gravimetrically or titrimetrically. These techniques are not only time-consuming but also usually applicable only to hard coals with low mineral contents. Relatively large amounts of volatile components may present serious problems, and constituents such as calcium and barium salts interfere strongly [1].

The reviving interest in coal as a fuel or base material for conversion processes made it expedient to develop a rapid method for the determination of total sulphur in a wide variety of coal types. Such a method could be particularly valuable for laboratories faced with large demands for analyses of less traditional coals, e.g. for surveying coal fields or for process development.

In 1974 Thürauf [2] described a rapid method for sulphur determination in coal based on flash combustion at 1250°C followed by non-dispersive infrared measurement of the sulphur dioxide formed during combustion. A prerequisite for obtaining correct results by Thürauf's method is a constant and high SO_2:SO_3 ratio in the combustion gases. However, this ratio is influenced by mineral matter in the coal which may occur in the ash. The method therefore seems less suitable for coals with high ash contents. In 1952 Radmacher [3] proposed the addition of iron(III) phosphate during coal combustion, to assist the conversion of all the sulphur present in refractory compounds to sulphur dioxide. This work, along with the conversion of all the sulphur compounds to sulphuric acid, followed by microcoulometric titration or thorin titration of the acid, formed the basis of the present investigation.

Experimental

Apparatus. A flow scheme of the combustion apparatus is given in Fig. 1. The layout is based on the open-tube principle; the gas is made to flow through combustion tube and scrubber by applying a vacuum to the gas outlet of the scrubber. The sample is burnt in the inlet section of the combustion tube, which is heated at 1200°C by a platinum heating coil. At this temperature iron(III) phosphate converts all the inorganic sulphates to sulphur oxides. To promote complete combustion of volatile organic material, the gases pass through a wider part of the quartz combustion tube which is heated at 1050°C. The ball joint at the end of the combustion tube is provided with a removable outlet capillary which is connected inside the male part of the joint with an O-ring. Finally the gases pass through a scrubber containing hydrogen peroxide in which all sulphur oxides are trapped and converted to sulphuric acid.

Procedure. Adjust the oxygen flow to 300 ml min^{-1}. Turn the oxygen valve until a slight excess of gas passes through the opening of the combustion tube. Set the prescribed temperatures.

Introduce 12 ml of 3% hydrogen peroxide into the absorption vessel. Weigh (to the nearest 0.1 mg) 30—50 mg of sample in a platinum boat and cover with about 50 mg of iron(III) phosphate. Introduce the sample boat into the combustion tube with the ladle. Move the sample boat slowly into the 1200°C zone in such a way that the sample burns steadily. Keep the boat in the combustion zone for 7 min. Disconnect the absorption vessel and flush the outlet capillary with 3 ml of a solution containing 1% orthophosphoric acid and 3% hydrochloric acid. Transfer this solution along with the

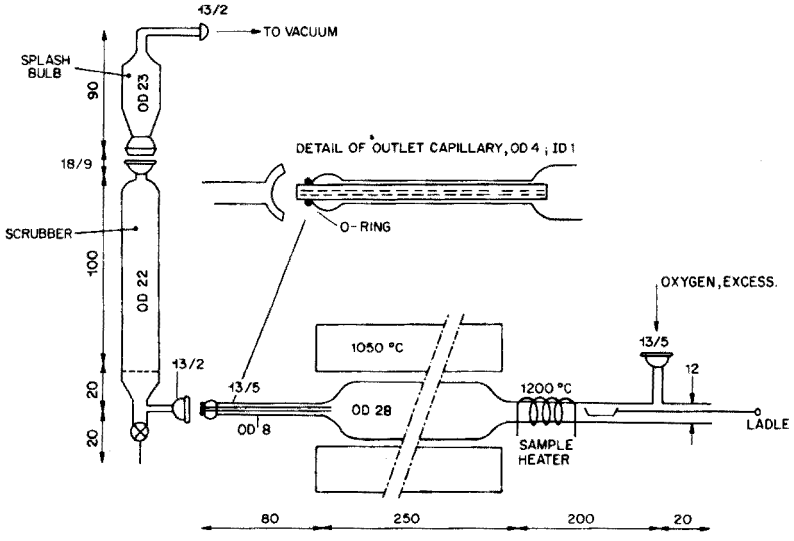

Fig. 1. Apparatus for the determination of total sulphur in coal. Dimensions are given in nm.

TABLE 1

Determination of sulphur by combustion and microcoulometry

Sample	S present (%w)	S found (%w)	Recovery (%)
S-Benzylthiuronium chloride	15.82	15.64 ± 0.12	98.9
Barium sulphate	13.70	13.90 ± 0.20	101.4

contents of the absorption vessel quantitatively to a 50-ml volumetric flask and top up with distilled water. Determine the sulphur concentration by using an aliquot containing 2—3 μg of sulphur in the microcoulometric titration procedure described by van Grondelle et al. [4]. The thorin titration described by Fritz and Yamamura [5] and other methods (gravimetric) may also be used.

Results and discussion

Because coal often contains both organic and inorganic sulphur compounds, the latter of which may be in a very stable form, the combustion system was tested with an organic sulphur compound and with barium sulphate. Quantitative yields were obtained for both types of compound (Table 1). The rinsing of the outlet capillary is essential; semi-volatile inorganic constituents of samples may deposit in the outlet capillary, presumably because of its relatively low temperature. The rinsing obviates frequent cleaning of the combustion tube itself. The procedure is not affected by the SO_2:SO_3 ratio, as all sulphur oxides are oxidized to sulphuric acid by the peroxide.

The results obtained for sulphur in coals by the standard Eschka mineralization and by the recommended procedure showed good agreement (Table 2), even when the coals had extremely high ash contents (Table 3).

TABLE 2

Comparison of methods for sulphur in coal (Results in % S)

Procedure	Brown lignite	Lignite coke	Fat Sahr coal	Ruhr coal	Lean coal "Ibbenbüh-ren"	Welsh anthracite
ISO/R 334	0.37	0.61	0.68	0.88	1.34	0.97
Eschka method[a]	0.35	0.61	0.64	0.92	1.37	0.96
Recommended procedure[a]	0.35	0.60	0.64	0.93	1.38	0.97
	0.34	0.62	0.64	0.92	1.36	0.94
						0.97

[a]With microcoulometric finish.

The titrations were mainly done by the microcoulometric method [4]. However, because this technique involves rather expensive apparatus, the simpler thorin titration [5] was also tested; a Metrohm E 1009 Spectrocolorimeter was used. This simpler titration procedure is also satisfactory (Table 4).

A duplicate analysis by the proposed method requires less than 1 h of working time, whereas e.g. the ISO/R 334 method which prescribes Eschka sintering and gravimetry takes several hours.

TABLE 3

Comparison of methods for sulphur in coal with high ash content

Ash content (%)	Sulphur (%)	
	ISO/R 334	Proposed method (microcoulometric)
76.3	0.88	0.89—0.91
33.0	0.95	0.92—0.93
52.9	0.83	0.83—0.84
87.2	0.51	0.54—0.58

TABLE 4

Comparison of the microcoulometric method with the thorin titration (Results in % S)

Finish	NBS standard coal (SRM 1632)[a]	Kentucky coal	Limburg coal
Microcoulometric	1.99	0.83	0.79
Thorin titration	2.02	0.80	0.80

[a]Sulphur content not specified.

REFERENCES

1 P. J. Jackson, Fuel, 35 (1956) 212.
2 W. Thürauf, Erdöl Kohle, 27 (1974) 135.
3 W. Radmacher, Brennstoff-Chemie, 33 (1952) 129.
4 M. C. van Grondelle, F. van de Craats and J. D. van der Laarse, Anal. Chim. Acta, 92 (1977) 267.
5 J. S. Fritz and S. S. Yamamura, Anal. Chem., 27 (1955) 1461.

Analytica Chimica Acta, 94 (1977) 217—220

Short Communication

PURIFICATION OF XYLENOL ORANGE BY ION-EXCHANGE CHROMATOGRAPHY, AND CHELATE FORMATION WITH LEAD(II) AND ZINC(II)

HISAKUNI SATO*, YUKIO YOKOYAMA and KOZO MOMOKI

Laboratory for Industrial Analytical Chemistry, Faculty of Engineering, Yokohama National University, Ooka 2-31-1, Minami-ku, Yokohama-shi (Japan)

(Received 15th March 1977)

Xylenol orange [1] is an excellent analytical reagent, but the synthesized reagent usually contains considerable amounts of impurities, such as cresol red, iminodiacetic acid and semixylenol orange. Purification by partition chromatography [2, 3] and by thin-layer chromatography [4] have been proposed, but the separation of iminodiacetic acid from xylenol orange is troublesome, and much time and labour are needed to obtain pure xylenol orange. Moreover, it has been reported [5] that purification of xylenol orange by these methods is unsuccessful, probably because the procedures require considerable experience.

The work reported here has shown that such mixtures of organic acids can be separated effectively by ion-exchange chromatography. With DEAE-cellulose, xylenol orange and semixylenol orange can easily be separated and isolated from other impurities by elution with sodium chloride solution. Chelate formation of pure xylenol orange with lead(II) and zinc(II) is also discussed.

Experimental

Reagents. The reagents used were of analytical grade, except for hydrochloric acid (Special grade; Wako SSG). Water was purified by passing through a mixed-bed ion-exchange column followed by distillation. Potassium hydroxide solution (carbonate-free) was standardized against potassium hydrogenphthalate. Lead(II) and zinc(II) nitrate solutions were standardized by EDTA titration.

Apparatus. A Toa Denpa Co. (type HM-5A) pH meter was used with glass and calomel electrodes, and a digital voltmeter. The HITAC 8700/8800 computer system in the Computer Center of the University of Tokyo was used.

Synthesis of xylenol orange. Impure xylenol orange was synthesized by Mannich condensation [1, 3] at 65 ± 2°C. After 9 h, the solvent was distilled off under reduced pressure.

Preparation of DEAE-cellulose column. Commercial DEAE-cellulose (Brawn or Whatman DE-23) was soaked in water for 2—3 h, and the slurry was introduced into a glass tube (1—5-cm diameter), to give a 15-cm column length; this was covered with filter paper. The column was washed with 0.1 M HCl, water, 0.1 M NaOH, water, 0.1 M HCl, and water, in that order.

pH titration. About 30 mg of solid xylenol orange was weighed and dissolved in 25 ml of water and 25 ml of 0.2 M KNO_3. The solution was titrated with 0.1 M KOH at 25 ± 0.1°C under a nitrogen atmosphere. To investigate the chelate formation with Pb(II) and Zn(II), similar pH titrations were performed by adding suitable amounts of the metal-ion solutions. The ionic strength was 0.1 (KNO_3).

Spectrophotometric measurement. At about pH 5 (hexamine — HNO_3), the visible spectra of the lead— and zinc—xylenol orange systems were recorded (Shimazu UV200). Transmittance values at 10-nm intervals in the range 400—600 nm were used to confirm the equilibrium data obtained by the pH titrations.

Results and discussion

Separation of xylenol orange. When a suitable amount of xylenol orange solution is loaded on the column and eluted with 0.1 M NaCl, three or more colored bands appear gradually, the elution order being cresol red, semixylenol orange, and xylenol orange; other colored bands were observed, but the amounts of these impurities were small if xylenol orange was synthesized at 60—65°C and the solvent (acetic acid) was distilled off rapidly at low temperature; iminodiacetic acid is colorless, but ninhydrin tests showed that it was eluted before cresol red, which is an improvement on partition chromatography [3].

For the preparative separation of semixylenol orange and xylenol orange, step-wise elution with 0.05, 0.1, and 0.2 M NaCl solutions proved suitable. For analytical purposes, gradient elution gives better chromatograms. The separation of xylenol orange, semixylenol orange, and other impurities appears not to depend on column diameter (up to 5 cm); again this is an improvement on partition chromatography. The amount of xylenol orange loaded on to the column at one time should be less than 0.1 mmol per 100 meq of DEAE-cellulose. As eluant, potassium nitrate solution is as suitable as sodium chloride, but sodium perchlorate gives poorer separations.

The eluted xylenol orange fraction can ordinarily be used as the reagent for complexiметric titrations or spectrophotometric determinations. The concentration of xylenol orange in the eluate with 0.2 M NaCl is about 10^{-3} M. This can be established accurately by measuring (at 430 nm) the absorbance of the diluted solution at pH 4—5. The apparent molar absorptivity under these conditions is 2.64×10^4 l mol^{-1} cm^{-1}.

Although Murakami et al. [3] used cation-exchange resin to obtain the free acid form, xylenol orange is adsorbed on the cation exchanger, and considerable amounts of water are necessary to elute it. The DEAE-cellulose

column can again be used effectively to remove sodium ion from the xylenol orange fraction. Once chromatographed and purified, the xylenol orange solution is diluted about four-fold with water, and the solution is poured onto the column, which is then washed with water until sodium ion is no longer detected (flame reaction). Xylenol orange is then eluted with 0.1 M HCl, giving a ca. 0.01 M solution. This eluate is collected in a polypropylene cup, and dried in a desiccator over sulfuric acid and silica gel. Evaporation under reduced pressure was difficult because of violent frothing on boiling. The solid xylenol orange was obtained as the hydrochloride; partition chromatography [3] showed only one colored band.

Elemental analysis of the purified xylenol orange gave 47.9% C, 5.0% H, 3.5% N, 4.3% S and 7.9% Cl. The pH titration showed the presence of a strong acid other than xylenol orange (H_6L); the acid concentration coincided with the chloride concentration obtained by elemental analysis. The molecular weight was estimated as about 761 from the pH titration curve. These results indicate that the composition of the solid xylenol orange is $H_6L \cdot 2H_2O \cdot 1.8HCl$.

Acid formation constants. The pH titration data were processed by the computer program, SCOGS [6]. The acid formation constants obtained were: $\log k_2 = 10.35 \pm 0.02$ $\log k_3 = 6.66 \pm 0.03$, $\log k_4 = 2.79 \pm 0.04$, $\log k_5 = 2.11 \pm 0.05$; the first and sixth constants could not be obtained by the pH titration method. These values agree with those of Murakami et al. [3].

Proton n.m.r. The n.m.r. spectrum of a 4.44% solution of xylenol orange in D_2O was measured. The spectrum showed methyl protons resonating at about 2 ppm from TMS, two types of methylenic proton resonating at a lower field broadened by the adjacent ^{14}N, and benzene ring protons at a lower field than active protons. The relative ratio of the peak areas for the methyl and two types of methylenic protons was about 6:8:4. This agrees with the known structure of xylenol orange, where two methyliminodiacetic acid groups are introduced into the symmetrical positions of *o*-cresol red.

Chelate formation of xylenol orange with lead(II) and zinc(II). The Pb—xylenol orange [7—10] and Zn—xylenol orange [11, 12] systems have often been studied but the molar ratios and the formation constants were re-examined with the pure reagent. The pH titration curves indicated the direct formation of 2:1 and 1:1 chelates. Since there are several possible combinations of metal ion (M), proton (H), and ligand (L), the titration data were processed by computer to obtain the most probable model and the formation constants by a least-squares treatment. The experimental data were satisfactorily explained by the assumption that ML, MHL, MH_2L, and M_2L were all formed under the experimental conditions. The overall formation constants are shown in Table 1.

The spectrophotometric data for the lead—xylenol orange system at pH 5.67 showed that the absorption maximum of Pb_2L occurs at about 580 nm (molar absorptivity, 7.74×10^4 l mol^{-1} cm^{-1}). The absorption maximum of Zn_2L is located at about 570 nm (molar absorptivity, 6.63×10^4 l mol^{-1} cm^{-1}).

TABLE 1

Formation constants for the lead— and zinc—xylenol orange systems

($\beta_{ijk} = [M_iH_jL_k]/[M]^i[H]^j[L]^k$; 25.0°C; $\mu = 0.1$)

	Pb—xylenol orange	Zn—xylenol orange
$\log \beta_{101}$	15.24 ± 0.07	15.41 ± 0.06
$\log \beta_{111}$	25.32 ± 0.04	24.91 ± 0.05
$\log \beta_{121}$	30.01 ± 0.02	29.84 ± 0.04
$\log \beta_{201}$	26.70 ± 0.04	25.37 ± 0.03

REFERENCES

1 J. Körbl, R. Pribil, and E. Emr, Collect. Czech. Chem. Commun., 22 (1957) 961.
2 D. C. Olson and D. W. Margerum, Anal. Chem., 34 (1962) 1299.
3 M. Murakami, T. Yoshino, and S. Harasawa, Talanta, 14 (1967) 1293.
4 M. Yamada and M. Fujimoto, Bull. Chem. Soc. Jpn., 49 (1976) 693.
5 Analytical Methods Committee, Analyst, 100 (1975) 675.
6 I. G. Sayce, Talanta, 15 (1968) 1397.
7 A. Ringbom, Complexation in Analytical Chemistry, Interscience, New York, N.Y., 1963.
8 P. V. Marchenko, Ukr. Khim. Zh., 30 (1964) 224.
9 M. Otomo, Jpn. Anal., 14 (1965) 457.
10 A. Cabrera-Martin, Quim. Anal., 28 (1974) 38.
11 K. Studlar and I. Janousek, Talanta, 8 (1961) 203.
12 V. Chromy and V. Svoboda, Talanta, 12 (1965) 437.

Analytica Chimica Acta, 94 (1977) 221—223

Book Reviews

Ralph B. Turner (Ed.), *Analytical Biochemistry of Insects*, Elsevier, Amsterdam, 1977, vii + 315 pp., price Dfl. 74, U.S. $30.25.

This is a very specialised book; its publication is justified because "it is the rare insect biochemist or physiologist who has not had the unrewarding experience of struggling unsuccessfully with a published analytical method devised for some other organism" (p. 3). Strangely enough, the only compounds not requiring special consideration are the carbohydrates, for which the routine, general methods appear to be adequate. Full marks go to the editor, if only for stressing that rigorous (amusingly misprinted as "vigorous" (p. VII)) analytical methodology is essential for success in this field; Chapter 2 elaborates as follows:- "Rigorous analytical methodology requires that several essential conditions are met. Since classical analytical chemistry courses have been dropped from many chemistry and biology curricula, these conditions are unknown or overlooked with the result that too many biochemical measurements appearing in the literature are questionable. This is a common criticism in the evaluation of research grants and manuscripts."

This book is written, in effect, by 11 American authors and one from each of Canada, Brazil and Switzerland. The eight chapters are entitled The Analysis of Nucleosides and Nucleotides; The Biochemical Analysis of Insect DNA; Preparation and Analysis of RNA; Analysis of Amino Acids, Peptides and Related Compounds; Insect Lipid Analysis; Chemical Analysis of Insect Moulting Hormones; Analysis of Naturally Occurring Juvenile Hormones; Analytical Biochemistry of Insect Neurotransmitters and their Enzymes. Each chapter presents many references (ranging from 37 to 244) and each refers to work published in 1975.

The technique of direct reproduction of typed manuscripts has been used, with the usual mixed results. Some chapters come out well (e.g. Chapter 2, where the effect is comparable to a normal type-set job) but in others the text is uncomfortably faint. When publishers decide on this method of production, why do they not, for all it would cost, have *all* the MSS. typed professionally on one machine so that some standard of uniformity is achieved, as in the book reviewed immediately below? This criticism apart, this is a good book that can be recommended unreservedly to those for whom it was written.

A. P. de Leenheer and R. R. Roncucci (Eds.), *Quantitative Mass Spectrometry in Life Sciences*, Elsevier, Amsterdam, 1977, viii + 253 pp., price Dfl. 74, U.S. $30.25.

This book contains the texts of the 4 plenary lectures and 20 papers read at the First International Symposium on Quantitative Mass Spectrometry in Life Sciences, held at the State University of Ghent, Belgium, June 16—18, 1976, when 155 delegates from 14 countries attended.

This book is worth reading by all life scientists, if only for the excellent reviews presented by the plenary lecturers, viz E. C. Horning (Quantification of drugs by mass spectrometry); P. Padieu (Evaluation by mass fragmentography of metabolic pathways of endogenous and exogenous compounds in Eukaryote cell cultures); H. Adlercreutz (Quantitative mass spectrometry of endogenous and exogenous steroids in metabolic studies in man); and C. C. Sweeley (Techniques for quantitative measurements by mass spectrometry). The majority of the contributed papers dealt either with aspects of mass fragmentography, field desorption mass spectrometry, or g.c.—m.s.

Although the direct reproduction of typed manuscripts has been used, the effect is acceptable because all the typing has been done accurately, with the same type-face. Unfortunately, several of the more complex figures have not reproduced clearly, possibly because they had to be reduced greatly in size. In a publication of this standard of quality, all figures submitted should be re-drawn professionally. Nevertheless, those concerned with such rapid publication of this book will earn the gratitude of all those who were unable to attend the Symposium.

L. Lang (Ed.), *Absorption Spectra in the Infrared Region, Vol. 1*, Butterworth, London, 1974, 320 pp., price £13.00; Vol. 2, Butterworth, London, 1976, 320 pp., price £17.50; Vol. 3, Akademiai Kiado, Budapest, 1977, 320 pp., price £17.50.

These large volumes are edited by Professor Lang of the Department of Atomic Physics, Technical University of Budapest, who is well known for his series, already extending to 21 volumes, on absorption spectra in the ultraviolet and visible region. In this infrared series he has the collaboration of S. Holly and P. Sohar; it was the intention, at the outset, to produce approximately 2 volumes per annum. The first two volumes, printed in Hungary, were joint editions published by the Butterworth Group and Akademiai Kiado. The spectra were obtained in various Hungarian Universities, Institutes, or Works, on the UR10 instrument (UR20 for some spectra in Vol. 3). The spectra are all of good quality and more than adequate for identification purposes. Each volume contains spectra that range from very simple, well-known compounds e.g. pyridine, octan-1-ol etc. to very unusual compounds which can only be of specialised research

interest, if any. Each volume has a well-prepared subject index, and there is also a molecular formula index. These volumes may be of interest for reference purposes to laboratories that do not already have collections of the well-known systems of punched cards.

D. M. W. Anderson

(continued from page 4 of cover)

Short Communications

VOL. 94 No. 1 ANALYTICA CHIMICA ACTA NOVEMBER 1, 1977

CONTENTS

(continued on inside page of the cover)